KINETICS AND MECHANISM OF OXIDATION OF DIOLS BY [BIS(TRIFLUOROACETOXY)IODO]BENZENE

Jayshree Banerji[a] and Kalyan K. Banerji[b]*

The oxidation of some vicinal and non-vicinal diols and two of their monoethers by [bis(trifluoroacetoxy)iodo]benzene (TFAIB) in aqueous acetic acid solution has been studied. The oxidation of vicinal diols leads to glycol-bond fission. The non-vicinal diols behave like monohydric alcohols and leads to the formation of hydroxy carbonyl compounds. The reaction is first order in TFAIB and a Michaelis-Menten kinetics was obtained with respect to the reductant. The reaction showed a first order dependence on hydrogen-ions. The oxidation of $[1,1,2,2-^2H_4]$ethandiol exhibited the absence of a kinetic isotope effect. Suitable mechanisms have been proposed.

Corresponding Authors
Fax: +91 291 2577530
E-Mail: banerjikk@gmail.com
[a]   Department of Chemistry, RGP Mahavidyalaya, Kolar Road, Bhopal 462042, India
[b]   Faculty of Science, National Law University, Mandore, Jodhpur 342304, India

Introduction

Oxidation of hydroxy compounds to the corresponding carbonyl compounds is an important transformation in synthetic organic chemistry. A large number of oxidants are known to bring about this transformation. However, most of these reagents are salts of toxic heavy metals. Hypervalent iodine compounds present an eco-friendly option. Bis(trifluoroacetoxy)-iodo]benzene (TFAIB) is well-known oxidant and some reports about the mechanism of oxidation reactions of TFAIB, including that of alcohols, have emanated recently from our laboratory.[1-6] However several oxidations of monohydric and polyhydric alcohols are known to follow different mechanistic pathways.[7] Therefore, we have studied the kinetics of oxidation several diols and two of their monoethers by TFAIB in 1:1 acetic acid-water (v/v), in the presence of perchloric acid. Mechanistic conclusions are discussed.

Experimental Section

Materials

TFAIB was a commercial product (Aldrich) and was used as received. The diols and the monoethers were commercial products and were distilled under reduced pressure before use. $[1,1,2,2-^2H_2]$Ethandiol (DED) was prepared by the reported methods.[8] Its isotopic purity, as ascertained by the ^{1}H NMR (100 MHz) spectra, is 96±3 %. Acetic acid was refluxed for 3 h with acetic anhydride and chromic oxide and then distilled. Perchloric acid was used as a source of hydrogen ions.

Product analysis

The product analysis was performed under kinetic conditions i.e. with an excess of the diol over TFAIB. In a typical experiment, the diol (0.1 mol) and TFAIB (4.3 g, 0.01 mol) were made up 100 ml in 1:1 acetic acid-water (v/v), in the presence of perchloric acid (0.2 mol), and was allowed to stand for *ca.* 12 h for the completion of the oxidation. It was then treated with an excess (200 ml) of a saturated solution of 2,4-dinitrophenyl-hydrazine in 2 mol dm^{-3} HCl and kept overnight in a refrigerator. The precipitated 2,4-dinitrophenylhydrazone (DNP) was filtered dried, weighed, recrystallized from ethanol and weighed again. The DNP derivatives were found to be homogenous by TLC except in the oxidation of propane-1,2- and butane-1,2-diols. In these cases the mixtures were separated by fractional crystallization. The identities of the products were confirmed by comparing the m.p. with the literature values.[9] In the oxidation of ethanediol, pinacol and butane-1,4-diol, the identity of the products were confirmed by mixed m.p. with authentic samples of DNP of formaldehyde, acetone and 4-hydroxybutanal respectively. The m.p. were determined in open capillaries and are uncorrected. The results are summarized in Table 1. The yield of DNP of ethanediol was 95 % and 88 % before and after recrystallization respectively.

Kinetic measurements

The reactions were studied under pseudo-first-order conditions by keeping an excess (x 10 or greater) of the diol over TFAIB. The solvent was 1:1 acetic acid-water (v/v), unless mentioned otherwise. The reactions were studied at constant temperature (± 0.1 K) and were followed by monitoring the decrease in [TFAIB] iodometrically for up to 80% reaction extent. Pseudo-first-order rate constants, k_{obs}, were evaluated from linear plots ($r^2 > 0.995$) of log [TFAIB] against time. Duplicate kinetic runs showed that the rate constants are reproducible to within ±3 %. Preliminary experiments showed that the reaction is not sensitive to changes in ionic strength. Therefore, no attempt was made to keep the ionic strength constant.

Table 1. Analysis of the products in the oxidation of diols by TFAIB

Diol	Product	m.p. of DNP (°C)	Yield[a]
Ethanediol	HCHO	166	89
Propane-1,2-diol	MeCHO, HCHO	147, 165	88
Butane-2,3-diol	MeCHO	148	90
Butane-1,2-diol	EtCHO, HCHO	140, 165	86
Pinacol	MeCOMe	127	91
Propane-1,3-diol	$HOCH_2CH_2CHO$	130	86
Butane-1,3-diol	$MeCH(OH)CH_2CHO$	95	87
Butane-1,4-diol	$HOCH_2CH_2CH_2CHO$	118	90
Pentane-1,5-diol	$HOCH_2(CH_2)_3CHO$	77	85
3-Methoxybutan-1-ol	$MeCH(OMe)CH_2CHO$	106	89
2-Methoxyethanol	$MeOCH_2CHO$	119[b]	85

[a] The yield is of DNP derivative after recrystallization in percentage; [b] Instead of DNP, 4-nitrophenylhydrazone derivative was prepared.
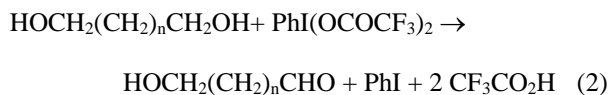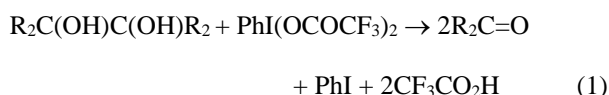
Simple and multivariate regression analyses were carried out by the least-squares method. We have used standard deviation (sd), coefficient of determination (R^2 or r^2), and Exner's[10] parameter, ψ, as measures of the goodness of fit in correlation analysis.

Results

Kinetic data were obtained for all the diols studied. Since the results are similar, only representative data are reproduced here.
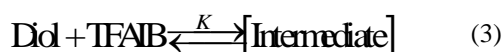
Stoichiometry

The oxidation of vicinal diols by TFAIB resulted in the formation of the products arising out of glycol-bond fission. The other diols are oxidized as simple alcohols to yield hydroxy aldehydes/ketones. The overall reactions may be represented as follows.

$$R_2C(OH)C(OH)R_2 + PhI(OCOCF_3)_2 \rightarrow 2R_2C=O$$

$$+ \, PhI + 2CF_3CO_2H \qquad (1)$$

$$HOCH_2(CH_2)_nCH_2OH + PhI(OCOCF_3)_2 \rightarrow$$

$$HOCH_2(CH_2)_nCHO + PhI + 2\,CF_3CO_2H \quad (2)$$

Rate laws

The reaction is of first order with respect to TFAIB and hydrogen ions. Michaelis-Menten type kinetics were observed with respect to diols (Table 2). A plot of $1/k_{obs}$ against $1/[diol]$ is linear with an intercept on the rate-ordinate (Figure 1). This indicates the following overall mechanism and the rate law (5).

$$Diol + TFAIB \underset{}{\overset{K}{\rightleftharpoons}} [Intermediate] \qquad (3)$$

$$[Intermediate] \xrightarrow{k_2} Product \qquad (4)$$

$$Rate = \frac{Kk_2[diol][TFAIB]}{1+K[diol]} \qquad (5)$$

The variation in diol concentration was studied at four different temperatures and the values of K and k_2 were obtained from the double reciprocal plots. The thermodynamic parameters for the formation of the intermediate and activation parameters for its disproportionation were also calculated (Tables 3 and 4).

Table 2. Rate constants of the oxidation of ethanediol by TFAIB at 298 K

10^3 [TFAIB], mol dm^{-3}	[ethanediol], mol dm^{-3}	[H$^+$], mol dm^{-3}	$10^4\,k_{obs}$, s^{-1}
1.0	0.10	0.10	0.64
1.0	0.20	0.10	1.03
1.0	0.30	0.10	1.26
1.0	0.50	0.10	1.59
1.0	0.75	0.10	1.80
1.0	1.00	0.10	1.95
1.0	1.50	0.10	2.11
1.0	2.00	0.10	2.10
1.0	2.50	0.10	2.50
2.0	1.00	0.10	1.97
4.0	1.00	0.10	1.96
6.0	1.00	0.10	1.94
8.0	1.00	0.10	1.95
1.0	1.00	0.20	3.96
1.0	1.00	0.30	5.92
1.0	1.00	0.40	8.00
1.0	1.00	0.60	11.8
1.0	1.00	1.00	19.7
1.0	1.00	0.20	3.97*

*contained 0.001 mol dm^{-3} acrylonotrile

Table 3. Formation constants and thermodynamic parameters of diol-TFAIB intermediate

| Diol	K, dm^{-3} mol^{-1}				ΔH, kJ mol^{-1}	ΔS, J mol^{-1} K^{-1}	ΔG, kJ mol^{-1}
	288 K	298 K	308 K	318 K			
Ethanediol	3.77	3.43	3.11	2.83	-9.8±0.1	-15.2 ±0.3	-5.5±0.1
Propane-1,2-diol	4.33	4.11	3.94	3.74	-6.2±0.1	-11.3 ±0.4	-6.0±0.2
Butane-2,3-diol	5.35	4.84	4.40	3.92	-10.3±0.2	-14.1 ±0.8	-6.4±0.2
Butane-1,2-diol	4.65	4.35	4.08	3.77	-9.4±0.3	-14.0 ±0.9	-5.5±0.2
Pinacol	3.54	3.27	3.05	2.79	-7.8±0.2	-6.5±0.2	-6.1±0.2
Propane-1,3-diol	5.90	5.45	5.00	4.39	-9.9±0.5	-11.3 ±0.8	-6.7±0.4
Butane-1,3-diol	4.05	3.80	3.53	3.31	-7.7±0.1	-6.9±0.3	-5.8±0.2
Butane-1,4-diol	4.10	3.61	3.29	3.01	-10.3±0.2	-15.8 ±0.6	-5.7±0.3
Pentane-1,5-diol	4.41	4.08	3.72	3.41	-9.1±0.2	-10.9 ±0.6	-6.0±0.2
3-Methoxy-butan-1-ol	4.60	4.24	3.89	3.59	-8.0±0.4	-7.3±0.2	-6.1±0.3
2-Methoxy-ethanol[*]	4.51	4.25	3.98	3.77	-7.1±0.1	-14.5 ±0.2	-6.1±0.2
DED	3.87	3.53	3.20	2.92	-9.7±0.2	-14.5 ±0.3	-5.6±0.1

[*]Data from Ref.5.

Table 4. Rate constants and activation parameters for the disproportionation of the diol-TFAIB intermediate

Diol[a]	$10^4\,k_2$, s^{-1}				ΔH^*, kJ mol^{-1}	ΔS^*, J mol^{-1} K^{-1}	ΔG^*, kJ mol^{-1}
	288 K	298 K	308 K	318 K			
Ethanediol	1.32	2.51	4.80	9.10	46.5±0.7	- 157±2	93.5±0.5
Propane-1,2-diol	1.86	3.51	6.68	12.3	45.5±0.5	- 159±2	92.7±0.4
Butane-2,3-diol	2.62	4.93	9.09	17.0	44.8±0.6	- 158±2	91.9±0.5
Butane-1,2-diol	4.38	8.08	14.6	26.7	43.1±0.6	- 160±2	90.6±0.5
Pinacol	5.19	9.57	17.3	31.4	43.1±0.7	- 159±2	90.2±0.6
Propane-1,3-diol	4.12	9.45	21.4	47.6	59.6±0.6	- 103±2	90.2±0.5
Butane-1,3-diol	7.34	15.4	32.2	68.2	53.9±0.9	- 118±1	89.0±0.5
Butane-1,4-diol	6.85	15.0	31.3	64.9	54.4±0.4	- 117±1	89.1±0.3
Pentane-1,5-diol	7.52	15.8	33.1	69.2	53.8±0.8	- 119±2	88.9±0.6
3-Methoxy-butan-1-ol	8.03	18.0	36.3	73.5	52.1±0.6	- 124±2	88.7±0.4
2-Methoxy-ethanol[*]	3.43	7.85	18.7	41.2	60.8±0.7	- 120±2	96.3±0.6
DED	1.29	2.50	4.84	9.07	47.0±0.5	- 156±2	93.5±0.4

Test for free radicals

The oxidation of ethanediol, in an atmosphere of nitrogen, failed to induce the polymerization of acrylonitrile. In blank experiments, with the diol absent, no noticeable consumption of TFAIB was observed. The addition of acrylonitrile had no effect on the rate of oxidation (Table 2).
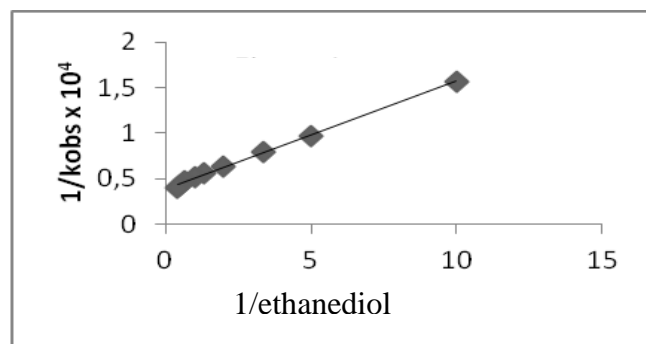
Figure 1. Oxidation of ethanediol by TFAIB: A double reciprocal plot

To further confirm the absence of free radicals in the reaction pathway, the reaction was carried out in the presence of 0.05 mol dm^{-3} of 2,6-di-*t*-butyl-4-methylphenol (butylated hydroxytoluene or BHT). It was observed that BHT was recovered unchanged, almost quantitatively.

Kinetic isotope effect

To ascertain the importance of the cleavage of the α-C – H bond in the rate-determining step, oxidation of deuterated ethanediol was studied. The results (Tables 3 and 4) showed that the neither the formation nor the disproportionation of the diol-TFAIB intermediate exhibit a kinetic isotope effect.

Solvent composition effect

The oxidation of ethanediol was studied in solvents containing different amounts of acetic acid and water. The rate of oxidation increases with an increase in the amount of acetic acid in the solvent (Table 5). This may be attributed to the change in the acidity of the medium with a change in the amount of acetic acid. Wiberg and Evans[11] have determined the Hammett's acidity function, H_0, for low concentration of perchloric acid in a series of acetic acid-water mixtures. They observed that the acidity increases as the concentration of acetic acid increases. The present reaction is an acid-catalyzed one and with an increase in the acidity of the solution, the rate is expected to increase.

Table 5. Effect of solvent composition on the oxidation rate of ethanediol by TFAIB

% AcOH, v/v	25	40	50	60	70
$10^5 k_{obs}$, s^{-1}	8.56	12.7	19.5	28.7	40.6

[ethanediol] 1.00 mol dm^{-3}; [TFAIB] 0.001 mol dm^{-3}; [H$^+$] 0.10 mol dm^{-3} ; T = 298 K.

Table 6. Effect of trifluoroacetic acid on the oxidation of ethanediol by TFAIB at 298 K

10^3 [TFA], mol dm^{-3}	0.0	0.5	1.0	2.0
$10^5 k_{obs}$, s^{-1}	19.5	13.4	9.42	7.58

[ethanediol] 1.00 mol dm^{-3}; [TFAIB] 0.001 mol dm^{-3}; [H+] 0.10 mol dm^{-3}.

Effect of trifluoroacetic acid

Addition of trifluoroacetic acid (TFA) reduces the rate of reaction (Table 6).

Discussion

The diverse nature of the products formed in the oxidation of vicinal diol and other diols suggests that these compounds follow different mechanistic pathways. This further confirmed by the two linear plots obtained between log k_2 at 288 K and at 318 K, one for the vicinal diols and another for the rest (Figure 2). Therefore, it was considered best to treat the oxidation of vicinal and other diols separately.
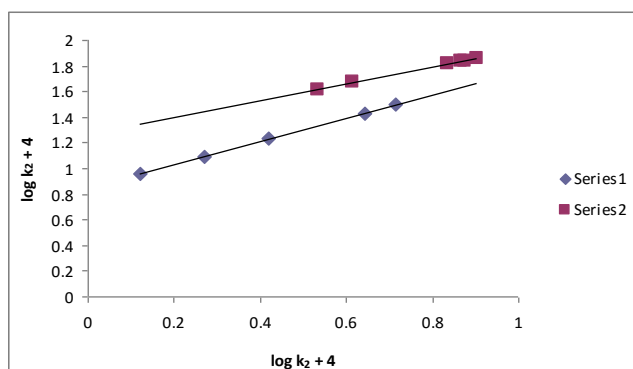
Figure 2. Isokinetic relationship in the oxidation of diols by TFAIB: vicinal diols (series 1); other diols (series 2)

Oxidation of vicinal diols

There is no significant correlation between the activation enthalpies and entropies of the oxidation of five vicinal diols ($r^2 = 0.6373$), indicating the absence of a compensation effect.[12] A correlation between the calculated values of enthalpies and entropies is often vitiated by the experimental errors associated with them. The reaction, however, exhibited an excellent isokinetic relationship, as determined by Exner's method.[13] An Exner's plot between log k_2 at 288 K and at 318 K was linear ($r^2 = 0.9989$, $sd = 0.02$, slope = 0.9039±0.0108). The value of isokinetic temperature evaluated from the Exner's plot is 451±11 K. The linear isokinetic correlation implies that all the diols are oxidized by the same mechanism and the change in the rate of oxidation is governed by changes in both the enthalpy and entropy of the activation.

The absence of a primary kinetic isotope effect confirms that the α-C-H bond is not cleaved in the rate-determining step. In contrast, a substantial primary kinetic isotope effect was observed in the oxidation of ethanol[5] by TFAIB. Thus it is apparent that the oxidation of monohydric alcohols and vicinal diols follow different mechanisms.

A perusal of data of Table 3 showed that the formation constants of the diol-TFAIB intermediate do not exhibit much variation with the structure of the diol. However, the rate constants of the disproportionation of the intermediate vary considerably with the nature of the diol. The rate constants of the disproportionation were, therefore, subjected to correlation analysis.

The rate constants, k_2, of the disproportionation failed to yield any satisfactory correlation separately with Taft σ_I and E_s values.

$$\log k_2 = -2.50 \pm 1.17 \, \Sigma\sigma_I - 3.48 \tag{6}$$

$r^2 = 0.6035$, $sd = 0.18$, $\psi = 0.70$, $n = 5$, $T = 298$ K

$$\log k_2 = -1.53 \pm 0.35 \, \Sigma E_s - 3.54 \tag{7}$$

$r^2 = 0.8615$, $sd = 0.11$, $\psi = 0.42$, $n = 5$, $T = 298$ K

The rates were, therefore, correlated in terms of Pavelich-Taft's[14] dual substituent-parameter (DSP) equation (8).

$$\log k_2 = \rho_I \, \Sigma \, \sigma_I + \delta \, \Sigma \, E_s + \log k_0 \tag{8}$$

The correlations are excellent; the reaction constant being negative (Table 7). Though the number of compounds is rather small (five) for correlation with a DSP equation, the correlations are excellent and results can be used qualitatively.

**Table 7.** Temperature dependence of the reaction constants

T, K	ρ_I	δ	R^2	sd	ψ
288	-1.18±0.01	-1.28±0.01	0.9998	0.01	0.02
298	-1.16±0.01	-1.25±0.01	0.9999	0.01	0.02
308	-1.12±0.02	-1.18±0.01	0.9996	0.02	0.03
318	-1.09±0.02	-1.15±0.02	0.9995	0.03	0.04

The negative polar reaction constants indicate an electron-deficient carbon centre in the transition state of the rate-determining step. The negative steric reaction constant shows a steric acceleration of the reaction. This may be explained on the basis of high ground state energy of sterically crowded diols. Since the crowding is relieved in the product carbonyl compound as well as in the transition state leading to it, the transition state energies of the crowded and uncrowded diols do not differ much and steric acceleration, therefore, results.
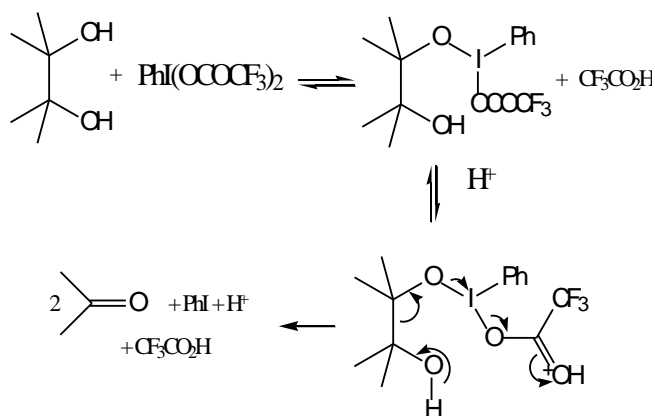
Scheme 1.
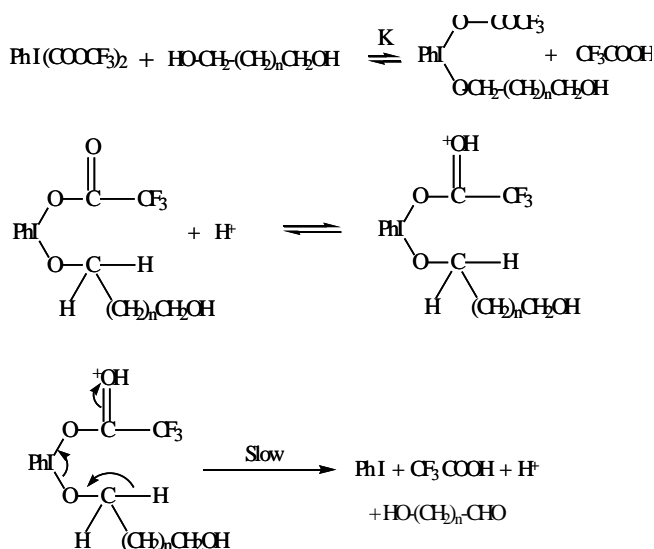
Scheme 2.

The absence of a kinetic isotope effect confirms that the α-C–H bond is not cleaved in the rate-determining step. The retardation of the reaction by the addition of TFA points to an equilibrium in which TFA is one of the products. The Michaelis-Menten kinetics also indicates the formation of an intermediate in a rapid pre-equilibrium. This may well be a ligand exchange round trivalent iodine. Similar exchanges are known in the oxidations by lead tetraacetate.[15] The observed acid-catalysis suggest that the intermediate is protonated in a fast reversible reaction, prior to the slow step.

The mechanism depicted in Scheme 1 explains all the observed data. The low negative values of the polar reaction constant support the proposed mechanism. In an oxidation reaction, the net flow of the electrons is from the reductant to the oxidant. Therefore, an electron-deficiency is created, in the transition state, in the reductant moiety.

Oxidation of other diols

The linear correlation between log k_2 at 288 K and 318 K (r^2 = 0.9980, slope = 0.6555±0.0148) for the oxidation of four non-vicinal diols, 3-methoxybutan-1-ol, and 2-methoxyethanol shows that all the compounds are oxidized by the same mechanism.[12] The value of isokinetic temperature is 397±22 K. 3-Methoxybutan-1-ol and 2-methoxyethanol are typical monohydric alcohols and, therefore, it is highly likely that the non-vicinal diols are oxidized by a mechanism similar to that operative for monohydric alcohols. The oxidation of ethanol and 2-propanol[5] exhibited a substantial primary kinetic isotope effect confirming the cleavage of the α-C-H bond in the rate-determining step. Therefore, a mechanism similar to one proposed earlier by Banerji et al,[5] accounts for the experimental results obtained in the oxidation of non-vicinal diols (Scheme 2)

Acknowledgements

References

[1]Kansara, A., Sharma, P. K., Banerji, K. K. *J. Chem. Res.,* **2004**, 581.

[2]Kansara, A., Sharma, P. K., Banerji, K. K. *J. Chem. Res.,* **2004**, 315.

[3]Kansara, A., Sharma, P. K., Banerji, K. K. *Indian J. Chem.,* **2004**, *43A*, 1056.

[4]Purohit, P., Banerji, J., Sharma, P. K., Banerji, K. K. *Prog. React. Kinet. Mech.,* **2009**, *34*, 141.

[5]Banerji, J., Sharma, P. K., Banerji, K. K., *Indian J. Chem.,* **2008**, *47A***,** 1213.

[6]Banerji, J., Sharma, P. K., Banerji, K. K., *Prog. React. Kinet. Mech.,* **2005**, *30*, 267;

[7]Banerji, J., Sharma, P. K., Banerji, K. K., *Indian J. Chem.,* **2007**, *46A***,** 445.

[8]Kemp, T. J. Waters, W. A. *Proc. Roy. Soc.,* **1963**, *A274*, 480.

[9]Coffey, S. (Ed), *Rodd's Chemistry of Carbon Compounds,* Vol. I, Elsevier, Amsterdam **1965**; Rodd, E. H. (Ed), *Chemistry of Carbon Compounds,* Vol. I A, Elsevier, Amsterdam, **1951**; Buckingham, J. (Ed), *Dictionary of Organic Compounds,* Vol. 3, Chapman and Hall, New York, **1982**; West R C, *Handbook of Chemistry and Physics,* 58th edition, CRC Press, Ohio, **1977-78**.

[10]Exner, O., *Collect. Czech. Chem. Commun*., **1966**, 31 3222.

[11]Wiberg, K. B., Evans, R. J., *J. Am. Chem. Soc.,* **1958**, *80* 3019.

[12]Liu, L. Guo, Q.-X., *Chem. Rev.,* **2001**, *101* 673.

[13]Exner, O.m *Collect. Czech. Chem. Commun*., **1964**, 29 1094.

[14]Pavelich, W. A., Taft, R. W, *J. Am. Chem. Soc.,* **1957**, *79*, 4835.

[15]Banerji, K. K., Banerjee, S. K., Shanker, R. *Bull. Chem. Soc. Jpn.,* **1978**, *51*, 2153.

EFFICIENT CATALYSTS FOR THE RAPID SYNTHESIS OF BENZYLIDENE BIS(4-HYDROXYCOUMARIN) DERIVATIVES IN AQUEOUS MEDIA

## Zahed Karimi-Jaberi[a]* and Mohammad Reza Nazarifar[a]

Trichloroacetic acid, CCl_3COOH, efficiently catalyzed the reaction of an aromatic aldehydes and 4-hydroxycoumarin in aqueous media under mild conditions to afford the corresponding α,α′-benzylidene bis(4-hydroxycoumarin) derivatives in high yields. Ceric sulfate, $(Ce(SO_4)2.4H_2O)$, has also been used as another solid catalyst for this reaction.

* Corresponding Authors
    Fax: +98 7126224402
    E-Mail: zahed.karimi@yahoo.com
[a]   Department of Chemistry, Firoozabad Branch, Islamic Azad University, P.O. Box 74715-117 Firoozabad, Fars, Iran

Catalyst: A: 10 Mol % trichloroacetic acid
B: 10 Mol % ceric sulfate 4.H_2O
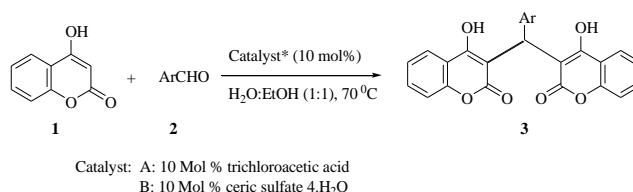
Scheme 1. Synthesis of benzylidene bis(4-hydroxycoumarin)

Introduction

It is well known that coumarin derivatives exhibit a wide range of biological activities, pharmaceutical and therapeutic properties, such as, antitumour, anticoagulant, antihelminthic, hypnotic, antifungal and antibacterial activities.[1-5] Recently, the synthesis of biscoumarin derivatives have attracted great interest due to their biological and pharmacological activities. The condensation of 4-hydroxycoumarin with aldehydes is the most convenient methods for the synthesis of biscoumarins. Various new techniques,[6-16] such as microwave-assisted synthesis technique,[6] ionic liquids,[10,17] solvent-free techniques[11] and acid catalysts,[7,12,13] were used to improve this reaction. In spite of their potential utility, many of these methods involve expensive reagents, harsh reaction conditions, high temperatures, long reaction times and unsatisfactory yields. Thus, the introduction of milder, faster and more eco-friendly methods is still in great demand.

From the environmental acceptability, recently inorganic acidic salts have widely used in organic synthesis because of minimized wastes, simplicity in handling and decreased reactor corrosion problems.[18] Trichloroacetic acid has been used by our group for the synthesis of enaminones,[19] dihydropyrano[2,3-c]pyrazoles,[20] and xanthenes.[21]

With our continuous investigation on the methodology of green synthesis,[19-22] we report the results that led to an extremely convenient method for the preparation α,α′-benzylidene bis(4-hydroxycoumarins) from aromatic aldehydes and 4-hydroxycoumarin in the presence of trichloroacetic acid or ceric sulfate in excellent yield (Scheme 1).

Experimental

Typical procedure for the synthesis of α,α′-benzylidene bis(4-hydroxycoumarin) Derivatives

A solution of aromatic aldehyde (1 mmol), 4-hydroxycoumarin (2 mmol), and CCl_3COOH or $Ce(SO_4)_2.4H_2O$ (10 mol %) in 5.0 mL aqueous ethanol (50%) was stirred at 70 °C for the appropriate times (Table 1). Upon completion of the reaction, monitored by TLC, the reaction mixture was allowed to cool to room temperature. The solid was filtered off and washed with water (2 × 10 ml) and purified by recrystalization from ethanol.

Selected spectral data

3,3′-(3-Nitrobenzylidene)-bis-(4-hydroxycoumarin) (3c) :IR(KBr): 3424, 2925, 1655, 1616, 1564, 1494, 1450, 1347, 762 cm⁻¹; ¹H NMR (400 MHz, DMSO-d6):δ 6.39 (s, 1H, CH), 7.28-8.04 (m, 12H, ArH), 8.04-9.52 (m, 2H, OH).

3,3′-(4-Cholorobenzylidene)-bis-(4-hydroxycoumarin) (3f): IR(KBr): 3420, 2923, 1668, 1606, 1563, 1490, 1451, 1351, 765 cm⁻¹; ¹H NMR (400 MHz, DMSO-d6):δ 6.63 (s, 1H, CH), 7.16-7.90 (m, 12H, ArH), 7.90-9 (m, 2H, OH).

3,3′-(4-Methoxybenzylidene)-bis-(4-hydroxycoumarin) (3h): IR(KBr): 3443, 2926, 1668, 1606, 1563, 1510, 1452, 1352, 767 cm⁻¹; ¹H NMR (400 MHz, DMSO-d6):δ 3.71 (s, 3H, CH3O), 6.31 (s, 1H, CH), 6.80-7.93 (m, 12H, ArH), 8.16-8.78 (m, 2H, OH).

3,3′-(4-Chloro-3-nitrobenzylidene)-bis-(4-hydroxycoumarin) (3k): IR(KBr): 3423, 2920, 1665, 1613, 1558, 1536, 1450, 1348, 765 cm^{-1}; ^{1}H NMR (400 MHz, DMSO-d6):δ 6.28 (s, 1H, CH), 7.26-7.85 (m, 11H, ArH), 8.15-8.56 (m, 2H, OH); 13C NMR (DMSO-d6):δ 36.42, 103.23, 116.24, 119.31, 121.99, 123.81, 124.03, 124.51, 131.39, 132.07, 132.89, 143.87, 147.94, 152.90, 164.70, 167.34. Anal. Calcd. for $C_{25}H_{14}ClNO_8$: C, 60.80; H, 3.27; N, 2.84; Found: C, 60.89; H, 3.25; N, 2.90.

Results and Discussion

To optimize the amount of catalyst, effect of solvent and effect of temperature, reaction of benzaldehyde and 4-hydroxycoumarin was selected as the model reaction to afford α,α′-(benzylidene)-bis-(4-hydroxycoumarin). The optimized reactant ratios were found to be 1.0 equiv. benzaldehyde and 2.0 equiv. 4-hydroxycoumarin in the presence of catalysts (10 mol %) in 5 ml aqueous ethanol (1:1, H$_2$O–EtOH). The expected α,α′-benzylidene bis(4-hydroxycoumarin) was produced in 88 % yield after 5 min at 70 °C, for trichloroacetic acid and 86 % yield after 7 min at 70 °C for ceric sulfate. With respect to the quantity of the catalyst, there was no significant enhancement in yields when the concentration was increased from 10 mol % to 20 mol %.

After optimizing the reaction conditions, different aldehydes, both with electron donating and electron withdrawing groups were investigated for the present protocol. It was found that all the reactions proceeded well and produced the corresponding products in good yields and in very short reaction times (Table 1). No significant change

in yield was observed when either substituted aromatic aldehydes were used. However, the synthesis could not be achieved in the absence of the catalyst.

The reaction proceeds via condensation of 1 equiv. of aldehyde with 2 equiv. of 4-hydroxycoumarin to form the corresponding product as has been suggested earlier.13 The reaction pathway is shown in Scheme 2.
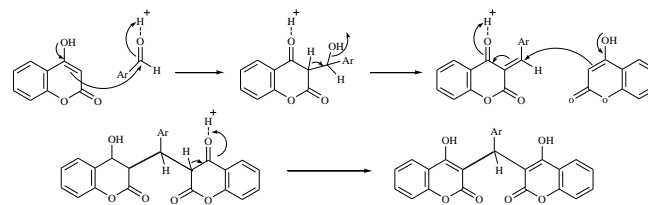
Scheme 2. Proposed mechanism

As shown in Table 2, we compared results of 3-methyl-1-(4-sulfonic acid)butylimidazolium hydrogen sulfate [MIM(CH$_2$)$_4$SO$_3$H],[10] sodium dodecyl sulfate (SDS),[12] phosphotungstic acid,[13] H$_{14}$[NaP$_5$W$_{30}$O$_{110}$])-SiO$_2$,[7] piperidine,[8] HBF$_4$ and tetrabutylammoniumbromide (TBAB),[9] [bmim]BF$_4$,[11] in the synthesis of α,α′-(enzylidene bis(4-hydroxycoumarin) derivatives with present method and demonstrated that CCl$_3$COOH or (Ce(SO$_4$)$_2$.4H$_2$O) can act as effective catalysts. Thus, the present work using CCl$_3$COOH or (Ce(SO$_4$)$_2$.4H$_2$O) as catalysts is an efficient route for production of α,α′-benzylidene bis(4-hydroxycoumarin) derivatives.

All products were identified by ^{1}H-NMR, ^{13}C NMR and IR spectroscopic methods and the results were confirmed by comparison with those available in the literature.

Table 1. Synthesis of benzylidene bis(4-hydroxycoumarin) derivatives

Entry	Aldehyde	Product	Method A[a]		Method B[b]		M.p. (°C)[ref.]
			Time, min	Yield, %	Time, min	Yield, %	
1	Benzaldehyde	**3a**	5	88	7	86	230-232[6]
2	4-Nitrobenzaldehyde	**3b**	3	98	5	97	232-234[6]
3	3-Nitrobenzaldehyde	**3c**	3	87	5	85	229-231[12]
4	4-Cyanobenzaldehyde	**3d**	4	89	5	82	242-244[16]
5	4-Fluorobenzaldehyde	**3e**	4	90	6	84	211-212[12]
6	4-Chlorobenzaldehyde	**3f**	3	94	5	88	256-258[6]
7	3-Methoxybenzaldehyde	**3g**	3	84	6	81	238-240[9]
8	4-Methoxybenzaldehyde	**3h**	4	83	7	80	246-248[6]
9	4-Bromobenzaldehyde	**3i**	3	95	5	91	264-266[12]
10	4-Methylbenzaldehyde	**3j**	5	86	6	84	266-268[6]
11	4-Chloro-3-nitrobenzaldehyde	**3k**	3	90	5	88	269-270

[a]Method A: Trichloroacetic acid; [b] Method B: Ceric sulfate

Table 2. Comparison results of CCl$_3$COOH and (Ce(SO$_4$)$_2$.4H$_2$O) with other catalysts reported in the literature.

Entry	Conditions	Catalyst	Time (min)	Yield (%)
1	Solvent-free, 80 °C	[MIM(CH$_2$)$_4$SO$_3$H] (20mol%)	25-30	86-96
2	H$_2$O, 60 °C	SDS (20mol%)	2.5-3 h	80-96
3	H$_2$O, 80 °C	Phosphotungstic acid (15mol%)	14-25	90-98
4	EtOH, 25 °C	H$_{14}$[NaP$_5$W$_{30}$O$_{110}$])-SiO$_2$ (0.3 mol%)	20-30	90-98
5	EtOH, r.t.	Piperidine	4 h	89-97
6	H$_2$O, 25 °C	HBF$_4$ (10 mol%)	10-12h	55-70
7	H$_2$O, reflux	TBAB (10 mol %)	25-40	82-95
8	Solvent-free, 60-70 °C	[bmim]BF$_4$ (4 mmol)	2-3h	77-91
9	H$_2$O: EtOH (1:1), 70 °C	CCl$_3$COOH (10 mol %)	3-5	83-98
10	H$_2$O: EtOH (1:1), 70 °C	(Ce(SO$_4$)$_2$.4H$_2$O)(10 mol %)	5-7	80-97

Conclusion

In conclusion, we have demonstrated that CCl₃COOH and Ce(SO₄)₂.4H₂O are efficient catalysts for synthesis of α,α′-benzylidenebis(4-hydroxycoumarin). Simple reaction procedures, inexpensive catalysts and single product formation make this an attractive protocol over the existing procedures.

References

[1] Manian, R. D. R. S., Jayashankaran, J., Raghunathan, R., *Tetrahedron Lett.,* **2007**, *48*, 1385.

[2] Kostova, I., Momekov, G., Zaharieva, M., Karaivanova, M., *Eur. J. Med. Chem*., **2005**, 40, 542.

[3] Lee, J. H., Bang, H. B., Han, S. Y., Jun, J. G., *Tetrahedron Lett*., **2007**, *48*, 2889.

[4] Zhao, H., Neamati, N., Hong, H., Mazumder, A., Wang, S., Sunder, S., Milne, G. W. A., Pommier, Y., Burke, T. R., *J. Med. Chem.,* **1997**, *40*, 242.

[5] Maria, G. K., Marian, E. J., *Med. Pharm. Chem*. **1961**, *3*, 583.

[6] Gui-Xia, G., Jian-Feng, Z., Li-Tao, A., Xiu-Li, D., Shun-Jun, J., *Synth. Commun*., **2009**, *39*, 497.

[7] Heravi, M. M., Nahavandi, F., Sadjadi, S., Oskooie, H. A., Bamoharram, F. F., *Synth. Commun*., **2010**, *40*, 498.

[8] Khan, K. M., Iqbal, S., Lodhi, A. M., Maharvi, G. M., Ullah, Z., Choudhary, M. I., Rahman, A. U., Perveen, S., *Bioorg. Med. Chem.,* **2004**, *12*, 1963.

[9] Khurana, J. M., Kumar, S., *Tetrahedron Lett.,* **2009**, *50*, 4125.

[10] Tavakoli-Hoseini, N., Heravi, M. M., Bamoharram, F. F., Davoodnia, A., Ghassemzadeh, M., *J. Mol. Liq*., **2011**, *163*, 122.

[11] Khurana, J. M., Kumar, S., *Monatsh. Chem*., **2010**, *141*, 561.

[12] Mehrabi, H., Abusaidi, H., *J. Iran. Chem. Soc*., **2010**, *7*, 890.

[13] Singh, P., Kumar, P., Katyal, A., Karla, R., Dass, S. K., Prakash, S., Chandra, R., *Catal. Lett*., **2010**, *134*, 303.

[14] Wang, J., Shi, D. Q., Zhuang, Q. Y., Wang X. S., Tu, S. J., *Chin. J. Org. Chem*., **2005**, *25*, 926.

[15] Mazaahir, K., Bansal, V., Mothsra, P., Saxena, S., Somvanshi, R. K., Dey, S., Singh, T. P., *J. Mol. Catal. A: Chem*., **2007**, *268*, 76.

[16] Tabatabaeian, K., Heidari, H., Khorshidi, A., Mamaghani, M., Mahmoodi, N. O., *J. Serb. Chem. Soc*., **2011**, *76*, 1.

[17] Yadav, U. N., Shankarling, G. S., *J. Mol. Liq*., **2014**, *191*, 137.

[18] Salehi, P., Zolfigol, M. A., Shirini, F., Baghbanzadeh, M., *Curr. Org. Chem*., **2006**, *10*, 2171.

[19] Karimi-Jaberi, Z., Takmilifard, Z., *Eur. Chem Bull.,* **2013**, *2*, 211.

[20] Karimi-Jaberi, Z., ReyazoShams, M. M., *Heterocycl. Commun.* **2011**, *17*, 177.

[21] Karimi-Jaberi, Z., Abbasi, S. Z., Pooladian, B., Jokar, M. *E-J. Chem*., **2011**, *8*, 1895-1899.

[22] Karimi-Jaberi, Z., Nazarifar, M. R., Pooladian, B., *Chin. Chem. Lett.* **2012**, *23*, 781.

DFT CALCULATIONS ON MOLECULAR STRUCTURES OF "SELF-ASSEMBLED" METALMACROCYCLES IN M(II)-DITHIOOXAMIDE-PROPANE-1,3-DIOL(M=3D METAL) SYSTEMS

Oleg V. Mikhailov[a]* and Denis V. Chachkov[b]

Using density functional theory (DFT) at the OPBE/TZP level, the calculation of the geometric parameters of the molecular structures of M(II) (5656)macrotetracyclic complexes with a tetradentate macrocyclic ligand with (NNNN)-coordination of donor centers, resulting from "self-assembly" process in M(II)– dithiooxamide– propandiol-1,3 ternary systems, where M= Mn, Fe, Co, Ni, Cu, Zn was performed. The calculation of the molecular structure of this ligand itself was also carried out. The values of the bond lengths, bond and torsion angles in the resulting complexes and macrocyclic ligand indicated above, are presented. The values of the standard enthalpy, entropy and Gibbs free energy of formation of these compounds were also calculated.

Corresponding Authors*

   E-Mail: olegmkhlv@gmail.com

[a] Analytical Chemistry Department, Kazan National Research Technological University, K. Marx Street 68, 420015 Kazan, Russia

[b] Kazan Branch of Joint Super-Computer Center of RAS, Lobachevsky Street 2, 420008 Kazan, Russia

Introduction

Previously a quantum-chemical calculations of the selected (5656) M(II) macrotetracyclic metalchelates of types I and II (where M= Mn, Fe, Co, Ni, Cu, Zn), each with two five-membered and two six-membered metal chelate cycles arranged symmetrically to each other, namely those that are formed in "self-assembly" processes (1).[1]
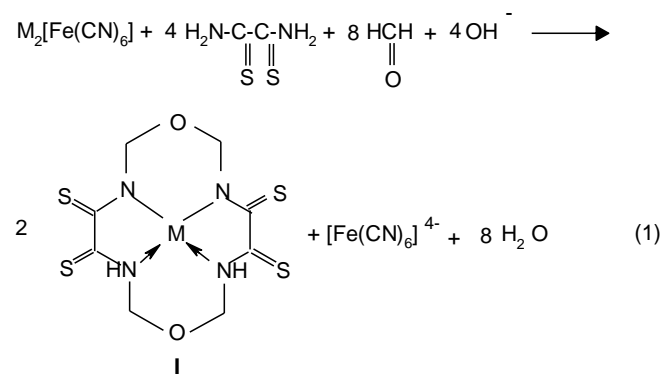
and (2)[2,3]
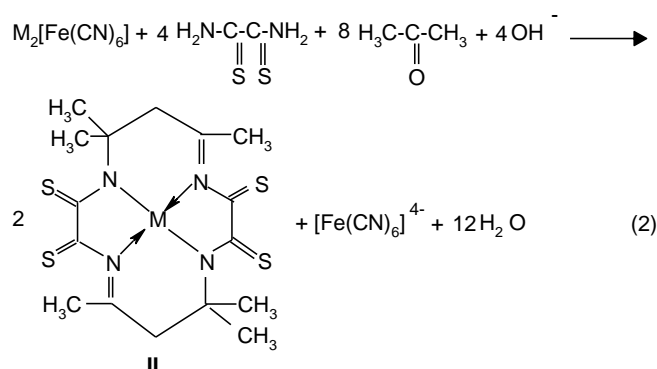
were carried out. Macrocycles of chelants (ligands resulting from "self-assembly") consisted of 14 atoms, and coordination of chelants to M(II) was carried out through four nitrogen atoms. When in the replacing formaldehyde in the reaction (1) or acetone in the reaction (2) with propandiol-1,3 $H_2C(OH)$–CH_2–$CH_2(OH)$, (5656) macro-tetracyclic metalchelates of type III can arise according to the "self-assembly" process (3) where chelant also contains a 14-membered macrocycle and, also, is coordinated to M(II) through four nitrogen atoms:
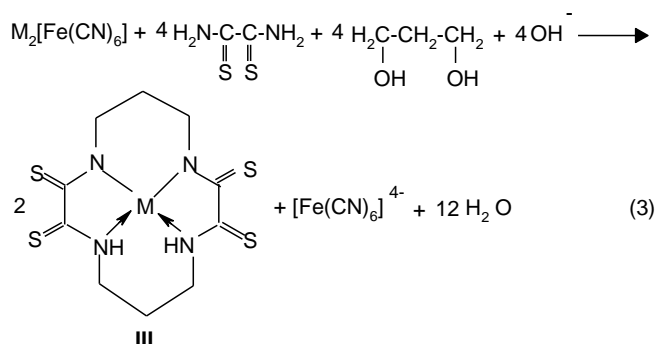
The principal possibility to form such complexes was mentioned in review.[4] In this connection it is very interesting to get and analyze the objective data on structural and geometric parameters of these metal chelates using non-empirical quantum-chemical calculation. This is just the subject of this article.

Method

As in previous our article[5] to carry out quantum-chemical calculations, the density functional theory (DFT) was applied. It combined the standard extended TZVP split-valence basis sets, described in papers[6,7] and non-hybrid OPBE functional described in Refs.[8,9] According to publications,[9-13] in the case of $3d$-element complexes, this method gives more accurate ratio of the high-spin state energy stability to the low-spin one as compared to the most popular B3LYP method. At the same time, DFT method accurately characterizes the basic geometric parameters of the molecular structures of the indicated compounds. The calculations were performed using the Gaussian09 program.[14] As in previous article,[5] the correspondence of the obtained stationary points to the energy minima in all cases was proved by the calculation of the second energy derivatives in coordinates of atoms. Thus, all the equilibrium structures, corresponding to the minimum points on the potential energy surfaces, only had real positive values of frequency.

Results and Discussion

According to our calculations, the ground state of the Mn(II) complex is a spin sextet and it is high-spin complex. For the Fe(II) complex, a ground state is spin triplet and it occupies an intermediate position between the low-spin and high-spin complexes. The ground states for the Co(II) and Ni(II) complexes are a spin doublet and a spin singlet, respectively, so both of them are low-spin. As for the Cu(II) and Zn(II) complexes, spin doublet and singlet, respectively, are their ground states in full agreement with theoretical expectations. In this case, the energy difference of structures with spin multiplicity (which is different from the ground state multiplicity) [quartet in the Mn(II), quintet in the Fe(II), quartet in the Co(II), triplet in the Ni(II), quartet in the Cu(II) and triplet in the Zn(II)] is 20.2, 24.2, 51.4, 68.8, 71.9 and 62.3 kJ mol^{-1} respectively. There is also a very negligible (more than 30 kJ mol^{-1}) energy difference between the ground and the nearest different from it in spin multiplicity excited states; it is only less than this value in the case of the Mn(II) and Fe(II) complexes.

Calculated bond lengths, bond (valence) angles and torsion (dihedral) angles for Mn(II), Fe(II), Co(II), Ni(II), Cu(II) and Zn(II) complexes of type III are listed in *Tables 1-3*. Their molecular structures are outwardly very similar to each other. Metal–nitrogen d(M-N) bond lengths in these macrotetracyclic coordination compounds do not coincide between each other; besides, the shortest M-N lengths can be observed in the Ni(II) complex, the longest – in the Mn(II) one. In average, in the Mn – Zn series they decrease in the proceeding from Mn to Ni, and increase in the proceeding from Ni to Zn (Table 1). However, it should be noted in this connection that d(M1N3) and d(M1N4) values in the same

series decrease in the proceeding from Mn to Fe, increase in the proceeding from Fe to Co, decrease in the proceeding from Co to Ni, increase in the proceeding from Ni to Cu, and, finally, decrease in the proceeding from Cu to Zn. Besides, in the each of these complexes a pairwise equality of d(M–N) values, namely, (M1N1) and (M1N2), (M1N3) and (M1N4), is observed; similar situation takes place for series of pair C–N, C–C and C=S bond lengths, for example (N1C5) and (C6N2), (C8C9) and (C9C7), (C1S4) and (C4S3) (*Table 1*). M(II) chelates under study have either a pyramidal [in the case of Mn(II) and Zn(II)] or quasi-planar [in the case of Fe(II), Co(II), Ni(II) and Cu(II)] coordination of the ligand donor centers relative to M [the sum of the four (N1M1N2), (N2M1N3), (N3M1N4) and (N5M1N2) bond angles, formed by donor atoms and M(II) ion (VAS) is equal to 340.6° (Mn), 356.3° (Fe), 358.6° (Co), 358.7° (Ni), 356.2° (Cu), 352.2° (Zn)].

It should be noted that only two of the above mentioned bond angles, namely, (N2M1N3) and (N4M1N1), have equal values (Table 2). However, the sum of the internal (non-bond) (N1N2N3), (N2N3N4), (N3N4N1) and (N4N1N2) (NVAS) angles in any of these complexes is exactly 360.0°; consequently, the group of N$_4$ donor atoms can be considered as strong planar. It is noteworthy that in the five of six complexes a pairwise equality of these non-bond angles, namely, (N1N2N3) and (N4N1N2), (N2N3N4) and (N3N4N1) occurs, and in the Cu(II) complex all these non-bond angles even are quite equally (each in 90°) (Table 2). The degree of deviation from co-planarity of each of the five-membered metal chelate rings in all these complexes is rather considerable (the sums of bond angles VAS$_{51}$ and

Table 1. Bond lengths in the M(II) complexes of type III.

M	Mn	Fe	Co	Ni	Cu	Zn
Bond lengths in the MN$_4$ chelate node, *pm*						
(M1N1)	236.6	200.1	196.4	193.4	210.0	224.8
(M1N2)	236.6	200.1	196.4	193.4	210.0	224.8
(M1N3)	201.4	187.2	187.8	186.4	194.4	194.2
(M1N4)	201.4	187.2	187.8	186.4	194.4	194.2
Selected bond lengths outside of the chelate node, *pm*						
(N1C5)	148.1	149.3	149.2	149.4	148.9	148.7
(C5C10)	152.5	152.7	152.7	152.4	152.5	152.5
(C10C6)	152.5	152.7	152.7	152.4	152.5	152.5
(C6N2)	148.1	149.3	149.2	149.4	148.9	148.7
(N2C3)	141.8	144.8	145.6	145.7	143.1	143.0
(C3C4)	150.1	148.2	147.9	147.5	149.2	150.0
(C4N3)	133.5	135.6	134.5	134.6	133.4	133.6
(N3C8)	145.4	144.9	144.7	144.6	144.7	145.2
(C8C9)	153.0	151.8	151.8	151.6	152.4	153.0
(C9C7)	153.0	151.8	151.8	151.6	152.4	153.0
(C7N4)	145.4	144.9	144.7	144.6	144.7	145.2
(N4C1)	133.5	135.6	134.5	134.6	133.4	133.6
(C1C2)	150.1	148.2	147.9	147.5	149.2	150.0
(C2N1)	141.8	144.8	145.6	145.7	143.1	143.0
(C2S1)	164.3	163.7	163.2	163.1	163.5	163.6
(C1S4)	167.0	166.8	167.4	167.4	167.6	167.0
(C3S2)	164.3	163.7	163.2	163.1	163.5	163.6
(C4S3)	167.0	166.8	167.4	167.4	167.6	167.0

Table 2. Bond angles in the M(II) complexes of type III.

| M	Mn	Fe	Co	Ni	Cu	Zn
Bond angles in the MN4 chelate node, *deg*						
(N1M1N2)	83.2	89.3	90.4	90.3	90.7	85.7
(N2M1N3)	79.0	84.3	84.5	84.5	82.6	81.1
(N3M1N4)	99.4	98.4	99.0	99.4	100.3	104.3
(N4M1N1)	79.0	84.3	84.5	84.5	82.6	81.1
VAS	340.6	356.3	358.4	358.7	356.2	352.2
Non-bond angles in the N4 group, *deg*						
(N2N3N6)	89.3	90.2	90.8	91.1	90.0	90.1
(N3N6N5)	90.7	89.8	89.2	88.9	90.0	89.9
(N6N5N2)	90.7	89.8	89.2	88.9	90.0	89.9
(N5N2N3)	89.3	90.2	90.8	91.1	90.0	90.1
VAS	360.0	360.0	360.0	360.0	360.0	360.0
Bond angles in the 5-membered chelate ring 1, *deg*						
(M1N2C2)	92.4	103.3	105.6	107.4	103.0	98.0
(N1C2C1)	112.7	111.3	111.0	110.6	112.3	112.6
(C2C1N4)	110.4	110.8	110.5	110.7	111.5	110.7
(C1N4M1)	115.7	116.0	116.6	117.1	116.0	117.2
(N4M1N1)	79.0	84.3	84.5	84.5	82.6	81.1
VAS51	510.2	525.7	528.2	530.3	525.3	519.6
Bond angles in the 5-membered chelate ring 2, *deg*						
(M1N2C3)	92.4	103.3	105.6	107.4	103.0	98.0
(N2C3C4)	112.7	111.3	111.0	110.6	112.3	112.6
(C3C4N3)	110.4	110.8	110.5	110.7	111.5	110.7
(C4N3M1)	115.7	116.0	116.6	117.1	116.0	117.2
(N3M1N2)	79.0	84.3	84.5	84.5	82.6	81.1
VAS52	510.2	525.7	528.2	530.3	525.3	519.6
Bond angles in the 6-membered chelate ring 1, *deg*						
(M1N1C5)	104.0	102.0	102.5	104.1	100.2	101.2
(N1C5C10)	112.9	110.9	110.9	110.8	112.1	112.5
(C5C10C6)	117.7	116.8	117.0	116.5	117.7	117.7
(C10C6N2)	112.9	110.9	110.9	110.8	112.1	112.5
(C6N2M1)	104.0	102.0	102.5	104.1	100.2	101.2
(N2M1N1)	83.2	89.3	90.4	90.3	90.7	85.7
VAS61	634.7	631.9	634.2	636.6	633.0	630.8
Bond angles in the 6-membered chelate ring 2, *deg*						
(M1N4C7)	121.0	125.4	124.5	124.5	122.0	119.1
(N4C7C9)	112.6	112.1	112.3	112.4	112.4	112.6
(C7C9C8)	117.8	115.1	114.8	114.5	116.7	118.0
(C9C8N3)	112.6	112.1	112.3	112.4	112.4	112.6
(C8N3M1)	121.0	125.4	124.5	124.5	122.0	119.1
(N3M1N4)	99.4	98.4	99.0	99.4	100.3	104.3
VAS62	684.4	688.5	687.4	687.7	685.8	685.7
Bond angles outside of the chelate rings, *deg*						
(C5N1C2)	120.1	118.0	116.9	115.3	117.4	118.3
(N1C2S1)	120.6	119.5	119.3	119.4	120.2	120.3
(S1C2C1)	126.1	129.0	129.5	129.9	127.3	126.7
(C2C1S4)	118.8	121.4	121.1	121.5	120.6	119.6
(S4C1N4)	130.7	127.8	128.4	127.9	127.9	129.7
(C1N4C7)	120.6	118.5	118.5	118.3	120.6	121.0
(C4N3C8)	120.6	118.5	118.5	118.3	120.6	121.0
(C6N2C3)	120.1	118.0	116.9	115.3	117.4	118.3
(N2C3S2)	120.6	119.5	119.3	119.4	120.2	120.3
(S2C3C4)	126.1	129.0	129.5	129.9	127.3	126.7
(C3C4S3)	118.8	121.4	121.1	121.5	120.6	119.6
(S3C4N3)	130.7	127.8	128.4	127.9	127.9	129.7

VAS=valence angle sum

VAS52 differ from the sum of the interior angles in a plane pentagon (540º) at least by 9.7º). Nevertheless, VAS51 and VAS52 in each of the metal chelates under study are equal each other (*Table 2*). The distortion is even more in the six-membered cycles, where the sums of the bond angles VAS61 and VAS62 differ from the sum of the interior angles in a flat hexagon (720º) by not less than 30º. It is significant that similar bond angles both within the chelate cycles and outside of them, in all of these complexes are pairwise equal to each other. The same equality between bond lengths, forming sides of these angles, is also observed. So the bond angle values both within the chelate cycles and outside of them only slightly depend on the nature of the M(II) ion. The values of torsion angles, which are often strongly different both from 0° and 180°, confirm the general *non*-coplanarity of molecular structures of complexes having general formula I (Table 3). As an example the structures of the Mn(II), Co(II) and Zn(II) chelates are shown in Fig. 1-3.

As you can see from them, all coordination compounds under examination are non-coplanar, have only one element of symmetry, namely symmetry flatness.
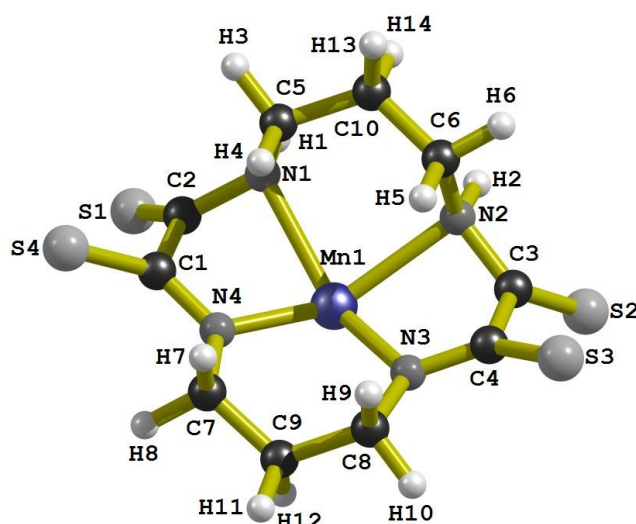
Figure 1. The molecular structure of the Mn(II) complex of type III.
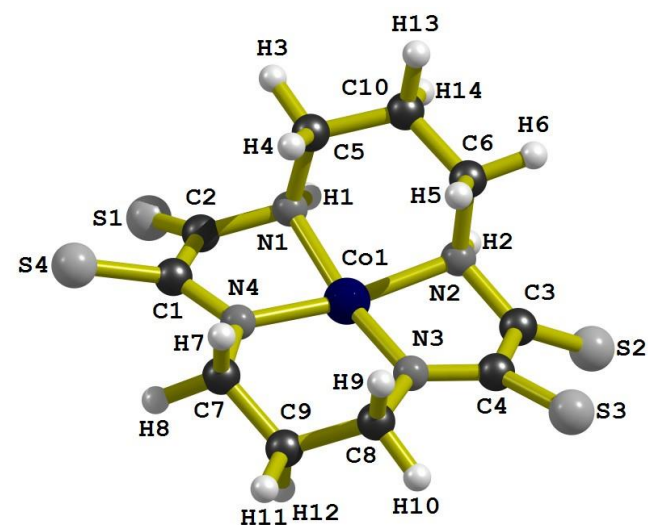
Figure 2. The molecular structure of the Co(II) complex of type III.

Table 3. Torsion (dihedral) angles in the M(II) complexes of type III.

M	Mn	Fe	Co	Ni	Cu	Zn
			Torsion (dihedral) angles, *deg*			
(N1M1N3C8)	92.1	98.1	104.2	111.8	98.1	101.8
(N2M1N4C7)	−92.1	−98.1	−104.2	−111.8	−98.1	−101.8
(M1N1C5C10)	72.0	70.1	69.1	68.8	69.7	72.0
(M1N2C6C10)	−72.0	−70.1	−69.1	−68.8	−69.7	−72.0
(N1C5C10C6)	−71.1	−61.5	−60.2	−59.2	−66.0	−68.3
(N2C6C10C5)	71.1	61.5	60.2	59.2	66.0	68.3
(M1N3C8C9)	24.0	29.4	31.9	30.7	30.4	28.5
(M1N4C7C9)	−24.0	−29.4	−31.9	−30.7	−30.4	−28.5
(N3C8C9C7)	−68.6	−63.3	−64.2	−64.0	−67.0	−68.1
(N4C7C9C8)	68.6	63.3	64.2	64.0	67.0	68.1
(M1N1C2C1)	55.3	40.0	36.6	33.1	39.5	45.4
(M1N4C1C2)	18.4	7.3	12.4	11.8	17.6	20.5
(N1C2C1N4)	−57.5	−33.0	−33.1	−29.8	−40.2	−48.5
(M1N1C2S1)	−116.6	−135.5	−138.4	−143.3	−135.0	−127.6
(M1N4C1S4)	−157.9	−171.7	−166.3	−167.6	−162.0	−157.3
(M1N2C3C4)	−55.3	−40.0	−36.6	−33.1	−39.5	−45.4
(M1N3C4C3)	−18.4	−7.3	−12.4	−11.8	−17.6	−20.5
(N2C3C4N3)	57.5	33.0	33.1	29.8	40.2	48.5
(M1N2C3S2)	116.6	135.5	138.4	143.3	135.0	127.6
(M1N3C4S3)	157.9	171.7	166.3	167.6	162.0	157.3
(S1C2C1S4)	−69.3	−38.9	−39.8	−34.3	−46.6	−58.0
(S2C3C4S3)	69.3	38.9	39.8	34.3	46.6	58.0
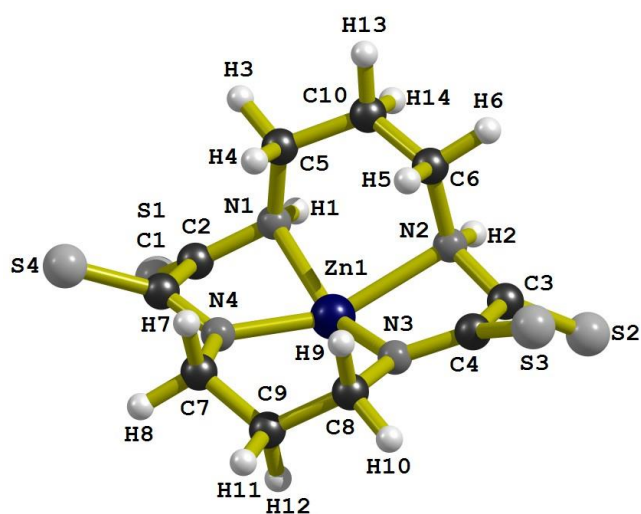
Figure 3. The molecular structure of the Zn(II) complex of type III.

In this connection, for all these complexes, rather high values of the electric dipole moment (μ) can be expected. And the OPBE/TZVP calculation method fully confirms these expectations, as calculated values of μ are very high and are 4.15, 5.80, 5.94, 5.73, 5.34 and 4.80 Debye units for the Mn(II), Fe(II), Co(II), Ni(II), Cu(II) and Zn(II) complexes respectively.

The values of the key thermodynamic parameters of the examined metalchelates (standard enthalpy, entropy and Gibbs energy of formation) are given in Table 4. As can be seen, all of them are positive, which shows that they can not be formed from individual elements and suggests that the above-mentioned template synthesis process (3) is likely to

be thermodynamically forbidden for its implementation in a solution or a solid phase. However, it seems to be quite possible under the specific conditions of complex formation in the organizing systems, based on the metal-complex gelatin-immobilized matrices.[4]

Table 4. Standard enthalpy $\Delta H^0_{f,298}$, entropy $\Delta S^0_{f,298}$ and Gibbs energy $\Delta G^0_{f,298}$ for the formation of the various M(II) chelates of type III.

M	$\Delta H^0_{f,298}$, kJ mol^{-1}	$\Delta S^0_{f,298}$, J mol^{-1} K^{-1}	$\Delta G^0_{f,298}$, kJ mol^{-1}
Mn	490.8	740.1	487.5
Fe	243.9	762.5	235.5
Co	394.4	735.6	392.7
Ni	431.9	732.4	432.0
Cu	424.8	727.6	426.2
Zn	552.0	739.0	551.0

The calculation of the chelant IV molecular structure which may be considered as part of the metalmacrocyclic chelates, being under study, showed that it is not planar by itself. The molecular structure of IV is shown in Fig. 4. It should be noted in this connection that sum of internal bond angles (VAS$_{14}$) in the fourteen-membered macrocycle in this chelant, and in all metallachelates under examination is less than the sum of the internal angles of a flat fourteen-sided polygon, equal to 2160°, and this difference is quite significant (in the chelant – by 82.6°, in the Mn(II) complex – by 68.7°, in the Fe(II) complex – by 70.9°, in the Co(II) complex – by 69.6°, in the Ni(II) complex – by 67.2°, in the Cu(II) complex – by 65.0°, in the Zn(II) complex – by 66.5°) (*Table 5*). Besides, in the each of complexes the deviation from the value of 2160° is less than in chelant IV.

Table 5. Bond angles of fourteen-membered macrocycle in chelant IV and type III complexes formed by it

Bond angle	Chelant	Mn	Fe	Co	Ni	Cu	Zn
(C10C6N2)	115.0	112.9	110.9	110.9	110.8	112.1	112.5
(C6N2C3)	228.0	239.9	242.0	243.1	244.7	242.6	241.7
(N2C3C4)	120.3	112.7	111.3	111.0	110.6	112.3	112.6
(C3C4N3)	111.6	110.4	110.8	110.5	110.7	111.5	110.7
(C4N3C8)	233.7	239.4	241.5	241.5	241.7	239.4	239.0
(N3C8C9)	112.8	112.6	112.1	112.3	112.4	112.4	112.6
(C8C9C7)	116.6	117.8	115.1	114.8	114.5	116.7	118.0
(C9C7N4)	112.8	112.6	112.1	112.3	112.4	112.4	112.6
(C7N4C1)	233.7	239.4	241.5	241.5	241.7	239.4	239.0
(N4C1C2)	111.6	110.4	110.8	110.5	110.7	111.5	110.7
(C1C2N1)	120.3	112.7	111.3	111.0	110.6	112.3	112.6
(C2N1C5)	228.0	239.9	242.0	243.1	244.7	242.6	241.7
(N1C5C10)	115.0	112.9	110.9	110.9	110.8	112.1	112.5
(C5C10C6)	117.8	117.7	116.8	117.0	116.5	117.7	117.7
Angles sum (VAS_{14})	2077.4	2091.3	2089.1	2090.4	2092.8	2095.0	2093.9
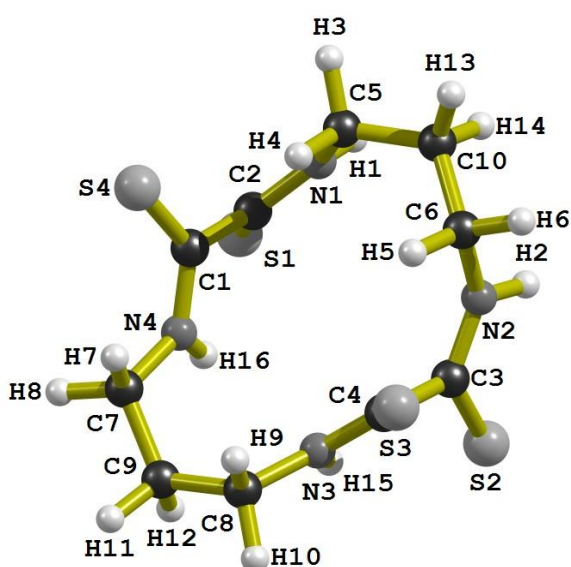
Figure 4. The molecular structure of the chelant IV.

In this regard, it can be stated that the complex formation of the above mentioned M(II) ions with chelant IV is accompanied by decrease of its structure distortion degree.

References

[1] Mikhailov, O. V.; Chachkov, D. V.; *Macroheterocycles* **2009**, *2*, 271.

[2] Mikhailov, O. V.; Chachkov, D. V.; *J. Coord. Chem.* **2010**, *63*, 4309.

[3] Chachkov, D. V.; Mikhailov, O. V.; *Russ. J. Inorg. Chem.* **2013**, *58*, 1073.

[4] Mikhailov, O. V.; *Inorg. Chim. Acta* **2013**, *394*, 664.

[5] Mikhailov, O. V.; Chachkov, D. V.; Grigorieva, O. N.; *Central Eur. J. Chem.* **2013**, *11*, 1822.

[6] Schaefer, A.; Horn, H.; Ahlrichs, R.; *J. Chem. Phys.* **1992**, *97*, 2571.

[7] Schaefer, A.; Huber, C.; Ahlrichs, R.; *J. Chem. Phys.* **1994**, *100*, 5829.

[8] Hoe, W.-M.; Cohen, A.; Handy, N.C.; *Chem. Phys. Lett.* **2001**, *341*, 319.

[9] Perdew, J.P.; Burke, K.; Ernzerhof, M.; *Phys. Rev. Lett.* **1997**, *78*, 1396.

[10] Paulsen, H.; Duelund, L.; Winkler, H.; Toftlund, H.; Trautwein, A.X.; *Inorg. Chem.* **2001**, *40*, 2201.

[11] Swart, M.; Groenhof, A. R.; Ehlers, A. W.; Lammertsma, K. *J. Phys. Chem. A.* **2004**, *108*, 5479.

[12] Swart, M.; Ehlers, A. W.; Lammertsma, K.; *Mol. Phys.* **2004**, *102*, 2467.

[13] Swart, M.; *Inorg. Chim. Acta* **2007**, *360*, 179.

[14] Frisch, M. J.; Trucks, G. W.; Schlegel, H. B.; Scuseria, G. E.; Robb, M. A.; Cheeseman, J. R.; Scalmani, G.; Barone, V.; Mennucci, B.; Petersson, G. A.; Nakatsuji, H.; Caricato, M.; Li, H.; Hratchian, H. P.; Izmaylov, A. F.; Bloino, J.; Zheng, G.; Sonnenberg, J. L.; Hada, M.; Ehara, M.; Toyota, K.; Fukuda, R.; Hasegawa, J.; Ishida, M.; Nakajima, T.; Honda, Y.; Kitao, O.; Nakai, H.; Vreven, T.; Montgomery, J. A., Jr.; Peralta, J. E.; Ogliaro, F.; Bearpark, M.; Heyd, J. J.; Brothers, E.; Kudin, K. N.; Staroverov, V. N.; Kobayashi, R.; Normand, J.; Raghavachari, K.; Rendell, A.; Burant, J. C.; Iyengar, S.S.; Tomasi, J.; Cossi, M.; Rega, N.; Millam, J. M.; Klene, M.; Knox, J. E.; Cross, J. B.; Bakken, V.; Adamo, C.; Jaramillo, J.; Gomperts, R.; Stratmann, R. E.; Yazyev, O.; Austin, A. J.; Cammi, R.; Pomelli, C.; Ochterski, J. W.; Martin, R. L.; Morokuma, K.; Zakrzewski, V. G.; Voth, G. A.; Salvador, P.; Dannenberg, J. J.; Dapprich, S., Daniels, A. D.; Farkas, O.; Foresman, J. B.; Ortiz, J. V.; Cioslowski, J.; Fox, D. J.; *Gaussian 09, Revision A.01,* Gaussian, Inc., Wallingford CT, 2009.

COMPARISON OF DEGRADATION OF METHYLENE BLUE DYE BY ZnO, N DOPED ZnO AND IRON ORE REJECTS

Vrinda Borker[a], Rajashri Karmali[b] and Koyar Rane[c]

Textile effluent containing unused dye when released in surroundings pollutes water bodies. It requires processing before disposal. Iron ore reject created during mining creates environmental pollution but contains minerals of technological importance. It has ~30-50 % iron in the form of γ-Fe_2O_3, α-Fe_2O_3 and Fe_3O_4 is wasted if thrown in fields, so can be used to degrade organic dyes. Mineralization of methylene blue, MB a model dye is carried out using photocatalyst either iron ore reject, synthesized ZnO or $ZnO_{1-x}N_x$ and the results are compared. ZnO is synthesised from oxalate and nitrogen doped ZnO from hydrazinated oxalate precursors. FTIR study of zinc complexes indicates formation of precursors and XRD of decomposed complexes reveal formation of zinc oxide with wurtzite structure. The presence of nitrogen in $ZnO_{1-x}N_x$ is confirmed by chemical estimation and XPS studies. SEM reveals the particle size of $ZnO_{1-x}N_x$ ~69 nm and ZnO ~0.5-1μm. $ZnO_{1-x}N_x$ absorbs in the visible region and ZnO in UV region. Band gap energy calculated using Diffuse reflectance Spectrum is 2.48 eV for the former, 3.19eV for the later and 2.38 eV for ore reject. Mineralizing property of ore reject, ZnO and $ZnO_{1-x}N_x$ are compared by electrons spray ionisation mass spectrometry study (ESI-MS) of degradation products, COD measurement and CO_2, NO_3^- and SO_4^{-2} estimation. Reusability study, kinetic study of degradation of MB dye using photocatalysts and ESI-MS study of degraded products of MB reveal better efficacy of iron ore rejects amongst three. Thus efficiency of iron ore reject > $ZnO_{1-x}N_{x.}$ > ZnO as photocatalyst.

* Corresponding Author
  Fax: +9108322462315,
  Email: borkarvp@gmail.com
[a*] Dhempe college of Arts and Science, Panaji Goa, 403001, India.
[b]   Department of Chemistry, Government College of Arts, Science and Commerce, Khandola, Goa, 403107, India
[c]   Rani Chennamma University, Belgaum 591156, India

Introduction

The dyes present in textile effluent pollute the water bodies. Materials like agricultural waste, ash, oxides of zinc, titania, iron[1-9] etc. are used in waste treatment of industrial effluent. The oxides are also used in degradation of hazardous gases, removal of organic pollutants and inhibition of undesirable microorganisms from water.[10] Zinc and titanium oxides are used as photocatalyst in organic dye degradation using UV radiation of ~378 nm. Zinc oxide is a semiconductor with an average bandgap of 3.37 eV and has varied applications.[11] It generates electron–hole pairs on exposure to ultraviolet radiations. However, sunlight consists ~2 % UV, limits the use of solar radiation for the photodegradation. Cation/anion doping of oxides is tried to enhance the photocatalytic properties.[12] Increased photocatalytic activity under visible light is mostly due to the synergistic effect of substantial nitrogen doping, high surface area and presence of oxygen vacancy in oxides.[13] Zinc oxide when doped with nitrogen replaces oxygen from the lattice forming $ZnO_{1-x}N_x$ (x$\le$ 0.15).[14] Decomposition of hydrazinated zinc oxalate forms yellow $ZnO_{1-x}N_x$ (absorbs in the visible region of the sunlight).[15] Hydrazine modified precursors yield spinels, perovskites with large surface area.[15-19] $ZnO_{1-x}N_x$ obtained from hydrazinated oxalate has surface area ~11.8 $m^2 g^{-1}$ and found to be good bactericidal agent effective against *E. coli* in our earlier work.[20] In the present investigation it is used for dye degradation.

The pollution in mining area is mainly because of ore reject: material remaining after beneficiation of the ore. These rejects/tailings are generally stored in the pits developed during mining. During rains they flow in the fields and ruin crops. They contain more than 40 % Fe which is wasted. We used iron ore reject for degradation of model organic dye methylene blue (MB) giving rejects a value addition.[21]

Methylene blue (MB belongs to thiazine class of dyes) is difficult to decompose under visible light and is chosen as a model dye to evaluate photocatalysis.

Present study aims at comparison of MB degradation results using iron ore, zinc oxide and N doped zinc oxide. So oxalate and hydrazinated oxalate of zinc are synthesized, analysed and decomposed to yield ZnO and $ZnO_{1-x}N_x$. These oxides as well as iron ore reject are characterized and their efficacy is tested by photo-catalytic degradation of MB. Photodegradation products generated during investigation are compared to understand the relative efficacy of three photocatalysts.

Experimental

Synthesis of zinc oxide precursor

Zinc oxalate is prepared by the addition of aq. ammonium oxalate solution (0.5M, 100 mL) to an aq. zinc chloride solution (0.5M, 100mL). The precipitate of zinc oxalate is filtered and dried. Hydrazination of oxalate is done by keeping the dried zinc oxalate over hydrazine hydrate (Merck, 99 %) in a dessicator. The hydrazine uptake is monitored by KIO_3 titration.[22]

Characterization of precursors and oxides

Standard chemical analysis, Infrared analysis (Shimadzu IR Prestige 21), TG/DTA studies (STA 409 PC LUXX-NETZCH) and isothermal weight loss study are carried out to fix formula for the zinc oxalate and its hydrazinated precursor. The decomposition temperature of both the precursors are obtained by TG/DTA recorded from room temperature to 1000 ℃ (heating rate-10K/min). The precursors are decomposed at ~700 ℃ to obtain zinc oxides.

Phase identification of the metal oxide is carried out by X-ray diffraction (Rigaku Powder X-ray diffractometer using CuK$_\alpha$ radiation, λ=1.5418 Å). Scanning electron micrographs (SEM) of oxides are obtained on JEOL JSM – 5800.

Nitrogen analysis is made on HIROBA EMGA 2800. The diffuse reflectance spectra (DRS) of oxides are recorded on UV-2401-Rev A 6700 with diffuse reflectance accessory to determine the absorption in the range of 200-800 nm. BaSO$_4$ is used as reference. The bandgap energies are calculated using equation: Band gap (E_g) in eV=1239.8/$\lambda_{max.}$ ($\lambda_{max.}$ is maximum wavelength of absorbtion from differential plots of reflectance spectra).

X ray photoelectron spectra, XPS is obtained at 298 K using MgK$_\alpha$ radiation on a VG Microtech Multilab ESCA 3000 spectrometer.

Characterization of iron ore reject

The various studies carried out of iron ore reject such as chemical analysis by standard methods,[22] infrared analysis by Shimadzu IR Prestige 21, elemental analysis by EDS, diffuse reflectance spectrum (DRS) by UV-visible spectrophotometer (Shimadzu UV-2401-Rev A 6700) and saturation magnetization measurement by Satmagan (Saturation Magnetization Analyser) Model 135 of Corrigan make. The phase identification of the metal oxides present in reject is carried out by X-ray diffraction (Rigaku Powder X-ray diffractometer) and Scanning electron micrographs (SEM) by JEOL JSM – 5800.

Photodegradation studies

Photodegradation or decolorization of an aqueous solution of methylene blue (MB), was monitored spectrophotometrically (Shimadzu UV-2401-Rev A 6700) at λ_{max} = 665 nm. The solution of MB was maintained at neutral pH. 50 mL aqueous solution of MB dye (0.5x10^{-4} M) with 200 mg of catalyst (ZnO or ZnO$_{1-x}$N$_x$ or iron ore reject) added was exposed to sunlight. 2 mL of test solution was filtered after every 30 minutes of sunlight exposure and tested on spectrophotometer. Simultaneously solution of MB, without the catalyst was also exposed to sunlight and checked on spectrophotometer after every 30 minutes (to check photolysis). Solar light intensity and the power generated were measured every 30 minutes using Luxmeter LX-101 and solar kit of TATA BP Solar Bangalore, India respectively. The average light intensity during the experiment was 300 to 724 lux units. The power was 0.24 W cm^{-1} to 0.52 W cm^{-1}.

Chemical and ESI-MS studies of the photodegradation products of methylene blue

The chemical oxygen demand (COD) test allows measurement of organic waste in water in terms of the total quantity of oxygen required for the oxidation of organic matter to CO$_2$ and water.

COD of MB solution during degradation is measured by the standard K$_2$Cr$_2$O$_7$ method.[23] The percentage of MB degraded or chemical oxygen demand removal (φ, %) is calculated according to the equation,

$$\varphi = 100 \frac{C_0 - C}{C_0}$$

C$_o$ is the initial chemical oxygen demand (mg L^{-1}) and
C is the chemical oxygen demand after treatment (mg L^{-1}).

The concentrations of nitrate ions, NO$_3^-$, sulfate ions, SO$_4^{2-}$ and free CO$_2$ (mg L^{-1}) are tested after complete de-colorization of MB by standard chemical methods.[24, 25] The decolorized solution is extracted with chloroform and the residue obtained after drying is dissolved in methanol and products are analyzed by electrospray ionization mass ESI-MS using an electrospray/quadrupole/time-of-flight (QTOF) mass spectrometer (QstarXL, MDS Sciex).

Zinc oxides and iron ore rejects are washed and dried after use and then reused for degradation. The reusability is tested three times.

Results and discussion

We confirm formation of zinc oxalate and hydrazinated zinc oxalate from infra red studies (Fig.1) of precursors. The band positions are observed at 1300, 1654 cm^{-1} due to v$_s$ (o-c-o) and v$_{as}$ (o-c-o) respectively. A broad band between 3000 to 3600 cm^{-1} is due to v (OH).[26-28] Hydrazine linkage is developed with band position between 1130-1200 cm^{-1} due to δ (NH$_2$) and between 3100-3500 cm^{-1} due to v(N-H) stretching in hydrazinated zinc oxalate.
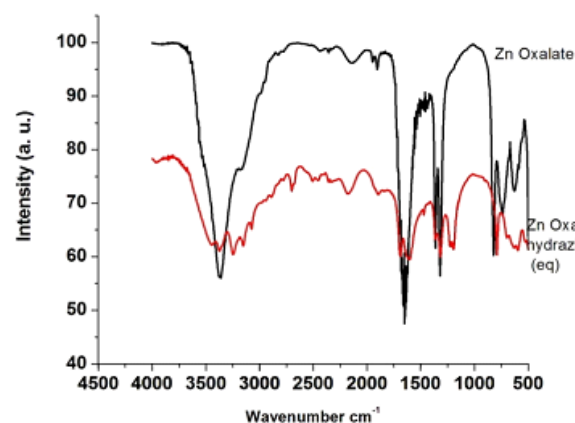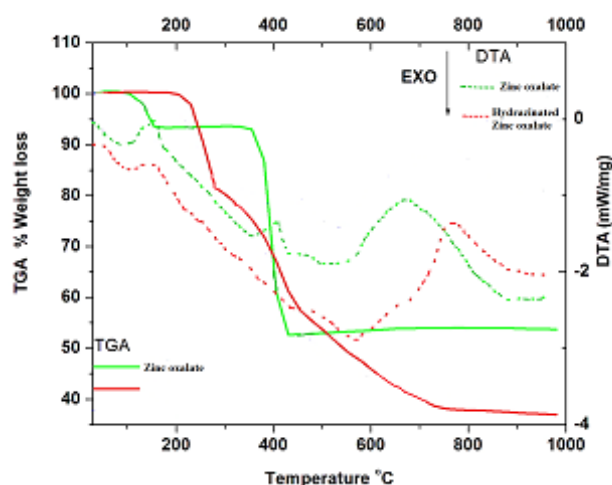

**Figure 1.** FTIR spectra of zinc oxalate and hydrazinated zinc oxalate

Table 1. Hydrazine *content*, oxalate content and weight loss study of precursors

Precursor	Hydrazine content, %		Oxalate content, %		Total Weight loss %		
	Calculated	Observed	Calculated	Observed	Calculated	TG	Isothermal
$ZnC_2O_4.2H_2O$	-	-	46.4	46.2	57.0	60.5	57.03
$ZnC_2O_4.N_2H_4.H_2O$	15.7	15.5	43.2	44.0	59.9	61.3	59.60

TG (Fig. 2) showed major weight loss of ~60 % till 600 °C in both precursors. he endotherms and exotherms till 600 °C in DTA suggested that dehydration, decarboxylation, dehydrazination and decomposition occurs till this temperature. A small endotherm at ~678 °C in zinc oxalate and ~759.4 °C in hydrazinated complex is due to structure formation (no weight loss occurs in TG at these temperatures).

Figure 2. TG/DTA of zinc oxalate and hydrazinated zinc oxalate

Total weight loss study, TG/DTA study and chemical analysis (hydrazine and oxalate content) of complex confirmed formula of zinc oxalate as $ZnC_2O_4.2H_2O$ and hydrazinated complex as $ZnC_2O_4.N_2H_4.H_2O$ (Table 1).
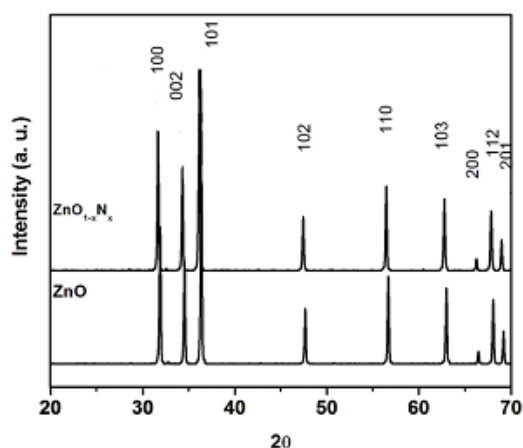
Figure 3. XRD of ZnO and $ZnO_{1-x}N_x$

The complexes were decomposed at 700°C; the former yielded white oxide and the later yellow. XRD of decomposed complexes, Fig. 3 match well with the Joint Committee on Powder Diffraction Standards (JCPDS) file of

ZnO (Wurtzite). 13.75 % Nitrogen was present in $ZnO_{1-x}N_x$ (yellow), measured by oxygen and nitrogen analyzer. However there was no difference in XRD pattern of ZnO and $ZnO_{1-x}N_x$. Similar observations were reported.[14]

XPS studies of $ZnO_{1-x}N_x$ were recorded for N1s and $Zn2p_{3/2}$ core levels. The N1s core level appeared at a binding energy (B.E.) ~ 398 eV Fig. 4.
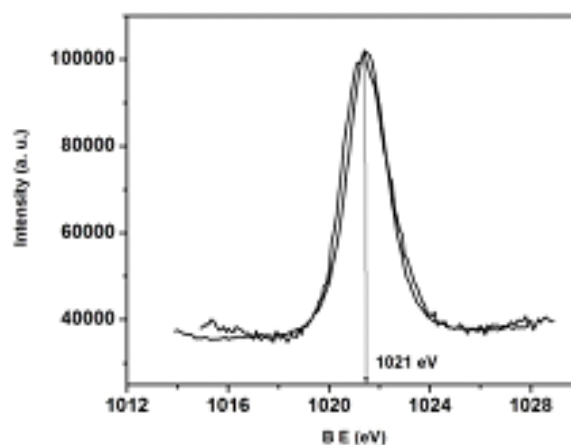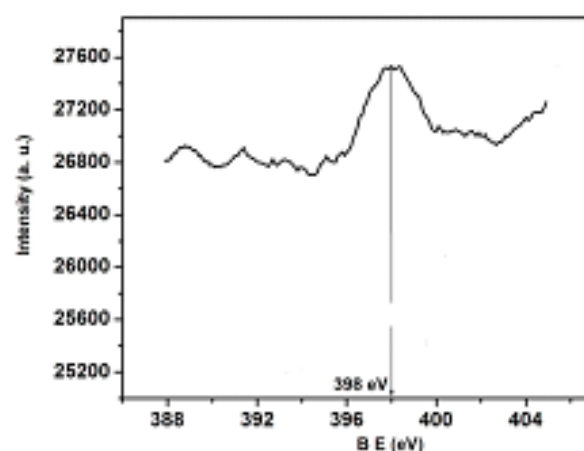
Figure 4. X-ray photoelectron spectrum of (a) N 1s and (b) Zn 2p electron in $ZnO_{1-x}N_x$

This suggests N in $ZnO_{1-x}N_x$ is similar to NH_3 or amines. The nitride B.E. is reported to be ~397 eV. So electron density on nitrogen is less than that of nitrides. Zn 2p core level shows B. E. ~ 1021 eV (Fig.4b). The lower B.E. of Zn 2p core level (reported, 1022 eV[14]) is due to covalent nature of Zn-N bond. These observations were similar to reported.[14] They suggest that electron density on Zn in $ZnO_{1-x}N_x$ is slightly more than ZnO. Nitrogen donated some electrons to Zn. This enhanced photocatalytic degradation of MB.

Diffuse reflectance spectra (Fig. 5) of ZnO and $ZnO_{1-x}N_x$ showed that the former absorbed in UV region and later in the visible region; indicating the possibility of photocatalysis by $ZnO_{1-x}N_x$ with visible light.
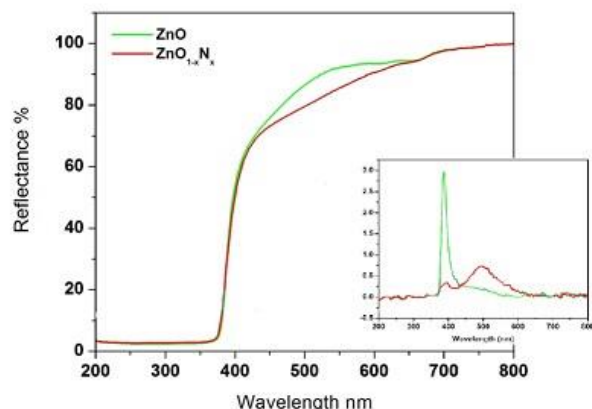
Figure 5. Diffuse reflectance spectra of ZnO and $ZnO_{1-x}N_x$ (inset derivative of the diffuse reflectance spectra)

The band gap energy calculated from derivative of the spectra is 3.19 eV for ZnO and 2.48 eV for $ZnO_{1-x}N_x$. The lower value of energy of $ZnO_{1-x}N_x$ helped in increasing number of electron hole pair thus enhancing the dye degradation. Scanning electron micrographic studies (Fig. 6) of $ZnO_{1-x}N_x$ indicated uniform particles ~69 nm and ZnO, ~0.5-2 μm with BET surface area of ~ 11.8 $m^2 g^{-1}$ and 8.137 $m^2 g^{-1}$ respectively. The large surface area of $ZnO_{1-x}N_x$, and less band gap energy (electrons excitation better) are important parameters in photocatalysis.
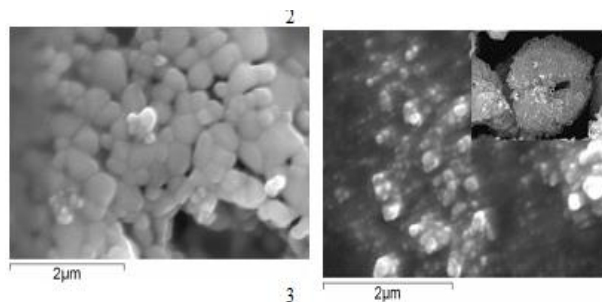
Figure 6. SEM pictures (a) ZnO (b) $ZnO_{1-x}N_x$

Chemical analysis of ore reject revealed the presence of 54% total Fe reported in earlier work[21]. XRD analysis of iron ore rejects Fig. 7 and EDS results[21] (Table 2) showed the presence of Fe_2O_3 (α, γ, ε), Fe_3O_4, α- FeOOH, SiO_2, Al_2O_3 and small amounts of MnO_2. The peak positions were matched with the JCPDS files.

Table 2. EDS results of analysis on iron ore reject

Element	Weight%	Atomic%
O K	43.64	71.07
Al K	2.74	2.64
Si K	2.60	2.42
K K	0.32	0.21
Mn K	0.70	0.33
Fe K	50.00	23.33
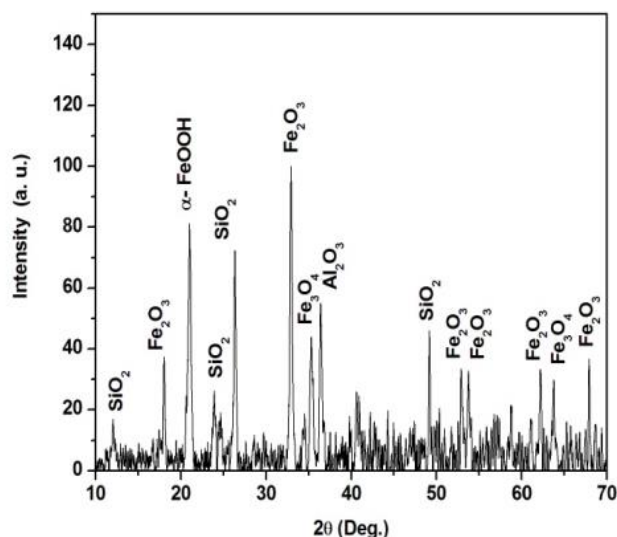
Figure 7. XRD of iron ore reject

FTIR of ore reject Fig. 8, showed absorption at 545 cm^{-1} due to Fe-O in Fe_3O_4.
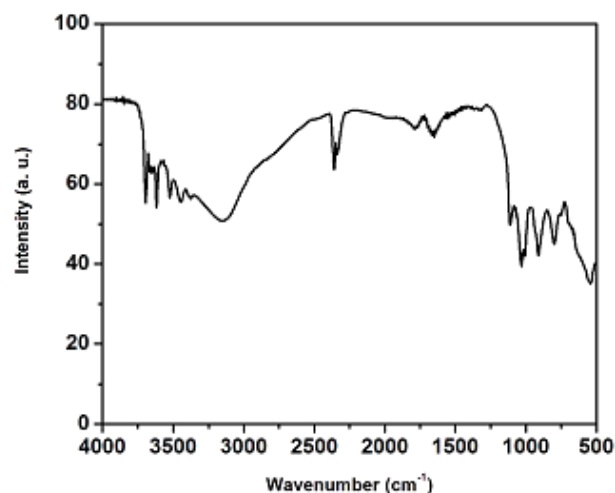
Figure 8. FT-IR of iron ore reject

The presence of broad and intense absorption band at 3100-3200 cm^{-1} was due to FeOOH, at 795, 913 cm^{-1} due to O-H bending, 1650 cm^{-1} due to H-O-H bending and at 3694 cm^{-1} due to surface hydroxyl groups. These results agreed well with results of XRD and EDS.

Iron ore reject showed different sizes and shapes of particles Fig. 9.
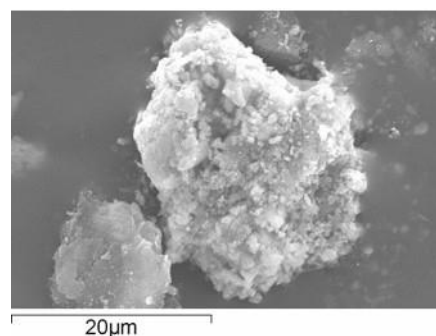
Figure 9. SEM picture of iron ore reject

Diffuse reflectance spectra (Fig.10) of iron ore reject revealed the absorption in visible region.
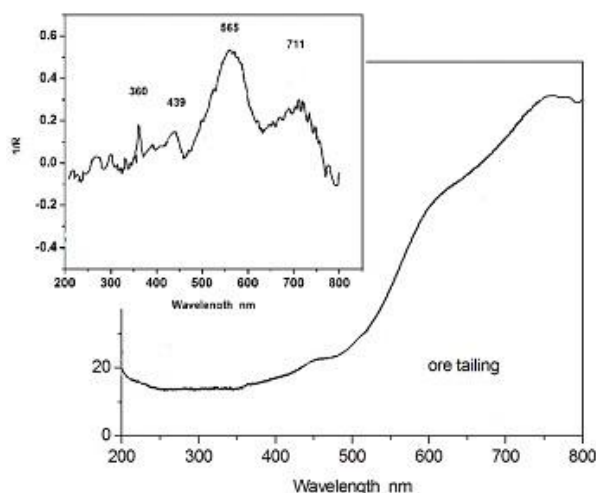
Figure 10. Diffuse reflectance spectra of iron ore reject (inset derivative of the diffuse reflectance spectra)

The band gap energy calculated was 2.39 eV. The derivative peaks may be assigned to the phases Goethite (α-FeOOH) at 439 nm, Maghemite (γ-Fe_2O_3) at 360 nm, Hematite (α-Fe_2O_3) at 565 nm and Magnetite (Fe_3O_4) at 711nm.[29-31] Components present in reject absorb in visible region enhancing the photo catalysis in sunlight.
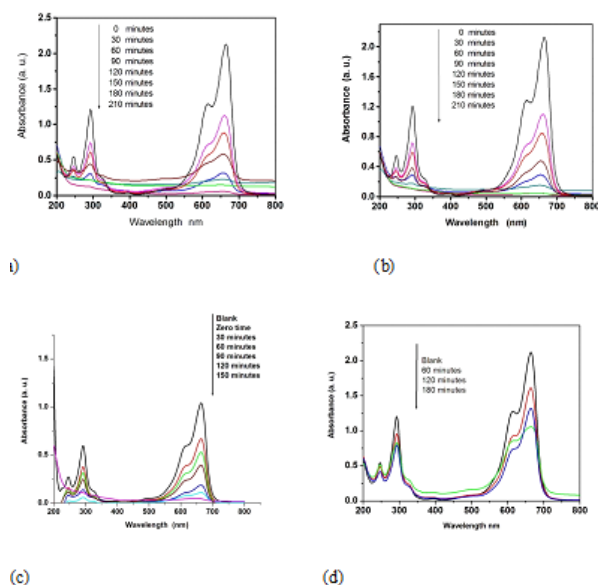
Figure 11. UV-Visible spectra of MB (pH=7)during degradation using a) ZnO; b) $ZnO_{1-x}N_x$; c) iron ore rejects; d) photolysis(absence of catalyst)

Maxima of UV-Visible absorbance spectra of methylene blue (λ_{max}=665 nm) diminished with increase in sunlight exposure time in presence of ZnO, $ZnO_{1-x}N_x$ and iron ore reject (Fig. 11a, b, c) due to breaking of the dye molecule. In presence of sunlight and ZnO (white) MB showed decolorisation in 210 minutes, in presence of $ZnO_{1-x}N_x$ (yellow) in 210 minutes, and in presence of iron ore reject in 150 minutes. Only sunlight exposure (photolysis-without addition photocatalyst), showed decrease in absorption

maxima but required 1200 minutes for decolorisation. The plot (Fig. 12) of variation in Absorbance of MB solution with time of sunlight exposure in presence of $ZnO_{1-x}N_x$ and iron ore reject showed a sharp decrease. Photolysis (absence of any catalyst) degraded MB marginally.
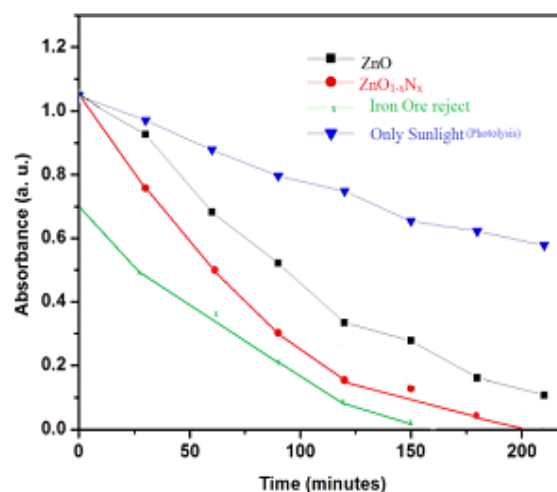
Figure 12. Decrease in absorbance of 0.5×10^{-4} M MB solution with sunlight exposure (the average light intensity, 300 to 724 lux units and the power, 0.24 to 0.52 W cm^{-1}).

The kinetic study of MB degradation in sunlight using photocatalysts revealed that it follows first order equation:

$$kt = \ln \frac{C_0}{C}$$

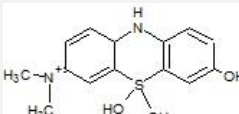where k is rate constant. The rate constants were listed in Table 3.
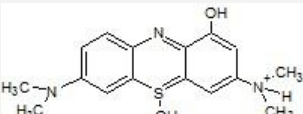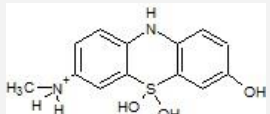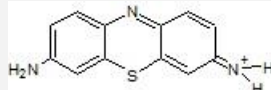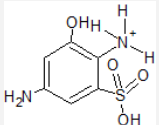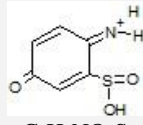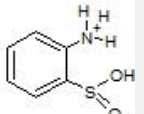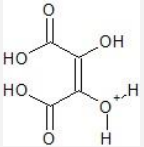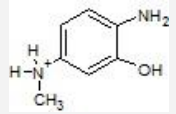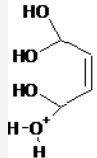
Table 3. Percent degradation and the rate constants for MB degradation

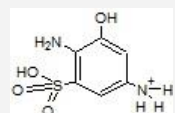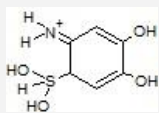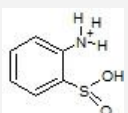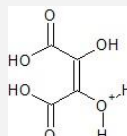| Photocatalyst	% degradation for 0.5×10^{-4} M MB	k, min^{-1}
ZnO	90%	8.36×10^{-3}
$ZnO_{1-x}N_x$	98%	14.7×10^{-3}
Iron ore reject	97%	17.3×10^{-3}
Photolysis	45%	3.11×10^{-3}

The rate constant values indicated efficiency of $ZnO_{1-x}N_x$ (14.7×10^{-3}min^{-1}) compared to the ZnO (8.36×10^{-3}min^{-1}) in dye degradation. The rate constant, k was highest for iron ore reject degradation, 17.3×10^{-3}min^{-1}. Degradation by ore rejects[21] is due to formation of H_2O_2 by Fe^{2+}/Fe^{3+} similar to explanation by Fenton.[32]

$$O_2(ads) + e^- \rightarrow O_2^{\bullet-} \qquad (1)$$

$$O_2^{\bullet-} + H_2O \rightarrow HO_2^{\bullet} + OH^- \qquad (2)$$

$$2HO_2^{\bullet} \rightarrow H_2O_2 + O_2 \qquad (3)$$

$$HO_2^{\bullet} + Fe^{3+} \rightarrow Fe^{2+} + O_2 \qquad (4)$$

$$Fe^{2+} + H_2O_2 \rightarrow OH^{\bullet} + OH^- + Fe^{3+} \qquad (5)$$
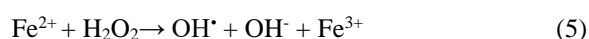
Table 4. Products of MB degradation on iron ore reject photocatalyst analyzed by ESI-MS.
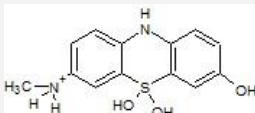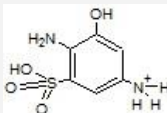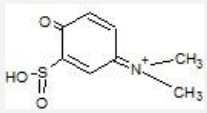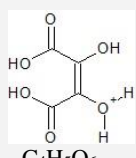
$C_{16}H_{20}N_3O_2S$
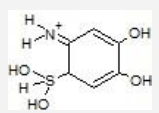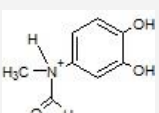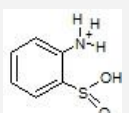$(M^+)=318.0305$

$C_{14}H_{17}N_2O_3S$
$(M^+)=293.0952$

$C_{13}H_{15}N_2O_3S$
$(M^+)=279.0897$

$C_{12}H_{10}N_3S$
$(M^+)=228.1013$

$C_6H_9N_2O_4S$
$(M^+)=205.0275$

$C_6H_6NO_3S$
$(M^+)=172.0599$

$C_6H_8NO_2S$
$(M^+)=158.0504$

$C_4H_5O_6$
$(M^+)=148.9778$

$C_7H_{11}N_2O$
$(M^+)=139.0138$

$C_4H_6O_4$
$(M^+)=121.0012$

Table 5. Products of MB degradation using $ZnO_{1-x}N_x$ analyzed by ESI-MS.

$C_6H_9O_4N_2S$,
$(M^+)=205.0523$

$C_6H_{10}O_4NS$,
$(M^+)=192.0268$

$C_6H_8O_2NS$,
$(M^+)=158.0668$

$C_4H_5O_6$,
$(M^+)=148.9939$

Table 6. Products of MB degradation on ZnO photocatalyst analyzed by ESI-MS.
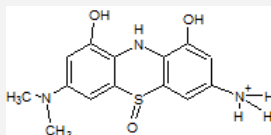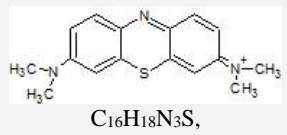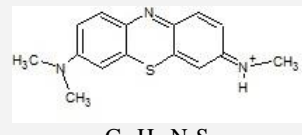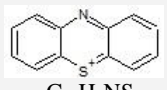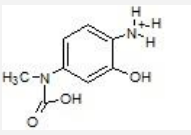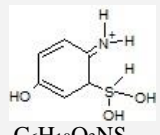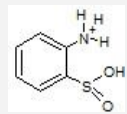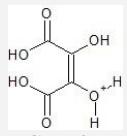

$C_{13}H_{15}O_3N_2S$,
$(M^+)=279.1189$

$C_6H_9O_4N_2S$,
$(M^+)=205.0545$

$C_8H_{10}O_3NS$,
$(M^+)=200.0814$

$C_6H_{10}O_4NS$,
$(M^+)=192.0265$

$C_8H_{10}O_3N$,
$(M^+)=167.9653$

$C_6H_8O_2NS$,
$(M^+)=158.0668$

$C_4H_5O_6$,
$(M^+)=148.9934$

Table 7. Products of solar degradation of MB without catalyst (photolysis) analyzed by ESI-MS.

$C_{14}H_{16}O_3N_3S$,
$(M^+)=306.1127$

$C_{16}H_{18}N_3S$,
$(M^+)=284.07774$

$C_{15}H_{16}N_3S$,
$(M^+)=270.0679$

$C_{12}H_8NS$,
$(M^+)=198.0964$

$C_8H_{11}O_3 N_2$,
$(M^+)=183.0843$

$C_6H_{10}O_3NS$,
$(M^+)=176.1126$

$C_6H_8O_2NS$,
$(M^+)=158.0690$

$C_4H_5O_6$,
$(M^+)=148.9956$

Oxygen adsorbed on surface of iron ore reject takes electron from the substrate and forms oxygen radical, which later reacts with water molecule forming hydrogen peroxide. Fe^{2+} of the ore gets oxidized by hydrogen peroxide to form Fe^{3+}, a hydroxyl radical and a hydroxyl anion.

$$Fe^{3+} + H_2O_2 \rightarrow Fe^{2+} + OOH^{\bullet} + H^+ \qquad (6)$$

Another molecule of hydrogen peroxide converted Fe^{+3} back to Fe^{2+}, a peroxide radical and a proton. The hydroxyl radicals ($OH^{\bullet}$) are effective in destroying organic dye molecules. This chain reaction continuously generates hydroxyl radical at each conversion.

Continuous formation of Fe^{2+} and Fe^{3+} during MB degradation by iron ore is responsible for fast decolorisation in 150 minutes and highest k (17.3×10^{-3} min^{-1}). SATMAGAN study has confirmed increased amount of Fe^{2+} after each use. Fe_3O_4 content of reject was 5.02 %.

It increased to 5.55 % after first use. Fe_3O_4 contains Fe^{2+} so efficiency of ore rejects increases after each use.

Following reactions are followed during degradation of MB by ZnO.[33]

$$\text{ZnO semiconductor} + h\nu \rightarrow \text{ZnO } (e_{cb}^- + h_{vb}^+) \qquad (7)$$
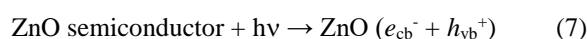
where

e_{cb}^- = electrons in the conduction band (cb);
h_{vb}^+ = holes in the valence band (vb)

$$\text{ZnO } (e_{cb}^-) + O_2 \text{ (adsorbed)} \rightarrow \text{ZnO} + O_2^{\bullet-} \qquad (8)$$

$$\text{ZnO } (h_{vb}^+) + H_2O\text{(ads)} \rightarrow \text{ZnO} + OH^{\bullet}_{ads} + H^+ \qquad (9)$$
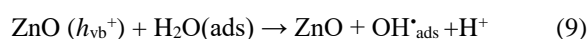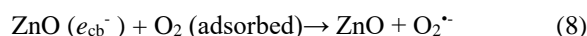
Direct oxidation of organic molecule by surface holes was also possible.

$$ZnO\ (h_{vb}^{+}) + \text{org. compd.} \rightarrow ZnO + H_2O + CO_2 \qquad (10)$$
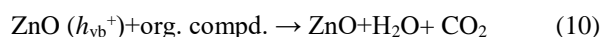
Using ESR spectroscopic data it is reported that the formation of active $OH^{\bullet}$ and $O_2^{\bullet-}$ species takes place during photodegradation of organic compounds.[34]

$$O_2^{\bullet-} + H^+ \rightarrow HO_2^{\bullet} \qquad (11)$$

$$2HO_2^{\bullet} \rightarrow H_2O_2 + O_2 \qquad (12)$$

$$H_2O_2 \rightarrow 2\,OH^{\bullet} \qquad (13)$$

Thus hydroxyl radicals are formed during degradation of MB in presence of all three photocatalyst. More the number of electron hole pairs formed more will be formation of these radicals. $ZnO_{1-x}N_x$ was yellow in colour due to loss of oxygen from lattice. Such non stoichiometric oxygen deficiencies lead to n-type semiconductor and absorb radiation in the visible region. Higher amount of visible radiations in sunlight compared to UV enhances electron pair formation when yellow $ZnO_{1-x}N_x$ is used then white ZnO. XPS results also have inferred that nitrogen in the lattice donates electrons to Zn, so these electrons generate hydroxyl radicals. Increased formation of hydroxyl radical formation in $ZnO_{1-x}N_x$ is responsible for higher value of rate constant k (14.7×10^{-3} min^{-1}) compared to the ZnO (8.36×10^{-3} min^{-1}). Reports[14] claim that $ZnO_{1-x}N_x$ is effective in catalysis application as compared to ZnO and our study confirms the same.

However when iron ore reject is used there is continuous formation of hydroxyl radicals and so the degradation is faster than zinc oxides.

It is reported[33] that the $OH^{\bullet}$ radicals attack the $C-S^{+}=C$ functional group in MB ($C_{16}H_{18}N_3S^{+}Cl^{-}$) forming sulfoxide (RS(=O)R') (equation 14). The attack of the second $OH^{\bullet}$ radical on the sulfoxide produces sulfone (RSO$_2$R') (equation 15) and causes the dissociation of two benzenic rings. Sulfone then gives rise to sulfonic acid (RSO$_3$H) (equation 17) which further gets oxidised to sulphate ion (equation 18).

Methylene blue degradation

$$C_{16}H_{18}N_3S + OH^{\bullet} \rightarrow C_{16}H_{18}N_3S=O \qquad (14)$$

$$C_{16}H_{18}N_3S=O + OH^{\bullet} \rightarrow C_8H_{11}O_2N_2S + C_8H_{11}N \qquad (15)$$

$$C_{16}H_{18}N_3S=O + OH^{\bullet} \rightarrow C_8H_{10}NSO_2 + C_8H_{11}N\text{-}NH_2 \qquad (16)$$

$$C_8H_{10}NSO_2 + OH^{\bullet} \rightarrow C_8H_{10}N\text{-}SO_3H \qquad (17)$$

$$C_8H_{10}NSO_3H + OH^{\bullet} \rightarrow [C_8H_{10}N]^{\bullet} + SO_4^{-2} + 2H^+ \qquad (18)$$
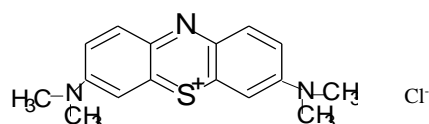
So degradation is directly proportional to hydroxyl radicals formed.

Detection of hydroxylated products in ESI-MS study (Table 4, 5, 6, and 7) confirmed that photodegradation of MB by three photocatalysts proceeded through hydroxyl radical mechanism.

The peak at m/z=284 in photolysed MB (without catalyst) correspond to methylene blue molecular ion. The peak at m/z = 270, and 198 correspond to loss of methyl groups, and dimethyl amino groups from aromatic rings on both sides of MB respectively. The peaks at m/z = 306, 279 were due to successive addition of hydroxyl in the MB molecule. The breaking of MB molecule was suggested by the presence of peaks at m/z = 205, 200, 192, 183, 176, 168, 158 and 149. Thus ESI-MS indicated presence of some organic moieties in the decolorized solution of MB. A careful comparison the degradation products of MB using ZnO, $ZnO_{1-x}N_x$, iron ore reject, and photolysis is

ZnO: $C_{13}H_{15}O_3N_2S$, $C_6H_9O_4N_2S$, $C_8H_{10}O_3NS$, $C_6H_{10}O_4NS$, $C_8H_{10}O_3N$, $C_6H_8O_2NS$, $C_4H_5O_6$

$ZnO_{1-x}N_x$: $C_6H_9O_4N_2S$, $C_6H_{10}O_4NS$, $C_6H_8O_2NS$, $C_4H_5O_6$

Iron ore rejects: $C_{16}H_{20}N_3O_2S$, $C_{14}H_{17}N_2O_3S$, $C_{13}H_{15}N_2O_3S$, $C_{12}H_{10}N_3S$, $C_6H_9N_2O_4S$, $C_6H_6NO_3S$, $C_6H_8NO_2S$, $C_4H_5O_6$, $C_7H_{11}N_2O$, $C_4H_6O_4$

Photolysis: $C_{14}H_{16}O_3N_3S$, $C_{16}H_{18}N_3S$, $C_{15}H_{16}N_3S$, $C_{12}H_8NS$, $C_8H_{11}O_3N_2$, $C_6H_{10}O_3NS$, $C_6H_8O_2NS$, $C_4H_5O_6$

It suggests that photolysis of MB, $C_{16}H_{18}N_3SCl$, lead to organic moiety having C_{16}, C_{15}, C_{14} in them while $ZnO_{1-x}N_x$ showed organic moieties having C_6 and C_4, so better degradation. When iron ore and ZnO were used decolourised solution also contained some molecules with C_{16}, C_{13}, etc.

Decolorisation of MB did not convey about total degradation to nontoxic molecules. MB, $C_{16}H_{18}N_3SCl$ is blue in colour and leuco MB, reduced form of MB is colorless. It can be converted back to MB. Thus it should be confirmed that decolourisation in our investigation was not formation of leuco MB. The complete mineralization of the molecule[35] may be written as follows:

$$2C_{16}H_{18}N_3SCl + 25\,O_2 \rightarrow 2\,HCl + 2\,H_2SO_4 + 6\,HNO_3 +$$

$$32\,CO_2 + 12\,H_2O$$
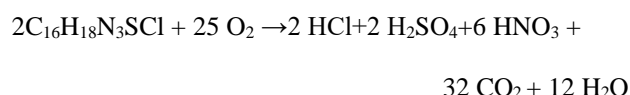
Formation of SO_4^{2-}, NO_3^{-} and CO_2 from the degraded MB solution (Table 8) indicated the mineralization of the dye.

Concentration of free CO_2 after 150 minutes was; 14.25 mg L^{-1} in presence of $ZnO_{1-x}N_x$, 10.69 mg L^{-1} in presence of ZnO, and 49.89 mg L^{-1} in case of iron ore reject. Thus iron ore reject was able to convert more organic moiety into CO_2. % COD removal was highest when $ZnO_{1-x}N_x$ (90 %) and iron ore reject (86 %) were used. Direct photolysis showed an increase in the COD from 84 % to 294 % after 30 minutes of light exposure. It further increased to ~572 % on complete decolourization (required ~ 20 h) revealing presence of organic moiety in solution after decolourisation.

Table 8. % COD, amount of free CO_2, nitrate and sulphate generated during MB photo degradation in presence of catalyst

Catalyst added	COD mg L^{-1}			% COD removal	Free CO_2	Nitrate, mg L^{-1}	Sulphate mg L^{-1}	
	t_0	t_{30}	t_{150}		t_{150}	t_{150}	t_{30}	t_{150}
Iron ore reject	84	44	12	86	49.89	0.77	2.55	3.10
$ZnO_{1-x}N_x$	84	36	08	90	14.25	0.80	0.11	0.90
ZnO	84	44	28	67	10.69	0.80	0.16	0.88
Photolysis (only sunlight)	84	294	572.4	COD added	-	2.60	0.75	32.5

Table 9. %COD, amount of free CO_2, nitrate and sulphate generated during MB photo degradation when catalysts are reused

	ZnO			$ZnO_{1-x}N_x$			Iron ore reject		
	COD %	sulphate mg L^{-1}	nitrate mg L^{-1}	COD %	sulphate mg L^{-1}	nitrate mg L^{-1}	COD %	sulphate mg L^{-1}	nitrate mg L^{-1}
1 cycle	67	0.88	0.8	90.47	0.8	0.99	85.71	3.101	0.77
2 cycle	69.05	3.0	1.8	69.05	2.4	1.32	90	1.92	3.0
3 cycle	80.95	2.2	1.8	78.5	7.9	2.6	73.8	4.6	5.99

ESI-MS study (Table 7) supported this observation. The photolysis led to incomplete mineralization and formation of oxygen demanding organic species. ZnO with its wide band gap of ~3.19 eV effectively absorbed the UV radiation of the sunlight (~2 % UV in sunlight reaches earth crust) and produced the electron hole pair and initiated photodegradation. N-doped ZnO due to the band gap modification (~2.48 eV in DRS study) and absorption of visible light lead to increased electron hole production, enhancing photocatalysis, higher % COD removal and CO_2 formation. Electron-hole recombination also decreased due to the band gap modifications.

Lack of nitrate content in the early stages of degradation was due to formation of ammonium ions initially and later oxidation to nitrates. Quantity of sulphate ions released was low due to the formation of gases, H_2S/SO_2.[31, 33]

200 mg $ZnO_{1-x}N_x$ was able to degrade 50 mL of 0.5×10^{-4} M MB in 150 minutes with ~90 % COD removal, 0.8 mg L^{-1} NO_3^{1-} and 0.99 mg L^{-1} SO_4^{2-}. It also showed reusability (Table 9) with increased formation of sulphates and nitrates. Time required for de-colorization of MB by $ZnO_{1-x}N_x$ was constant during reuse but showed a decrease in COD removal in the 2nd run (Table 9).

200 mg of ore reject was able to degrade 50 mL of 0.5×10^{-4} M MB in 150 minutes with ~86 % COD removal, 0.77 mg L^{-1} NO_3^{1-} and 3.1 mg L^{-1} SO_4^{2-} Thus ore had better mineralizing action as compared to ZnO and $ZnO_{1-x}N_x$. Degradation enhanced during its reuse due to conversion of Fe^{3+} to Fe^{2+} ions which increased formation of hydroxyl ions. The degradation time decreased from 150 minutes to 120 minutes and 90 minutes during the second and third use, respectively. $ZnO_{1-x}N_x$ did not show this trend. 2 g of reject added to 50 mL of 0.5×10^{-4} M MB was able to degrade the dye instantaneously. This was also not observed when 2 g $ZnO_{1-x}N_x$ were used.

All catalysts were reused three times (Table 9) without losing the original activity suggesting that there was negligible adsorption of the degradation products on their surface.

Conclusions

The two precursors zinc oxalate and hydrazinated zinc oxalate were synthesized. On decomposition, zinc oxalate yielded white ZnO and hydrazinated zinc oxalate yellow $ZnO_{1-x}N_x$. Presence of nitrogen in yellow oxide was confirmed by XPS and oxygen nitrogen analyser. N-doped zinc oxide, $ZnO_{1-x}N_x$ obtained from the hydrazinated precursor required less time for degradation of the methylene blue dye as compared to ZnO. ESI-MS results indicate presence of small amounts of some organic moieties on complete decolourization. Photolysis of MB, $C_{16}H_{18}N_3SCl$, lead to formation of organic moiety having C_{16}, C_{15}, C_{14} in them while $ZnO_{1-x}N_x$ lead to formation of molecules with C_6 and C_4. No loss in the efficiency of ZnO and $ZnO_{1-x}N_x$ makes them suitable for reuse. The electron-hole pair formation in ZnO and $ZnO_{1-x}N_x$ on exposure to sunlight lead to hydroxyl radical formation, those are responsible for degradation. $ZnO_{1-x}N_x$ absorbs in visible region and so more electron hole pairs are formed. In XPS study it is inferred that nitrogen is likely to donate some electrons to Zn. So they also enhance generation of hydroxyl radicals. This increases efficiency of $ZnO_{1-x}N_x$. Band gap energy calculated from DRS are 2.48 eV and 3.19 eV for $ZnO_{1-x}N_x$ and ZnO respectively indicating easier electron excitation in the former than later. Thus $ZnO_{1-x}N_x$ showed better dye degradation. Iron ore reject contained about 54 % total Fe with lower band gap energy 2.39 eV. The time required for dye degradation using iron ore rejects is least, 150 minutes with higher first order rate constant 17.3×10^{-3} min^{-1} as compared to ZnO which required 210 minutes with k, 8.36×10^{-3} min^{-1} and $ZnO_{1-x}N_x$ with k, 14.7×10^{-3} min^{-1}. During degradation ore reject forms hydroxyl ion radicals similar to fenton reagent. Chain reaction during the process supplies hydroxyl ions continuously due to formation of Fe^{3+}/Fe^{2+}. Hence efficacy of ore reject is best amongst the three. Increased amount of Fe^{2+} during reuse is proved by SATMAGAN. The dye molecule is converted to gases. Formation of SO_4^{2-}, NO_3^- and CO_2 indicated the mineralization of the dye. Concentration of SO_4^{2-} and free CO_2 is found higher when ore reject is used for degradation. % COD removal is higher for iron ore reject and $ZnO_{1-x}N_x$.

Thus Iron ore rejects, an environmental pollutant, easily available on mining sites can be used to degrade dyes and other unsaturated organic compounds then synthesizing oxides. Comparing the three photocatalysts for dye degradation, iron ore reject > $ZnO_{1-x}N_x$ > ZnO.

Acknowledgement

References

[1]Smelcerovic M., Dordevic D., Novakovic M., Mizdrakovic M., *J. Serbian Chem. Soc.*, **2010,** *75(6)*, 855.

[2]Sriwong C., Wongnawa S., Patarapaiboolchai O., *J. Environ. Sci.*, **2012**, *24*, 464.

[3]Elghniji K**,** Hentati O., Mlaik N., Mahfoudh A., Ksibi M., *J. Environ. Sci., 2012, 24*, 479.

[4]Rashed M. N., El-amin A.A., *Intern. J. Phys. Sci.*, **2007**, *2*, 73.

[5]Noorjahan M., Pratap Reddy M., Durga Kumari, V., Lavedrine, B., Boule, P., Subrahmanyam, M., *J. Photochem. Photobiol. A: Chem.*, **2003**, *156*, 179.

[6]Chakrabarti, S., Dutta B. K., *J. Hazard. Mater.*, **2004**, *112,* 433.

[7]Byrappa K., Subramani, A. K., Ananda, S., Lokanatha Rai, K. M. and Dinesh, R., *Bull. Mater. Sci.*, **2006**, *29*, 433.

[8]Daneshvar N., Aber S., Seyed Dorraji M. S., Khataee A. R. and Rasoulifard M. H., *Int. J. Chem. Biomol. Eng.*, **2008**, *1*, 24.

[9]Liu, H., Yang, Y., Kang, J., Fan, M., Qu, J., *J. Environ. Sci.*, **2012**, *24*, 242.

[10]Padmavathy, N., Vijayaraghavan, R., *Sci. Techn. Adv. Mater.*, **2008**, *9*, 1.

[11]Moezzi, A., McDonagh, A. M., Cortie, M. B., *Chem. Eng. J.*, **2012**, *185*, 1.

[12] Rane, K. S., Mhalsiker, R., Yin, S., Sato, T., Cho, K., Dunbar E. and Biswas, P., *J. Solid State Chem.*, **2006**, *179*, 3033.

[13]Noor, A., Mishra, T., Sahu, R. K. and Tiwari, J. P., *J. Mater. Chem.*, **2010**, *20*, 10876.

[14]Mapa, M. and Gopinath, C. S., *Chem. Mater.*, **2009,** *21*, 351.

[15]Rane, K. S., Uskaikar, H., Pednekar, R. and Mhalsikar, R., *J. Therm. Anal. Calor.*, **2007**, *90*, 627.

[16] Moye, V., Rane, K. S. and Kamat Dalal, V. N., *J. Mater. Sci. Mater. Electr.*, **1990**, *1*, 212

[17]Borker, V., Rane, K. S., Kamat Dalal, V. N., *J. Mater. Sci. Mater. Electr.*, **1993**, *4*, 241.

[18]Rane, K. S., Verenkar, V. M. S. and Sawant, P. Y., *Bull. Mater. Sci.*, **2001**, *24*, 323.

[19]Rane, K. S., Verenkar, V. M. S. and Sawant, P. Y., *Bull. Mater. Sci.*, **2001**, *24*, 331

[20]Karmali, R. S., Bartakke, A., Borker, V. P., Rane, K. S., *Biointerface Res. Appl. Chem.*, **2011**, *1*, 57.

[21]Karmali, R. S., Borker, V. P., Rane, K. S., Naik, C. G., *J. Solid Waste Manag.*, **2012**, *38*, 232.

[22]Vogel I. A., *"Textbook of Quantitative Inorganic analysis"*, Longman, UK., **1978**.

[23]Feng, X., Zhu, S., Hou, H., *Water S. A.*, **2006**, *32*, 43.

[24]Manivasakam, N., *Physicochemical examination of water sewage and industrial effluents,* Pragati Prakashan, Meerut, **1980**.

[25]Ramesh, R. and Anbu, M., *Chemical methods for environmental analysis, water and sediment,* Macmillan India Press, **1996**.

[26]Fujita, J., Martell, A. E., Nakamoto, K., *J. hem, Phys.*, **1962**, *36*, 324.

[27]Fujita, J., Martell, A. E., Nakamoto, K., *J. Chem,Phys.,* **1962**, *36*, 331.

[28]Braibanti, A., Dallavalle, F., Pellinghelli, M. A., Leporati, E., *Inorg. Chem.*, 1968, *7*, 1430.

[29]Scheinost, A. C., Chavernas, A., Barron, V., Torrent, J., *Clays Clay Minerals,* **1998**, *46*, 528.

[30]Shen, Z. X., Cao, J. J., Zhang, X. Y., Arimoto, R., Ji, J. F., Balsam, W. L., Wang, Y. Q., Zhang, R. J., Li, X. X., *Sci. Total Environ.*, **2006**, *367*, 899.

[31]Cornell, R. M., Schwertmann, U., *The iron oxides: structure, properties, reactions, occurrences and uses*, 2nd Edition, Wiley-VCH, 2003.

[32]Fenton, H. J. H., *J. Chem. Soc. Trans.*, **1894**, *65*, 899.

[33]Houas, A., Lachheb, H., Ksibi, M., Elaloui, E., Guillard, C., Herrmann, J., *Appl, Catal, B*: *Environ.*, **2001**, *31*, 145.

[34]Fu, H., Zhang, L., Zhang, S., Zhu, Y. and Zhao, J., *J. Phys. Chem. B,* **2006**, *110*, 3061.

[35]Nath, S., Ghosh, S. K., Panigrahi, S., Thundat, T., Pal, T., *Langmuir*, **2004**, 20, 7880.

SPECTROSCOPIC, THEORETICAL AND BIOLOGICAL STUDIES OF BINUCLEAR Mn(II), Ni(II), Cu(II) AND Cd(II) COMPLEXES WITH POLYDENTATE LIGAND DERIVED FROM DEHYDROACETIC ACID AND DIETHYLENETRIAMINE

Mahmoud N. Al-Jibouri,[a]* Taghreed M. Musa[a] and Omar Hamad Al-Obaidi[b]

A series of binuclear acyclic polydentate complexes of Mn(II), Ni(II), Cu(II) and Cd(II) ions with a ligand derived from the condensation of dehydroacetic acid and diethylenetriamine (3,3'-[iminobis(ethane-2,1-diylnitrilo-(1E)-eth-1-yl-1-ylidene)]bis(4-hydroxy-6-methyl-2H-pyran-2-one)]), [Mn₂LCl₂(H₂O₄)] and [M₂LCl₂], M=Ni, Cd and Cu(II), have been prepared and characterized by¹H and ¹³C NMR, FT-IR and UV-Visible spectroscopy and micro-elemental analysis, as well as with the measurement of the magnetic moments of solid complexes and molar conductivity in DMSO solution. The new acyclic poly dentate ligand 3,3'-[iminobis(ethane-2,1-diylnitrilo-(1E)-eth-1-yl-1-ylidene)]bis(4-hydroxy-6-methyl-2H-pyran-2-one)] are identified on the basis of (CHN) elemental analysis, ¹H, ¹³C NMR, as well as FT-IR and UV-Visible spectroscopy. The antimicrobial activity of the free ligand and its Mn(II), Ni(II), Cu(II) and Cd(II) complexes were tested against *Staphylococcus aureus* and *Escherichia coli* and fungicidal activity against *Aspergillus Niger* and *Candida albicans*. The minimum inhibitory concentration (MIC) method revealed that all metal complexes showed enhanced activity toward the selected micro-organisms compared with the free ligand H₂L and Amoxicillin. The octahedral geometry is proposed for Mn(II) complex, square planar for Ni(II) and Cu(II) complexes and tetrahedral symmetry is suggested for Cd(II) complex.

* Corresponding Authors
    E-Mail: **Mahmoudnajim71@yahoo.com**
[a] Chemistry Department, College of Science, Al-Mustansirya University
[b] Chemistry Department, College of Science for Women, Al-Anbar University

Introduction

The binuclear metal complexes containing heterocyclic rings are widely used as antibiotics, antifungal agents and semiconductor sensors.[1-4] Development of new microbicides including fungicides has increasing importance in modern medicinal chemistry[5] because appearance of large number of provoking factors that depress or destroy the immune system such as chemotherapy of cancer, using drugs to avoid organ rejection in transplanted patients and AIDS.[6]

3-Acetyl-6-methyl-2H-pyran-2,4(3H)-dione (**1**) (dehydroacetic acid or DHA) is a widely used compound usually obtained through the condensation of ethyl acetate.[7] It has been modest antifungal properties.[8] Dehydroacetic acid is an excellent chelating agent and its various derivatives including theirs metal complexes are promising fungicides, bactericides, herbicides and insecticides.[10-11] Dehydroacetic acid is also a versatile starting material for the synthesis of a wide variety of heterocyclic ring systems and other organic compounds.[12]

Recent studies related to coordination chemistry of (3,3'-[iminobis(ethane-2,1-diylnitrilo-(1E)-eth-1-yl-1-ylidene)]-bis(4-hydroxy-6-methyl-2H-pyran-2-one by Al-Obaidi[13] motivated us to prepare and study some new binuclear metal complexes with different stoichiometry.

Experimental

Physical measurements

Electronic spectra of the new ligand and its metal complexes were recorded in the region 800-200 nm on a Shimadzu 670 spectrophotometer. IR-spectra were recorded on PC Shimadzu FT-IR spectrophotometer in KBr in the range of 400 - 4000 cm⁻¹. The ¹H and ¹³C NMR spectra of the ligand were recorded in DMSO-d⁶ on a 300MHZ Bruker spectrometer. The effective magnetic moment measurements of the solid complexes were carried out on a Magnet Balance MG. The molar conductivity of metal complexes in DMSO solution was measured on a HPG G-3001 digital conductivity meter. The carbon, hydrogen and nitrogen analysis of ligand and its metal complexes were done on Carlo Elba 1108 instrument, the metal content in the complexes were measured on a Shimadzu 670 spectrophotometer by using standard addition method.

Calculation method

The quantum chemical calculations were made with using Hyper Chem-8 program.[14]

Reagents and solvents

Dehydroacetic acid and diethylenetriamine were obtained from Aldrich Co. The hydrated metal chlorides (MnCl₂.4H₂O, NiCl₂.6H₂O, CuCl₂.2H₂O) and CdCl₂ (Fluka and Merck) were used for the synthesis of complexes without any purification.

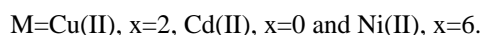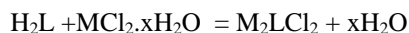**Synthesis of ligand 3,3'-[iminobis(ethane-2,1-diylnitrilo-(1E)-eth-1-yl-1-ylidene)]bis(4-hydroxy-6-methyl-2H-pyran-2-one)] (H₂L)**

The ligand (H₂L) was prepared by refluxing (2 g, 1.1 mol) of dehydroacetic acid in 30 ml absolute ethanol with (0.613 g, 5.91 moles) of diethylenetriamine for about 9 h on water bath. The polydentate acyclic ligand (H₂L) formed is deposited upon cooling the mixture to room temperature overnight. (Scheme 1).
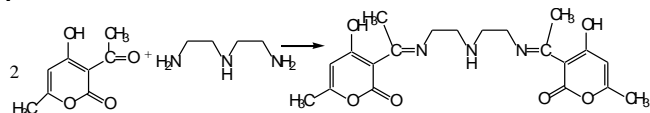
Scheme 1. Synthesis of Ligand H₂L

Synthesis of metal complexes

2 mmol of CuCl₂. 2H₂O, MnCl₂.4H₂O, NiCl₂.6H₂O and CdCl₂ in 20 mL methanol was added to 0.403g, (1 mmol) of H₂L ligand dissolved in methanol containing KOH (1 %, w/v). The resulting mixture was refluxed under nitrogen atmosphere until the complex precipitated (ca. 3 h) then the solution was cooled to room temperature, the precipitate was filtered off, washed several times with 15 ml of diethyl ether and dried under vacuum to afford Mn₂LCl₂.4H₂O and M₂LCl₂ (M=Cu, Ni and Cd) complexes in 51-65 % yield.

$$H_2L + MnCl_2.4H_2O = Mn_2LCl_2.4H_2O$$

$$H_2L + MCl_2.xH_2O = M_2LCl_2 + xH_2O$$

M=Cu(II), x=2, Cd(II), x=0 and Ni(II), x=6.

Anti-bacterial Activity

The *in-vitro* biological activity of the investigated free ligand H₂L and its metal complexes were tested against the bacteria *Escherichia coli* and *Staphylococcus aureus* by disc diffusion method using nutrient agar as medium and streptomycin as control. The antifungal activities of the compounds were also tested by the well diffusion method against the fungi *Aspergillus Niger* and *Candida albicans*, on potato dextrose agar as the medium and ketaconazole as control. Each compound was dissolved in DMSO and solutions of different concentrations (25, 50 and 100 ppm) were prepared separately. In a typical procedure, a well was made on agar medium inoculated with microorganism. The well was filled with the test solution using a micropipette and the plate was incubated 24 h for bacteria at 37 ºC and 72 h for fungi at 30 ºC. During this period, the test solutions were diffused into the gel, the growth of the inoculated microorganism was affected, and the inhibition zone was developed. All determinations were performed three times.

The bacteria subcultures, *Staphylococcus aureus* and *Escherichia coli* were used for antibacterial test, whereas *Aspergillus flavus* and *Candida albicans* were used for antifungal test using the modified Kirby-Bayer disc diffusion method.[11] Briefly, 100 ml of the tested bacteria/

fungi were grown in 10 ml of breath media until they reached 100 cells ml⁻¹ for bacteria and 110 cells ml⁻¹ for fungi. 100 ml of microbial suspension was spread on the agar plate corresponding to the broth in which they were maintained.

Result and Discussion

The new acyclic Schiff base [H₂L] ligand derived from condensation of one mole diethylenetriamine with two moles of dehydroacetic acid behaves as tetradentate dibasic chelating agent towards the studied metal(II) ions. The stoichiometry of the complexes was confirmed by their elemental analysis. (Table 2). All the complexes were sparingly soluble in common organic solvents but completely soluble in DMF, DMSO, and acetonitrile. The analytical data (Table 1) indicate that the complexes are binuclear. The molar conductance (Table 3) values measured in DMF solution (1x10⁻³ mol dm⁻³) fall in the range 9.0-22 ohm⁻¹ cm² mol⁻¹. These observed values of the molar conductance agree well within the expected values for non-electrolytes.[15]

¹H and ¹³C NMR spectra

The **¹H** NMR spectra of free ligand in DMSO-d₆ shows six signals for the ligand in the regions 13.6-13.7, 5.96-5.60, 4.65 and 3.53- 3.10 ppm which merged with each other except high deshielded –OH proton of pyranone-ring[14] (Figure 1).
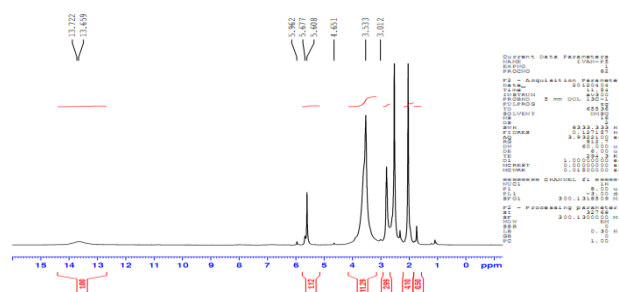
Figure 1. ¹H NMR to the H₂L in DMSO-d₆ solvent.
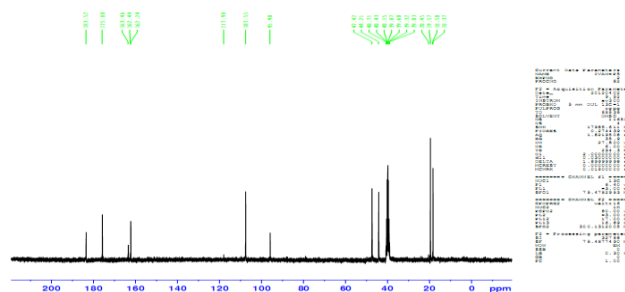
Figure 2. ¹³C NMR to the H₂L in DMSO-d⁶ solvent

The ¹³C NMR spectrum of the free ligand in DMSO-d₆ displays chemical shifts of tautomers (20 signals for twice 10 chemical environment) and the sharp Me-signals of DMSO solvent around 40 ppm. All the signals of the pyranone ring and the azomethine group could tentatively be

Table 1. Analytical data for ligand and its metal complexes

Formula	Molecular weight	Colour	Composition Calculated (Found)				
			C%	N%	H%	Cl%	M%
H₂L, C₂₀H₂₅N₃O₆	403	Off white	59.55 (59.54)	11.91 (10.42)	6.20 (6.25)	-	-
[Ni₂LCl₂]	589.4	Brown	40.72 (39.55)	8.14 (7.20)	4.24 (3.01)	12..05 (11.88)	19.91 (18.52)
[Cu₂LCl₂]	599.1	Green	40.06 (39.09)	8.01 (7.96)	4.17 (4.66)	11.85 10.98	21.21 (20.88)
[Mn₂LCl₂.4H₂O]	653.8	Brown	36.70 (35.77)	7.34 (6.61)	5.05 (4.88)	10.86 (9.97)	16.80 (15.89)
[Cd₂LCl₂]	696.8	Dark yellow	34.44 (33.99)	6.02 (4.98)	3.59 (3.11)	10.19 (10.09)	32.26 31.93

[a]Analysis of metal content were done on the basis of FAAS

assigned (**Me**-C6 group-107.55 ppm, Me-**C6**(ring)-163.50 ppm, **C5**H(ring)-183.5 ppm, **C4**(OH)(ring)-96.9 ppm, **C5**CMeN(ring)-162.4 ppm, **C6**=O(ring)-20.45 ppm, **C**(CH₃)=N-175.8 ppm and **CH₃**C=N-19.57 ppm, and methyl or methylene groups respectively.[29] The residual signals belong to the diethylenetriamine link and to the tautomer forms of the pyranone part. (Figure 2). The ^{1}H NMR spectra of Cd(II) complexes in DMSO-d₆ solution can be seen in Figure 3). The changes of ^{1}H signals belong to the Schiff base ligand reveals the coordination of nitrogen –C=N- and –OH groups with the metal ions.[15,29]
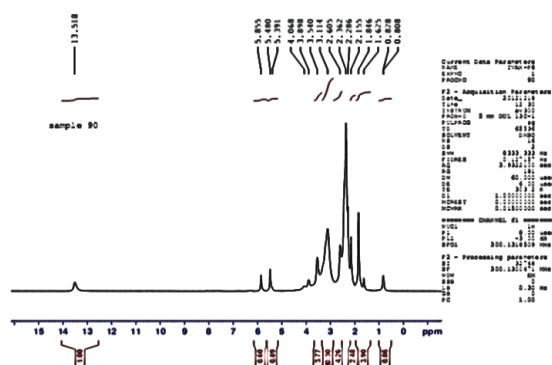
Figure 3. ^{1}H NMR of the [Cd₂LCl₂] in DMSO-d[6] solvent.

Infrared Spectra

The FT-IR spectrum of the free ligand (H₂L) in KBr disk displays broad and strong absorptions in the regions 3400 cm⁻¹ and 1695-1655cm⁻¹ that could be assigned to -OH and C=O bands located on the pyrane ring.[13,16] The medium intensity absorption band at 3571-3357 cm⁻¹may be assigned to υ(NH) stretching of diethylenetriamine moiety. The IR spectra of all metal complexes show bands in the regions 3160-3550, 1655-1688 and 1522-1560 cm⁻¹ that are assignable to υ_{NH}, $\upsilon_{C=O}$ and $\upsilon_{C=N}$ bands, respectively. These band positions confirm the coordination of bivalent metal ions to C=N and deprotonated C-O groups active sites. Moreover, the far infrared spectra of all metal complexes show weak

absorption bands in the range 510-422 and 468-414 cm⁻¹ which may be confirmed as υ_{M-N} and υ_{M-O} bands. The Mn(II) complexes show broad bands at 3650 cm⁻¹ and strong bands at 1590 cm⁻¹ that related to coordinated water molecules. The bands at 1581, 1431, 1259 cm⁻¹ may be assigned to bending of NH, and asymmetrical vibration modes of C=C and C-N stretching, respectively. This confirms the condensation of carbonyl group of dehydroacetic acid with amino groups of diethylentriamine.[11,13] The bands around 3400 cm⁻¹ and 1656cm⁻¹ can be assigned to υ_{OH} and $\upsilon_{C=N}$ stretchings.[17] The band at 1695cm⁻¹ can be attributed to the $\upsilon_{C=O}$ of the pyranone ring. The NH bands are probably overlapped by the OH bands and did not appear for the free NH₂ group bands of diethylenetriamine.[16-18] The Cd(II) complex shows weak bands in the far infrared spectra between 336 and 370 cm⁻¹ which probably belong to Cd-Cl bonds.

Electronic spectra and magnetic properties

The free ligand (H₂L) spectrum in methanol exhibits three distinct absorptions around 42735, 37878 and 31847 cm⁻¹ which are assigned to $\pi{\rightarrow}\pi^*$ of benzenoid ring and E_1, E_2 and $n{\rightarrow}\pi^*$ transitions of C=N, and C=O chromophores.[18] The diamagnetic properties of Ni(II) reveals the square planar symmetry of low spin d[8] state, and agree well with the high energy absorptions in the region 23255 – 25316 cm⁻¹ of $^1A_1g \rightarrow {}^1B_1g$ and $^1A_1g \rightarrow {}^1B_2g$ transitions, respectively.[19] However, the diamagnetic properties of binuclear copper(II) complex indicate the spin–spin coupling of Cu-Cu form.[17] The weak intensity peak of copper(II) complex in DMF in the region 19500 cm⁻¹ with a shoulder on the low energy side at 15500 cm⁻¹ may confirms the transitions of distorted octahedral, with LFSE=17 500cm⁻¹.[19-20] The pale pink solution of manganese(II) complex in DMF displays weak intensity peak at 22333 cm⁻¹ which may be assigned to $^6A_1g \rightarrow {}^4T_1g$ and other in the UV region 33421 cm⁻¹ that are entirely related to LMCT transitions. The magnetic moment obtained (5.30 B.M.) was within the range expected for magnetically high spin Mn(II) complex with octahedral symmetry.[21-22]

Table 2. IR spectral data of the free ligand and its metal complexes

Compound	$\upsilon_{C=O, C=N}$	$\upsilon_{OH}, \upsilon_{NH}$	$\delta_{OH}, \delta_{NH}, \upsilon_{C-N}$	$\upsilon_{Ar-H}, \upsilon_{CH2CH2}$	$\upsilon_{M-N}, \upsilon_{M-O}, \upsilon_{M-Cl}$
H₂L	1695(s), 1656, 1595	3400(br) 3571	1581 1509, 1259	2995-29249(m)	-
[Ni₂LCl₂]	1688, 1522(s)	3160(m)	1433, 1200, 1207	2988, 3044(w)	510(m), 440, 330(w)
[Cu₂LCl₂]	1680 1537,	3419(br)	1450, 1188, 1233(m)	3030(w), 2804	468, 422, 310(w)
[Mn₂LCl₂.4H₂O]	1670(s), 1505(s)	ᵃ3550(br) ᵃ3510 ᵇ1590	1522, 1388, 1188(m)	2890, 3060(w)	522, 414(w), 280-333
[Cd₂LCl₂]	1669-1655 1560(s)	3350(m)	1544(s)	3080(w), 2966(m)	422, 414, 336-370(w)

sh=shoulder, br=broad. s=strong, m=medium,vw = very weak , w=weak and a,b=absorption of O-H for coordinated H₂O.

Table 3. UV-Vis spectra data, magnetic moments and molar conductance results of the prepared complexes.

Compound	Absorption bands, υ (cm⁻¹)	Assignment	Geometry	μ, BM	ᵃΩ, S cm² mol⁻¹
H₂L	42735 37878 31847	INCT $\pi \rightarrow \pi^*$ $n \rightarrow \pi^*$	-	-	-
[Ni₂LCl₂]	23255 25316	$^1A_{1g} \rightarrow {}^1B_{1g}$ $^1A_{1g} \rightarrow {}^1B_{2g}$	square planar	0	9
[Cu₂LCl₂]	19500 15500	$^2B_{1g} \rightarrow {}^2B_{2g}$ $^2B_{1g} \rightarrow {}^2Eg$	square planar	1.2	18
[Mn₂LCl₂.4H₂O]	33421 27567	LMCT $^6A_{1g} \rightarrow {}^4T_{1g}$	octahedral	5.43	11
[Cd₂LCl₂]	33400 28900	LMCT $\pi \rightarrow \pi^*$	tetrahedral	0	22

a=molar conductance in DMF solutions, INCT-intraligand field

The metal (II) complexes in DMF solutions showed nonelectrolyte properties with 15-30 ohm⁻¹ cm² mol⁻¹ conductivity values indicating that there are no chloride ions in the outer sphere of metal complexes.[15] The cadmium(II) complex in DMF solution exhibits two sharp peak in the region 34300-29800 cm⁻¹ that belong to ligand to metal charge transfer and $\pi \rightarrow \pi^*$ transitions, respectively.

Theoretical Study

The optimized geometry of manganese-complex and some selected bond lengths and angles can be seen in Fig. 4 and Table 4 respectively.

The values of the bond lengths and angles are quite similar to the experimental results of analogous compounds.[23-24]
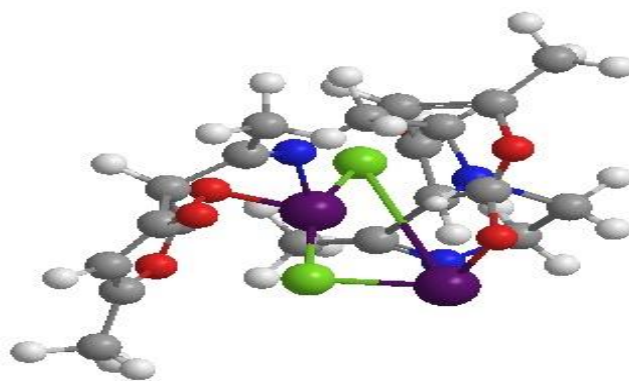
Figure 4. The geometry of Mn(II) complex optimized with Hyperchem MP3 semi-empirical method using Hyperchem-8 program.

Table 4. **S**tructural parameters, bond lengths (Å) and angles (º) of the [Mn₂L₂] complex.

Bond lengths (Å)		Bond angles(º)		Bond angles(º)	
N(1)-C(2)	1.4700	C(20)-C(27)-H(50)	109.4993	C(16)-C(28)-H(53)	109.4999
N(1)-C(16)	1.2600	C(20)-C(27)-H(51)	109.4416	C(16)-C(28)-H(54)	109.4419
N(1)-Mn(29)	1.8460	C(20)-C(27)-H(52)	109.4617	C(16)-C(28)-H(55)	109.4618
C(2)-C(3)	1.5230	H(50)-C(27)-H(51)	109.4419	H(53)-C(28)-H(54)	109.4419
C(2)-H(35)	1.1130	H(50)-C(27)-H(52)	109.4620	H(53)-C(28)-H(55)	109.4618
C(2)-H(36) 1.1130		H(51)-C(27)-H(52)	109.5209	N(1)-Mn(29)-O(15)	72.8134
C(3)-N(4)	1.4380	C(20)-C(21)-C(22)	94.9350	N(1)-Mn(29)-Cl(32)	109.4999
C(3)-H(37)	1.1130	C(20)-C(21)-H(46)	132.5325	N(1)-Mn(29)-Cl(33)	90.0000
C(3)-H(38)	1.1130	C(22)-C(21)-H(46)	132.5324	O(15)-Mn(29)-Cl(32)	109.5001
N(4)-C(5)	1.7721	C(17)-C(22)-C(21)	115.0000	O(15)-Mn(29)-Cl(33)	90.0001
N(4)-H(31)	1.0200	C(17)-C(22)-O(23)	122.5000	Cl(32)-Mn(29)-Cl(33)	155.4959
C(5)-C(6)	1.5230	O(19)-C(18)-O(25)	130.3984	N(1)-C(16)-C(12)	115.0997
N(7)-Mn(30)	1.8460	C(18)-O(25)-Mn(30)	109.5005	N(1)-C(16)-C(28)	122.4499
C(8)-C(9)	1.3491	C(24)-C(34)-H(56)	109.5006	C(12)-C(16)-C(28)	122.4504
C(13)-C(8)	1.3510	C(24)-C(34)-H(57)	109.4422	C(2)-N(1)-C(16)	108.0001
Mn(29)-O(15)	1.7097	C(24)-C(34)-H(58)	109.4617	C(2)-N(1)-Mn(29)	119.9999
C(16)-C(28)	1.4970	H(56)-C(34)-H(57)	109.4416	C(16)-N(1)-Mn(29)	120.0000
C(17)-C(18)	1.5090	H(56)-C(34)-H(58)	109.4617	C(6)-C(5)-H(39)	113.5837
O(19)-C(20)	1.4100	H(57)-C(34)-H(58)	109.5195	C(6)-C(5)-H(40)	119.2535
C(20)-C(21)	1.6036	C(18)-C(17)-C(22)	109.4698	H(39)-C(5)-H(40)	99.9980
C(20)-C(27)	1.4970	C(18)-C(17)-C(24)	154.3598	C(3)-N(4)-C(5)	127.8364
C(21)-C(22)	1.3510	C(18)-C(17)-H(45)	65.2800	C(3)-N(4)-H(31)	116.0821
C(21)-H(46)	1.1000	C(22)-C(17)-C(24)	96.1702	C(5)-N(4)-H(31)	116.0815
C(22)-O(23)	1.2080	C(22)-C(17)-H(45)	174.7458	C(2)-C(3)-N(4)	109.4697
C(24)-C(34)	1.4970	C(24)-C(17)-H(45)	89.0805	C(2)-C(3)-H(37)	109.4491
Mn(30)-O(25)	1.8100	N(7)-Mn(30)-O(25)	109.4997	C(2)-C(3)-H(38)	109.4791
Cl(32)-Mn(29)	2.1600	N(7)-Mn(30)-Cl(32)	90.0000	N(4)-C(3)-H(37)	109.4491
Cl(33)-Mn(29)	2.1600	N(7)-Mn(30)-Cl(33)	33.3581	N(4)-C(3)-H(38)	109.4798
Cl(32)-Mn(30)	2.1600	O(25)-Mn(30)-Cl(32)	109.4999	H(37)-C(3)-H(38)	109.5005
Cl(33)-Mn(30)	4.3970	O(25)-Mn(30)-Cl(33)	89.7988	Mn(29)-Cl(33)-Mn(30)	39.4475
N(1)-Mn(29)	1.8460	Cl(32)-Mn(30)-Cl(33)	71.0216	Mn(29)-Cl(32)-Mn(30)	90.0002
N(4)-C(5)	1.7721	N(7)-C(24)-C(17)	67.6349	C(9)-C(26)-H(47)	109.5003
N(4)-H(31)	1.0200	N(7)-C(24)-C(34)	146.1829	C(9)-C(26)-H(48)	109.4421
C(5)-H(39)	1.1130	C(17)-C(24)-C(34)	146.1822	C(9)-C(26)-H(49)	109.4620
C(5)-H(40)	1.1130	C(6)-N(7)-C(24)	107.9999	H(47)-C(26)-H(48)	109.4418
C(6)-N(7)	1.4700	C(6)-N(7)-Mn(30)	120.0001	H(47)-C(26)-H(49)	109.4614
N(7)-Mn(30)	1.8460	C(24)-N(7)-Mn(30)	120.0003	H(48)-C(26)-H(49)	109.5197
Mn(29)-O(15)	1.7097	C(5)-C(6)-N(7)	110.7399	C(11)-O(15)-Mn(29)	91.9842
Mn(30)-O(25)	1.8100	C(5)-C(6)-H(41)	109.1315	C(9)-O(10)-C(11)	120.0000
Cl(32)-Mn(29)	2.1600	N(4)-C(5)-C(6)	92.1467	C(8)-C(9)-O(10)	123.3719
Cl(33)-Mn(29)	2.1600	N(4)-C(5)-H(39)	113.5836	C(8)-C(9)-C(26)	118.3141
Cl(32)-Mn(30)	2.1600	N(4)-C(5)-H(40)	119.2539	O(10)-C(9)-C(26)	118.314
Cl(33)-Mn(30)	4.3970				

Biological Study

The inhibition zone was measured by the disc method,[13,25] the diameters of the inhibition zone were measured in millimeters. Standard disc of *Amoxycilline* (antibacterial agent) and *Ketoconazole* (antifungal agent) were used as controls for antimicrobial activity. However, the filter discs impregnated with 10 ml of (DMSO solvent + distilled water) were used as a negative control. The used agar (Mueller-Hinton) was rigorously tested for composition and pH.

$$RI(\%) = 100 \frac{A - B}{C - B}$$

where

A= area of inhibition sample plate.

B= area of inhibition in the DMSO (control).

C= area of inhibition in the standard plate.

The effect of free ligand H₂L and it complexes on gram-negative and gram-positive bacteria and fungi were compared and the results are given in Table 5.
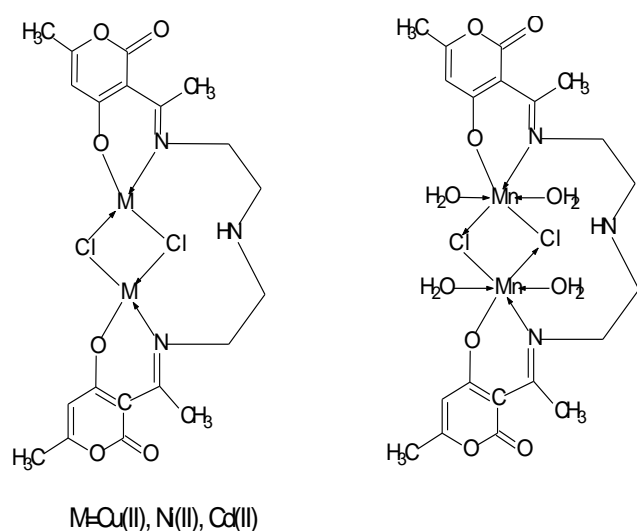
The ligand and its metal complexes were screened for their antibacterial and fungal activities at the same concentration and conditions.

Table 5. Antibacterial activity of ligand and its metal complexes

Compound	Inhibition, mm			
	Escherichia Coli	*Staphylococcus aurea*	*Fungi*	
	G⁻	G⁺	*A. flavus*	*C. albicans*
H_2L	27.22±0.22	33.7±0.03	35.3±0.31	18.0±0.1
Mn(II)	22.01±0.55	34.51±0.11	20.91±0.09	12.11±0.1
Ni(II)	19.41±0.29	12.95±0.84	34.05±0.10	17.0±0.2
Cu(II)	34.43±0.16	39.51±0.11	42.71±0.23	20.0±0.33
Cd(II)	11±1.2	19.51±0.21	12.71±0.93	15.0±0.77
	Control DMSO			
Reagent	**Antibacterial**		**Antifungal**	
	G⁺	G⁻	*A. flavus.*	*C. albicans*
Amoxycilline	18 ±0.2	22±0.2	-	-
Ketoconazole	-	-	31.89±0.2	32.5±0.2

G⁺, G⁻ = gram Positive and gram negative *bacteria*

The ligand and all its metal complexes exhibit inhibition zone against *E. Coli* bacteria in the range 19-34 mm, supporting their activity toward gram-negative bacteria against *Amoxycilline* control.[13,27] It is found obviously (Table 5) that Cu(II) complex proved to be a potentially better antifungal agent against *A. Flavus* than the *Ketoconazol* (standard) and this complex has improved antimicrobial activity than the free ligand. It cannot be explained on the basis of chelation theory[26,28] but would rather with the releasing of Cu(II) ion form the complex. Although the decrease in the polarizing ability of the metal could enhance the lipophilicity of the complexes, which would lead to a breakdown of the permeability of the cells, resulting in interference in normal cell processes,[27-29] but only the Cu(II) complex showed higher value of inhibition against all types of microorganisms than the free eligand comparing it with nickel, manganese(II) or cadmium(II) chelates.

Conclusion

According to the results obtained from elemental analyses, spectroscopic studies and magnetic moment measurements, square planar central atom geometry was proposed for Ni and Cu(II) complexes, while the Mn(II) complex was found to be octahedral, and the Cd(II) complex was found to be tetrahedral. Theoretical study for the Mn(II) complex supported the expected structure derived foerm spectroscopic data. Except cadmium complex, the all studied compounds have antimicrobial activity toward gram negative and gram positive bacteria and fungi.

References

[1]Constable, E. C., *Coordination Chemistry of Macrocyclic Compounds,* Oxford University Press, Oxford, **1999**.

[2]Singh, D. P. Kumar, Malik V. R. and Tyagi, P., *Transition Met.Chem*., **2007**, *32*, 1051-55.

[3]Mane, P. S., Salunke, S,. M., More, B. S., E-J. Chem., **2011**, *8(1)*, 245-252.

[4]Munde, A. S., Jagdale, A. N., Jadhav, S. M. and Chondhaker, T. K., *J. Korean Chem. Soc.*, **2004**, *53*, 407.

[5]Munde, A. S., Jagdale, A. N., Jadhav, S. M. and Chandhekar, T. K., *J. Serb. Chem. Soc*., **2010**, *75*, 349.

[6]Zucolotto, M., Danicl, C. J., Javior, A. E. and Castellana, E. E., *Inorg. Chim. Acta*, **2000**, *328*, 45-50.

[7]Sakurai, H., Inohara, T., Adachi, Y., Kawabe, K., Yasui, H., *Bioorg. Med. Chem.,* **2004**, *14(5)*, 1093-1096.

[8]Levai, A. Jeko, J., *Monatsh. Chem*., **2006**, *137*, 339-346.

[9]Mane, P. S., Shirodkar, S. G., Arbad, B. R., Chondhekar, T. K., *Indian J. Chem*., **2001,** *40*, 648-655.

[10]Rao, P. V., Narasaiah, A. V., *Indian J. Chem.*, **2003**, 42A, 896.

[11]Raman, N.,Johnson, S. R and Sukthicevel, A., *J. Coord. Chem*., **2009**, *62*, 691.

[12]Vandpitte J, , Basic laboratory procedures in clinical bacteriology, WHO, Geneva, **1991**, 78-110.

M=Cu(II), Ni(II), Cd(II)

Figure 5. Proposed structure of metal(II) complexes.

[13]Al-Obaidi, O. H., *J. Chem., Biol. Phys. Sci.,* **2014,** *4(1)*, 31-37.

[14]Chojnacki, H. and Pruchnik, F., Int. J. Mol. Sci., **2001**, *2*, 44.

[15]Geary W. J., *Coord. Chem. Rev.,* **1971,** *7(1)*, 81-122.

[16]Silverstein, R. M., Bassler, G. C. and Morrill, T. C., *Spectrometric methods for Identification of organic compounds*, 4th Ed., Wiley, London, **1986**

[17]Raman, N.,Johnson, S. R and Sukthicevel, A., *J. Coord. Chem.*, **2009**, *62*, 691.

[18]Nakamato, K., *Infrared and Raman spectra of Inorganic and coordination Compounds*, 4th ed., Wiley, New York, **1986**

[19]Dyer, J. R., *Application of absorption spectroscopy of organic compounds*, Prentice Hall., Eaglewood Cliffs, N.J., **1965,**

[20]Lever, A. B., *Inorganic Electronic Spectroscopy*, 2nd, Elsevier.,**1984.**

[21]Sutton, D., *Electronic Spectra of Transition Metal Complexes*, McGraw Hill., London, **1968,**

[22]Cotton, F. A., Wilkinson, G., Murillo, C. A., Bochmann, M., *Advanced Inorganic Chemistry*, 6th Edition, John Wiley and Sons., **1999**.

[23]Satyanarayane D. N., *Electronic Absorption spectroscopy and Related Techniques*, Universities press, Hyderabad, **2001.**

[24]Manku, G. S., *Theoretical Principles of Inorganic Chemistry***,** McGraw-Hill Offices, **2004**, 21st, 449-500.

[25]Stewart, J. P., *J. Comput. Chem.,* **1999,** 10(2), 209-220.

[26]Chandra, S., Sharma, D., *Transit. Met. Chem.*, **2002,** *27*, 732-735.

[27]Negam, N. A., Said, M. M., Morsy, S. M. I., *J. Surfactants Detergents*, **2008,** 13(4), 521-528.

[28]Perrin, D. D., Armarego, W. L. F., *Purification of laboratory chemicals*, 3rd Ed., Pergamon Press, Oxford, UK, **1988.**

[29]Ullah, H., Wattoo, F.-H., Wattoo, M. H. S., Gulfraz. M., Tirmizi, S. A., Ata, S., Wadood, A., *Turk. J. Biochem.,* **2012**; *37(4)* ; 386−391.

REMOVAL OF AMITROLE FROM AQUEOUS SOLUTIONS BY ACID ACTIVATED CLAY

Jale Gülen,[a]* Fatma Turak[b] and Mahmure Özgür[b]

In this study, the adsorption behavior of amitrole on acid activated clay (AC) was investigated using a spectrophotometric method to obtain information on the pesticide removal. The adsorption of amitrole from aqueous solutions by AC has been performed using a batch-adsorption technique. The effect of various experimental parameters, such as initial concentration of pesticide, contact time, temperature and pH on the adsorption process, were investigated. Original pH at the beginning was 5. It was observed that the adsorption percentage of amitrole on AC remained practically constant with increasing temperature and contact time of around 3 h was sufficient to reach the equilibrium for all temperature. Temkin and Harkins-Jura adsorption models were applied to describe the equilibrium isotherms and the isotherm constants were calculated. It was found that the data were fitted Temkin adsorption model better than Harkins-Jura adsorption model. The present study showed that the asit activated clay was abundant snd low-cost. Clay can be used as sorbent for the removal of amitrole from aqueous solutions.

*Corresponding Author
Tel: +90212 383 47 54
    E-Mail: gulenj@yildiz.edu.tr
[a]   Yildiz Technical University, Chemical Engineering
    Department, 34210, Esenler, Istanbul-Turkey
[b]   Yildiz Technical University, Chemistry Department, 34210,
    Esenler, Istanbul-Turkey

Introduction

Increasing use of pesticides in agriculture and domestic activities for controlling pests is polluting the environment day by day.[1] The contamination of soils, ground water and surface water by pesticide is currently a significant concern throughout the world due to the detrimental effect of them to both human life and environment.[2] Toxicity of present pesticides and their degradation products is making these chemical substances a potential hazard. When these pesticides are introduced into the environment through spraying on crops, the pesticide droplets fall on soil, plant and water. While some part of these chemicals stays in the area where it is applied, major parts are transported to various environmental media. The adsorption/desorption phenomena of pesticides in soil are of great importance from environmental point of view. Pesticide sorption process affects other processes like transport, degradation, volatilization and bioaccumulation, which influence the final fate of these compounds in the soil.[3-5]

In industry, the cost of water not only includes the direct cost but also costs incurred in bringing the water to certain specifications prior to use. Present and future legislation will lead to more stringent controls on industrial effluent pollution.[6] Industries such as food and beverage industry, chemical, petrochemical, pharmaceutical and refining industries, pulp and paper industry and the electronics industry all generate large volumes of waste streams with significant residue content for treatment and recycling.[7] In general, reduction of waste water in any given industry can be achieved by a number of ways including process modification, changes in raw materials used or water consumption reduction programmes leading to significant environmental and economic benefits.[8, 9]

Current technologies for waste stream treatment and recycling include membrane technology encompassing reverse osmasis, micro filtration and ultra filtration.[10-13] Alternatives to membrane systems include oxidation methods based on chemical oxidation an air/oxygen based catalytic (or noncatalytic) oxidation. The first category includes advanced oxidation processes such as the use of ozone, hydrogen peroxide and UV radiation to generate hydroxyl radicals used for oxidation.[14-17] These processes tend to be limited by their intensive costs. The second category includes dry oxidation, wet air oxidation and catalytic wet air oxidation.[18-20]

Adsorption is another example of a physical procedure used in waste water treatment. Adsorption technology has been used for the removal of organics from waste waters, primarily focusing on the use of activated carbon as the adsorbent choice. Regeneration of the spent adsorbent material can be a costly and intensive process.[21] This has led to an interest in developing alternative adsorbents for the removal of organic pollutants from aqueous waste streams.[22,23]

This study aims to remove the undesired pesticide termed amitrole from water using a natural clay material which is sulphuric acid washed and dried. This study is furnissed with some experimental parameters.

Experimental studies

Adsorbate

Amitrole is a pesticide used in agriculture that is supplied by Hektaş AŞ. in Turkey. It is used as a herbicide to control grass and weeds growing around fruit trees, bushes, vines and cereal crops. It is also used on weeds along paths,

railways tracks and industrial areas as well as on aquatic weeds in marshes and ditches. Amitrole is toxic to some types of aquatic organisms. It slows down the growth of bacteria and the energy-processing mechanisms in plants. Due to its high solubility in water, amitrole is likely to end up in water resources where it may take up a month or so to break down. It does not accumulate in aquatic organisms. In soils, amitrole is broken down by microbia within 2-4 weeks. It is not considered likely that amitrole pollution has any effect on the global environment.[24] The chemical formula is given in Fig. 1 and its characteristic properties are listed in Table 1.
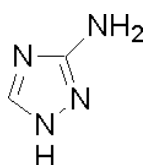
Figure 1. Chemical structure of amitrole

Table 1. The characteristics properties of amitrole

Molecular weight	84.08 g mol^{-1}
Color	Beige
Form	Pullar
Smell	none
Melting point	149-152 ºC
İgnition point	225 ºC
pH (20 ºC)	6.5 (100 g L^{-1})

Adsorbent

The chemical composition of the clay sample was estimated by X-ray fluorescence (XRF) (Philips) Magic PW 2424. X-ray diffraction spectroscopy (XRD) analysis was carried out with PANanytical X-ray diffractomer (Philips) and the results are given in Table 2. The observed chemical composition of clay as given below indicated that silica, alumina and iron(III) oxide are major constituents.

Table 2. Chemical composition of clay

Compound	%
SiO$_2$	60.89
Al$_2$O$_3$	17.35
Fe$_2$O$_3$	8.48
K$_2$O	0.67
CaO	2.156
TiO$_2$	0.86
MgO	4.69
Moisture	4.904

Acid activated clay was prepared from the natural clay by refluxing for 1 h with 36 N sulphuric acid. The resulting activated sample was washed with distilled water to remove all the excess acid and dried in a drier for 2 h at 110 °C until a constant weight was reached. It was then ground in a ball mill and sieved to particular size -75+180 μm for the adsorption study. The BET surface areas of clay were measured with nitrogen as 165 m^2 g^{-1}.

Adsorption studies

The amitrole stock solution was prepared by dissolving 0.01 g amitrole in 100 ml distilled water. A 5 ml solution was diluted to 20 ml with distilled water. The absorbance-calibration data were obtained from this stock solution at the selected wavelength (λ=214 nm).

The experimental solutions were prepared by using 5 ml stock solution diluted to 20 ml with distilled water as 25 μg mL^{-1} concentration. The amount of adsorbent used in the experiments was kept constant as 0.1 gram. The solutions were shaken in a water bath until adsorption equilibrium was attained as was indicated by ATI/UNICAM UV/VIS spectophotometer at λ=200 nm and 214 nm for λ$_{max}$ max absorbance and λ$_{min}$ first derivative, respectively. λ$_{min}$ data were taken into consideration. The adsorption data were measured in half an hour intervals. After the liquid phase was centrifuged at 100 rpm for 5 minutes, 2 ml supernatant was diluted to 10 mL. The experiments were done at 25, 35, 45 and 55 ºC. And they were performed at different pH values to see the effect of pH changes on the adsorption yield.

Effect of pH

The experiments were performed at different pH values such as 1.5, 3, 5, 7, 9, 11. The pH value of the stock solution was monitored using either 0.1 N hydrochloric acid or 0.1 N sodium hydroxide solution. The measurements were performed using WTW Inolab pH meter. The pH value of the initial experimental solution was 5. 0.1 g adsorbent was added to each solution. After 3 hours, the absorbance values at equilibrium were measured by UV spectrophotometer. The experiments were performed at temperature of 25 ºC.

Uptake (φ, %) was determined from the formula given below.

$$\varphi\% = \frac{C_0 - C_e}{C_0} \times 100 \tag{1}$$

C_o = initial concentration of pesticide, μg mL^{-1}
C_e = equilibrium concentration of pesticide, μg mL^{-1}

Effect of initial concentration

The effect of initial amitrole concentrations in the range of 2-10 μg mL^{-1} on the adsorption mechanism was determined. The samples were continuously agitated with a speed of 300 rpm at the room temperature for 3 hours.

Effect of Temperature

The effect of temperature was searched by performing the experiments at different temperatures like 25, 35, 45 and 55 °C temperatures.

Adsorption isotherm model

Some adsorption isotherm models were applied for describing the relationship between adsorbate and adsorbent patterns. The Temkin equation suggest a linear decrease of sorption energy as the degree of completion of the sorptional centers of an adsorbent is increased . The heat of adsorption and the adsorbent-adsorbate interaction on adsorption isotherms were studied by Temkin and Pzyhev.[25] The Temkin isotherm equation is given as

$$q_e = B_T(\ln A_T + \ln C_e) \tag{2}$$

where $\quad B_T = \dfrac{RT}{b}$

T is the absolute temperature in K,
R is the universal gas constant, 8.314 J mol^{-1} K^{-1},
A_T is the equilibrium binding constant (L mg^{-1}) and
B_T is related to the heat of adsorption.

The Harkins-Jura adsorption isotherm can be expressed as[26]

$$\frac{1}{q_e^2} = \left(\frac{B}{A}\right) - \left(\frac{1}{A}\right)\log C_e \tag{3}$$

where

B and A are the isotherm constants.

The Harkins-Jura adsorption isotherm accounts to multilayer adsorption and can be explained with the existence of heterogeneous pore distribution.

Adsorption kinetics

The adsorption kinetics are searched using the pseudo first order and pseudo second order equation by Lagergen and Svenska.[27]

The pseudo first order equation is determined by

$$\ln(q_e - q_t) = \ln q_e - k_1 t \tag{4}$$

where

q_e is the amount of pesticide adsorbed (mg g^{-1}) at equilibrium
q_t is the amount of pesticide adsorbed at time t (mg g^{-1})
k_1 is the rate constant of the adsorption process (h^{-1})

The second order of pseudo kinetic model was implemented to verify the suitability of the experimental data. The pseudo second order kinetic model is given by the following equation

$$\frac{t}{q_t} = \frac{1}{k_2 q_e^2} + \left(\frac{1}{q_t}\right)t \tag{5}$$

where

k_2 is the rate constant of the adsorption process (mg mL^{-1} h^{-1})

Thermodynamic parameters

The thermodynamic parameters like $\Delta G°$, $\Delta H°$ and $\Delta S°$ were calculated to determine the nature of the adsorption. Adsorption standard free energy changes ($\Delta G°$) are determined using the following equation.[28]

$$\Delta G^0 = -RT \ln K \tag{6}$$

where

R is the gas constant 8.314x10^{-7} kJ K^{-1} mol^{-1}),
T is the temperature (K) and
$\Delta G°$ is the Gibbs free energy of adsorption.

The equilibrium constant was calculated from

$$K = \frac{q_e}{C_e} \tag{7}$$

where

q_e (mgg^{-1}) and C_e (μgmL^{-1}) are the equilibrium concentrations of pesticide on the sorbent and in solution, respectively.

The sorption distribution coefficient can be expressed in terms of enthalpy and entropy changes as a function of temperature

$$\ln K = -\frac{\Delta H^0}{RT} + \frac{\Delta S^0}{R} \tag{8}$$

The enthalpy change ($\Delta H°$) and the entropy change ($\Delta S°$) can be calculated from the plot of ln K versus 1/T. The slope and the intercept represent -$\Delta H°$/R and $\Delta S°$/R, respectively.

Results and discussion

Phase contact time and initial adsorbate concentration

The effect of initial concentration of amitrole was studied . The adsorption became constant after 3 hours. Fig 2 shows the relationships between equilibrium concentration and time at different temperatures. Fig 3 shows the variation of q_e as a function of time and temperature. The amount of adsorption at equilibrium, q_e(mg g^{-1}) was calculated using the following equation:

$$q_e = \frac{(C_0 - C_e)V}{W} \tag{9}$$

Table 3. Isotherm constants

Temperature, °C	Temkin			Harkins-Jura		
	A_T(L mg^{-1})	B_T	R^2	A	B	R^2
25	1.75	0.57	0.99	-9.73	690.83	0.78
35	1.55	0.51	0.91	-4.29	288.1	0.74
45	1.67	0.31	0.99	-1.68	2462.88	0.53
55	1.65	0.31	0.99	-1.01	3115.45	0.35

where,

C_o (µgmL^{-1}) and C_e (µgmL^{-1}) are liquid phase pesticide concentrations at initially and at equilibrium, respectively.

V is the volume of the pesticide solution (mL) and

W is the mass of adsorbent (mg)

As the temperature was increased, the removal percent was decreased that was seen on Fig. 3.

Figure 4. Uptake % versus pH at 25 °C (Adsorbent dose:0.1 g/25 ml, equilibrium time:3 h)

Effect of initial concentration

The effect of initial amitrole concentration in the range of 2-10 µg mL^{-1} on adsorption mechanism was investigated under the specified conditions. Figure 5 shows the adsorption of amitrole on clay (q_e) vs initial pesticide concentration. Increasing the pesticide concentration led to an increase in the amitrole adsorption by clay. The maximum adsorption capacity found to be 0.105 mg g^{-1}. The acid treatment has the positive effect of the adsorption capacity of clay.

Figure 2. Concentration versus time at different temperatures (T: 25 °C, 35 °C, 45 °C, 55 °C; adsorbent dose: 0.1 g/25 ml)
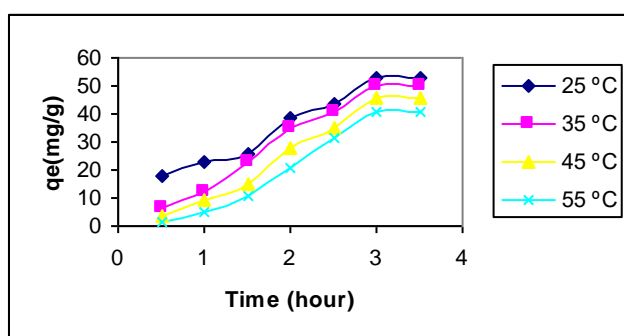
Figure 3. q_e versus time and temperature (T:25, 35, 45 and 55 °C, adsorbent dosage: 0.1 g/25 ml)
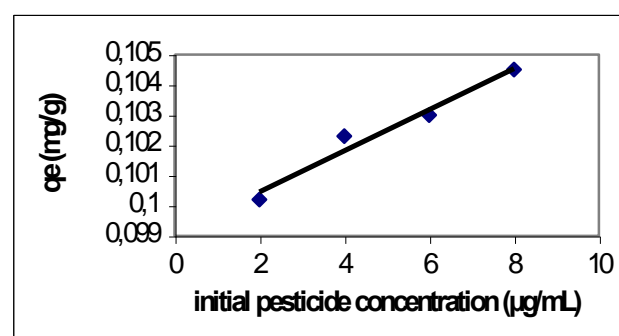
Figure 5. Effect of initial concentration on amitrole adsorption (T=25 °C)

Effect of pH

The effect of pH is shown in Figure 4 in terms of uptake % - pH. The uptake percent was reached to approximately 80 % at pH 3. The H$^+$ ions of amine group has the positive effect on the adsorption. Hameed found the highest adsorption of 2,4-6 trichlorophenol onto activated clay at pH=2.[29] The pesticide removal capacity is gradually decreased until the pH value of 8. Later, it is almost stable around the pH value of 12.

Adsorption isotherms

A Temkin plot of q_e vs ln C_e at studied temperature is shown in Fig 6. The Temkin isotherm constant, B_T shows that the heat of adsorption increases with increase in temperature, indicating endothermic adsorption. In our study, this value decreases showing the exothermic behavior. Hameed studied the adsorption of 2,4-6 trichlorophenol adsorption onto HCl activated clay. He applied Langmuir, Freundlich and Temkin isotherms to the experimental data.

The R^2 values are good (0.95, 0.90 and 0.89) and B_T constants of isotherms are decreased with increasing temperature as 25.24, 17.45 and 14.73 showing exothermic nature of adsorption.[29]
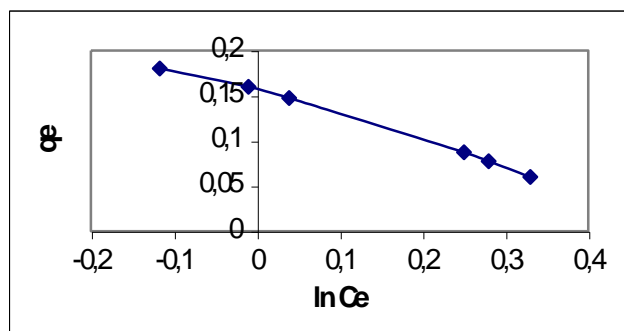
Figure 6. Temkin isotherm at 25 °C

The Harkins Jura plot ($1/q_e^2$ vs log C_e) is given in Fig 7. The low R^2 values indicate that the adsorption of amitrole by clay does not support this isotherm model.
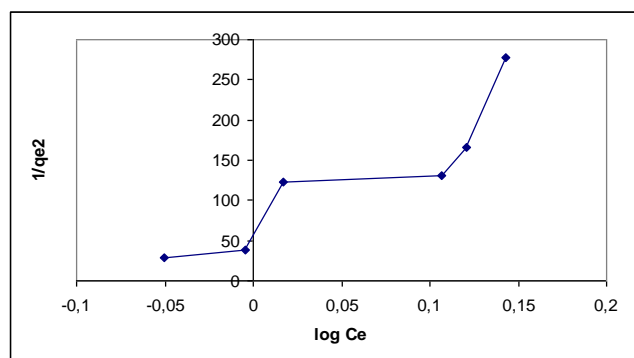
Figure 7. Harkins Jura isotherm at 25 °C

Nevine Kamal Amin studied the removal of direct blue 106 dye from aqueous solution using new activated carbon derived from pomegranate peel. She applied some isotherm models to the adsorption data like Langmuir, Freundlich, Temkin, Dubunin-Raduskevich (D-R) and Harkins-Jura isotherms. The correlation coefficients (R^2) of Harkins-Jura and D-R isotherms are lower than the other models.[30]

The constants and correlation coefficients of the study are summarized in Table 3.
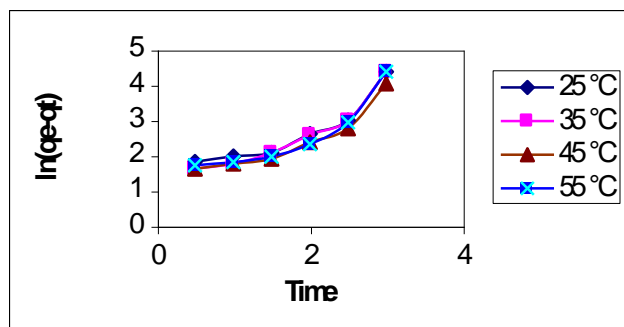
Figure 8. Pseudo first order kinetic of amitrole by AC

Table 4. Kinetic parameters

Temp °C	k_1	R^2	k_2	R^2
25	0.93	0.84	0.92	0.66
35	1.03	0.88	0.32	0.54
45	0.89	0.85	1.31	0.88
55	0.97	0.81	5.50	0.88

Adsorption kinetics

The adsorption kinetic behavior was shown in Fig. 8 and 9 for pseudo first and pseudo second order kinetics, respectively. The kinetic parameters were given in the Table 4. At low temperatures (25, 35 °C) the reaction progressed as pseudo first order but at high temperature (45, 55 °C) both models support the adsorption mechanism.
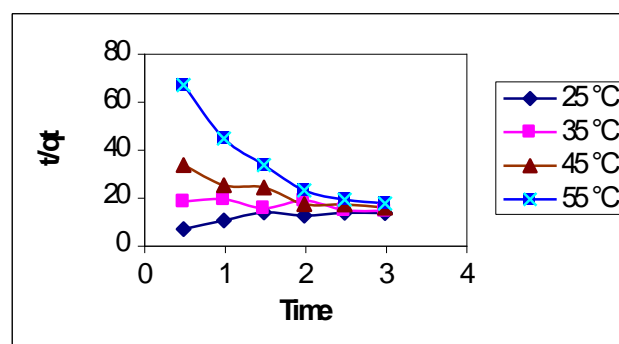
Figure 9. Pseudo second order kinetic of amitrole by AC

Thermodynamic approach

The thermodynamic parameters are calculated from the plot and were shown in Figure 10 and Table 5. The negative value obtained for $\Delta H°$ confirms the exothermic nature of the sorption processes. The negative $\Delta S°$ value reflects the fact no significant change occurs in the internal structure of clay during the pesticide adsorption. The negative $\Delta G°$ values indicate the feasibility and spontaneous nature of amitrole adsorption on acid treated clay.
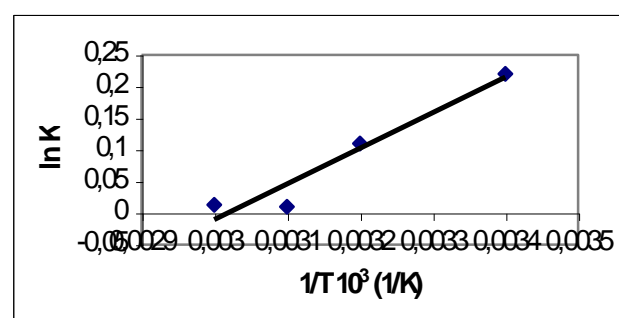
Figure 10. ln K versus 1/T plot for thermodynamic parameters

Bakouri et al. studied the acid activated olive stones for removal of pesticides like aldrin, dieldrin and endrin. They found the exothermic and spontaneous behavior of the process at the studied temperatures (10, 15, 20, 25, 30, 35, 40 °C).[31]

Table 5. Thermodynamic parameters

Temperature °C	$\Delta H°$ (J g^{-1})	$\Delta S°$ (J g^{-1} K^{-1})	$\Delta G°$ (J g^{-1})
25(298 K)	-4680.8	-14.1	-509
35(308 K)			-369
45(318 K)			-229
55(328 K)			-89

Conclusion

In this study, adsorption of amitrole from aqueous solutions on acid activated clay (AC) was investigated under different experimental conditions in batch model. The removal of pesticide was found to be depending on phases contact time, initial concentration of pesticide, pH and temperature. Maximum pesticide was sequestered from the solution within 3 h after the adsorption experiment beginning for all temperatures. The equilibrium adsorption data were very best represented by Temkin isotherm. The reaction is well represented with pseudo first order kinetic model at 25 °C.

Given the facts that clay necessitates no pretreatment, it is ecofriendly and low-cost, and that it has a satisfying adsorption capacity. Present clay especially asit activated clay can well be used in different types of removal activities like textile dyes, phenolic compounds and pesticides.

Acknowledgement

References

[1]Singh, R. P., Kumari, F., Singh, D., *Ecotoxicol. Environment. Safety*, **1994**, 70-79.

[2]Memon, G. Z., Bhanger, M. I., Akthar, M., Talpur, F. N., Memon, J. R., *Chem. Eng. J.,* **2008**, *138*, 616-621.

[3]Rama Krishna, K., Philip, L., *J. Hazard. Mater.*, **2008**, *160*, 559-567.

[4]Gao, J. P., Maguhn, J., Spitzauer, P., Kettrup, A., *Water Resour.*, **1998**, *32*, 1662-1672.

[5]Kumar, M., Philip, L., *Chemosphere*, **2006**, *62(7)*, 1064-1077

[6]O'Brien, J., O'Dwyer, T. F., Curtin, T., *J. Hazard. Mater.*, **2008**, *159*, 476-482.

[7]Hancock, F. E., *Catal. Today*, **1999**, *53*, 3-9

[8]Zbantar Zver, L., Glavic, P., *Resour. Conserv. Recycl.*, **2005**, *43*, 133-145.

[9]Saha, N. K., Balakrishnan, M., Batra, V. S., *Resour. Conserv. Recycl.,* **2005**, *43,* 163-174.

[10]Benneth, A., Filtration Separ., **2000**, *39*, 26-28

[11]Ko, C., Chen, S., *Bioresor. Technol.*, **2008**, *99*, 2293-2298

[12]Ahmad,A. I., Tan, K. Y., *Desalination*, **2004**, *165*, 193-199

[13]Goncharuk, V. V., Kucheruk, D. D., Kochkodan, V. M., Badekha, V. P., *Desalination,* **2002**, *143*, 45-51.

[14]Hirakawa, T., Daimon, T., Kitazawa, M., Ohguri, N., Koga, C., Negishi, N., Matsuzawa, S., Nosaka, Y., *J. Photochem. Photobiol. A*, **2007**, *190*, 58-68.

[15]Amat, A. M., Arques, A., Miranda, M. A., Segui, S., Vercher, R. F., *Desalination*, **2007**, *212*, 114-122.

[16]Puma, G. L., Yue, P. L., *Ind. Eng. Chem. Res.*, **2002**, *41*, 5594-5600.

[17]Bastaki, A., Nader, M., *Chem. Eng. Process.: Process Intens.*, **2004**, *43*, 935-940.

[18]Morent, R. Dewulf, J. Steenhaut, N. Leys, C. Van Lagenhove, H. J., *Adv. Oxidn. Technol.*, **2006**, *9*, 53-58.

[19]Levec, J., Pintar, A., *Catal. Today*, **2007**, *124*, 172-184.

[20]Bhargava, S. K., Tardio, J., Jani, H., Akolekar, D. D., Foeget, K., Hoang, M., *Catal. Surveys Asia*, **2007**, *11*, 70-86.

[21]Shu, H. T., Li, D., Scala, A. A., Ma, Y. H., *Separ. Purif. Technol.*, **1997**, *11*, 27-36.

[22]Kelleher, B. K., Doyle, A. M., O'Dwyer, T. F., Hodnett, B. K., *J. Chem. Technol. Biotechnol.*, **2001**, *76*, 1216-1222.

[23]Gülen, J., Turak, F., Özgür, M., *Int. J. Modern Chem.*, **2012**, *2(2)*, 47-56.

[24]internet available February 2014 (http://en.wikipedia.org/wiki/ 3-amino-1,2,4-triazole.

[25]Temkin M. J. and Pyzhev, V., *Acta Physiochim. USSR*, **1940**, *12*, 217-222.

[26]Basar, C. A., *J. Hazard. Mater.*, **2006**, *B135*, 232-241.

[27]Ho, Y. S., *Scientometrics*, **2004**, *59*, 171-177.

[28]Çoruh, S., Geyikçi, F., Ergun, O.N., *Environment. Technol.*, **2011**, *32(11)*, 1183-1193.

[29]Hameed, B. H., *Colloids Surfaces A: Physichem. Eng. Aspects,* **2007**, *307*, 45-52

[30]Kamal Amin, N., *J. Hazard. Mater.*, **2009**, *165,* 52-62.

[31]El Bakouri, H., Usero, J., Morillo, J., Oussini, A. H., *Bioresour. Technol.*, **2009,** *100*, 4147-4155.

SYNTHESIS AND NEUROTROPIC ACTIVITY OF NOVEL SULFOLANE-CONTAINING CAGE SULFONAMIDES

Iryna S. Zarovnaya[a], Helen T. Zlenko[b] and Vitaliy A. Palchikov[a]*

Keywords: sulfonamides; sulfolane; norbornene; adamantane; neurotropic activity; NOE experiments

A novel water soluble cage sulfonamides was prepared and their neurotropic effects were evaluated. *In vivo* tests showed high level of analgesic and tranquilizing activity of *trans*-N-(bicyclo[2.2.1]hept-5-en-*endo*-2-ylmethyl)-4-hydroxytetrahydrothiophene-3-sulfonamide-1,1-dioxide, greater than well known sodium metamizole used as the internal standard. Stereochemical structure of the title compounds was confirmed using the NOE and 2D NMR experiments.

* Corresponding Author
  E-Mail: palchikoff@mail.ru; palchikoff82@gmail.com
[a] Oles Honchar Dnipropetrovsk National University
    72, Gagarin Av., Dnipropetrovsk, 49010, Ukraine
[b] Dnipropetrovsk Medical Institut Traditional and Alternative Medicine. 17, Sevastopolska Str., Dnipropetrovsk, 49005, Ukraine

Introduction

Sulfonamides are one of the oldest groups of the drugs, they have been in clinical use for over 70 years.[1] Sulfonamides play an important role in medicinal chemistry: many antimicrobial, anti-inflammatory, anticonvulsant, antihypertensive, antipsychotic, diuretic, hypoglycemic, and anticancer drugs contain the sulfonamide subunit.[2] Today, the presence of sulfonamides in medicinal agents is widespread; close to 10 % of the top 100 pharmaceuticals prescribed in 2011-2012 either bear a sulfonamide fragment or are coadministered with a sulfonamide-containing drug.[3] At the same time, biological properties of the polycyclic hydrocarbon structures such as the bicylic norbornane, norbornene and tricyclic adamantane have attracted the attention since the 1930s. The medicinal chemistry of these cage compounds gained momentum in the 1980s with the discovery of the calcium-channel-modulating effects and antiviral activity thereof. The 1990s and 2000s saw several reports on a variety of pharmacological areas, i.e., dopaminergic, catecholaminergic, and focusing on disorders of the central nervous system, such as neurodegeneration (Parkinson's and Alzheimer's disease).[4] These polycyclic structures have proved to be very useful tools in drug design, in particular during the past 30 years.

In our previous papers we described many new cage sulfonamides.[5] The presented paper extends our earlier research, we used the sulfolane-containing sulfonyl chloride **1** as a versatile scaffold for the synthesis of a new series potentially biologically active cage compounds. The main purpose of this work was to develop simple methods for the preparation of cage sulfonamides containing pharmacophore sulfolane (thiolan-1,1-dioxide) fragment. This fragment is known because of its unique biological properties and found in many compounds with neurotropic activity.[6] Realizing the importance of polycyclic structures and sulfolanes, it is planned to conjugate these two ligands under one construct and to study their biological activity.

We envision that studies on the synthesis and chemistry of cage sulfonamides can further expand their scope and utility.

Results and Discussion

It is well known that isothiuronic salts may be oxidized to the corresponding sulfonyl chlorides at the low temperature by using excess of gaseous chlorine in different conditions.[7] We screened a number of possible routes for the synthesis of starting sulfonyl chloride **1** and ultimately developed a simple protocol (Scheme 1). Unfortunately, attempts to obtain of compound **1** by known method[8] has not been successful, we found than in described conditions only *trans*-chlorohydrin **2** was formed. The good, scalable and reproducible yield of **1** was obtained under the following conditions: treatment of isothiuronic salt **3** by solution of chlorine in carbon tetrachloride at the temperature about 0-5 °C. The reaction is rapid, avoids the use of chlorine gas, and succeeds with easily available salt **3**. This method allows the preparation of the sulfonyl chloride **1**, which are stable enough to be purified and stored, making them potentially useful starting material in parallel chemistry efforts. In our investigation we used the classical approach to sulfonamides relies on a reaction between sulfonyl chloride **1** and amines in the presence of a triethylamine (TEA) (Scheme 1).
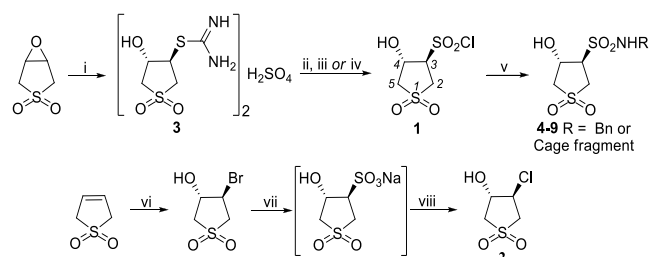
Scheme 1. *Reagents and conditions*: i) (NH₂)₂CS (1 eq.), H₂SO₄ (0.5 eq.), H₂O, 60-70 °C, 2 h (83%); ii) Cl₂ (gaseous, excess), EtOAc-H₂O, 5-10 ºC, 8 h (68%); iii) Cl₂ (solution in CCl₄, excess), EtOAc-H₂O (1:1 v/v), 5-10 °C, 8 h (62%); iv) H₂O₂ (6 eq.), SOCl₂ (2 eq.), MeCN, 80 °C, 2 h (traces); v) NH₂R (1 eq.), TEA (1 eq.), EtOAc, 20 °C, 24 h (42-87%); vi) NBS (2 eq.), H₂O, 70-75 °C, 3 h (75%); vii) Na₂SO₃ (1.6 eq.), THF-EtOH-H₂O (1:2:2 v/v), microwave irradiation (300W), 45 min, then viii) SOCl₂ (2.6 eq.), PhH-DMF (70:1), 60 °C, 3 h (64%).

To study the title reaction, we chose a series of known cage-amines such as stereochemically pure *endo-* and *exo*-bicyclo[2.2.1]hept-5-en-2-ylmethanamines, 1-(bicyclo-[2.2.1]heptan-2-yl)ethanamine, 1-aminoadamantane, (1-adamanthyl)methylamine and also benzylamine. Column chromatography on silica allowed to isolate individual products. The synthesized novel sulfonamides have the following structures **4-9** (Scheme 2).
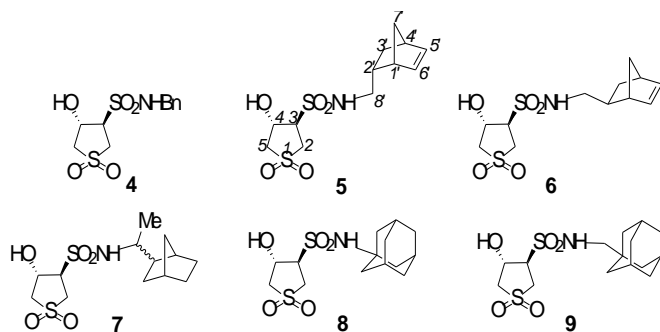
Scheme 2. Structures of sulfonamides **4-9**.

The study of stereochemical features of compound **1** is key importance because it determines the structure of the final products. Stereochemical structure of 4-hydroxytetrahydrothiophene-3-sulfonyl chloride 1,1-dioxide **1** and chlorohydrine **2**, in particular *trans*-orientation of substituents in position 3 and 4 of sulfolane ring were confirmed using the NOE experiments as well as ^{1}H, ^{13}C, COSY and HSQC studies. Most important spectral data showing on Fig. 1 are summarized in Table 1.
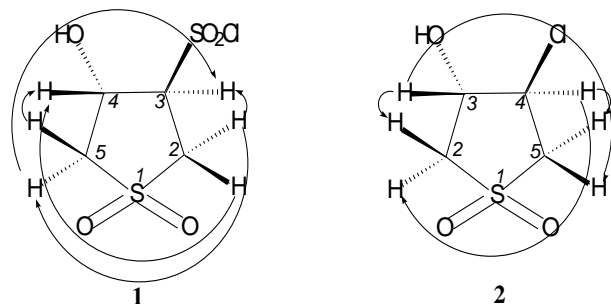
Figure 1. Most important correlations in the NOE spectra of sulfonyl chloride **1** ((CD₃)₂CO, 500 MHz) and chlorohydrin **2** (DMSO-*d₆*, 500 MHz).

The analysis of the IR spectra of synthesized products leads to following conclusions: the spectra of all products are characterized by absorption bands in the region of 1396-1319 and 1198-1162 cm⁻¹, which corresponds to the asymmetric and symmetric stretching vibrations of the SO₂ group in the sulfolane heterocycle. Also, the presence of intense absorption bands in the region of 3445-3380 and 3362-3275 cm⁻¹ (*v* OH, *v* NH) has been detected. Additionally, and the bands of strained double bond at 3034-3025 and 725-717 cm⁻¹ (*v* (=CH) and *δ* (=CH)) are present in the spectra of compounds **5** and **6**.

Assignment of the chemical shifts for compounds **3** and **5** were determined using coordinates of cross peaks in their COSY and HSQC spectra.

Table 1. All correlations in the NOE spectra of sulfonyl chloride **1** ((CD₃)₂CO, 500 MHz) and chlorohydrin **2** (DMSO-*d₆*, 500 MHz).

Sulfonyl chloride 1		
Atom	**Chemical shift of irradiated signal, ppm**	**Chemical shifts, ppm, and NOE values, %**
H⁵ᵃ	3.37	3.82 (4.0), 4.99 (0.3)
H²ᵃ	3.69	4.05 (3.4), 4.99 (1.4), 5.19 (0.2)
H⁵ᵇ	3.82	3.37 (2.4), 5.19 (2.3)
H²ᵇ	4.05	3.69 (1.8), 4.99 (1.0)
H³	4.99	3.37 (0.3), 4.05 (1.3)
H⁴	5.19	3.69 (0.3), 3.82 (0.9)
Chlorohydrin 2		
Atom	**Chemical shift of irradiated signal, ppm**	**Chemical shifts, ppm, and NOE values, %**
H²ᵇ	3.12	3.43 (0.2), 3.55 (11.1), 4.51 (0.8), 4.62 (0.5)
H²ᵃ	3.55	3.12 (16.0), 3.43 (2.0), 4.51 (10.3)
H⁵ᵃ	3.77	3.43 (8.1), 4.62 (2.1)
H³	4.51	3.12 (1.0), 3.43 (1.1), 3.55 (2.9)
H⁴	4.62	3.12 (0.4), 3.43 (1.0), 3.77 (2.1)

The structure of sulfonamide **5** was additionally proved by the mass spectrum. The spectrum of compound **5** lacks the molecular ion peak *m/z* 321 that indicates a low stability of the compound under electron impact. The major pathway of the mass-spectral fragmentation is the retrodiene reaction of the norbornene fragment giving intensive fragment ions F₁ (*m/z* 66, 22.8 %) and F₂ (*m/z* 56, 100 %). Homolysis of the N-S sulfonamide bond leads to formation of metastable ion F₃, elimination of SO₂ and H₂O from which gives cyclobutene radical F₄ (*m/z* 54, 14.9 %) (Scheme 3).
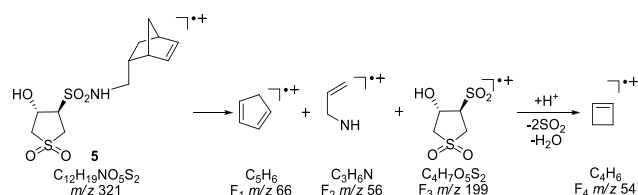
Scheme 3. The major pathway of the mass-spectral fragmentation sulfonamide **5**.

In the present paper, the neurotropic activity of the derivatives **5** and **8** via *in vivo* tests are briefly described. As the internal standard we used well known sodium metamizole (Analgin, injected in the doses of 100 mg/kg). Compound **5** is found to be the most potent analgesic and tranquilizing agent in this series synthesized by our laboratory.

Table 2. Neurotropic activity of the sulfonamides **5** and **8**.

Comp.	LD$_{50}$ mg kg^{-1}	Analgesic effect, %				Anticon-vulsant effect,%	Tranquili-zing effect, %	Antihypoxic effect, %
		Time after the injection, min						
		30	60	90	120			
5	734±80.8	+111	+145	+127	+116	+50	+127	+13
8	500±52.2	+31	+29	+124	+83	+49	+35	–
Sodium metamizole	–	+127	+72	–	–	+20	+43	–

Analgesic effect of sulfonamide **5** is prolonged (even after 2 hours analgesic effect remains at the level 116%) and significantly exceeds analogue (sodium metamizole). In addition, the compound **5** has the moderate anticonvulsant (50%) and significant tranquilizing effects (127%). Such instances may lead to increased resistance to oxygen deficiency, however, anti-hypoxic activity is low (only 13%). Adamantane-containing analogue **8** has a moderate and short-term analgesic activity, moderate tranquilizing and anticonvulsant effects. Results of research are summarized in Table 2. The title sulfonamides are water-soluble, which may be important for further research of their biological activity.

Experimental

Solvents were dried and distilled immediately prior to use. Commercially available reagents were used as purchased. Melting points were determined in open capillaries and are uncorrected. Analytical thin layer chromatography was carried out on Silufol UV-254 precoated plates using ethyl acetate and 2-propanol as eluents; the plates were visualized with iodine vapors. Flash chromatography was performed with Merck silica gel 60 (40–63 µm). FT-IR spectra were recorded on Spectrum One (Perkin Elmer) or Nicolet iS10 spectrometers using KBr pellets, absorption maxima (ν_{max}) are reported in wavenumbers (cm^{-1}). The NMR spectra were measured in the indicated solvents with either a 400 or 500 MHz Bruker spectrometers. Chemical shifts are reported in parts per million (ppm) with respect to the solvent residual signal (CDCl$_3$ ^{1}H: δ=7.26 ppm, ^{13}C: δ=77.16 ppm; DMSO-d_6 ^{1}H: δ=2.50 ppm, ^{13}C: δ=39.52 ppm; (CD$_3$)$_2$CO ^{1}H: δ=2.05 ppm, ^{13}C: δ=206.26 ppm). Coupling constants (*J*) are expressed in Hertz (Hz), and spin multiplicities are given as s (singlet), d (doublet), dd (doublet of doublets), t (triplet), q (quartet), qd (quartet of doublets), dt (doublet of triplets), ddd (doublet of doublets of doublets), m (multiplet) and br.s (broad singlet). NOE spectroscopic data were recorded using Bruker AVB 500 spectrometer (500 MHz, gradient NOE T_{mix}=800 msec). Low resolution mass-spectrum of compound **5** were recorded on Varian 1200L spectrometer with 70 eV electron impact ionization (EI). Elemental analysis (C, H, N) were carried out using a Carlo Erba microanalyzer. *trans*-4-Bromotetrahydrothiophene-3-ol-1,1-dioxide was prepared according to literature method.[9]

Bis-*trans*-4-hydroxy-1,1-dioxidotetrahydro-3-thienylimidothio-carbamate sulfate, 3

Thiourea 3.80 g (0.05 mol) was stirred with 2.50 g (1.36 ml, 0.025 mol) 98% sulfuric acid in 25 ml water at 60-70 °C

until complete dissolution of thiourea, then 6.70 g (0.05 mol) 3,4-epoxytetrahydrothiophene-1,1-dioxide was added and stirred at the same temperature for 2 h. The reaction mixture was cooled to 5 °C, the white salt **3** was filtered and washed with several portions of cold water. Yield 10.75 g (83%), m.p. 191-192 °C (dec). For IR and elemental analysis data see.[10] ^{1}H NMR ((CD$_3$)$_2$SO, 400MHz): δ 3.11 (dd, 1H, H^{5a}, $^2J_{5a,5b}$ 13.4 Hz, $^3J_{5a,4}$ 6.6 Hz), 3.40 (dd, 1H, H^{2a}, $^2J_{2a,2b}$ 13.7 Hz, $^3J_{2a,3}$ 8.9 Hz), 3.63 (dd, 1H, H^{5b}, $^2J_{5a,5b}$ 13.4 Hz, $^3J_{5b,4}$ 6.9 Hz), 3.80 (dd, 1H, H^{2b}, $^2J_{2a,2b}$ 13.7 Hz, $^3J_{2b,3}$ 7.6 Hz), 4.28 (m, 1H, H^3), 4.43 (m, 1H, H^4), 5.41 (br.s, 1H, OH), 8.75 (br.s, 4H, C=NH and –NH$_3$$^+$) ppm. ^{13}C NMR ((CD$_3$)$_2$SO, 100 MHz): δ 46.4 (C^3), 55.0 (C^2), 57.6 (C^5), 71.3 (C^4), 95.4 (C=NH) ppm.

***trans*-4-Hydroxytetrahydrothiophene-3-sulfonyl chloride-1,1-dioxide, 1**

Method A. Chlorine gas was passed through the stirred mixture of 10.00 g (0.019 mol) bis-*trans*-4-hydroxy-1,1-dioxidotetrahydro-3-thienyl imidothiocarbamate sulfate **3** in 40 ml ethyl acetate and 40 ml water at 5-10 °C (ca. 7-8 h). The reaction mixture was concentrated to half-volume *in vacuo* and cooled to -20 °C. The white solid **1** was filtered and washed with small portion of water. Yield 6.16 g (68 %), m.p. 105-108 °C (lit. m.p. 121-122 °C from ethyl acetate[7]), R$_f$ 0.27 (2-propanol). For IR and elemental analysis data see.[7] ^{1}H NMR ((CD$_3$)$_2$CO, 500 MHz): δ 3.37 (ddd, 1H, H^{5b}, $^2J_{5b,5a}$ 13.7 Hz, $^3J_{5b,4}$ 6.8 Hz, $^4J_{5b,2a}$ 1.4 Hz), 3.69 (ddd, 1H, H^{2b}, $^2J_{2a,2b}$ 14.4 Hz, $^3J_{2b,3}$ 8.5 Hz, $^4J_{2b,5a}$ 1.3 Hz), 3.82 (ddd, 1H, H^{5a}, $^2J_{5a,5b}$ 13.7 Hz, $^3J_{5a,4}$ 7.3 Hz, $^4J_{5a,2b}$ 1.3 Hz), 4.05 (ddd, 1H, H^{2a}, $^2J_{2a,2b}$ 14.4 Hz, $^3J_{2a,3}$ 9.4 Hz, $^4J_{2a,5b}$ 1.4 Hz), 4.99 (m, 1H, H^3), 5.19 (m, 1H, H^4) ppm. ^{1}H NMR (CDCl$_3$, 400 MHz): δ 3.29 (d, 1H, OH, $^3J_{OH,4}$ 6.8 Hz), 3.37 (ddd, 1H, H^{5b}, $^2J_{5b,5a}$ 14.1 Hz, $^3J_{5b,4}$ 5.3 Hz, $^4J_{5b,2a}$ 1.9 Hz), 3.63 (ddd, 1H, H^{2b}, $^2J_{2a,2b}$ 14.3 Hz, $^3J_{2b,3}$ 9.5 Hz, $^4J_{2b,5a}$ 0.9 Hz), 3.67 (ddd, 1H, H^{5a}, $^2J_{5a,5b}$ 14.1 Hz, $^3J_{5a,4}$ 7.3 Hz, $^4J_{5a,2b}$ 0.9 Hz), 3.83 (ddd, 1H, H^{2a}, $^2J_{2a,2b}$ 14.3 Hz, $^3J_{2a,3}$ 8.9 Hz, $^4J_{2a,5b}$ 1.9 Hz), 4.49 (m, 1H, H^3), 5.12 (m, 1H, H^4) ppm. ^{1}H NMR ((CD$_3$)$_2$SO, 400 MHz): δ 2.97 (dd, 1H, H^{5b}, $^2J_{5a,5b}$ 13.4 Hz, $^3J_{5b,4}$ 3.2 Hz), 3.18 (dd, 1H, H^{2b}, $^2J_{2a,2b}$ 13.5 Hz, $^3J_{2b,3}$ 6.2 Hz), 3.27 (m, 1H, H^4), 3.44 (dd, 1H, H^{2a}, $^2J_{2a,2b}$ 13.5 Hz, $^3J_{2a,3}$ 9.0 Hz), 3.46 (dd, 1H, H^{5b}, $^2J_{5a,5b}$ 13.4 Hz, $^3J_{5a,4}$ 6.0 Hz), 4.61 (m, 1H, H^3), 7.77 (br.s, 1H, OH) ppm. ^{13}C NMR ((CD$_3$)$_2$CO, 100 MHz): δ 52.7 (C^2), 58.4 (C^5), 68.7 (C^4), 76.9 (C^3). ^{13}C NMR ((CD$_3$)$_2$SO, 100 MHz): δ 52.5 (C^2), 57.5 (C^5), 62.5 (C^4), 68.6 (C^3) ppm.

Method B. Chlorine gas was passed through the 200 ml carbon tetrachloride at 0 °C until its consumption ceased (yellow solution, solubility of chlorine in the carbon tetrachloride at 0 °C at atmospheric pressure is 32 mol %).[11]

Mixture of 10.36 g (0.02 mol) salt **3** and 200 ml prepared solution of chlorine was stirred in 80 ml ethyl acetate/water (1:1) at 0-5 °C for 8 h. The white solid **1** was filtered. Yield 5.77 g (62 %).

trans-4-Chlorotetrahydrothiophene-3-ol-1,1-dioxide, 2

Method A.[12] A mixture of salt **3** 1.04 g (2 mmol), 1.2 ml 30% aqueous solution hydrogen peroxide (12 mmol), and 0.28 ml (4 mmol) thionyl chloride was stirred in acetonitrile 80 °C for 2 h. The white solid was filtered. The reaction mixture was quenched by adding water (10 ml), extracted with ethyl acetate (3 × 50 ml), and the extract dried with magnesium sulfate. The filtrate was evaporated *in vacuo* and recrystallized from ethyl acetate. Yield 0.06 g (18 %), m.p. 166-167 °C. For IR, ^{1}H NMR (80 MHz) and elemental analysis data see.[13] ^{1}H NMR ((CD$_3$)$_2$SO, 500 MHz): δ 3.12 (dd, 1H, H^{2b}, $^2J_{2a,2b}$ 13.8 Hz, $^3J_{3,2b}$ 3.6 Hz), 3.43 (dd, 1H, H^{5b}, $^2J_{5a,5b}$ 14.3 Hz, $^3J_{4,5b}$ 4.1 Hz), 3.55 (dd, 1H, H^{2a}, $^2J_{2a,2b}$ 13.8 Hz, $^3J_{3,2a}$ 5.8 Hz), 3.77 (dd, 1H, H^{5a}, $^2J_{5a,5b}$ 14.3 Hz, $^3J_{4,5a}$ 6.4 Hz), 4.51 (m, 1H, H^3), 4.62 (m, 1H, H^4), 6.33 (br.s, 1H, OH) ppm. ^{1}H NMR ((CD$_3$)$_2$CO, 500 MHz): δ 3.15 (dd, 1H, H^{2b}, $^2J_{2a,2b}$ 13.8 Hz, $^3J_{3,2b}$ 3.6 Hz), 3.35 (dd, 1H, H^{5b}, $^2J_{5a,5b}$ 14.2 Hz, $^3J_{4,5b}$ 4.2 Hz), 3.58 (dd, 1H, H^{2a}, $^2J_{2a,2b}$ 13.8 Hz, $^3J_{3,2a}$ 5.6 Hz), 3.80 (dd, 1H, H^{5a}, $^2J_{5a,5b}$ 14.2 Hz, $^3J_{4,5a}$ 6.3 Hz), 4.68 (m, 1H, H^4), 4.71 (m, 1H, H^3) ppm. ^{13}C NMR ((CD$_3$)$_2$SO, 100 MHz): δ 56.7 (C^2), 57.2 (C^5), 58.3 (C^4), 73.3 (C^3) ppm. ^{13}C NMR ((CD$_3$)$_2$CO, 100 MHz): δ 57.7 (C^2), 58.4 (C^5), 59.1 (C^4), 74.9 (C^3) ppm.

Method B.[8] A mixture *trans*-4-bromotetrahydro-thiophene-3-ol-1,1-dioxide 1.5 g (7 mmol) and 1.4 g (11.2 mmol) sodium sulfite in THF/EtOH/H$_2$O (1:2:2 v/v) was heated for 45 min under microwave irradiation (300 W). The reaction mixture was cooled to room temperature and volatile components were removed *in vacuo*. The residue was used in the next step without further purification. To a stirred suspension of sulfonate in anhydrous benzene (50 ml) and DMF (0.7 ml) was added 1.3 ml (18.2 mmol) thionyl chloride and the mixture was heated at 60 °C for 3 h. The reaction mixture was quenched by adding water (20 ml) and evaporated *in vacuo*. The white solid **2** was recrystallized from ethanol. Yield 0.76 g (64 %).

General procedure for the synthesis of sulfonamides 4-9

To a stirred mixture of 5 mmol corresponding amine and 0.51 g (0.69 ml, 5 mmol) triethylamine in 20 ml dry ethyl acetate was added dropwise a solution of sulfochloride **1** (1.17 g (5 mmol) in 40 ml hot ethyl acetate. The reaction mixture was stirred at room temperature for 24 h. The solid was filtered and purified by flash column chromatography on silica (ethyl acetate/hexane 1:1 v/v).

trans-N-Benzyl-4-hydroxytetrahydrothiophene-3-sulfonamide 1,1-dioxide, 4

Yield 0.64 g (42 %), m.p. 109-112 °C, R$_f$ 0.64 (2-propanol). IR (cm^{-1}): 3442, 3347, 2938, 1341, 1286, 1162, 1126, 1053. ^{1}H NMR ((CD$_3$)$_2$SO, 400 MHz): δ 3.16 (m, 1H, H^{2b}), 3.27-3.66 (m, 3H, H^{2a}, H^{5a,b}), 3.91 (m, 1H, H^3), 4.22 (s, 2H, CH$_2$), 4.75 (m, 1H, H^4), 6.05 (br.s, 1H, OH) 7.35 (m, 5H, Ph) ppm. Anal. calcd. for C$_{11}$H$_{15}$NO$_5$S$_2$: C, 43.26; H, 4.95; N, 4.59 %. Found: C, 43.31; H, 4.91; N, 4.72 %.

trans-N-(Bicyclo[2.2.1]hept-5-en-*endo*-2-ylmethyl)-4-hydroxy-tetrahydrothiophene-3-sulfonamide-1,1-dioxide, 5

Yield 0.71 g (44 %), m.p. 188-190 °C, R$_f$ 0.45 (2-propanol). IR (cm^{-1}): 3437, 3275, 3034, 1648, 1522, 1328, 1289, 1174, 1129, 1048, 725. ^{1}H NMR ((CD$_3$)$_2$SO, 500 MHz): δ: 0.54 (ddd, 1H, H$^{3'n}$, $^2J_{3'n,3'x}$ 11.6 Hz, $^3J_{3'n,2'}$ 4.1 Hz, $^4J_{3'n,7's}$ 2.7 Hz), 1.24 (d, 1H, H$^{7'a}$), 1.36 (d, 1H, H$^{7's}$, $^2J_{7's,7'a}$ 7.5 Hz), 1.85 (ddd, 1H, H$^{3'x}$, $^2J_{3'n,3'x}$ 11.6 Hz, $^3J_{3'x,2'}$ 8.5 Hz, $^3J_{3'x,4'}$ 3.5 Hz), 2.26 (m, 1H, H$^{2'}$), 2.43 (d, 1H, H$^{8'a}$, $^2J_{8'a,8'b}$ 10.8 Hz), 2.50 (m, 1H, H$^{8'b}$), 2.80 (m, 1H, H$^{1'}$), 2.90 (m, 1H, H$^{4'}$), 2.98, 3.21, 3.30, 3.43, 3.47 (m, 5H, H^3, H^{2a,b}, H^{5a,b}), 4.62 (m, 1H, H^4), 5.38 (br.s, 1H, OH), 5.99 (dd, 1H, H$^{6'}$, $^3J_{5',6'}$ 5.6 Hz, $^3J_{1',6'}$ 2.8 Hz), 6.20 (dd, 1H, H$^{5'}$, $^3J_{5',6'}$ 5.6 Hz, $^3J_{4',5'}$ 3.0 Hz), 7.68 (br.s, 1H, NH) ppm. ^{13}C NMR ((CD$_3$)$_2$SO, 125 MHz): δ 29.8 (C$^{3'}$), 36.7 (C$^{2'}$), 41.9 (C$^{4'}$), 42.8 (C$^{1'}$), 43.4 (C$^{8'}$), 49.1 (C$^{7'}$), 52.5 (C^2), 57.5 (C^5), 62.5 (C^3), 68.5 (C^4), 131.8 (C$^{6'}$), 138.0 (C$^{5'}$) ppm. EI-MS, m/z (I, %): 67 (46.1), 66 (22.8), 56 (100), 54 (14.9). Anal. calcd. for C$_{12}$H$_{19}$NO$_5$S$_2$: C, 44.84; H, 5.96; N, 4.36 %. Found: C, 44.95; H, 6.10; N, 4.31 %.

trans-N-(Bicyclo[2.2.1]hept-5-en-*exo*-2-ylmethyl)-4-hydroxy-tetrahydrothiophene-3-sulfonamide-1,1-dioxide, 6

Yield 0.76 g (45 %), m.p. 179-182 °C, R$_f$ 0.40 (2-propanol). IR (cm^{-1}): 3380, 3351, 3025, 2962, 1633, 1435, 1319, 1280, 1213, 1190, 1137, 1118, 1060, 717. ^{1}H NMR ((CD$_3$)$_2$SO): δ 0.54 (d, 1H, H$^{3'n}$, $^2J_{3'n,3'x}$ 10.8 Hz), 1.29 (d, 1H, H$^{7'a}$), 1.34 (d, 1H, H$^{7's}$, $^2J_{7's,7'a}$ 7.4 Hz), 1.59 (m, 1H, H$^{3'x}$), 1.84 (m, 1H, H$^{2'}$), 2.29 (m, 1H, H$^{8'a}$), 2.40 (m, 1H, H$^{8'b}$), 2.81 (m, 2H, H$^{1'}$, H$^{4'}$), 2.97 (m, 1H, H^{2b}), 3.16-3.49 (4H, H^{2a}, H^{5a,b}, H^3), 4.61 (m, 1H, H^4), 5.47 (br.s, 1H, OH), 6.09 (m, 2H, H$^{5',6'}$) 8.00 (br.s, 1H, NH). Anal. calcd. for C$_{12}$H$_{19}$NO$_5$S$_2$: C, 44.84; H, 5.96; N, 4.36 %. Found: C, 44.78; H, 5.98; N, 4.40 %.

trans-N-(1-{Bicyclo[2.2.1]heptan-2-yl}ethyl)-4-hydroxytetra-hydrothiophene-3-sulfonamide 1,1-dioxide, 7

Yield 1.51 g (86 %), m.p. 107-111 °C, R$_f$ 0.79 (2-propanol). IR (cm^{-1}): 3420, 3315, 3068, 2935, 1703, 1516, 1455, 1415, 1320, 1167. ^{1}H NMR ((CD$_3$)$_2$SO, 400 MHz) : δ 0.64 (d, 1H, H$^{3'n}$, $^2J_{3'n,3'x}$ 11.0 Hz), 1.07 (m, 3H, CH$_3$), 1.22-1.33 (m, 4H, H$^{5'n}$, H$^{6'n}$, H$^{7'a}$, H$^{7's}$), 1.45 (m, 3H, H$^{2'}$, H$^{5'x}$, H$^{6'x}$), 1.81 (m, 1H, H$^{3'x}$), 2.78 (m, 1H, H$^{4'}$), 2.81 (m, 1H, H$^{1'}$), 3.16-3.48 (m, 5H, H^{2a,b}, H^{5a,b}, H^3), 4.61 (m, 1H, H^4), 5.36 (br.s, 1H, OH), 8.12 (br.s, 1H, NH). Anal. calcd. for C$_{14}$H$_{26}$NO$_5$S$_2$: C, 47.70; H, 7.43; N, 3.97 %. Found: C, 47.77; H, 7.39; N, 3.86 %.

trans-N-1-Adamantyl-4-hydroxytetrahydro-thiophene-3-sulfonamide-1,1-dioxide, 8

Yield 1.52 g (87 %), m.p. 245-250 °C, R$_f$ 0.76 (2-propanol). IR (cm^{-1}): 3445, 2914, 1517, 1378, 1297, 1197, 1175, 1120, 1048. ^{1}H NMR ((CD$_3$)$_2$SO, 400 MHz): δ 1.75 (s, 12H, CH$_2^{Ad}$), 2.10 (s, 3H, CH^{Ad}), 3.15-3.50 (m, 5H, H^{2a,b}, H^{5a,b}, H^3), 4.61 (m, 1H, H^4) 5.45 (br.s, 1H, OH), 7.70 (br.s, 1H, NH). Anal. calcd. for C$_{15}$H$_{26}$NO$_5$S$_2$: C, 49.43; H, 7.19; N, 3.84 %. Found: C, 49.38; H, 7.13; N, 3.96 %.

trans-N-(1-Adamantylmethyl)-4-hydroxytetrahydrothiophene-3-sulfonamide-1,1-dioxide, 9

Yield 1.11 g (61 %), m.p. 163-165 °C, R_f 0.73 (2-propanol). IR (cm^{-1}): 3434, 3362, 2903, 2677, 2495, 1751, 1519, 1319, 1196, 1039. ^{1}H NMR ((CD$_3$)$_2$SO, 400 MHz): δ 1.51 (s, 12H, CH$_2^{Ad}$), 1.96 (s, 3H, CH^{Ad}), 2.99-3.08 (m, 2H, NHCH$_2$), 3.16-3.50 (m, 5H, H^{2a,b}, H^{5a,b}, H^3), 4.61 (m, 1H, H^4), 5.40 (br.s, 1H, OH), 8.10 (br.s, 1H, NH). Anal. calcd. for C$_{15}$H$_{25}$NO$_5$S$_2$: C, 49.56; H, 6.93; N, 3.85 %. Found: C, 49.68; H, 6.89; N, 3.92 %.

In vivo tests: The neurotropic activity of the newly synthesized compounds **5** and **8** was studied on a mice of both sexes weighing 20-30 g. The room temperature was maintained within the limits 21±2 °C. Solutions of compounds in aqueous suspensions of the remaining substances, prepared with the addition of Tween-40, were introduced intraperitoneally 30 min before the test. The same volume of the sodium chloride isotonic solution was injected into the control animals. The effect of the substances injected in the doses of 1/10 LD$_{50}$ was compared in groups of animals, consisting of 6 individuals. The experimental data were treated statistically. The mean values of LD$_{50}$ for 12 observations were determined by a rapid method given in.[14] The arithmetical means and their standard deviations ($M\pm m$) were calculated to assess the average duration of the anesthetic effect of the hexenal stereotypy, the protective properties in the corazol spasms and hypoxia. The significance of differences between mean values were assessed by Student's criterion: differences were considered as significant at a probability level $p < 0.05$. The effect of the substances on the central nervous system was estimated: (*a*) from the analgesic effect, determined by the "hot plate" method at 55 °C; (*b*) from the corazol spasms caused by the intravenous titration with 10% corazol solution at a rate of 0.01 ml/sec; (*c*) from the influence on the duration of the hexenal anesthesia (60 mg/kg); (*d*) from the influence of the life time of animals under hypoxic hypoxia, created by placing the mouse in a separate chamber with a volume of 125 ml without absorption of CO$_2$. The acute toxicity was determined by the intraperitoneal injection of the investigated substances and by establishing the lethal dose (LD$_{50}$).

Conclusion

In summary, we have described a convenient method for the synthesis of small library water soluble sulfolane-containing cage sulfonamides, starting from easily available 3,4-epoxysulfolane. For the first time the NOE and 2D NMR spectra of sulfochloride **1** and chlorohydrine **2** has been studied in detail and confirmed their *trans*-structure. Sulfonamide **5** can be used as a lead compound in the future biological studies. The title compounds, which are not easily accessible by other means, are poised for subsequent functionalization and should offer great opportunities as building blocks in synthesis, and particularly in the elaboration of chemical libraries of cage sulfonamides for pharmaceutical industry (*e.g.* provide better coverage of the chemical space). Further research on the synthetic and medicinal applications of this compounds is ongoing and the results will be reported in due course.

References

[1]Ruggy, G., *Ohio J. Sci.*, **1945**, *45*, 115; Seydel, J. K., *J. Pharm. Sci.* **1968**, *57*, 1455.

[2]Shah, S. S. A., Rivera, G., Ashfaq, M., *Mini-Rev. Med. Chem.* **2013**, *13*, 70 and references therein.

[3]Ding, H. X., Liu, K. K.-C., Sakya, S. M., Flick, A. C., O'Donnell, C. J., *Bioorg. Med. Chem.* **2013**, *21*, 2795; Graul, A. I., Lupone, B., Cruces, E., Stringer M., *Drugs Today.* **2013**, *49*, 33.

[4]Oliver, D. W., Malan, S. F., *Med. Chem. Res.* **2008**, *17*, 137; Wanka, L., Iqbal, K., Schreiner, P. R., *Chem. Rev.* **2013**, *113*, 3516.

[5]Pal'chikov, V. A., Prid'ma, S. A., Tokar', A. V., Turov, A. V., Omel'chenko, I. V., Shishkin, O. V., Golodaeva, E. A., Kas'yan, L. I., *Russ. J. Org. Chem.* **2013**, *49*, 1122; Kas'yan, L. I., Pal'chikov, V. A., Prid'ma, S. A., Turov, A. V., Kas'yan, A. O., Mazepa, A. V., Rybalko, V. E., *Russ. J. Org. Chem.* **2011**, *47*, 994; Kas'yan, L. I., Prid'ma, S. A., Pal'chikov, V. A., Kas'yan, A. O., Turov, A. V., Tokar', A. V., Tret'yakov, S. V., *Russ. J. Org. Chem.* **2010**, *46*, 637; Kas'yan, L. I., Pal'chikov, V. A., Turov, A. V., Prid'ma, S. A., Tokar', A. V., *Russ. J. Org. Chem.* **2009**, *45*, 1007; Kas'yan, L. I., Prid'ma, S. A., Turov, A. V., Pal'chikov, V. A., Kas'yan, A. O., Karat, L. D. *Russ. J. Org. Chem.* **2009**, *45*, 505.

[6]Pal'chikov, V. A., *Bull. Dnipropetrovsk Univ., Ser. Chem.* **2010**, *18*, 63; Zlenko, H. T., Zarovnaya, I. S., Palchikov, V. A., *Eur. Psych.* **2013**, *28* (supp. 1), 1284; Zlenko, H. T., Palchikov, V. A., Prishlyak, I. S., *Eur. Psych.,* **2012**, *27* (supp. 1), 912; Zlenko, H. T., Palchikov, V. A., Tretjakov, S. V., *Eur. J. Pain Suppl.*, **2011**, *5*(1), 90; Zlenko, H., Kasyan, L., Palchikov, V., Prishlyak, I., *Eur. Arch. Psych. Clin. Neurosci.*, **2011**, *261* (suppl. 1), S88.

[7]Bezuglyi, Yu. V., Tukhar, A. A., Bezmenova, T. E., Bratunets, A. G., Shakhvorost, A. M., *Zh. Org. Khim. (USSR).* **1986**, *22*, 880; Tukhar, A. A., Bezuglyi, Yu. V., Foremnaya, V. P., Bratunets, A. G., Shakhvorost, A. M., *Chem. Heteroc. Comp.* **1989**, *25*, 393.

[8]Alapafuja, S. O., Nikas, S. P., Shukla, V. G., Papanastasiou, I., Makriyannis, A., *Tetrahedron Lett.*, **2009**, *50*, 7028.

[9]Ohno, M., Koide, N., Sato, H., Eguchi, S., *Tetrahedron.*, **1997**, *53*, 9075.

[10]Bezuglyi, Yu. V., Tukhar, A. A., Bezmenova, T. E., *Ukr. Khim. Zh.* **1982**, *48*, 1307.

[11]Schmittinger, P., Florkiewicz, T., Curlin, L.C., Lüke, B., Scannell, R., Navin, T., Zelfel, E., Bartsch, R., *Chlorine in Ullmann's Encyclopedia of Industrial Chemistry*, **2006**, 1.

[12]Bahrami, K., Khodaei, M. M., Soheilizad, M., *J. Org. Chem.,* **2009**, *74*, 9287.

[13]Novitskaya, N. N., Flekhter, B. V., Tolstikov, G. A., *Chem. Heterocycl. Comp.* **1977**, *13*, 843.

[14]Germane, S. K., Eberlinjsh, O. E., Kozhuhov, A. N. In: *Scientific and Methodological Aspects of Biological Study of Novel Drugs.* Zinatne, Riga, **1987**, 86.

STUDY ON THE HESPERIDIN – CYCLODEXTRINS INTERACTIONS BY THIN LAYER CHROMATOGRAPHY

Andreia Corciova[a]* and Bianca Ivanescu[b]

Keywords: hesperidin, cyclodextrin, thin layer chromatography, thermodynamics

In this study, the interaction of hesperidin with β-CD, HP-β-CD, β-CD sulfate was investigated by thin layer chromatography. The chromatographic conditions included: Kieselgel G_{25} stationary phase, mobile phase of butanol: acetic acid: water (4:1:5) and increasing concentrations of the three cyclodextrins. Visualization was performed by examination in UV light and by exposure to iodine vapors. Also, the thermodynamic parameters were calculated: the Gibbs free energy change (ΔG^0_{tr}), free energy change (ΔG^0), enthalpy change (ΔH^0) and entropy change (ΔS^0). The results show that the best inclusion capacity is obtained for HP-β-CD, the inclusion process is favored by increasing the concentration of cyclodextrin, and by increasing the temperature.

* Corresponding Authors
     E-Mail: acorciova@yahoo.com
[a]   University of Medicine and Pharmacy "Grigore T. Popa" Iasi, Faculty of Pharmacy, Department of Drugs Analysis, University Street 16, 700150 Iasi, Romania
[b]   University of Medicine and Pharmacy "Grigore T. Popa" Iasi, Faculty of Pharmacy, Department of Pharmaceutical Botany, University Street 16, 700150 Iasi, Romania

Introduction

Hesperidin (Figure 1) is a flavanone glycoside (hesperetin-7-rutinoside) and the most abundant flavonoid in citrus fruits. It is found in highest quantities in the peel and membranous parts of sweet orange and lemon. Hesperidin reduces the permeability and fragility of capillary walls and can be used in chronic venous insufficiency, haemorrhoids, varicose veins, various ulcers and bruising. Hesperidin also manifests other effects on the vascular system, such as: antihypercholesterolaemic, antihyperlypidemic, calcium channel blocker, antihypertensive and diuretic effects.[1]

Numerous studies confirm a significant antiinflammatory activity of hesperidin, both *in vivo* and *in vitro*, possibly through the inhibition of eicosanoid synthesis and/or antioxidant free radical scavenger activity. One study showed analgesic activity in mice on subcutaneous administration, exerted through a peripheral mechanism.[2]
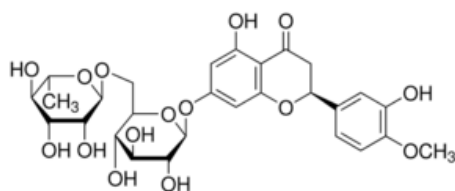
Figure 1. Hesperidine structure

Like most other flavonoids, hesperidin manifests antioxidant activity and radical scavenging properties. Lately, a considerable amount of research has been carried out on the anticarcinogenic activity of hesperidin against different human cancer cell lines, with remarkable results.[3] The sedative effect of hesperidine was also investigated, as the property to decrease bone density loss.[4,5]

Hesperidin has found to possess antibacterial, antifungal, antiviral properties, antiallergic and antianaphylactic activities. Further, it has been shown to inhibit platelet and cell aggregation and the activity of some enzymes (hyaluronidase, aldol reductase, aromatase). The aglycone, hesperetin, protects liposomes from UV-irradiation induced peroxidation and might be successfully employed as a topical photo-protective agent.[6]

Since hesperidin is poorly soluble in water it can be a challenge when using it in different pharmaceutical formulations. In order to increase the solubility of the substance, one of the most used methods is complexation with cyclodextrins, because the cyclodextrin - substance complex has the ability to change the physicochemical properties of the inclusion compound. Complexation can be defined as the formation of the reversible interaction between the active substance and cyclodextrin in order to form a new compound by means of intermolecular forces such as: covalent bonds, Van der Waals bonds, ion – dipole forces, dipole – dipole forces, hydrogen bonds. Some of the chemical and physical properties that can be modified during complexation include: increased stability and solubility of substances, protection against degradation, reduced gastric toxicity and irritancy, masking the unpleasant smell and taste, enhanced bioavailability of substances.[7]

The inclusion constants (K) and dissociation constants are a measure of changes in the physicochemical properties of a compound as a result of the inclusion process. The thermodynamic parameters, i.e. Gibbs free energy change (ΔG^0_{tr}), free energy change (ΔG^0), enthalpy change (ΔH^0) and entropy change (ΔS^0) can be calculated according to the effect of temperature on the stability constants of the complex.[8,9]

The interaction between the active compounds and cyclodextrins can be investigated by various analytical methods, such as: in solid state-thermal methods, IR spectroscopy, X-ray diffractometry, Scanning Electron Microscopy, Thin Layer Chromatography, in solution - electrochemical methods, spectroscopic methods (UV-Vis, NMR, RES, fluorescence).[7]

This study investigates the interaction between hesperidin and three types of cyclodextrins by thin layer chromatography, calculating the inclusion constants and the thermodynamic parameters of the inclusion process.[8-13]

Materials and method

Materials

Hesperidin, beta cyclodextrin (1135 g mol^{-1}), HP-β-CD (1460 g mol^{-1}) and β-CD-sulfated sodium salt (3277 g mol^{-1}) were obtained from Sigma-Aldrich (USA). Chromatographic plates were coated with silica gel G_{25} 0.25 mm (Sigma-Aldrich, Switzerland), 10 x 20 cm, 0.2 mm thickness. All the reagents and substances used were of analytical grade.

Methods

Chromatographic separation was achieved at room temperature by the ascending method. The mobile phase was butanol: acetic acid: water (4:1:5) containing different concentrations of cyclodextrin. The chromatographic plates were spotted with 20 µl solution containing 1 mg/ml hesperidin, at 2 cm distance from the bottom edge, and the separation chamber was saturated for 1 hour. The migration distance was 12 cm. Visualization was performed by examination in UV light and by exposure to iodine vapors. R_f values were calculated by the ratio between the distance covered by flavone and the distance covered by the mobile phase containing increasing concentrations of cyclodextrin.

Results and discussions

Figures 2-4 show the effect of different concentrations of cyclodextrin on the R_f values of hesperidin.
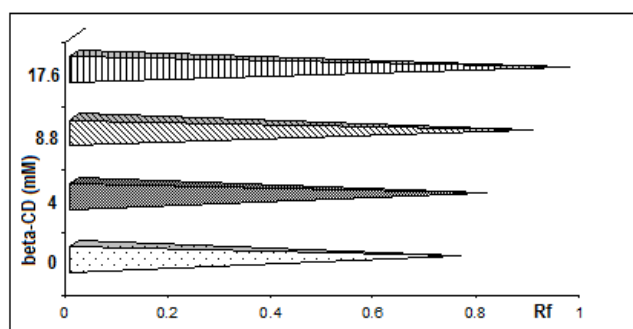
Figure 2. The effect of β-CD concentration on the R_f values of hesperidin

It is apparent that by raising the concentration of cyclodextrin in the mobile phase, the migration distance decreases and thus the value of R_f increases. The most obvious change in R_f values was observed for HP-β-CD, followed by β-CD and β-CD sulfate.
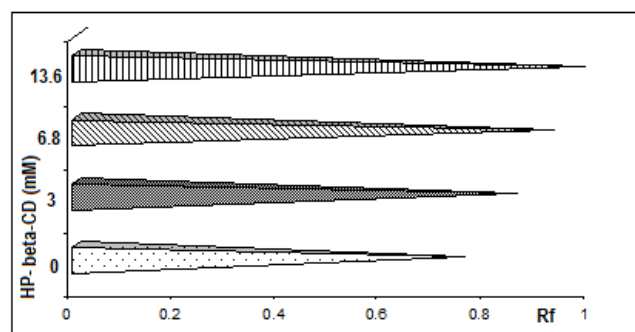
Figure 3. The effect of HP-β-CD concentration on the R_f values of hesperidin
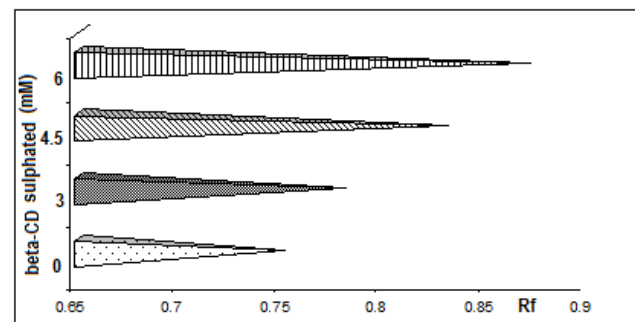
Figure 4. The effect of β-CD sulfate concentration on the R_f values of hesperidin

From the diagrams obtained, where the R_f values are expressed based on the concentrations of cyclodextrins, the inclusion constants (K) were calculated according to the formula:

$$K = (slope/intercept)*1000$$

Figure 5 shows a comparison between the values of inclusion constants depending on cyclodextrins, and Figure 6 presents the values of dissociation constants ($1/k$) according to cyclodextrins.
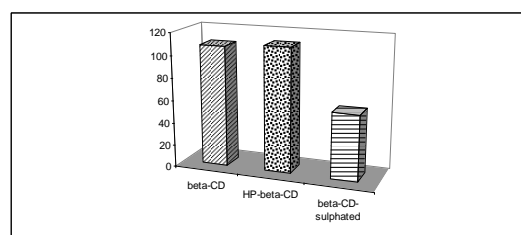
Figure 5. Inclusion constants of hesperidin depending on the cyclodextrin used
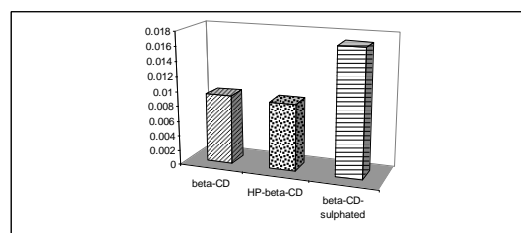
Figure 6. Dissociation constants of hesperidin depending on the cyclodextrin used

From the above figures it appears that the inclusion capacity decreases in order of HP-β-CD> β-CD> β-CD sulfate and HP-β-CD and β-CD compounds are more stable than those with β-CD sulfate. In order to determine the effect of temperature on the inclusion process, the values of inclusion constants were calculated at increasing temperatures: 293 K, 303 K and 313 K (Figures 7-9).
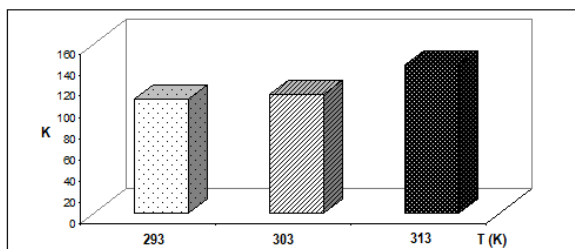
Figure 7. The effect of temperature on inclusion constants of hesperidin in β-CD
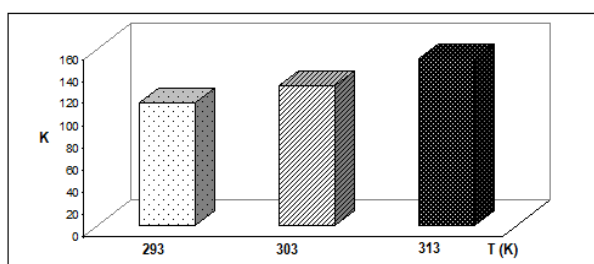
Figure 8. The effect of temperature on inclusion constants of hesperidin in HP-β-CD
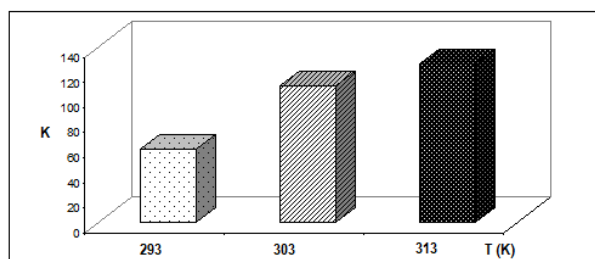
Figure 9. The effect of temperature on inclusion constants of hesperidin in β-CD sulfate

The values of inclusion constants rise with the increasing temperature, which indicates that the high temperature favors the inclusion process. Also, the thermodynamic parameters were calculated: Gibbs free energy change (ΔG^0_{tr}) (Table 1), free energy change (ΔG^0) (Table 2), enthalpy change (ΔH^0) and entropy change (ΔS^0) (Table 3), using the following equation:

$$\Delta G^0_{tr} = -RT \log \frac{R_f}{R_{f0}}$$

where

R = gas constant

T = absolute temperature of the reaction

R_f/R_{f0} = the ratio between the R_f values of hesperidin with CD and the R_f values of hesperidin without CD.

$$\Delta G^0 = - 2.303 RT \log K,$$

where

K = inclusion constant of the complex made

Table 1. ΔG^0_{tr} (kJ mol^{-1}) values depending on CD concentration

	CD concentration, mM	ΔG^0_{tr}, kJ mol-1		
		293 K	303 K	313 K
β-CD	4	- 0.068	0.239	0.703
	8.8	- 0.178	0.155	0.523
	17.6	- 0.258	0.042	0.453
HP-β-CD	3	- 0.13	0.681	0.546
	6.8	- 0.212	0.506	0.43
	13.6	- 0.280	- 0.082	0.307
β-CD sulfate	3	- 0.041	0.314	0.569
	4.5	- 0.106	0.222	0.322
	6	- 0.154	0.120	0.345

Negative values of ΔG^0_{tr} indicates advantageous conditions for migration of hesperidin in the presence of cyclodextrin, especially for HP-β-CD. Values decline with increasing concentrations of CD, which demonstrates that the reaction becomes more favorable with larger CD concentrations. However, at greater temperature the ΔG^0_{tr} values become positive, which indicates that a higher temperature is unfavorable for the migration of hesperidin along the stationary phase.

Table 2. ΔG^0 (kJ mol^{-1}) values depending on temperature

Temperature	293 K	303 K	313 K
β-CD	- 11.28	- 11.76	- 12.73
HP-β–CD	- 11.35	- 12.08	- 12.93
β-CD sulfate	- 9.79	- 11.71	- 12.46

Negative values of ΔG^0 show that the inclusion process takes place spontaneously. Given the van't Hoff equation and plotting log K vs $1/T$, the slope will give us the value of enthalpy change (ΔH^0):

$$Slope = \frac{\Delta H_0}{2.303 R}$$

The standard entropy change (ΔS^0) for the complexation reactions was calculated using the equation:

$$\Delta G^0 = \Delta H^0 - T \Delta S^0$$

Positive ΔH^0 values indicate an endothermic process and positive ΔS^0 values can be attributed to the transfer of hesperidin into the cyclodextrin cavity and to the formation of hydrophobic bonds.

Table 3. ΔS^0 (J mol^{-1} K^{-1}) and ΔH^0 (kJ mol^{-1}) values depending on the cyclodextrin used

	ΔS^0	ΔH^0
β-CD	0.042	1.10
HP-β–CD	0.043	1.28
β-CD sulfate	0.044	3.21

Conclusions

The present paper analyzed the interaction between hesperidin and β-CD, HP-β-CD and β-CD sulfate by thin layer chromatography. The results show that, the reaction between hesperidin and cyclodextrins with the formation of inclusion compounds is an endothermic and spontaneous process, and is more effective at increasing temperatures and CD concentrations. The best inclusion and more stable compounds were obtained with HP-β-CD.

Acknowledgements

References

[1] Garg, A., Garg, S., Zaneveld, L. J. D., Singla, A. K., *Phytother Res.,* **2001**, *15*, 655–69.

[2] Galati, E. M., Monforte, M. T., Kirjavainen, S., Forestieri, A.M., Trovato, A., Tripodo, M. M., *Farmaco,* **1994**, *40*, 709–712.

[3] Al-Ashaal, H. A., El-Sheltawy, S. T., *Pharm. Biol.*, **2011**, *49*, 276-282.

[4] Guzmán-Gutiérrez, S. L., Navarrete, A., *Planta Med.*, **2009**, *75*, 295–301.

[5] Chiba, H., Ueharam, M., Wu, J., Wang, X., Masuyama, R., Suzuki, K., Kanazawa, K., Ishimi, Y., *J. Nutr.*, **2003**, *133*, 1892–1897.

[6] Kuntić, V., Brborić, J., Holclajtner-Antunović, I., Uskoković-Marković, S., *Vojnosanit. Pregled.* **2014**, *71*, 60-65

[7] Anjana, M. N., Sreeja, C. N., Jipnomon, J., *Int. J. Pharm. Pharm. Sci.,* **2013**, *5*, 54-58.

[8] Guo, X., Shuang, S., Wang, X., Dong, C., Pan, J., Aboul-Enein, H. Y., *Biomed. Chromatogr.*, **2004**, *18*, 559–563.

[9] Hadžiabetdić, J., Elezović, A., Rahić, O., Mujezin, I., *Am. J. Anal. Chem.*, **2012**, *3*, 811-819.

[10] Hostettmann, K., Lederer, M., Marston, A., Leipzig-Pagani, E., *Phytochem. Anal.*, **1997**, *8*, 173–175.

[11] Hostettmann, K., Lederer, M., Marston, A., *Phytochem. Anal.,* **2000**, *11,* 380–382.

[12] Nikolova, M., Berkov, S., Ivancheva, S., *Acta Chromatogr.*, **2004**, *14*, 110-114.

[13] Nahla Nour El-Din Ahmed Salama, *J. Planar Chromatogr.-Mod. TLC*, **2008**, *21*, 441-44

CRYSTAL STRUCTURE OF 3,3,6,6-TETRAMETHYL-9-(3-CHLOROPHENYL)-3,4,6,7,9,10-HEXAHYDROACRIDINE-1,8-DIONE-DMF SOLVATE

Dalbir Kour,[a] D. R. Patil,[b] Madhukar B. Deshmukh,[b] and Rajni Kant[a]*

The crystal structure of dimethylformamide solvated 3,3,6,6-tetramethyl-9-(3-chlorophenyl)-3,4,6,7,9,10-hexahydroacridine-1,8-dione ($C_{26}H_{33}ClN_2O_3$) crystallizes in the triclinic space group P-1 with unit cell parameters: a=9.0814(4), b=11.5650(5), c=12.1354(5) Å, α=91.806(3)º, β=96.450(3)º, γ= 104.565(4)º and Z=2. The crystal structure was solved by direct methods and refined by full-matrix least-squares procedures to a final *R*-value of 0.056 for 2691 observed reflections. The central ring of the acridinedione system adopts a *boat* conformation and the two outer rings adopt *sofa* conformations. The solvent moiety (dimethylformamide) is involved in the existence of intra and intermolecular C-H...O interactions.

* Corresponding Authors
    Fax: +91 191 243 2051
    E-Mail: rkvk.paper11@gmail.com
[a]   X-ray Crystallography Laboratory, Post-Graduate
    Department of Physics & Electronics,
University of Jammu, Jammu Tawi - 180 006, India.
[b]   Department of Chemistry, Shivaji University, Kolhapur - 416
    004 (MS), India.

Introduction

A multicomponent reaction (MCR) provides influential implement for the synthesis of complex molecules by reacting three or more small bulding blocks. MCRs are economic, selective, minimizing waste, time and power, eco-friendly in organic synthesis.[1-3] Acridinediones containing a 1,4-DHP nucleus are used as laser dyes with very high efficiencies of photo initiators.[4,5] A latest literature review reveals that 1,4-DHP nucleus exhibit Calcium channels blockers and anti-aggregratory activity. Besides this, 1,4-DHP skeleton shows many biological activities such as anti-hypertension, anti-cancer, anti-diabetics, geroprotective, neuroprotactant and anti-HIV.[6]

Synthesis of 1,8-dioxoacridinedione is usually carried out by MCRs of active methylene compound, aldehydes and ammonium acetate or primary amine.[7-8] In continuation of our current endeavor on multicomponent reactions, we disclose herein report for the synthesis and structures of 3,3,6,6-tetramethyl-9-(3-chlorophenyl)-3,4,6,7,9,10-hexa-hydroacridine-1,8- dione (Scheme **1**).
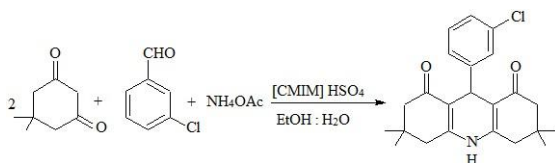
Scheme 1. Synthesis of title compound **I**.

Experimental

All the chemicals were purchased from SD Fine Chem Limited and Thomas Baker, used as received without further purification. Melting point was determined on Labstar melting apparatus. The IR spectra was run on a Perkin-Elmer, FTIR-1600 spectrophotometer and expressed in cm⁻¹ (KBr). ¹H NMR spectra was recorded on Bruker Avance (300 MHz) spectrometer in DMSO-d₆ using TMS as the internal standard. Elemental analysis was performed on a EURO-EA elemental analyzer.

Synthesis

In a 50 ml rounded bottom flask, a mixture of dimedone (2 mmol), 3-chlorobenzaldehyde (1 mmol) and ammonium acetate (1.2 mmol) in mixture of aqueous ethanol (5 ml) was stirred at RT for 5 min. To this [CMIM][HSO₄] (20 mol %) was added and the reaction mixture heated at 85 °C till completion of reaction. The progress of reaction was monitored by TLC. After completion of reaction, the mixture was gradually cool to RT and poured on ice water under stirring, solid were precipitate out. Filter the product and dried. The crude product were recrystallized from ethanol and characterized by IR, ¹H NMR, elemental and single crystal analysis. M.P.: > 300 °C, Yield: 80 %. IR (KBr): 3413, 3269, 2945, 1638, 1602 cm⁻¹. ¹H NMR (300 MHz, DMSO-d₆): δ 0.90(s, 6H, CH₃), 1.02(s, 6H, CH₃), 2.03-2.52(m, 8H, CH2), 4.85(s, 1H, CH), 7.10-7.31(m, 4H. Ar-H), 9.48(bs, 1H, NH). Analysis: calculated for $C_{23}H_{26}ClNO_2$ (383.911): C, 71.96 %; H, 6.83 %; N, 3.65 %; found: C, 71.91 %; H, 7.79 %; N, 3.70 %.

Crystal Structure Determination and Refinement

The X-ray intensity data of a well defined crystal (0.30 x 0.20 x 0.10 mm) were collected at room temperature (293 K) by using a CCD area-detector diffractometer (*X'calibur system – Oxford diffraction, 2010*) which is equipped with graphite monochromated MoKα radiation (λ=0.71073 Å).

The cell dimensions were determined by the least-squares fit of angular settings of 4587 reflections in the θ range 3.52 to 29.01°. A total number of 11110 reflections were collected of which 2691 reflections were treated as observed ($I > 2\sigma(I)$). Data were corrected for Lorentz, polarization and absorption factors.

The structure was solved by direct methods using SHELXS97.[9] All non-hydrogen atoms of the molecule were located from the E-map. Full-matrix least-squares refinement was carried out by using SHELXL97 software.[9] The geometry of the molecule is determined by PLATON.[10] All the hydrogen atoms were positioned geometrically and were treated as riding on their parent C/N atoms, with C-H distances of 0.93-0.98 Å and N-H distance of 0.84 Å; and with $U_{iso}(H) = 1.2U_{eq}(C/N)$, except for the methyl groups where $U_{iso}(H) = 1.5U_{eq}(C)$. The final refinement cycles yielded an *R*- factor of 0.056 ($wR(F^2) = 0.1473$) for the observed data. The residual electron density ranges from -0.355 to 0.185 eÅ⁻³.

Atomic scattering factors were taken from International Tables for X-ray Crystallography (1992, Vol. C, Tables 4.2.6.8 and 6.1.1.4). The crystallographic data are summarized in Table 1. CCDC-981749 contains the supplementary crystallographic data for this paper.

Table 1. Crystal data and other experimental details for (**1**)

CCDC	981749
Crystal description	Yellow block
Crysatl size	0.30x0.20x0.10
Emperical Formula	$C_{26}H_{33}Cl\,N_2O_3$
Formula weight (g mol⁻¹)	456.99
Radiation, Wavelength (Å)	Mo *K*α, 0.71073
Unit cell dimensions	a = 9.0814(4),
	b = 11.5650(5),
	c = 12.1354(5) Å,
	α= 91.806(3)°,
	β = 96.450(3)°,
	γ = 104.565(4)°
Crystal system, Space group	triclinic, P-1
Unit cell volume (Å³)	1223.40(9)
No. of molecules per unit cell, *Z*	2
No. of parameters refined	299
Absorption coefficient (mm⁻¹)	0.185
F(000)	488
θ range for entire data collection (º)	3.53 <θ < 26.00
Limiting indices	−11 ≤ *h* ≤ 11,
	−14 ≤ *k* ≤ 14,
	−14 ≤ *l* ≤ 13
Reflections collected/unique	11110 /4803
Reflections observed (*I*>2σ(*I*))	2691
Final *R*-factor	0.056
$wR(F^2)$	0.1473
Goodness-of-fit	1.024
$(\Delta/\sigma)_{max}$	0.001
Final residual electron density (eÅ⁻³)	-0.355< Δρ < 0.185

Results and discussion

An ORTEP view of the molecule with atomic labeling is shown in Figure 1.[11] Its geometry was calculated using the PLATON[10] and PARST[12] software. Bond lengths[13] and angles have normal values (Table 2) and correspond to those observed in some related structures.[14,15]
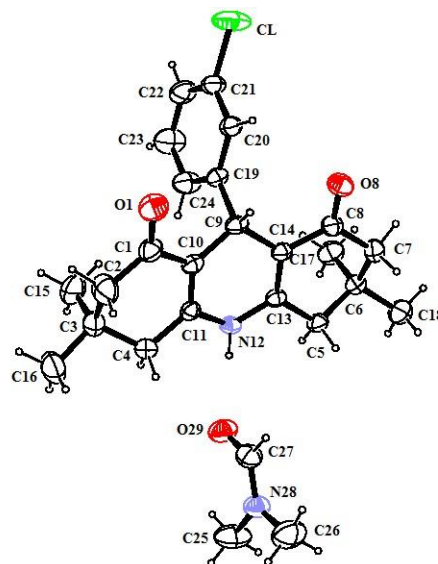
Figure 1. ORTEP view of the molecule with displacement ellipsoids drawn at the 50 % probability level. H atoms are shown as small spheres of arbitrary radii.

The central ring (C9/C10/C11/N12/C13/C14) of the acridinedione moiety adopts a *boat* conformation [ΔCs(C9)=0.66 & ΔCs (C10-C11)=7.12] and the four essentially planar atoms (C10/C11/C13/C14) of this ring [maximum deviation 0.1077 (2) Å for C9] form a dihedral angle of 82.06 (8)º with benzene ring. In this ring, N12 and C9 deviate from plane (C10/C11/C13/C14) by 0.0725 (2) and 0.1077 (2) Å, respectively. Both the outer rings adopt *sofa* conformations (ΔCs (C3) = 0.852; ΔCs (C6) = 3.482).[16] The atoms C3 and C6 deviate from the mean planes defined by (C1, C2, C4, C11, C10) and (C5, C7, C8, C14, C13) by 0.3328 (3) and 0.3345 (2) Å, respectively.

Table 2. Selected bond lengths (Å) and angles (°) for non hydrogen atoms (e.s.d.'s are given in parentheses) for (**1**)

Bond lengths		Bond angles	
Cl-C21	1.745(2)	C13- N12- C11	121.7(2)
O1- C1	1.228(3)	O1- C1- C10	120.5(2)
O8- C8	1.225(3)	O1- C1- C2	121.5(2)
N12- C13	1.373(3)	O8- C8- C14	121.2(2)
N12- C11	1.377(3)	O8- C8- C7	120.5(2)
C10- C11	1.352(3)	C10- C11- N12	120.3(2)
C13- C14	1.357(3)	N12- C11- C4	116.4(2)
O29- C27	1.215(3)	C14- C13- N12	120.6(2)
N28- C27	1.316(3)	N12- C13- C5	116.0(2)
N28- C25	1.438(3)	C27- N28- C25	120.6(2)
N28- C26	1.450(3)	C27- N28- C26	121.4(2)
		C25- N28- C26	118.0(2)
		O29- C27- N28	126.4(3)

Table 3. Geometry of intra- and inter molecular hydrogen bonds for (**1**)

D-H…A	D-H (Å)	H…A (Å)	D…A (Å)	θ[D-H…A(º)]	Symmetry code
N12-H12…O29	0.84	2.04	2.873	171	
C25-H25A…O29	0.96	2.37	2.781	105	
C5-H5A…O1	0.97	2.52	3.445	159	x+1,+y,+z
C15-H15B…O1	0.96	2.49	3.393	155	-x,-y+1,-z
C27-H27…O8	0.93	2.32	3.230	165	-x+1,-y+1,-z+1

A part of crystal structure is shown in Figure 2. In (I), molecules are connected to a dimeric formation via C15-H15B…O1 hydrogen bonds generating a R$_2^2$ (12) graph-set motif. The DMF solvent takes part in both intra (C25-H25...O29) and inter molecular (C27-H27...O8) interactions (Table 3).
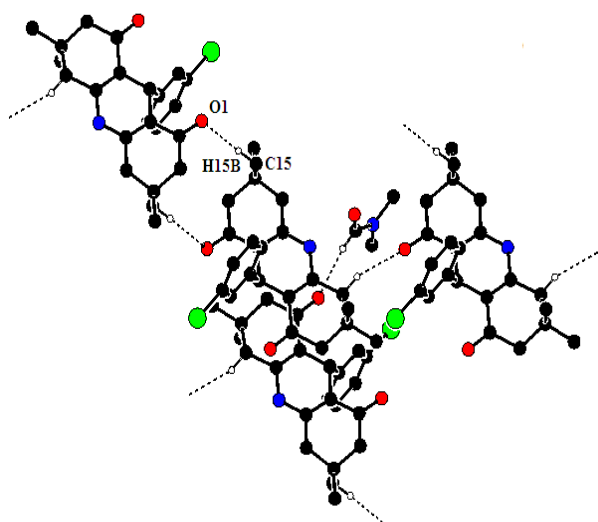
Figure 2. A part of crystal structure showing C-H….O intermolecular onteractions generating R$_2^2$(12) graph set motif

Acknowledgements

References

[1]Mistry, S. R., Maheria, K.C., *J. Mol. Catal. A*, **2012**, *355,* 210.

[2]Ganguly, C. N., Roy, S., Mondal, P., Saha, R., *Tetrahedron Lett*., **2012**, *53,* 7067.

[3]Khan, A.T., Das, D. K., *Tetrahedron Lett.*, **2012**, *53*, 2345.

[4]Kumar, S., Singh, K. N., *J. Heterocyclic Chem.*, **2011**, *48,* 69.

[5]Fan, X., Li, Y., Zhang, X., Qu, G., Wang, J., *Heteroatom. Chem.,* **2007**, *18(7)*, 786.

[6]Rajacka, A., Yuvaraju, K., Praveen, Murthy, Y. L. N., *J. Mol. Catal. A*, **2010**, *370*, 197.

[7]Kidwai, M., Bhatnagar, D., *Tetrahedron Lett.,* **2010,** *51*, 2700.

[8]Wang, G.-W., Miao, C.-B., *Green Chem.*, **2006,** *8*, 1080.

[9]Sheldrick, G. M., *Acta Cryst.*, **2008**, *A64*, 112.

[10]Spek, A. L., *Acta Cryst.*, **2009**, *D65*, 148.

[11]Farrugia, L. J., *J. Appl. Cryst.*, **2012**, *45*, 849.

[12]Nardelli, M., *J. Appl. Cryst*., **1995**, *28*, 659.

[13]Allen, F. H., Kennard, O., Watson, D. G., Brammer, L., Orphen, A. G., Taylor, R., *J. Chem. Soc. Perkin Trans. 2*, **1987**, S1-S19.

[14]Kant, R., Gupta, V. K., Kapoor, K., Patil, D. R., Patil, P. P., Deshmukh, M. B., *Acta Cryst.*, **2013a**, *E69*, o100.

[15]Kant, R., Gupta, V. K., Kapoor, K., Patil, D. R., Jagadale, S. D., Deshmukh, M. B., *Acta Cryst.*, **2013b**, *E69*, o101.

[16]Duax, W. L., Norton, D. A., *Atlas of Steroid Structures*, New York: Plenum Press, **1975**, 1.

CYTOTOXIC EVALUATION OF SUBSTITUTED BENZALDEHYDES

Felipe A. R. Rodrigues,[a] Augusto C. A. Oliveira,[a] Bruno C. Cavalcanti,[a] Marcília P. Costa,[a] Claudia Pessoa,[a] Alessandra C. Pinheiro[b] and Marcus V. N. de Souza[b]*

A series of fifty-four commercial aldehydes have been synthesized and evaluated for their activity against peripheral blood mononuclear cells (PBMC) and four human cancer cell lines, exhibiting potent citotoxicity (IC_{50} ranging from 0.36 to 4.75 µg mL^{-1}). The structure-activity relationship (SAR) analysis indicated that the number, the positions and the type of substituents attached into the aromatic and heteroaromatic ring are critical for the biological activity. The aldehydes **24**, **26**, **48** and **49** displayed a potent citotoxicity activity compared to the reference drug doxorubicin being, therefore, this discovery important for the rational design of new compounds against cancer.

Corresponding Authors
  Tel: +552139772404
  Fax: +552125602518
  E-mail: marcos_souza@far.fiocruz.br
[a] Laboratório de Oncologia Experimental, Faculdade de Medicina, Universidade Federal do Ceará, Fortaleza, CE, Brazil.
[b] FioCruz-Fundação Oswaldo Cruz, Instituto de Tecnologia em Fármacos-Far-Manguinhos, Rio de Janeiro, RJ, Brazil.

INTRODUCTION

The aldehyde function has a great versatility in organic synthesis since it is able to perform a large number of chemical transformations such as the preparation of alcohols, ethers, carboxylic acids, esters and alkanes. Aldehydes can also be used to form carbon-carbon bond, and may be used to obtain various systems and heteroaromatic compounds. In medicinal chemistry aldehydes are used in the formation of Schiff bases,[1] amines,[2] hydrazones and *N*-acylhydrazones,[3-8] which are present in many compounds with application in different diseases. One of them is cancer, which the National Institutes of Health (NIH) estimates that the over-all costs of cancer in 2007 were $226.8 billion[9] being a leading cause of death worldwide and accounted for 7.6 million deaths (13 % of all deaths) in 2008.[10] Due to the interest of our group in this field and the importance of the aldehydes[11] for the preparation of its respective hydrazones and *N*-acylhydrazones, classes of compounds which have potent activities against cancer, the aim of this article was to evaluate fifty-four commercial aldehydes against peripheral blood mononuclear cells (PBMC) and four human cancer cell lines. Although these commercial benzaldehydes have been used by research groups in the search of new anticancer drugs, they had not been tested previously against cancer cell lines. Considering that, the evaluation of commercial aldehydes common used in medicinal chemistry could be valuable information for the rational design of new compounds against cancer.

MATERIAL AND METHODS

Cytotoxicity Against Cancer Cell Lines

Initially, as a pre-screening procedure, all commercial aldehydes **1-54** (Scheme **1**) were tested *in vitro* only against three human cancer cells: SF-295 (glioblastoma), OVCAR-8 (ovary) and HCT-116 (colon) (National Cancer Institute, Bethesda, MD) at 5µg mL^{-1} by using MTT assay (Table **1**). Afterward, the compounds were classified by their growth inhibition (GI) percentage, at least in one cell line, as active (100 % *GI*), moderately active (75 % < *GI* < 100 %), or inactive (*GI* < 50 %).
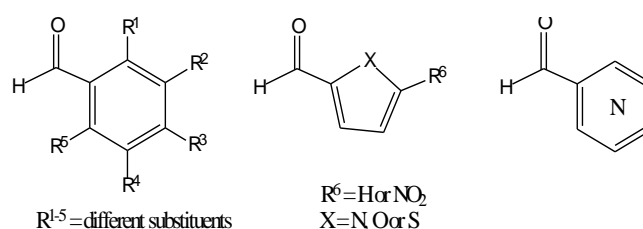
Scheme 1. Commercial aldehydes used in medicinal chemistry tested against cancer cell lines.

The aldehydes **24**, **26**, **48** and **49** which displayed more than 80 % of GI, were selected for *in vitro* anticancer activities evaluation against PBMCs and four human cancer cell lines: OVCAR-8, SF-295, HCT-116, HL-60, using the MTT cell proliferation assay. The concentrations that induce 50% inhibition of cell growth (IC_{50}) in µg mL^{-1} are reported in Table **2**.

Table 1. Growth Inhibition Percentage (*GI* %) for three human tumors cells line by the MTT Assay of commercial aldehydes **1**-**54**.

Com-pound	R on benzaldehyde	Growth Inhibition[a] (*GI*, %)					
		OVCAR-8	SD	HCT-116	SD	SF-295	SD
1	H	0.00	0.00	13.12	2.78	18.12	2.14
2	2-NO$_2$	6.91	1.89	43.00	4.19	55.60	4.72
3	3-NO$_2$	37.23	3.75	50.97	1.10	35.32	17.31
4	4-NO$_2$	17.92	5.97	33.18	19.74	64.53	2.68
5	2,6-diNO$_2$	69.07	1.51	87.71	2.25	68.16	2.42
6	2-F	14.54	0.21	19.86	1.95	51.17	2.92
7	3-F	0.00	0.00	9.90	0.38	24.09	7.22
8	3-Cl	0.00	0.00	12.81	2.78	17.12	5.89
9	4-Cl	0.15	0.34	9.49	9.65	20.20	6.16
10	2,3-diCl	36.62	5.26	55.34	0.45	51.65	5.30
11	2,4-diCl	39.25	3.10	62.77	1.65	69.99	1.52
12	2,6-diCl	1.63	0.39	6.93	2.96	28.59	2.26
13	3,4-diCl	23.12	2.97	31.79	2.05	60.50	10.50
14	2-Br	0.00	0.00	9.05	0.92	38.21	9.49
15	3-Br	4.74	3.00	10.63	3.01	46.78	4.18
16	4-Br	0.00	0.00	5.53	1.49	33.69	11.00
17	4-CH$_3$	3.63	4.36	32.23	20.53	63.13	1.00
18	2-CN	2.52	2.73	5.36	4.14	42.51	0.43
19	3-CN	19.25	0.53	67.51	0.62	50.39	1.31
20	4-CN	62.66	5.48	65.89	3.66	59.11	19.73
21	2-OH	4.24	0.68	0.53	0.06	19.24	2.98
22	3-OH	4.22	0.63	9.50	1.81	34.73	0.17
23	4-OH	6.70	0.63	9.94	1.27	48.77	1.73
24	2.3-diOH	84.41	3.39	64.38	6.07	80.42	0.13
25	2,4-diOH	22.73	3.39	18.09	1.28	31.02	13.92
26	2,5-diOH	84.07	2.37	63.32	5.75	84.57	0.31
27	3,4-diOH	47.10	3.79	46.10	14.13	68.18	2.13
28	3,4,5-triOH	41.27	2.53	48.81	5.16	67.79	0.58
29	2-OCH$_3$	19.08	6.50	54.21	0.65	69.60	4.66
30	3-OCH$_3$	16.32	0.21	44.31	25.59	52.58	4.07
31	4-OCH$_3$	4.48	4.29	4.64	10.92	22.67	20.48
32	2,6-diOCH$_3$	70.69	2.00	76.19	0.02	68.00	3.93
33	2,4-diOCH$_3$	8.62	5.95	27.22	4.53	51.46	4.57
34	2,3-diOCH$_3$	0.00	0.00	19.39	10.49	42.56	8.73
35	2,5-diOCH$_3$	45.49	3.51	46.04	5.51	55.18	4.71
36	3,4-diOCH$_3$	11.79	2.51	16.54	0.93	25.11	22.17
37	3-OEt	41.62	4.83	42.95	7.83	65.86	10.39
38	4-OEt	0.38	3.44	0.00	0.00	21.92	7.12
39	2-OH; 3-OCH$_3$	44.82	1.21	42.55	7.24	62.61	1.12
40	2-OH; 4-OCH$_3$	4.90	1.95	13.64	6.17	56.52	3.74
41	2-OH; 4-CH$_3$	7.44	0.46	32.41	1.77	43.71	5.08
42	2-OH; 5-CH$_3$	0.00	0.00	17.16	2.71	40.80	8.67
43	2-OH; 5-NO$_2$	57.43	4.23	39.17	32.34	78.17	0.16
44	3-NO$_2$; 4-Cl	71.26	0.12	63.26	2.90	62.79	4.31
45	3-Cl; 4-OH	11.89	3.65	19.57	1.33	60.08	1.48
46	4-N(CH$_3$)$_2$	5.18	1.66	0.00	0.00	22.49	8.85
47	4-N(Et)$_2$	9.56	0.18	4.98	0.27	44.78	2.26
Compound No. and name		OVCAR-8	SD	HCT-116	SD	SF-295	SD
48	5-NO$_2$-2-furaldehyde	85.60	2.08	82.88	3.28	75.83	1.89
49	5-NO$_2$-2-thiophene-C(O)H	86.38	1.77	80.38	0.80	89.46	0.13
50	2-thiophene-C(O)H	0.00	0.00	12.45	3.97	18.47	2.09
51	2-pyrrole-carboxaldehyde	0.00	0.00	11.19	1.52	18.66	0.95
52	2-pyridine-carboxaldehyde	4.41	0.90	13.72	1.53	32.53	1.59
53	3-pyridine-carboxaldehyde	8.61	0.28	13.60	4.55	40.64	13.09
54	4-pyridine-carboxaldehyde	6.09	3.17	23.02	3.66	26.02	2.41

Table 2. Cytotoxic activity of the aldehydes **24**, **26**, **48** and **49** [IC_{50} (μg mL^{-1})] on human tumor cell lines.

Compound	HCT-116 IC$_{50}$ (CI 95 %)[*]	OVCAR-8 IC$_{50}$ (CI 95 %)[*]	HL-60 IC$_{50}$ (CI 95 %)[*]	SF-295 IC$_{50}$ (CI 95 %)[*]	PBMCIC$_{50}$ (CI 95 %)[*]
2,3-dihydroxybenz-aldehyde	2.299 (1.929 to 2.741)	1.807 (1.558 to 2.096)	1.741 (0.5464 to 5.546)	4.750 (4.422 to 5.102)	>5
2,5-dihydroxybenz-aldehyde	1.931 (1.075 to 3.467)	1.284 (1.096 to 1.503)	0.8470 (0.2356 to 3.045)	3.826 (3.348 to 4.371)	2.839 (1.931 to 4.174)
5-nitro-2-furaldehyde	1.199 (0.9509 to 1.511)	1.563 (1.353 to 1.805)	0.3605 (0.1578 to 0.8235)	3.823 (3.538 to 4.131)	2.137 (1.296 to 3.525)
5-nitro-2-thiophene-carboxaldehyde	1.199 (0.5633 to 0.6610)	0.7508 (0.6526 to 0.8637)	0.3761 (0.1723 to 0.8211)	2.866 (2.618 to 3.139)	1.935 (1.151 to 3.253)
Doxorubicin	0.125 (0.09 to 0.17)	0.265 (0.17 to 0.305)	0.02 (0.01 to 0.02)	0.23 (0.19 to 0.25)	0,8 (0,72 to 0,88)

[*] Data are presented as IC_{50} values and 95 % confidence intervals (IC 95 %) obtained by nonlinear regression for all cell lines colon (HCT-116), ovary (OVCAR-8), leukemia (HL-60), glioblastoma (SF-295) and normal lymphocytes (PBMCs) from three independent experiments. Doxorubicin was used as positive control. Experiments were performed in triplicate. IC_{50} = concentrations that induce 50 % inhibition of cell growth in μg mL^{-1}.

RESULTS AND DISCUSSION

The evaluation of commercial benzaldehydes **1**-**54** tested against four human cancer cell lines suggested that the number, the positions and the type of substituent attached into the aromatic and heteroaromatic ring are critical for the biological activity (Figure 1).

For example, the structure-activity relationship (SAR) analysis indicated that the number and the positions of hydroxyl group into aromatic ring are critical for the biological activity. Dihydroxyl groups in 2,3 (**24**) or 2,5 (**26**) positions displayed good cytotoxic activities, however when these groups are in 2,4 (**25**); 3,4 (**27**) or 3,4,5 (**28**) positions no activity were detected. It is important to mention that when hydroxyl groups in 2,3 (**24**) or 2,5 (**26**) positions are replaced by dimethoxy groups **34** and **35**, respectively the aldehydes were inactive. The presence of a methoxy group and one hydroxyl group such as the aldehyde **34** leads to loss of activity. In this context, when one of hydroxyl group was replaced by methyl (**42**) or nitro group (**43**) the aldehydes were inactive. Another information is that aldehydes with only one hydroxyl group into the ring in the positions 2 (**20**), 3 (**21**) or 4 (**22**) were inactive.

Other substituent present in the aromatic aldehydes (mono or disubstituted) such as F, Cl, Br, CN, NO$_2$, OEt, N(Me)$_2$ or N(Et)$_2$ leads to loss of activity.

The cytotoxic evaluation of the heteroaromatic aldehydes suggested that the size, the substituents and its positions into the ring are important for the biological evaluation. For example, five-membered ring were more active than six being the aldehydes **48** and **49** were the most actives. Among them, **49** (5-nitro-thiophene carboxaldehyde) displayed the best result, indicating that the nitro group in the five position and the sulfur are important for the anticancer activity. The SAR for this class of compounds is summarizes in Figure 1.

EXPERIMENTAL

Cytotoxicity Against Cancer Cell Lines

The commercial aldehydes **1**-**54** (1.715–5.0 μg mL^{-1}) were tested for their cytotoxic activity against PBMCs (normal lymphocytes) and four human cancer cell lines: OVCAR-8 (ovary), SF-295 (glioblastoma), HCT-116 (colon), HL-60 (leukaemia) (National Cancer Institute, Bethesda, MD). All cell lines were maintained in RPMI 1640 medium supplemented with 10 % fetal bovine serum, 2 mM glutamine, 100 U mL^{-1} penicillin, and 100 μg mL^{-1} streptomycin at 37 °C with 5 % CO$_2$. Each compound was dissolved with DMSO, until reaching a concentration of 1 mg mL^{-1}. The final concentration of DMSO in the culture medium was kept constant, below 0.1 % (v/v). The commercial aldehydes **1**-**54** were incubated with the cells for 72 h. The negative control received the same amount of DMSO (0.001 % in the highest concentration). The cell viability was determined by reduction of the yellow dye 3-(4,5-dimethyl-2-thiazol)-2,5-diphenyl-2*H*-tetrazolium bromide (MTT) to a blue formazan product as described by Mosmann.[12]

Cytotoxicity Against Normal Peripheral Blood Mononuclear Cells

Fresh peripheral human heparinized blood was collected from healthy donors with no recent or chronic smoking, drinking or drug intake. Peripheral blood mononuclear cells (PBMCs) were obtained by a standard method of density-gradient centrifugation over Histopaque®-1077. The PBMCs were cultivated with RPMI 1640 supplemented with 20% fetal bovine serum, 2 mM glutamine, 100 U/ml penicillin, 100 g/ml streptomycin and phytohemagglutinin (final concentration: 2 %) at 37 ºC with 5% CO$_2$.[13-15] The study was approved by the Ethical Committee of Federal University of Ceará State, Brazil. For all experiments, cell viability was performed by using a hemocytometer and Trypan Blue assay.
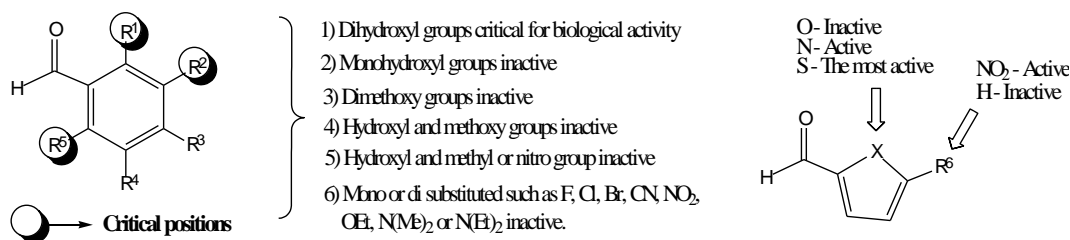
Figure 1. SAR of the benzaldehydes series tested against cancer cell lines.

CONCLUSION

In this work we report the cytotoxicity activity of a series of fifty-four commercial aldehydes, which have been evaluated for their activity against peripheral blood mononuclear cells (PBMC) and four human cancer cell lines. The SAR of this class indicated that the number, the positions and the type of substituents attached into the aromatic and heteroaromatic ring are critical for the biological activity. The position 2, 3 and 5 in aromatic ring and the dihydroxyl groups are critical for biological activity. In the heteroaromatic aldehydes the size, substituents and the heteroatom are important for cytotoxic activity. In this context, the compound **49** displayed a potent cytotoxicity activity compared to the reference drug doxorubicin. Considering the data of this current study, our findings are valuable information for the rational design of new compounds against cancer.

REFERENCES

[1]Ferreira, M. L., Vasconcelos, T. R. A., Carvalho, E. M., Lourenço, M. C. S., Wardell, S. M. S. V., Wardell, J. L., Ferreira, V. F., De Souza, M. V. N., *Carbohyd. Res.,* **2009**, *344*, 2042-2047.

[2]Delarue-Cochin, S., Paunescu, E., Mães, L., Mouray, E., Sergheraert, C., Grellier, P., Melnyk, P., *Eur. J. Med. Chem.*, **2008**, *43*(2), 252-260.

[3]Lourenço, M. C., De Souza, M. V. N., Pinheiro, A. C., Ferreira, M. L., Gonçalves, R. S. B., Nogueira, T. C. M., Peralta, M. A., *Arkivoc*, **2007**, *15*, 181-191.

[4]Lima, C. H. S., Henriques, M. G. M. O., Candéa, A. L. P., Lourenço, M. C. S., Bezerra, F. A. F. M., Kaiser, C. R., De Souza, M. V. N., *Med. Chem. (Hilversum)*, **2011**, *7*(3), 245-249.

[5]Ferreira, M. L., Cardoso, L. N. F., Goncalves, R. S. B., Silva, E. T., Lourenço, M. C. S., De Souza, M. V. N., *Lett, Drug, Des, Discov,,* **2008**, *5*(2), 137-140.

[6]De Souza, M. V. N., Vasconcelos, T. A., Mello, S. C. P., Wardell, S. M. S. V., Peralta, M. A., Ferreira, B., Henrique, M. G. M. O., Junior, I. N., Lourenco, M. C. S., *Lett. Drug. Des. Discov.*, **2005**, *2*(7), 563-566.

[7]Carvalho, S. A., Da Silva, E. F., De Souza, M. V. N., Lourenco, M. C. S., Vicente, F. R. C., *Bioorg. Med. Chem. Lett.,* **2008**, *18*(2), 538-541.

[8]De Souza, M. V. N., Junior, I. N., Miranda, G. B. P., Lourenco, M. C. S., Vasconcelos, T. A., Pais, K. C., *Lett. Drug. Des. Discov.*, **2006**, *3*(6), 424-428.

[9]American Cancer Society, http://www.cancer.org/ (Accessed July, **2013**).

[10]World Health Organization, http://www.who.int/gho/ncd/mortality_morbidity/cancer/en/index.html (Accessed July, **2013**).

[11]Ferreira, M. L., Candéa, A. L. P., Henriques, M. G. M. O., Lourenço, M. C. S., Kaiser, C. R., De Souza, M. V. N., *Lett. Drug. Des. Discov.*, **2010**, *7*(10), 754-758.

[12]Mosmann, T., *J. Immunol Methods*, **1983**, *65*(1-2), 55-63.

[13]Magalhães, H. I. F., Cavalcanti, B. C., Bezerra, D. P., Wilke, D. V., Paiva, J. C. G., Rotta, R., Lima, D. P., Beatriz, A., Burbano, R. R., Costa-Lotufo, L. V., Moraes, M. O., Pessoa, C., *Toxicol. in Vitro*, 2011, *25*(8), 2048-2053.

[14]Berthold, F., *Blut*, **1981**, *43*, 367-371.

[15]Hutchins, D., Steel, C. M., *Clin. Exp. Immunol.,* **1983***, 52*(2), 355-364.

SYNTHESIS AND CHARACTERIZATION OF SOME TRANSITION METAL COMPLEXES WITH TRIDENTATE N3 DONOR SCHIFF BASE DERIVED FROM 2-AMINOTHIAZOLE

Mahmoud Najim Al-Jibouri,[a]* Fadhil R. Hafidh[a] and Anaam Majeed Rasheed[a]

A 2,6-diacetylpyridine based novel acyclic tridentate compartmental ligand (E)-N-(1-(6-((E)-1-(thiazol-5-ylimino)ethyl)pyridin-2-yl)ethylidene)thiazol-2-amine was prepared by condensation of 2,6-diacetylpyridine and two equivalent of 2-thiazolamine in ethanol. The reaction of metal chlorides (Mn(II), Co(II), Ni(II), Cu(II), Zn(II)) and $VOSO_4.5H_2O$ with the new ligand in methanol results the formation of deep colored metal complexes with the formula [MLCl]Cl (M=Mn, Ni, and Zn), [MLCl_2(H_2O)], M=Co, Cu(II), and [VOL(SO_4)], respectively. The free ligand and its metal complexes were characterized by elemental analyses, conductivity measurements, magnetic susceptibility data, IR, UV-Vis and NMR spectral data. The physical measurements and FTIR spectral data showed that most of the complexes contain tetrahedrally coordinated central ion(II) except the square-pyramidal vanadyl complex and octahedral geometry for Co(II) and Cu(II) complexes.

* Corresponding Authors
   E-Mail: mahmoudnajim71@yahoo.com;
   anaam_m71@yahoo.com; fadhilrukays72@yahoo.com
[a]   Chemistry Department, College of Science, Al-Mustansiriya University, Baghdad, Iraq

Introduction

The presence of exocyclic nitrogen and sulphur atoms in the structure of Schiff bases gives mutative ability to coordination sites to link directly with the transition metal ions.[1-2] Azomethine ligands involving thiazole ring have attracted the chemists to prepare novel metal chelate due to their importance in antimicrobial,anti-inflamatory,and anti-HIV applications.[3-5] Aljibouri and co-workers [6-9] have been synthesized and studied the biological effect of Cr(III), Fe(III), Mn(II), Co(II), Ni(II), Cu(II) and Zn(II) chelates with N5 donor Schiff bases derived from 2,6-diacetylpyridine.[10-13] Due to the growing interest of metal chelates involving heterocyclic rings, here we report the synthesis and characterization of some first row transition metal complexes with new Schiff base derived from condensation of 2,6-diacetyl pyridine and 2-thiazolamine.

Experimental

All the organic chemicals and solvents used were analytical grade and procured from Sigma-Aldrich Co. The hydrated metal(II) chlorides of manganese, cobalt, nickel, copper(II), anhydrous zinc(II) chloride and vanadyl sulphate were purchases from Sigma-Aldrich company. As well as the 2,6-diacetylpyridine and 2-aminothiazole were used without any purification. The solvents used were ethanol, deuterated dimethyl sulfoxide (DMSO-d_6), methanol and DMF.

Electronic spectra were recorded in the region 800-200 nm on a Shimadzu 670 spectrophotometer. IR-spectra were recorded in the range of 200-4000 cm^{-1} on a Shimadzu PC FT-IR spectrophotometer in KBr and CsI discs. The ^{1}H NMR spectra of the ligand were recorded in DMSO-d_6 on a 300 MHz Bruker spectrometer. The effective magnetic moment measurements of the solid complexes were carried out an MG Magnet Balance.The molar conductance of metal complexes in N,N-dimethylformamide (DMF) solution were measured with using a HPG G-3001 digital conductivity meter. The carbon, hydrogen , nitrogen and sulphur analysis were done on a Carlo Elba 1108 elemental analyzer. The metal content of complexes were measured with using a Shimadzu 670 spectrophotometer with standard addition method.[14]

Synthesis of the Ligand (L)

The ligand was prepared by the mixing of hot ethanolic solution (20 mL) of 2-aminothiazole (2 g, 0.02 mol) and an ethanolic solution (20 mL) of 2,6-diacetylpyridine (1.63 g, 0.01 mol) with constant stirring in the presence of few drops of 36 % HCl. This mixture was refluxed for 4 h then allowed to cool overnight at 20 °C. The isolated light yellow colored precipitate was filtered off, washed with cold EtOH and dried under *vacuum* over anhydrous $MgSO_4$. Yield (80 %), mp. 155-157 °C. Element chemical analysis data is shown in Table 1.
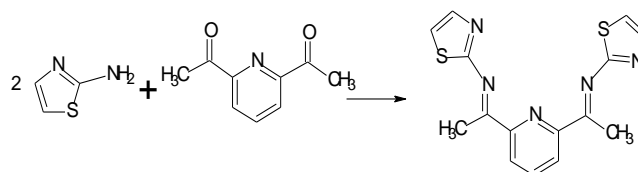
Scheme 1. Preparation of the ligand

Preparation of Mn(II), Co(II), Ni(II), Cu(II), Zn(II) and VO(IV) complexes

Methanolic (25 ml) solution of metal chlorides or $VOSO_4.5H_2O$ (1 mmol) was added to methanolic solution of the ligand (0.327g, 1 mmol) with keeping the pH to be neutral. The resulting mixture was refluxed on a water bath for 2-3 h then cooled to room temperature to afford deep colored precipitates of metal complexes.

Result and Discussion

The new acyclic Schiff base L ligand derived from condensation of 2,6-diacetylpyridine and two equivalents of 2-aminothiazole behaves as a tridentate chelating agent toward the studied metal ions. The stoichiometry of the ligand and its complexes were confirmed by their elemental analysis (Table 2). The Mn(II), Zn(II) and Ni(II) complexes showed 54-78 ohm^{-1} cm^2 mol^{-1} molar conductivity in DMF while the vanadyl(IV), cobalt(II) and copper(II) complexes gave 18-24 ohm^{-1} cm^2 mol^{-1} values, thus these later complexes proved to be non-electrolytes.[15]

The proton NMR spectrum of the ligand,figure(1), can be classified into two distinct classes, the methyl (C=N-CH$_3$), and aromatic protons appear as singlet peaks and resonate in the ranges 3.6-3.88 ppm and 7.5-8.4 ppm respectively.[12,16] Deshielding and splitting of signals in the ^{1}H NMR spectrum of Zn[LCl]Cl complex in DMSO-d$_6$ show the changes in electron density due to coordination of the nitrogen atoms of –C=N- to Zn(II) ion causing the shift of proton resonance toward deshielded field[16] (Figure 2.).

Electronic spectra and Magnetic moments

The free ligand in abs. EtOH shows high intensity peaks at 255 and 388 nm that related to $\pi\rightarrow\pi^*$ and $n\rightarrow\pi^*$ transitions of C=N-, C=O and C=C- groups.[17] (Table 2). The electronic spectra of the metal(II) complexes were recorded in DMF. The pale olive solution of VO(IV) complex exhibits two weak spin allowed peaks in the region 610-510 nm that are consistent with d-d transitions of square pyramidal oxovanadium(IV) complexes.
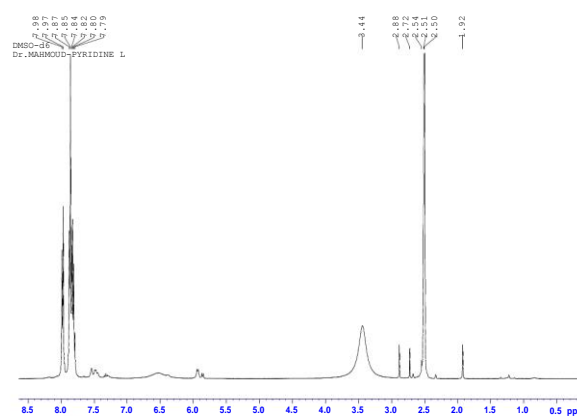
Figure 1. ^{1}H NMR spectrum of Schiff base ligand in DMSO-d$_6$
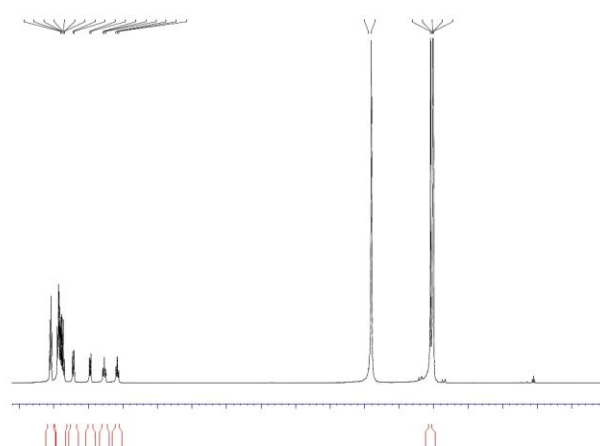
Figure 2. ^{1}H NMR spectrum of [ZnLCl]Cl in DMSO-d$_6$

The spectrum of the Mn(II) complex exhibits bands at 440 nm and 388 nm belong to d-d and charge transfer, respectively confirming the high spin octahedral symmetry around manganese(II) ion.[18] The magnetic moments for Mn, Co and Ni(II) complexes were 5.64, 3.66. and 3.96 *B.M.* which revealed the magnetic properties of well agreement with their electronic spectra.[19-20]

Table 1. Physical properties and elemental analyses of prepared compounds

Compound	Color	M.P., °C	C% Calc. (found)	H% Calc. (found)	N% Calc. (found)	S% Calc. (found)	M% Calc (found)
L	Yellow	155-157	55.02 (54.98)	4.01 (3.60)	21.39 (20.83)	19.59 (18.88)	-
[VOL]SO4	Olive	177-179	39.37 (38.81)	3.49 (3.11)	13.47 (14.07)	18.53 (18.00)	9.82 (8.696)
[MnLCl]Cl	Dark yellow	222^d	43.66 (42.78)	4.59 (4.21)	13.88 (14.00)	13.22 (12.88)	11.76 (10.80)
[CoL(H$_2$O)Cl$_2$]	Dark green	212^d	40.24 (39.71)	4.19 (3.92)	13.86 (14.99)	12.69 (12.00)	11.66 (10.99)
[NiL]Cl	Brown	225^d	42.03 (41.09)	3.74 (3.66)	11.97 (12.11)	10.77 (9.66)	10.54 (10.11)
[CuL(H$_2$O)Cl$_2$]	Pale brown	231^d	40.06 (39.51)	4.15 (3.81)	13.76 (14.10)	12.44 (11.61)	11.35 (10.88)
[ZnLCl]Cl	White off	241	38.88 (37.87)	3.65 (3.11)	10.28 (11.11)	8.56 (8.03)	10.36 (9.32)

Table 2. Electronic spectral, magnetic moment and molar conductance data of the metal(II) complexes

Compound	λ_{max}, nm	Band assignment	Λ, S mol^{-1} cm^{-2}	μ, B.M.	Geometry
L	255	$\pi \rightarrow \pi*$	10		—
	338	$n \rightarrow \pi*$			
[VOLSO$_4$]	610	$^2B_1g \rightarrow \ ^2B_2g(D)$	22	1.55	Square pyramidal
	510	$^2B_1g \rightarrow \ ^2E_2g(D)$			
	355	$^2B_1g \rightarrow \ ^2A_1g(F)$			
[MnLCl]Cl	440	$^6A_1 \rightarrow \ ^4T_1(F)$	60	5.64	Tetrahedral
	366	$^6A_1 \rightarrow \ ^4E_1(F)$			
[CoL(H$_2$O)Cl$_2$]	780	$^4T_1g \rightarrow \ ^4T_2g(F)$	24	3.66	Octahedral
	660	$^4T_1g \rightarrow \ ^4A_2g(F)$			
	398	LMCT			
[NiLCl]Cl	699	$^3T_1 \rightarrow \ ^3T_2$	78	3.96	Tetrahedral
	612	$^3T_1 \rightarrow \ ^3A_2$			
	388	LMCT			
[CuL(H$_2$O)Cl$_2$]	710	$^2B_1g \rightarrow \ ^2A_1g$	18	1.72	Octahedral
	404	$^2B_1g \rightarrow \ ^2B_1g$			
	311	MLCT			
[ZnLCl]Cl	390	CT	54	0	Tetrahedral
	255	$\pi \rightarrow \pi*$			

C.T=Charge transfer**,**m=molar conductivity in DMF solutions(ohm^{-1}.cm^2.mol.$^{-1}$)

The vanadyl complex recorded paramagnetic properties with 1.55 *B.M.* value suggesting the square pyramidal geometry around V(IV) ion. The cobalt(II) complex in its DMF solution showed two weak bands in the visible region at 660-780 nm, respectively, these absorptions support the octahedral structrue of Co(II) complex.[19,21] The electronic spectra of Cu(II) complex displays two prominent bands. A low intensity broad band around 404-710 nm is assignable to $^2T_{2g} \rightarrow \ ^2E_g$ transition. The other high intensity band at 300 nm belongs to a symmetry forbidden ligand to metal charge transfer. On the basis of electronic spectrum, a distorted octahedral geometry of Cu(II) ion can be suggested.[22-23] The Cu(II) complex showed magnetic moment 1.72 BM, is slightly higher than the spin-only value 1.73 BM expected for one unpaired electron, which offers possibility of an octahedral geometry.

The electronic spectra of the Mn(II) complex display weak absorption bands in the region 440-3660 nm supporting the electronic transitions of high spin Mn(II) tetrahedral.[22] In contrast, the red solution of Ni-complex in DMF shows two low energy bands in the region 612-699 nm that are related to tetrahedral geometry around nickel(II) ion.[20]

IR spectra

The infrared spectral data of the ligand and its metal complexes are presented in Table 3. The IR spectra of the Schiff base exhibited characteristic band of C=N- and C-S groups at 1640 cm^{-1} and 1000-1070 cm^{-1}, respectively.[23]

The strong band at 1614 cm^{-1} and a characteristic weak intensity band at 3090 cm^{-1} in the IR spectra of the Schiff base are assigned to C-H stretching of pyridine moiety. The disappearance of strong absorptions in the region 1730-1690 cm^{-1} of carbonyl groups related to 2,6-diacetylpyridine gives good indication to condensation with the –NH2 group of 2-aminothiazole to form the new Schiff base L that is involving-C=N-moiety.[24] All the metal complexes showed a downshift in the wavenumbers of C=N- stretching in the region 1522-1633 cm^{-1}which reveals the coordination of nitrogen atoms to the central metal ions. The weak bands appeared in the region 490-533 cm^{-1} belongs to M-N bonds[25] support this conclusion. The bands in the region 250-389 cm^{-1} can be ascribed to (M-Cl) bond formation.[23]

The FTIR spectra of all complexes in CsI disc showed downshift in the wavenumbers of imine group of range 1522-1633 cm^{-1}that support remarkably the bonding of nitrogen atoms of –C=N- to metal ions. The IR spectral results provide strong evidence for the interaction of the Schiff base with metal ions in a supposed tridentate N3 mode. The vanadyl complex in CsI disc showed strong and medium absorptions at 989 and 412 cm^{-1} that were assignable to vibrational modes of V=O and M-O bonds, respectively.[25]

The cobalt(II) and copper(II) complexes display broad bands in the region 3550-3600 cm^{-1} which indicate the presence of coordinated water molecules in the structure of the two mentioned complexes. The spectra of metal complexes do not show changes in intensity and position of C-S[26-27] bonds, thus it confirms the lack of S-metal coordination.

Table 3. Selected vibrational FTIR absorptions for the free ligand and its metal(II) complexes

Compound	$\nu C=N$	$\nu C-S$	$\nu M-N$, $\nu M-Cl$	Other bands
L	1640(s)	1070-1000(s)	—	
[VOL]SO$_4$	1630-1590(s)	1067-1005	490-533.	988[b], 412[c]
[MnLCl]Cl	1600-1588	1068-1010 (s)	460-488, 389	3022
[CoL(H$_2$O)Cl$_2$]	1610-1577	1072-1000 (s)	517(w), 300	3600[a]
[NiLCl]Cl	1590-1533	1065-1007	510(w), 250-322	2965
[CuL(H$_2$O)Cl$_2$]	1543-1522	1062-1000	568, 278-344	466[c], 3550[a]
[ZnLCl]Cl	1633-1559	1066-1009	422, 370(w)	3070, 2964

s=strong, m=medium, br=broud, w=weak, a=broad band of H$_2$O molecules coordinated to Co(II) and Cu(II) b - V=O and c - M-O bonds.

Conclusions

The complexes of Mn(II), Co(II), Ni(II), Cu(II), Zn(II) and vanadyl(IV) with Schiff base derived from 2,6-diacetylpyridine and 2-aminothiazole were synthesized and characterized. The Schiff base act as versatile tridentate ligand. The Co(II) and Cu(II)-complexes have octahedral geometry, Mn(II),Ni(II) and Zn(II) complexes are tetrahedral and vanadyl complex has square-pyramidal structure with monocoordinated sulphate ion.
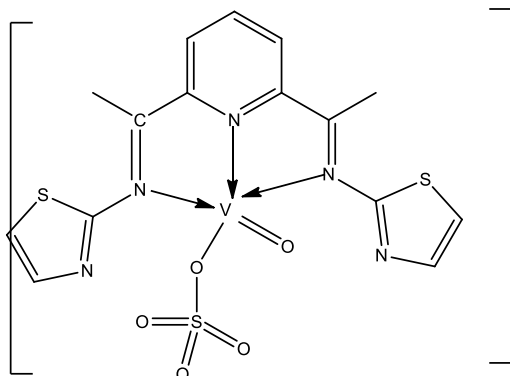
Figure 3. The proposed strcture of vanadyl-complex.

References

[1]Pattan, S. R., Dighe, N. S., Nirmal, S. A., Merekar, A. N. Laware, R. B., Shinde, H. V. and Musmade, S., *Asian J. Res. Chem.,* 2(2) (2009) 196-201.

[2]Thakar, A. S., Pandya, K. S., Joshi K. T. and Pancholi, A. M., *E-J. Chem.,* **2011,** *8(4),* 1556-1565.

[3]Pandya, K. S., Joshi, K. T., Pancholi, A. M. and Thakar, A. S., *J. Chem. Pharm. Res.,* **2011,** *3(4),* 741-749.

[4]Coombs, R. R., Ringer, M. K., Blacquiere, J. M., Smith, J. C., Neilsen, J. S., Uh, Y.-S., Gilbert, J. B., Leger, L. J., Zhang, H., Irving, A. M., Wheaton, S. L., Vogles, C. M., Westcott, S. A., Decken, A. and Baerlocher, F. J., *Transit. Met. Chem.,* **2005,** *30*, 411-418.

[5]Neelakantan, M. A., Marriappan, S. S., Dharmaraja, J., Jeyakumar, T. and Muthukumaran, K., *Spectrochim. Acta Part A.,* **2008,** *71,* 628-635.

[6]Al-Jibouri, M. N. Al-Obaidi, O. H., *Adv. Chem.,* **2013,** *2(2),* 96-105.

[7]Al-jibouri, M. N., Al-Obaidi, O. H., *Sci. J. Chem.,* **2013,** *1(2),* 14-20.

[8]Al-jibouri, M. N., Al-Obaidi, O. H., *Int. J. Biochem., Res. Review,* **2014,** *4(1),* 28-42.

[9]Al-Obaidi, O. H., *J. Chem. Biol. Phys. Sci.,* **2014,** *4(1),* 31-37.

[10] Chandra, S. and Kumar, A., *Spectrochim. Acta A,* **2007,** *66,* 1347-1351. doi:10.1016/j.saa.2006.04.047

[11]Chandra, S., Minika T., *Open J. Inorg. Chem.,* **2012,** *2,* 41-48. doi:10.1080/00958970802521076 .

[12]Kumar, U. and Chandra, S., *E-J. Chem.,* **2010,** *7,* 1238-1245.

[13]S. R. Kelode, *Int. J. Chem. Tech. Res..,* **2012,** *4(4),* 1442-1446.

[14]Drago, R. S. *Physical Methods for Chemists,* 2nd. Edition, Saunders Colleges Publishing, New York. **1977**.

[15]Geary, W. J., *Coord. Chem. Rev.,* **1971,** *7(1),* 81-122.

[16]Batterham, T. J., *NMR Spectra of Simple heterocycles* (Taylor, E. C. and Weissberger, A., eds. *General Heterocyclic Chemistry Series,* John Wiley and Sons, Inc. New York, USA. **1973**.

[17]Silverstein, R. M., Bassler, G. C. and Morrill, T. C., S*pectrometric Identification of Organic Compounds,* 4th Edit., Wiley, New York,**1981**.

[18]Sutton, D., *Electronic Spectra of Transition Metal Complexes,* McGraw-Hill, London, **1968**, 388.

[19]Siddappa, K., Reddy, T., Mallikarjun, M. and Reddy, C. V., *Eur. J. Chem.,* **2000,** 5(1), 155-162.

[20]Singh, D. P., Malik, V., Kumar, R., Kumar, K., Rasayan J. Chem., **2009,** 2(1), 133-138.

[21]Dyer, J. R., *Application of absorption spectroscopy of organic compounds,* Prentice Hall., Eaglewood Cliffs, N.J., **1965**,

[22]Sanmartin, J., Bermejo, M. R., Deibe, A. M. G., Maneiro, M., Lage, C., Filho, A. J. C., *Polyhedron,* **2000,** *19,* 185-192.

[23]Cotton, F. A., Wilkinson, G., Murillo, C. A., Bochmann, M., *Adv. Inorg. Chem.,* 6th edition, John Wiley & Sons, **1999**.

[24]Satish, M. A., Sathisha, M. P. and Revankar, V. K., *Trans. Met. Chem.,* **2007,** *32,* 81-87.

[25]Nakamoto, K., *Infrared and Raman spectra of Inorganic and Coordination Compounds,* **1986**, Wiley, New York.

[26]Chandra, S., Sharma, D., *Transit. Met. Chem.,* **2002,** *27,* 732-735.

[27]Kruger P. J. and Smith, D. W. *Can. J. Chem.,* **1967,** *45(14),* 1611-1618.

ASSESSMENT OF HYPERTENSION RISK IN CHILDREN BY CHEMOMETRICAL TECHNIQUES

Viera Mrázová,[a] Miroslava Makohusová,[a]* László Kovács[b] and Katarína Babinská[b]

The present work deals with the multivariate data analysis to elucidate the hypertension risk factors in children, which may contribute in some extent to their prospective medical treatment. Results of laboratory tests together with the data obtained from medical documentation were used to indicate as well as to predict the hypertension diagnosis in children. The best diagnostic classification outputs were obtained using artificial neural networks, the K-th nearest neighbour technique, general and linear discriminant analysis. In contrast to the assessment of single laboratory test results, a combination of several tests enables more comprehensive information that can help the physician in diagnosis. This work exemplifies a possible approach to computer-aided medical diagnosis.

* Corresponding Authors
    E-Mail: miroslava.makohusova@gmail.com
[a]   Department of Chemistry, Faculty of Science, University of SS Cyrilus and Methodius , Trnava, Slovak Republic.
[b]   2nd Department of Paediatrics, Faculty of Medicine of Comenius University, Bratislava, Slovak Republic.

Introduction

The very important advantage of chemometrics and its diverse techniques is versatility, facilitated by its high level of abstraction, characteristic for the scientific disciplines extensively utilizing mathematics. When processing various data of everyday life, exploitable e.g. in medicine or pharmacy, but also in food control or environmental monitoring, resembling algorithms and similar ways of the data processing and evaluation are implemented for different objects under investigation. Considering medicinal data, chemometrical approach allows characterization and quantification of the role of the influencing factors and may effectively support diagnosing and monitoring the progression of a disease. Moreover, this approach enables a total, multicomponent insight into diagnosis **1, 2, 3** instead of sequential view on laboratory results.

Paediatric hypertension is a field of increasing interest and importance. Early identification of children at risk for hypertension is important **4** to prevent serious, long-term complications associated with undetected disease. Although children do not typically suffer from hypertensive disease, an accumulation of medical data suggests that the systolic blood pressure elevation is as an important factor in the morbidity of hypertension in children, as in adults **5**.

Primary hypertension in childhood and adolescence is not a benign disease and cause significant damage of the target organ. Even though clinically evident cardiovascular disease is rare in childhood, the extent of target organ damage is the main risk factor for future cardiovascular events **6**. Patients with moderate to severe hypertension, as well as those with left ventricular hypertrophy, diabetes, cardiovascular and renal disease are considered to be at higher risk and should be considered for prompt pharmacological therapy **7**.

In children, blood pressure measurement is cumbersome and its categorization is based upon the normative data universally defined by National High Blood Pressure Education Program Working Group **8**. The prevalence of childhood obesity is increasing at an alarming rate in developed countries **9**. The prevalence of hypertension is higher in overweight and obese adolescents, and their health state appears to be independent of a family history of hypertension **10**. Obese children are approximately at a three-fold higher risk for hypertension than non-obese children **11**.

Diagnostic criteria for elevated blood pressure in children are based on the concept that blood pressure in children increases with age and body size, making it impossible to utilize a single blood pressure level to define hypertension, as done in adults **12**.

Optimal nutrition during the first year of life is critical to infants' healthy growth and development, and breastfeeding might be a key component. Its duration had no significant effect on infant weight within the first 6 months, but after the 7th month the breastfed infants were lighter than the ones not breastfed. Similarly, the height of the breastfed children is slightly smaller **13**.

Chemometrical multivariate data analysis may elucidate the risk factors in children, which contribute in some extent to prospective treatment of hypertension. The aim of this work is selection of the factors significantly influencing hypertension in children. It is based on exploitation of the results of clinical laboratory tests, as well as the data obtained from medical documentation; further descriptors like age, weight, height, period of breastfeeding are used to indicate or predict the hypertension diagnosis.

Experimental

Data description

The analysed data originate from the 2nd Department of Paediatrics, Faculty of Medicine of Comenius University in Bratislava. The data matrix involves 70 patients aged 3-18 years, among them 29 girls and 41 boys. Three categories of probands were created: (1) the probands without hypertension - 42 patients, (2) the patients with conditional hypertension caused by another disease - 17 non-obese patients with kidney disorders and obese patients associated with other diseases, (3) the patients with confirmed hypertension - 11 probands.

The data with potential effect on hypertension were obtained from the clinical laboratory tests, medical documentation and the data about family history. They represent a set of the following chemometrical descriptors, which all are continuous variables:

Haemoglobin content (g L^{-1}), *HB*; haematocrit (red blood cell volume fraction in the whole blood volume), *HCT*; mean corpuscular volume (fL), *MCV*; content of alanine aminotransferase (μkat L^{-1}), *ALT*; creatinine content (μmol/L), *CR*; sodium concentration (mmol L^{-1}), Na; potassium concentration (mmol L^{-1}), *K*; child's age (year), *AGE*; body mass index, *BMI*; actual weight during hospitalization (kg), *AW*; actual height during hospitalization (cm), *AH*; birth weight (g), *BW*; height at birth (cm), *BH*; period of breastfeeding (months), *BF*. The abbreviated descriptor names in italics were used in computations supported by software specified below.

Hypertension HT was used as the target categorical variable. The probands were categorized into three categories: 1-without hypertension, 2-with conditional hypertension caused by another illness, 3-the patients with hypertension.

Calculation techniques and software

Basic data processing was performed by MS Excel spreadsheet. The following techniques were used for calculations and graph preparations: principal component analysis (PCA), cluster analysis (CLU), correlation analysis (CA), analysis of variance (ANOVA), linear discriminant analysis (LDA), quadratic discriminant analysis (QDA), general discriminant analysis (GDA), the K-th nearest neighbour classification (KNN), logistic regression (LR) and artificial neural networks (ANN).

Data exploration and analysis was performed by using advanced contemporary software packages: SAS ver. 9.1.3 (SAS Institute, Inc. 2004), SAS JMP ver. 7.0 (SAS Institute, Inc. 2007), SPSS ver. 15.0 (SPSS, Inc. 2006), Statgraphics Centurion XV ver. 15.1.02 (Stat-Point, Inc. 2006).

Results and discussion

Principal components analysis and cluster analysis

Both techniques, PCA and CLU, enable better displaying of the investigated problem and demonstrate natural grouping of similar objects under study. In this work, all

fourteen continuous descriptors were used in calculations of principal component analysis. Acquired principal components result from a linear combination of the descriptors, optimized for maximum data variation. The rays corresponding to individual descriptors are depicted in the PCA loadings plot (Figure 1); the loadings mean in fact the ray end points. The risk factors predisposing the development of hypertension are located along the increasing values of the first principal component (PC1), which may be therefore indicated the quantity reflecting the hypertension risk. It is consistent with an axiom that the PC1 usually signifies the main effect of the given study (under condition that the descriptors are rationally selected).
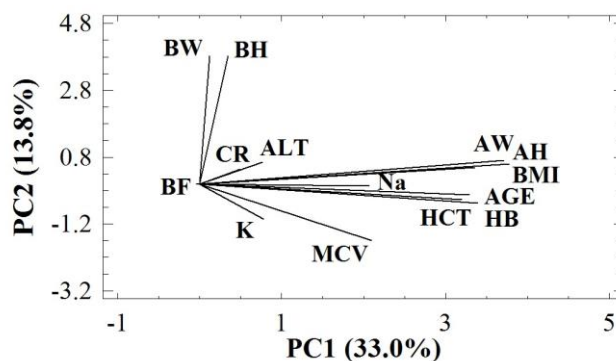
Figure 1. PCA loading plot illustrates 14 descriptors and 70 objects - the patient samples. Software Statgraphics Centurion XV.

The largest loadings with respect to PC1 exhibit *AH*, *AW*, *BMI*, *HB*, *AGE* and *HCT*; a lower effect upon PC1 has Na and *MCV*. The descriptors of the birth weight and height at birth are located along the PC2 axis, perpendicular to the PC1 axis. These two descriptors together with the breastfeeding duration should not have any significant effect upon hypertension in children.

The cluster analysis is a technique that sorts objects into groups by the greatest similarity within the groups and the maximum variability between the groups. The method is suitable for data where the observed variables (descriptors) are quantitative. CLU output is a dendrogram; in this work clustering among the descriptors was evaluated.

Figure 2 shows that the descriptors *HB* with *HCT*, then *AW* with *BMI*, and also *AGE* with *AH* are closely related and form the first common cluster. These six descriptors also most substantially contribute to the PC1 (Fig. 1) therefore they may be considered as most hazardous factors. The second cluster contains descriptors BW and BH, which are similar in some extent to *ALT*; the first two ones exclusively represent PC2 in PCA and their loadings versus PC1 are negligible therefore they have probably no effect upon hypertension. The third cluster is formed by the couples *MCV* and *Na*, *K* and *BF*, plus *CR*; these descriptors except the first two exhibit a small or even insignificant impact on hypertension risk. With regard to the problem of hypertension in children, the PCA and CLU techniques provide synergistic outputs and interpretation of the role of descriptors by their position in the PC2 – PC1 plane is similar to the way how they form the clusters.

Table 1. The correlation table with pairs correlation coefficients *r* for continual variables. Critical value $r_{crit} = 0.306$. Software SPSS.

	AGE	*AW*	*AH*	*HB*	*HMT*	*MCV*	*Na*	*BMI*
AGE	1.000							
AW	0.654	1.000						
AT	0.850	0.810	1.000					
HB	0.409	0.502	0.543	1.000				
HMT	0.472	0.563	0.592	0.964	1.000			
MCV	0.331	0.296	0.333	0.378	0.417	1.000		
Na	0.294	0.391	0.369	0.278	0.292	0.285	1.000	
BMI	0.519	0.895	0.662	0.475	0.517	0.201	0.344	1.000
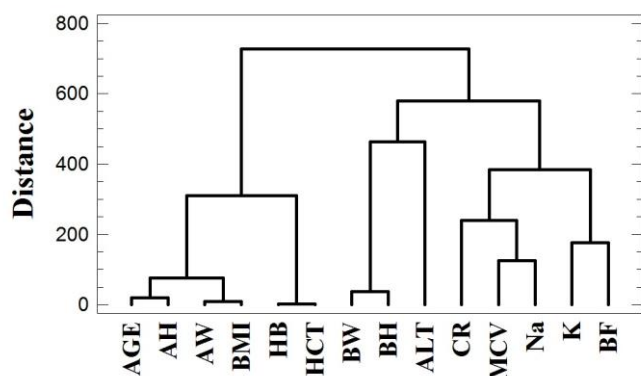
Figure 2. Cluster analysis of 14 investigated descriptors using Ward's method and squared Euclidean distance. Software Statgraphics Centurion XV.

Correlation analysis and analysis of variance

Correlation analysis demonstrates mutual correlations of all pairs of descriptors. Its output is a correlation table containing the pair correlation coefficients R. A part of the descriptors (*AH*, *AW*, *BMI*, *HB*, *HCT*, *Na*) is strongly and positively correlated to *AGE* and their values increase directly with the patient's age.

Found strong correlations between *BMI*, actual weight (*AW*) and height (*AH*) are expected since *BMI* is calculated from these descriptors. A high correlation between the patient's height at birth (*BH*) with the birth weight (*BW*) is also logical. The sodium content considerably increases with the patient's weight, height and *BMI* and is significantly but less strongly correlated to *AGE*, *MCV*, *HCT* and *HB*. Very strong positive correlation (R = 0.964) was found between *HCT* and *HB*, which is related to their shortest distance in the dendrogram and a close position of the corresponding rays in the PC2 - PC1 plane. The results of correlation analysis are consistent with the results of cluster analysis and PCA and are also in agreement with the expected relationships between some descriptors.

Analysis of variance (ANOVA) is a statistical method, which allows to find whether the value of a random variable (descriptor) is significantly affected by some categorical variable, called factor that has two or more levels – categories. In this work the effects of only one factor were investigated - factor *HT* with three categories reflecting different level of hypertension risk. The achieved ANOVA results point out that the strongest impact of hypertension (*HT*) to the investigated descriptors exhibits BMI, then AGE,

AW, *AH* and *ALT*; in case of other descriptors the effect is smaller or even insignificant. Except *ALT* this is fully consistent with the PCA output. The only descriptor which is different at the significance level p = 0.05 for all three categories of the *HT* factor is *BMI*. Further four above mentioned descriptors reflect only the differences between two category combinations (1 vs. 3, 2 vs. 3) but do not reflect the change between categories 1 and 2. On the other hand, the potassium content (*K*) is not significantly influenced by the change between the category 2 and 3, and finally, breastfeeding (*BF*) is not related to the distinction between the *HT* categories 1 and 3 even though the exchange between the categories 1 and 2 or 2 and 3 shows the significant relation. These findings were obtained by means of least significant difference (LSD) test as well as Bonferroni test in ANOVA.

Discriminant analysis and artificial neural networks

The aim of multidimensional classification in medicinal chemistry, decomposed into four steps, is creation of diagnostic categories, development of classification model by classifying the patients according to known relevancy to the given category, validation of the established model and, finally, categorization of the not yet classified subjects into one of possible classes. The classification efficiency is defined by the ratio of the successfully classified patient samples to the number of all samples; it is calculated in percentage for the training set of the patient samples as well as for the independent validation set.

The patients classified into three categories by the hypertension risk *HT* are displayed in Figure 3, which shows the graphical output of linear discriminant analysis. The samples of probands without hypertension (class 1) are located at negative values of the first discriminant function (DF1), while the patients with confirmed hypertension (class 3) are located at high DF1 values. The samples of the patients with hypertension as a result of another disease (class 2) are located between the groups 1 and 3.

Only two of seventy samples were incorrectly classified by LDA. The first one regards the patient with diagnosed secondary hypertension (class 2) but his values of biochemical tests were affected by metabolic disturbances and therefore he was classified into class 1. The second case regards the patient diagnosed into class 1, but due to gastrointestinal disease the tests values were altered and he was classified into class 2.
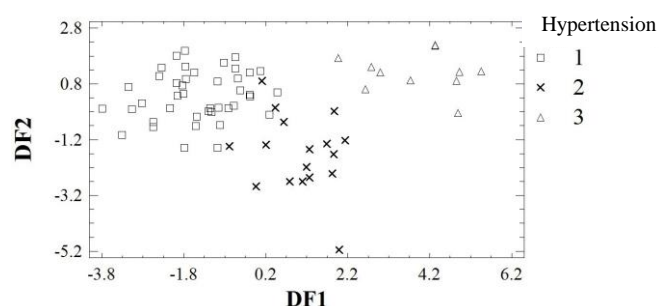
Figure 3. Classification of 70 patient samples by linear discriminant analysis according to hypertension diagnosis *HT*: 1 - patients without hypertension, 2 - patients with a conditional hypertension caused by another disease, 3 - patients with hypertension. Software Statgraphics Centurion XV.

Advanced approach to classification of the categorized samples involves application of several techniques of multidimensional data analysis and selection of that with the best classification efficiency, based mainly on the results achieved for the validation set. This way of valuation has already been successfully applied for diagnostic purposes and disease monitoring **1, 3, 14, 15**. In addition to LDA further classification techniques were used in this work – QDA, GDA, the non-metric KNN technique with different number of nearest neighbours, and logistic regression, which all belong to the discriminant analysis family **16**. Their results are compared to the outputs of ANN.

Table 2 summarizes the classification efficiency of 70 patient samples categorized into 3 classes using 14 continuous descriptors and different classification techniques. The LDA results were obtained by the software packages Statgraphics, SPSS and SAS, and by all software the same results were obtained. The quadratic discriminant analysis (QDA) and the K-th nearest neighbour method (KNN) were performed by using SAS software. The calculations by logistic regression were performed by means of JMP software. Most efficient ways of classification can be selected by the cross validation results in the last column of Table 2.

Table 2. Classification results (in %) in diagnosing hypertension in children.

Classification method	Training set	Cross-validation
LDA	97.1	90.0
QDA	98.6	58.6
GDA	96.5	91.2
KNN *K* = 3	82.9	77.1
KNN *K* = 5	91.4	87.1
KNN *K* = 7	91.4	88.6
KNN *K* = 9	95.7	91.4
KNN *K* = 11	94.3	91.4
LR	100.0	83.8
ANN*)	100.0	92.9*)

*)In ANN classification the test set results are shown instead of the cross-validation output.

Analysis by artificial neural networks was performed by using software Statistica 7.0. A three-layer perceptron with back error propagation was used. The whole data set was randomly divided into a training set (46 samples), validation set (10 samples) and a test set (14 samples). The best results were achieved using 12 optimally selected continuous

descriptors at the input: *AGE*, *AH*, *ALT*, *AW*, *BF*, *BH*, *BMI*, *BW*, *HB*, *K*, *MCV*, *Na* and 8 hidden neurons. The selection of the best network was made by comparing the classification efficiency of many networks evaluated for the validation data set, which was performed automatically by software using the option Intelligent Problem Solver).

The inspection of Table 2 reveals very good results of several techniques – over 90 % efficiency. The best results provide ANN with 92.9 % of the uncategorized patient samples classified into the appropriate category. Slightly lower, but still very successful are the classification efficiencies observed for KNN (for K = 9 or 11), GDA and LDA. All of them allow a valuable prediction of the hypertension risk in children.

Conclusions

Hypertension is not only a serious disease of adults, but as demonstrated in recent years, it is now increasingly encountered in children. The progress of this latent disease leads to damage and subsequent failure of vital organs. Diagnosis of hypertension in children is very difficult. The problems with the blood pressure measurement require a long-term monitoring of the state of the patient via biochemical tests leading the physician to diagnose. There exist several hidden risk factors that contribute to the development of hypertension and a possibility of their coincidence increases a real risk for its occurrence. Chemometrical approach, which makes complex analysis of the impact of all risk factors, may effectively support diagnosing and monitoring this disease. It was found that the factors most influencing hypertension risk in children are actual height and weight, body mass index, and age; the biochemical tests mostly reflecting children hypertension are haematocrit, haemoglobin and in a lower extent also sodium content and mean corpuscular volume. Applied multidimensional classification techniques enable a successful prediction of the hypertension risk in children. For this purpose the most successful are artificial neural networks but also simpler techniques – K-th nearest neighbour, linear and general discriminant analysis provide valuable risk prediction. They may considerably facilitate the diagnosis, start the therapy earlier and avoid complications from hypertension.

Acknowledgements

References

[1]Balla, B., Mocák, J., Pivovarníková, H., Balla, J*., Chem-Eur. J.*, **2004**, *72*, 259-267.

[2]Kavková, D., Varmusová, E., Tudík, I., Mocák, J., Balla, B. *Stud. Pneumol. Phtisiol*., **2007**, *5*, 199-203.

[3]Mrázová, V., Mocák, J., Varmusová, E., Kavková, D., Bednárová, A., *J. Pharm. Biomed*., **2009**, *50*, 210-215.

[4]Harrabi, I., Belarbia, A., Gaha, R., Essoussi, A. S., Ghannem, H., *Can. J. Cardiol.*, **2006**, *22*, 212-216.

[5]Sorof, J. M., *Am. J. Hypertens.*, **2002**, *15*, 57-60.

[6]Litwin, M., Niemirska A., Śladowska-Kozlowska, J., Wierbicka, A., Janas, R., Wawer, Z. T., Wisniewski, A., Feber, J., *Pediatr. Nephrol.,* **2010**, *25*, 2489-2499.

[7]Pierdomenico, S.D., Lapenna, D., Bucci, A., Di Iorio, A., Neri, M., Cuccurullo, F., Mezzetti, A., *Am. J. Hypertens.*, **2004**, *17*, 876-888.

[8]Falkner B, Gidding SS, Portman R, Rosner B., *Pediatrics,* **2008**, *122*, 238-242.

[9]Salvadori, M, Sontrop, J. M., Garg, A. X., Truong, J, Suri R. S., Mahmud, F. H., Macnab, J. J., Clark, W. F., *Pediatrics,* **2008**, *122*, 821-827.

[10]Benmohammed, K., Nguyen, M. T., Khensal, S., Valensi, P., Lezzar, A., *Diabetes Metab.*, **2011**, *37*, 291-297.

[11]Sorof, J., Daniels, S., *Hypertension*, **2002**, *40*, 441-447.

[12]Lurbe, E., Cifkova, R., Cruickshank, J. K., Dillon, M. J., Ferreira, I., Invitti, C., Kuznetsova, T., Laurent, S., Mancia, G., Morales-Olivas, F., Rascher, W., Redon, J., Schaefer, F., Seeman, T., Stergiou, G., Wühl, E., Zanchetti, A., *J. Hypertens.*, **2009**, *27*, 1719-1742.

[13]Li, S. C., Kuo, S. C., Hsu, Y. Y., Lin, S. J., Chen, P. C., Chen, Y. C. J., *J. Exp. Clin. Med.*, **2010**, *2*, 165-172.

[14]Mocák, J., Balla, B., *Chem. Listy.,* **2003**, *97*, 736-737.

[15]Ďurčeková, T., Mocák, J., Boronová, K., Balla, J., *J. Pharm. Biomed. Anal.* **2011**, *54*, 141-147.

[16]Khattree, R., Naik, N. N., *Multivariate data reduction and discrimination with SAS software,* **2002.**

IN- SILICO ANALYSIS OF DIFFERENT PLANT PROTEIN AND THEIR ESSENTIAL COMPOUND WITH SULFONYLUREA BINDING PROTEIN OF β-CELLS OF HOMO SAPIENS FOR CURING DIABETES MELLITUS TYPE II DISEASE

Rohit Sahu[a]* and Neerja Shukla[b]

Diabetes (type-2) is a chronic disorder affecting millions people all over the world. The disease is associated with long-term dysfunction, damage, and failure of various organs thus, affects almost every physiological system of the body. The chronic insulin resistance, progressive decline in β-cell function or increased rate of cell death results decreased insulin production and finally leads the disease. The sulfonylurea is known to regulate blood glucose homeostasis but have a characteristic profile of side effects. Some medicinal plant have showed hypoglycemic activities but the exact mechanism of action of these drugs at cellular level is yet not known and thus no better formulation of indigenous medicine could be developed till date for the treatment of type-2 diabetes. Therefore, the present study has been done to investigate the effect of the indigenous drugs, *in-silico* on the diabetic receptor, with a view to observe their effect on β-cell which could be helpful for the development of better formulation for the treatment of diabetes. Now days most of the drugs used in the treatment of type-2 diabetes either target the sulfonylurea receptor stimulating insulin release. Targeting of sulfonylurea may provide an important help for the development of drugs against type-2 diabetes. However, absence of tertiary structure of sulfonylurea limits the possibilities of structure based drug designing. In the present work we have explore the 3D structure of sulfonylurea receptor using homology approach. Based on the active sites we have screened the essential compound of Indigenous plants as a inhibitor as well as plant protein against modelled protein using iGEMDock 2.1 and Hex6.0 Cuda softwares. The Lead compound of plant as well as plant protein molecule would be scaled out on the basis of binding efficiency, starting from higher to lower and given the preference compare with the other one.

*Corresponding Authors
    E-Mail: homoimmuno@rediffmail.com
[a]   Center of Bioinformatics, University of Allahabad
[b]   Nehru Gram Bharti University, Allahabad

Introduction

Diabetes (type-2) is a chronic disorder affecting millions people all over the world and today India leads the world with the largest number of diabetics. The disease is associated with long-term dysfunction, damage, and failure of various organs thus, affects almost every physiological system of the body.

The management of diabetes mellitus (type II) has continued to be challenges all over the world[1] including the India where it is estimated that 19.4 million individuals are affected by the non-insulin dependent diabetes mellitus (NIDDM), which is likely to go up to 57.2 million by the year 2025.[2] India leads the world today with the largest number of diabetics in any given country. In the 1970s, the prevalence of the diabetes among the urban Indians was reported to be 2.1 percent, which has now risen to 12.1 percent. Moreover there is an equally large pool of individuals with impaired glucose tolerance (IGT) and many of them may eventually develop NIDDM in the coming future.[3]

Diabetes mellitus type 2 represents the final stage of a chronic and progressive syndrome representing a heterogeneous disorder caused by various combinations of insulin resistance and decreased pancreatic cell function caused by both genetic and acquired abnormalities.[1–7] Currently, type 2 diabetes mellitus is diagnosed when the underlying metabolic abnormalities consisting of insulin resistance and decreased cell function cause elevation of plasma glucose above 1260 mg L^{-1} (7 mmol L^{-1}) in the fasting state and/or above 2000 mg L^{-1} (11.1 mmol L^{-1}) 120 min after a 75-g glucose load.[8]

However, the fact that many newly diagnosed type 2 diabetic subjects already suffer from so called "late complications of diabetes" at the time of diagnosis[9] indicates that the diagnosis may have been delayed and, in addition, that the pre-diabetic condition is harmful to human health and requires increased awareness by physicians and the general public.

β-Cell dysfunction is initially characterized by impairment in the first phase of insulin secretion during glucose stimulation and may antedate the onset of glucose intolerance in type 2 diabetes.[10] Initiation of the insulin response depends upon the trans- membranous transport of glucose and coupling of glucose to the glucose sensor. The glucose/glucose sensor complex then induces an increase in glucokinase by stabilizing the protein and impairing its degradation. The induction of glucokinase serves as the first step in linking intermediary metabolism with the insulin secretory apparatus. Glucose transport in cells of type 2 diabetes patients appears to be greatly reduced, thus shifting the control point for insulin secretion from glucokinase to the glucose transport system.[11,12] This defect is improved by the sulfonylureas.[13,14]

Sulfonylureas are drugs that stimulate secretion of insulin from the pancreatic cells.[15,16] and are therefore used extensively in the treatment of type 2 diabetes. It is well established that sulfonylureas stimulate insulin release by interacting with the high-affinity 140-kDa SUR-1 protein of the ATP-regulated K^+ channel at the cytoplasmic leaflet of the plasma membrane. This interaction closes the channel, causing membrane depolarization, the opening of voltage-gated L-type Ca^{2+} channels, an increase in cytoplasmic-free Ca^{2+} concentration, and the activation of the secretory machinery.[17,18] Sulfonylureas also shows to stimulate insulin exocytosis by directly interacting with the secretory machinery and not through closure of the plasma membrane ATP-regulated K^+ channel.[19-21] This effect may constitute part of the therapeutic benefits of sulfonylureas and contribute to their hypoglycemic action in diabetes.

Nevertheless, some studies have clearly demonstrated that the second-generation sulfonylurea glibenclamide accumulates progressively in the β-cell. Moreover, autoradiography studies have shown that sulfonylureas are internalized by the β-cell and bind to intracellular sites such as secretory granules.[19, 20-22]

Medicinal plants used in curing diabetes mellitus

Diabetes mellitus is a common disease in the United States. It is estimated that over 16 million Americans are already caught with diabetes, and 5.4 million diabetics are not aware of the existing disease. Diabetes prevalence has increased steadily in the last half of this century and will continue rising among U.S. population. It is believed to be one of the main criterions for deaths in United States, every year. This diabetes information hub projects on the necessary steps and precautions to control and eradicate diabetes, completely.

There is an increasing demand by patients to use natural products with antidiabetic activity, because insulin and oral hypoglycaemic drugs have undesirable side effects.[23] Medicinal plants are a good source of natural antioxidants believed to exert their effect by reducing the formation of the final active metabolite of the drug-induced systems or by scavenging the reactive molecular species to prevent their reaching a target site.[24-26] It has been documented that several medicinal plants show their hypoglycaemic effects associated with a significant alteration in the activity of liver hexokinase,[27] glucokinase.[28] In addition, Bopanna et al.[27] and Eskander et al.[29] demonstrated that the administration of several herb extracts could restore the changes in the activities of serum enzymes, like alkaline phosphatase (ALT), acid phosphatase and transaminases, aspartate aminotransferase (AST) and alanine aminotransferase (ALT). Phytochemicals isolated from plant sources have been are used for the prevention and treatment of cancer, heart disease, DM, and high blood pressure.[30]

On the other hand in Indian medicine mentions various plant formulations helpful in the treatment of diabetes mellitus. These plant medicines are gaining considerable recognition world wide.[31] The *Gymnema sylvestre*, an indigenous medicine has been studied extensively for its beneficial action in diabetes mellitus. The active ingredients of *Gymnema sylvestre* are the gymnemic acid, which appears to correct the metabolic derangements in diabetic

liver, kidneys and muscles and reverse the hepatic pathological changes during the hyperglycemic phase. Results from the other studies show that its extracts may affect the insulin release by increasing the cellular permeability.[32] It was observed that it regulates well the blood sugar level in alloxan induced diabetic rabbits and increases the uptake and incorporation of glucose into glycogen and proteins.[33] It has also been documented that *Gymnema sylvestre* not only affects the blood glucose homeostasis but also increases the activity of glucose by insulin dependent pathways.

Pterocarpus marsupium is epicatechin also shows anti-hyperglycemic activity.[33] and exhibits alpha glucosidase inhibitory activity comparable to metformin.[32] It has been observed that it may renormalize the activities of hexokinase, glucokinase and phosphofructokinase.[30] It was also observed that *Pterocarpus marsuspium* treatment decreased the blood sugar level by 38–60 percent along with decreased hepatic and renal weight, whereas the renal glycogen content decreased by 75 %.[28] It was found that epicatechin increases the c–AMP content of the islets, which may be associated with the increased insulin release and conversion of proinsulin to insulin.[17]

Similarly, *Eugenia jambolana*, a very common indigenous medicine significantly decreases the level of blood glucose blood urea, and cholesterol with increased glucose tolerance and the levels of total protein and liver glycogen.[19] It also decreases the activities of glutamate oxaloacetate transaminase and glutamate pyruvate transaminase.[29] Although various works have been conducted in relation to hypoglycemic activities of various indigenous drugs but the exact mechanism of action of these drugs at cellular level remain elusive.

Materials and Methods

All computations and molecular modelling were carried out on the IBM Workstation with Fedora 7 operating system using MODELLER9v8, iGEMDOCK 2.1, HEX6.0 CUDA and GROMACS 4.0.1 package.

Sequence alignment and molecular modeling of SUR-1 receptor

The protein sequence of sulfonylurea receptor (SUR-1) in fasta format was obtained from the NCBI database[34] (Accession No. AAB02278). Protein-BLAST algorithm[35] against Protein DataBank[36] was carried out for the sequence homology search, in order to identify homologous sequences with known 3-D structure. Blast-p (protein query–protein database) program was run with BLOSUM62 as a scoring matrix,[37] word size 3, gap penalty of 11 and gap extension penalty of 1. High resolution crystal structure of homologous protein as a template was considered for homology modelling. The Blast-p alignments were further refined by using Clustal *W* 2.0.10 program[38] with default parameters. The sequence and 3D structure of template protein were extracted from the PDB database. Crystal structure of ATP-binding cassette (ABC)-transporter haemolysin (Hly)B (PDB ID: 2FF7.A)[39] was obtained as the best hit amongst 39 hits according to its sequence identity

score, lowest E-value and highest resolution. The 3D structure of SUR-1 receptor was generated by MODELLER 9v8[40] and SWISS-MODEL server.[41] Homology modelling of SUR-1 receptor was performed in the following steps: template selection from Protein Data Bank (PDB), sequence-template alignment, model building, model refinement and validation.[42]

Protein structure validation

MODELLER generated several preliminary models which were ranked based on their DOPE scores. Some models having low DOPE score were selected and stereo-chemical property of each models was assessed by PROCHECK.[43] PROCHEK server was used for the validation of modeled SUR-1 receptor structure. PROCHECK analysis of the model was done to check whether the residues are falling in the most favoured region in the Ramachandran's plot or not. The model with the least number of residues in the disallowed region was selected for the further studies. Quality of models was evaluated with respect to energy and stereochemical geometry. ProSA-Web server[44] to evaluate energy and Verify 3D[45] to evaluate the local compatibility of the model related to good protein structure.

Molecular Docking

The iGEM Dock 2.1 program[46] was used for the molecular docking analysis of SUR-1 receptor with Lead compound of plants. The two dimensional structure of lead compounds were taken from pubchem server[48] of NCBI and converted it into 3D coordinate via CORINA server. The Generic evolutionary method (GA)[47] was used in iGEMDock to perform the automated molecular dockings. Default parameters were used for the docking of lead compound with SUR-1 receptor.

Another docking was also performed with Hex 6.0 Cuda program. Such docking was performed for calculating protein-protein interaction between the plant protein and SUR1 receptor. The Hex 6.0 Cuda is based on FFT algorithm for performing macromolecular docking.

Results and Discussion

Homology modeling of SUR-1

The SUR-1 has (Accession No. AAB02278) is 1581 amino acids long and shows structural similarity with the crystal structure of ATP-binding cassette (ABC)-transporter haemolysin (Hly)B (PDB ID: 2FF7.A). ATP-binding cassette (ABC)-transporter haemolysin (Hly)B was selected as a template on the basis of lowest E-value (0.00E-1) and maximum identity (45.5 %) (Data shown in Table 1). MODELLER 9v8 was used to generate the homology model of SUR-1 according to the crystal structure of 2FF7.A. Total five models were generated and their discrete optimize potential energy (DOPE) was calculated using "model-single.top" script (Table 2). The model no. 3 (PBP.B99990003.pdb) having maximum score was consider as a best model of SUR1 shown in Fig. 1.

Pymol software was used to visualize the model and find out the maximum numbers of helixes, turns and sheets in the protein.

Table 1. Comparative study of DOPE score of five models predicted through MODELLER and overall quality factor determination through ERRAT

Model predicted through MODELLER	DOPE score kJ mol⁻¹	Overall quality factor ERRAT
PBP.99990001	-12225.373	78.71
PBP.99990002	-12225.373	78.71
PBP.99990003	-20151.761	93.562
PBP.99990004	-20016.876	91.953
PBP.99990005	-20128.563	92.392

Protein structure analysis

The final model was validated using different tools: PROCHECK, Verify3D and ERRAT programs were used for the validation of predicted model. PROCHECK analysis of the modelled protein showed that 94.17 % of the residues were found in allowed regions of Ramachandran plot (Fig. 2). Among the 355 residues 270 residues found in most favoured region, 25 in additional allowed region, 3 in generously allowed region and 1 residue in disallowed region. The statistical score of the Ramachandran plot shows that 90.3 % are in the most favoured region, 8.4 % in additional allowed region, 1.0 % in generously allowed region and 0.3 % in disallowed region. The above results indicate that the protein model is reliable (Table 2). Verify 3D score profile access the quality of the model. Fig. 1 shows the verify 3D profile of the modelled protein, residues have an averaged 3D-1D score greater than zero should be considered reliable. The computability score for all the residues in the modelled protein are above zero.
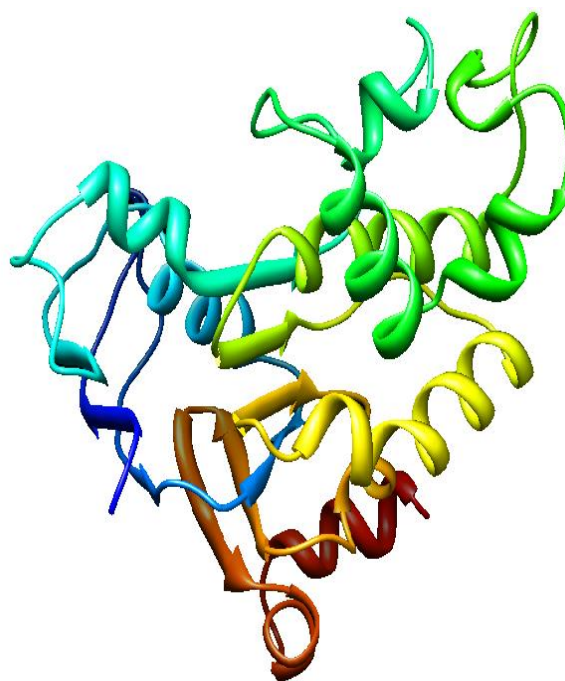
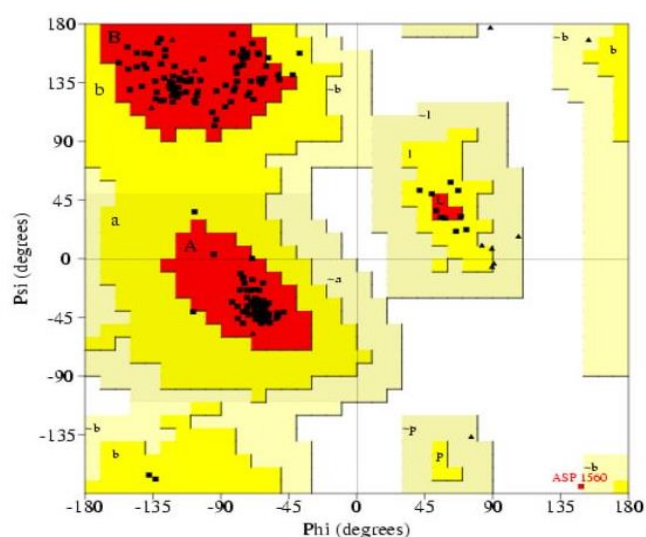**Figure 1.** 3D Structure of SUR1 of *Homo sapient*

Table 2. Ramachandran plot calculation for 3D model of SUR1

% Amino acid in	Modelled protein	Template
Favored regions	93.1	93.9
Additional allowed regions	14.0	12.0
Generously allowed regions	0.0	2.0
Disallowed regions	1.0	0.0

Homology modelling of Plant Protein

The plant protein have (GI No. 154082720, 270281938, 42491750, 327315251, 66970848, 345288139, 374711794, 68052751, 296012006) are long chain of amino acids and shows structural similarity with the crystal structures (PDB ID. 3kylA, 3h4iA, 1d8vA, 1ej7L, 1gp6A, 1ausN, 4rubA, 2w90B, 2pq6A).Such crystal structure was selected as a template on the basis of lowest *e*-value and maximum identity (%) (data shown in Table 3). MODELLER 9v8 was used to generate the homology model of plant protein according to the crystal structure of their selected templates. Total five models were generated and their discrete optimize potential energy (DOPE) was calculated using "model-single top" script. The model which having maximum score was consider as a best model of plant protein shown in Fig.3. Pymol software was used to visualize the model and find out the maximum numbers of helixes, turns and sheets in the protein.


Figure 2. Ramachandran's map of SUR1 of *Homo sapience*

Protein structure analysis of Plant Protein Model

The final model was validated using different tools: PROCHECK, Verify3D and ERRAT programs were used for the validation of predicted model. PROCHECK analysis of the modelled protein showed that maximum % i.e. >90 % of the residues were found in allowed regions of Ramachandran plot. Verify 3D score profile access the quality of the model. Fig. 3 shows the verify 3D profile of the modelled protein, residues have an averaged 3D-1D score greater than zero should be considered reliable.
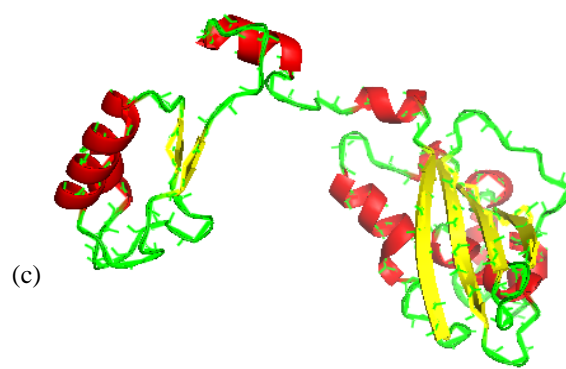
The computability score for all the residues in the modeled protein are above zero.
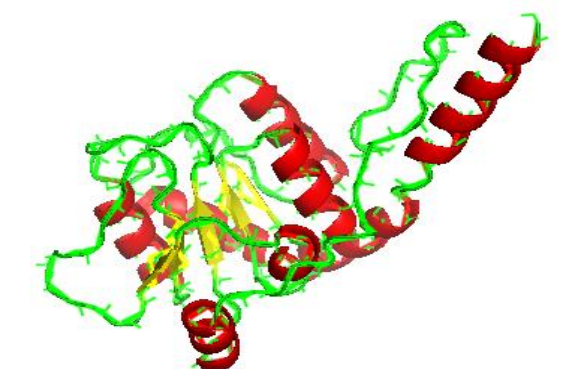

(a)

Phyllanthus emblica
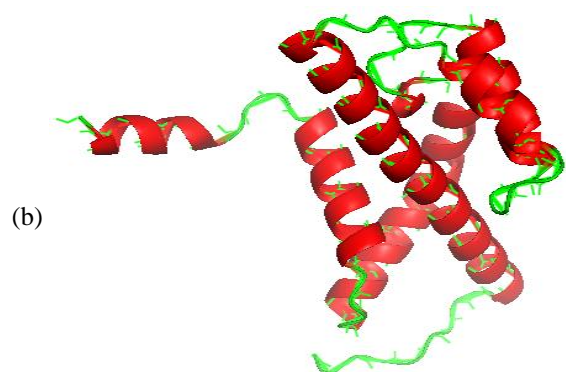


(b)

Trigonella foenum graecum


(c)

Swertia chirata

(d)

Gymnema sylvestre

Table 3. List of medicinal plant and their modelling properties

Plant	G.I number	Sequence identity [%]	Based on template	*E*-value	DOPE score kJ mol⁻¹
Azadirachta indica	154082720	10.993	3kylA	3.9E-06	-17560.344
Gymnema sylvestre	270281938	27.67	3h4iA	7.9E-41	-2892.445
Momordica charantia	42491750	100	1d8vA	5.4264E-136	-10898.884
Ocimum sanctum	327315251	98.361	1ej7L	2.16647E-101	-8356.080
Phyllanthus emblica	66970848	32.653	1gp6A	0	-10421.651
Pterocarpus marsupium	345288139	95.946	1ausN	1.86376E-123	-10666.641
Swertia chirata	374711794	96.585	4rubA	3.85617E-113	-8178.599
Trigonella foenum graecum	68052751	49.296	2w90B	0	-6055.666
Withania somnifera	296012006	51.271	2pq6A	0	-2838.410
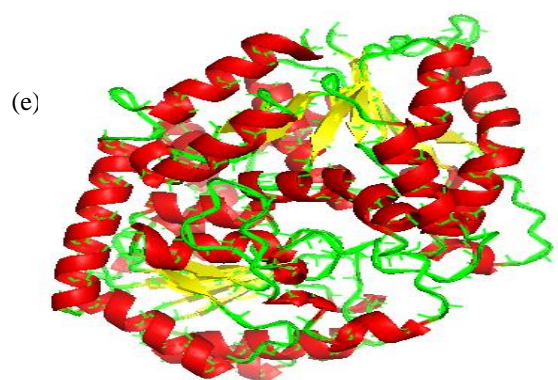
(e)

Withania somnifera

(f)

Momordica charantia

(g)

Ocimum sanctum

(h)

Azadirachta indica

(i))
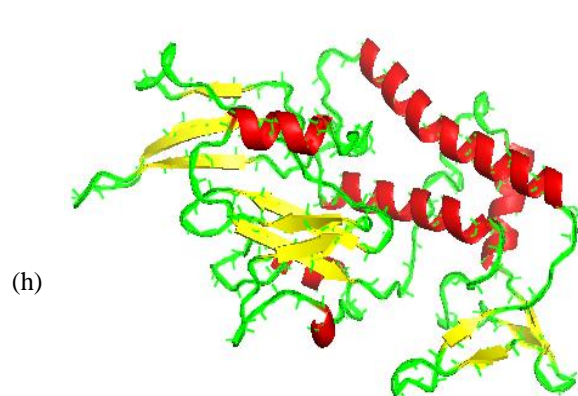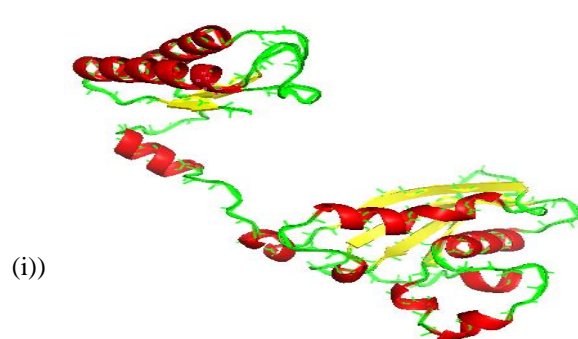
Pterocarpus marsupium

Figure 3a-i. 3D Structure of plant protein

Preparation of lead compound

According to the several studies it is found that there are several plants which help to stimulate β-cells to synthesize insulin for the treatment of Diabetes Mellitus Type II. It was found by studies that such plants have essential element which help in controlling Diabetes Mellitus Type II. So these essential compounds are taken as lead compound whose two dimensional structure were taken from pubchem server[48] of NCBI and converted it into 3D coordinate via CORINA server. The properties of Lead compound has been calculated both with the help of off-line tools as well as on-line web server

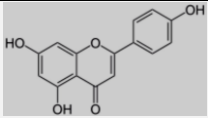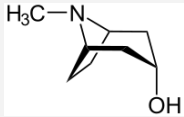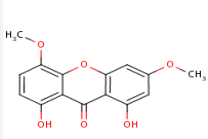**Table 4.** Lead compounds of medicinal plants and their properties
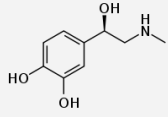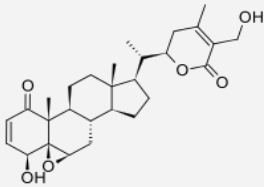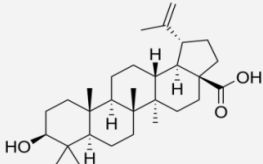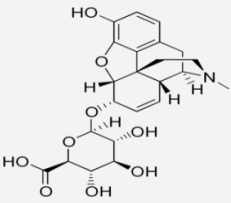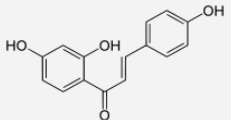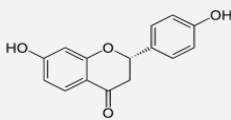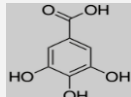
Name	Plant Source	I.U.P.A.C Name	Molecu-lar formula	Molecular Mass	Structure
Apigenin	*Ocimum sanctum*	5,7-dihydroxy-2-(4-hydroxyphenyl)-4H-1-benzopyran-4-one	$C_{15}H_{10}O_5$	270.24 g mol^{-1}	
Tropine	*Withania somnifera*	(3-endo)-8-methyl-8-azabicyclo[3.2.1]octan-3-ol	$C_8H_{15}NO$	141.21 g mol^{-1}	
Swerchirin	*Swertia chirata*	1,8-dihydroxy-3,5-dimethoxy-9H-xanthen-9-one	$C_{15}H_{12}O_6$	288.254 g mol^{-1}	
Adrenaline	*Azadirachta indica*	(R)-4-(1-hydroxy-2-(methylamino)ethyl)ben-zene-1,2-diol	$C_9H_{13}NO_3$	183.204 g mol^{-1}	
Withaferin A	*Withania somnifera*	(4β,5β,6β,22R)-4,27-dihydroxy-5,6:22,26-diepoxyergosta-2,24-diene-1,26-dione	$C_{28}H_{38}O_6$	470.60 g mol^{-1}	
Betulinic acid	*Gymnema sylvestre*	(3β)-3-hydroxylup-20(29)-en-28-oic acid	$C_{30}H_{48}O_3$	456.70 g mol^{-1}	
Morphine 6-glucuronide	*Gymnema sylvestre*		$C_{23}H_{27}NO_9$	461.46 g mol^{-1}	
Isoliquiriti-genin	*Pterocarpus marsupium*	(E)-1-(2,4-dihydroxyphenyl)-3-(4-hydroxyphenyl)prop-2-en-1-one	$C_{15}H_{12}O_4$	256.25 g mol^{-1}	
Liquiritige-nin	*Pterocarpus marsupium*	(2S)-7-hydroxy-2-(4-hydroxyphenyl)-2,3-dihydro-4H-chromen-4-one	$C_{15}H_{12}O_4$	256.25 g mol^{-1}	
Gallic acid	*Emblica officinalis and Syzygium cuminii*	3,4,5-trihydroxybenzoic acid gallic acid	$C_7H_6O_5$	170.12 g mol^{-1}	

Table 4. contg.
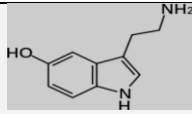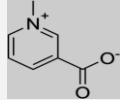
| Serotonin | *Momordica charantia* | 5-hydroxytryptamine | $C_{10}H_{12}N_2O$ | 176.215 g/mol | |
| Trigonelline | *Trigonella foenum-graecum* | 1-methylpyridinium- 3-carboxylate | $C_7H_7NO_2$ | 137.14 g mol^{-1} | |

Table 5. Docking result of Plant Protein and SUR1 Receptor

Plant Name	Clst	Soln	E_{total}	E_{shape}	Bmp	RMS
Momordica charantia	1	1	-441.3	-441.3	-1	-1
Azadirachta indica	1	1	-468.5	-468.5	-1	-1
Gymnema sylvestre	1	1	-516.0	-516.0	-1	-1
Ocimum sanctum	1	1	-416.8	-416.8	-1	-1
Phyllanthus emblica	1	1	-434.7	-434.7	-1	-1
Pterocarpus marsupium	1	1	-440.1	-440.1	-1	-1
Swertia chirata	1	1	-467.9	-467.9	-1	-1
Trigonella Foenum Graecum	1	1	-409.6	-409.6	-1	-1
Withania somnifera	1	1	-540.3	-540.3	-1	-1

Table 6. The interaction energies (kcal mol^{-1}) of SUR-1 receptor and plant ligands obtained from the molecular docking with iGEM Dock

Lead Compound	Total energy	VDW	H-bond	AverConPair
5-Hydroxytryptamine	-69.6924	-66.1924	-3.5	30
Adreline	-61.3787	-58.8847	-2.49403	30.4615
Apigenin	-81.5924	-78.1433	-3.44905	29.381
Gallic acid	-77.0755	-77.0755	0	29
Tropine	-57.45	-49.11	-8.34	0
Isoliquiritigenin	-86.39	-65.66	-20.74	0
Liquiritigenin	-96.42	-79.43	-16.99	0
Withaferin A	-91.33	-75.87	-15.46	0
Betulinic acid	-78.33	-65.93	-9.6	-2.8
Morphine 6-glucuronide	-104.24	-101.42	-2.5	-0.36
Lutelin	-102.811	-102.811	0	22.3871
Swerchirin	89.1252	89.1252	0	14.6667
Trigonelline	-63.0574	-56.5052	-6.5522	34.4

Molecular Docking Analysis

Molecular docking was performed on SUR-1receptor with Lead compounds using iGEMDock2.1. The interaction of these Ligands with modelled protein was selected on the basis of binding energy or Total Energy, VDW and Hydrogen bonding interaction. These values along with the hydrogen bond forming residues are presented in Table 5. The Lead compound that was showing smaller dissociation constant and higher binding energy, VDM with SUR-1 receptor, was considered to be a better Lead compound.

Another molecular docking was performed on SUR-1 receptor with Plant protein using Hex6.0Cuda. The interaction of these Proteins with modelled protein was selected on the basis of E_{total}, E_{shape}, Bmp, RMS. These values are presented in Table 6. The Plant Protein that was showing higher binding energy i.e. E_{total} with SUR-1 receptor, was considered to be a better protein.

The morphine 6-glucuronide was bound on the active amino acid of SUR-1 receptor with -104.24 kcal mol^{-1} binding energy (Fig. 4). While the other have less binding energy as compare with morphine 6-glucuronide. In the another docking process the protein of *Withania somnifera* is showing highest binding energy as compare with other plant protein molecules. Morphine 6-glucuronide is found in the *Gymnema sylvestre* plant which is popularly known as Diabetic plant. Such interaction value proving that it has highest efficiency in binding with SUR1 receptor compare with the other and can be used as the most potent Drug against the SUR-1 receptor amongst the other molecules in this study.

Binding energy calculated for each docked complex are shown in Tables 5 and 6. The values of molecular docking studies are presented in Tables 5 and 6, evidently describes the good correlation between lead compound and molecules to modelled protein of SUR-1 receptor. Our data revealed

a

b
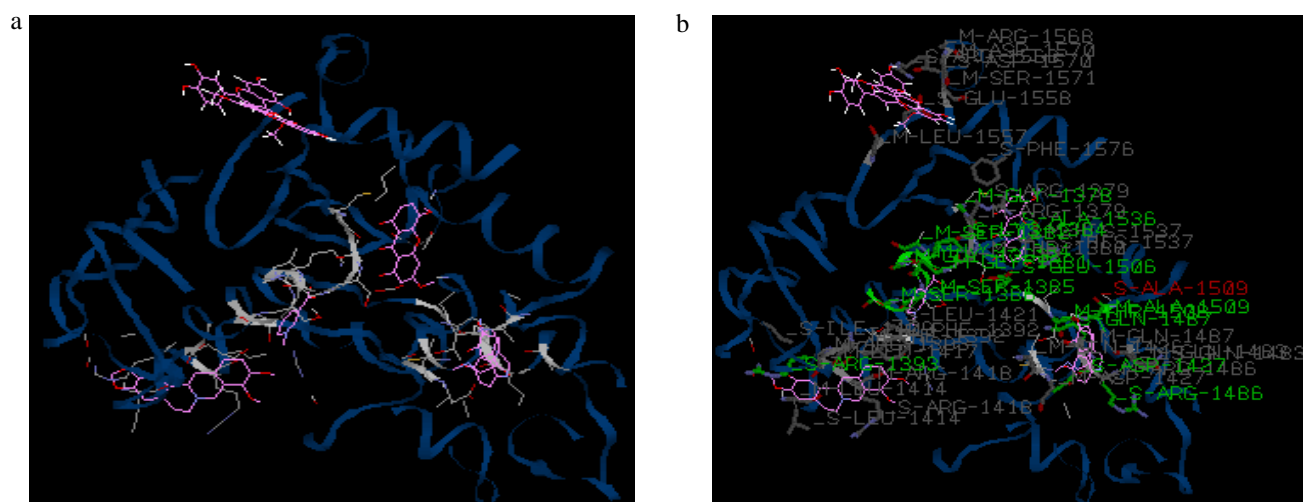
Figure 4. Docking Poses of iGEM DOCK2.1. a) Docking pose between lead compound and SUR1; b) Docking pose between lead compound and SUR1 showing binding with different amino acid of the receptor;
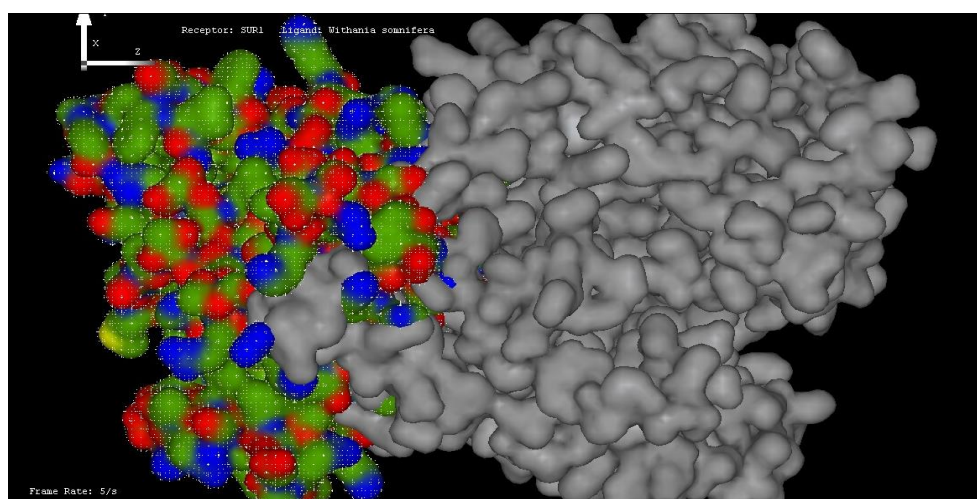
Figure 5. Docking Poses of HEX6.0 CUDA. **C)** Docking pose between protein structure of *Withania somnifera* and SUR1. The SUR1 is in dotted coloured on the basis atoms present and the protein is the pattern of colour selection with solid structure form.

that the efficacy of the entire compound and the plant protein was scaled out on the basis of their binding energy which help to choose or to develop the combine drug of such plant which would be used as thee best antibiotic against Diabetes Mellitus Type-II.

Discussion

The result of above experiment shows that the Morphine 6-glucuronide has high binding affinity as compared with other like lutelin, swerchirin, trigonelline, 5-hydroxytryptamine, adreline, apigenin, gallic acid, tropine, liquiritigenin and isoliquiritigenin on the basis of binding energy. The morphine 6-glucuronide was bound on the active amino acid of SUR-1 receptor, while the other was bound on the active amino acid of SUR-1 receptor lower less binding energy compare with Morphine 6-glucuronide. Similarly in protein-protein interaction performed by Hex operating software, *Withania somnifera* is showing highest binding energy as compare with other plant protein

molecules other like *Gymnema sylvestre, Momordica charantia, Azadirachta indica, Ocimum sanctum, Phyllanthus emblica* and *Pterocarpus marsupium.* So on that basis the morphine 6-glucuronide and *Withania somnifera* have higher binding affinity with the receptor than the other. This shows that the *Withania somnifera* and *Gymnema sylvestre* works much better than the other plants over the SUR1 receptor. Another reason for being better performance shown by the *Gymnema sylvestre* which could be utilized in place of other or used as essential drug during the preparation of combine drug is that *Gymnema sylvestre* also contain Betulinic acid as an essential compound in it. Betulinic acid also has a good binding energy with the SUR1 receptor. So due present morphine 6-glucuronide and betulinic acid as an essential element in *Gymnema sylvestre* makes the *Gymnema sylvestre* potential plant for curing Diabetes mellitus type II. The use of plant as an oral drug is least toxic and having little or no side effect than compare with chemical based drug. So come to the end, on the basis of molecular docking *Gymnema sylvestre* can be used as a drug as it have all the properties of stimulating the β-cells of pancreas for the synthesis of insulin.

Conclusion

In the present study, we build the 3 D structure of SUR-1 using homology modelling. The protein structure was verified to be a good quality and being used for the docking study. The Thirteen essential compound of the indigeneous plant and Nine indigenous plant protein were designed for the studies, and used for binding with SUR-1 receptor. Top ranked docking analysis was revealed that, Morphine 6-glucuronide and *Withania somnifera* binds at the active sites with higher binding energy. On the basis of binding energy, Morphine 6-glucuronide and other like lutelin, swerchirin, trigonelline, 5-hydroxytryptamine, adreline, apigenin, gallic acid, tropine, liquiritigenin and isoliquiritigenin found to be best and most effective inhibitor against diabetes mellitus Type-II. Similarly the plant protein of *Withania somnifera* and other like *Gymnema sylvestre, Momordica charantia, Azadirachta indica, Ocimum sanctum, Phyllanthus emblica* and *Pterocarpus marsupium* on the basis of binding energy found to be best and most effective inhibitor against diabetes mellitus type-II. This information would be also useful for the in new drug designing against diabetes mellitus type-II.

References

[1]Gerich, J. E., *Endocr. Rev.* **1998**, *19*, 491 –503.

[2]DeFronzo, R. A., *Diabetologia*, **1992**, 35, 389–397.

[3]Yki, J. H., *Lancet,* **1994**, *343*, 91–95.

[4]Ferrannini, E., *Endocr. Rev.,* **1998**, *19,* 477–490.

[5]Kahn, C. R., *Diabetes*, **1994**, *4*, 1066–1084.

[6]Olefsky, J. M., *Med. Biol.*, **1993**, *334*, 129–150.

[7]Haring, H. U., *Ex. Clin. Endocrinol. Diabetes,* **1999**, *107*, S17–S23

[8]Report of the Expert Committee., *Diabetes Care*, **1999**, 22[Suppl 1], S5–S19.

[9]Beck, N. H., Groop, L. C., *J. Clin. Invest.*, **1994**, *94*, 1714–1721.

[10]Ward, W. K., Beard, J. C., Porte, D., *Diabetes Metab.*, **1986**, *2*, 297–313.

[11]Leahy, J. L., *Diabetes Care*, **1991**, *13*, 992–1010.

[12]Porte, D., *Diabetes*, **1991**, *40*, 166–180.

[13]Luz, L., DeFronzo, R. A., *Am. J. Physiol.*, **1989**, *257*, E241–E246.

[14]Groop, L. C., Ratheiser, K., Luzi, L., Melander, A., Simonson, D. C., Petrides, A., Bonadonna, R. C., Widén, E., DeFronzo, R. A., *Acta Diabetol,* **1991**, *28*, 162–168.

[15]Otto, H., Mikosch, M., Otto-Bendfeldt, E., *Med. Welt*, **1966**, *3*, 1864 –1966.

[16]Krall, L. P., *Clin. Ther.,* **1984**, *6*, 764 –762.

[17]Ashcroft, F. M., Rorsman, P., *Mol. Biol.,* **1989**, *54*, 87–143.

[18]Aguilar-Bryan, L., Nichols, C. G., Wechsler, S. W., Clement, J. P., Boyd, A. E., Gonzalez, G., Herrera-Sosa, H., Nguy, K., Bryan, J., Nelson, D. A., *Science,* **1995**, *268*, 423– 426.

[19]Flatt, P. R., Shibier, O., Szecowka, J., Berggren, P. O., *Diabetes Metab.,* **1994**, *20*, 157–162.

[20]Hellman, B., Sehlin, J., Taljedal, I. B., *Acta Endocrinol.*, **1984**, *105*, 385–390.

[21]Carpentier, J. L., Sawano, F., Ravazzola, M., Malaisse, W. J., *Diabetologia*, **1986**, *29*, 259–261.

[22]Marynissen, G., Smets, G., Kloppel, L., Gerlache, L., Malaisse, W. J., *Acta Diabetol*, **1992**, *29*, 113–114.

[23]Bonner-Weir, S., *J. Mol. Endocr.*, **2000**, *24*, 297-302.

[24]Butler, A. E., Janson, J., Bonner-Weir, S., Ritzel, R., Rizza, R. A., Butter, P. C., *Diabetes*, **2002**, *52*, 102-110.

[25]Maedler, K., Sergeev, P., Ris, F., Oberholzer, J., Joller-Jemelka, H. I., Spinas, G. A., Kaiser, N., Halban, P. A., Donath, M. Y., *J. Clin. Invest.*, **2002**, *110*, 851-860.

[26]Maedler, K., Spinas, G. A., Lehmann, R., Sergeev, P., Weber, M., Fontana, A., Kaiser, N., Donath, M. Y., *Diabetes*, **2001**, *50,* 1683-1690.

[27]Maedler, K., Spinas, G. A., Dyntar, D., Mortiz, W., Kaiser, N., Donath, M. Y., *Diabetes*, **2001**, *50*, 69-76.

[28]Piro, S., Anello, M., Di Pietro, C., Lizzio, M. N., Patanè, G., Rabuazzo, A. M., Vigneri, R., Purrello, M., Purrello, F., *Metabolism*, **2002**, *51*, 1340-1347.

[29]Lupi, R., Dotta, F., Marselli, L., Del Guerra, S., Masini, M., Santangelo, C., Patané, G., Boggi, U., Piro, S., Anello, M., Bergamini, E., Mosca, F., Di Mario, U., Del Prato, S., Marchetti, P., *Diabetes*, **2002**, *51*, 1437-1442.

[30]Mathis, D., Vence, L., Benoist, C., *Nature*, **2001**, *114*, 792-798.

[31]Goldback-Wood, S., Doronzynski, A., Lie, G.L., *B. M. J.*, **1996**, *313*, 131-133.

[32]Shrikant., Sharma, S., *Ind. J. Clin. Pract.*, **2002**, *12a*, 49-56.

[33]Shanmugasundaram, E. R., Rajeshwari, G., Baskaran, K., Rajesh Kumar, B. R., Radha Shanmugasundaram, K., Kizar Ahmath, B., *J. Ethnopharmacol.*, **1990**, *3*, 281-294.

[34]Gasteiger, E., Gattiker, A., Hoogland, C., Ivanyi, I., Appel, R. D., Bairoch, A., *Nucl. Acids Res.*, **2003**, *31*, 3784 – 378.

[35]Altschul, S. F., Madden, T. L., Schaffer, A. A., Zhang, J., Zhang, Z., Miller, W., Lipman, D. J., *Nucl. Acids Res.,* **1997**, *25*, 3389 – 3402.

[36]Berman, H. M., Westbrook, J., Feng, Z., Gilliland, G., Bhat, T. N., Weissig, H., Shindyalov, I. N., Bourne, P. E., *Nucleic Acids Research*, **2000**, *28*, 235-242.

[37]Henikoff, S., Henikoff, J. G., *Proc. Natl. Acad. Sci.,* **1992**, *89*, 10915-10919.

[38]Thompson, J. D., Higgins, D. G., Gibson, T. J., *Nucleic Acids Res.*, **1994**, *22(22)*, 4673-80.

[39]Powell, A. J., Tomberg, J., Deacon, A. M., Nicholas, R. A., Davies, C., *J. Biol. Chem.*, **2009**, *284(2)*, 1202-12.

[40]Sali, A., Blundell, T. L., *J. Mol. Biol.*, **1993**, *234*, 779 – 815.

[41]Arnold, K., Bordoli, L., Kopp, J., Schwede, T., *Bioinformatics,* **2006**, *22,* 195 – 201.

[42]Martí-Renom, M. A., Stuart, A. C., Fiser, A., Sánchez, R., Melo, F., Sali, A., *Ann. Rev. Biophys. Biomol. Struct.*, **2000**, *29*, 291 – 325.

[43]Laskowski, R. A., MacArthur, M. W., Moss, D. S., Thornton, J. M., *J. Appl. Crystallogr.*, **1993**, *26*, 283 – 291.

[44]Ward, W. K., Beard, J. C., Porte, D., *Diabetes Metab. Rev.*, **1986**, *2*, 297–313.

[45]Leahy, J. L., *Diabetes Care*, **1991**, *13*, 992–1010.

[46]Yang, J. M., Chen, Y. F., Tu, Y. Y., Yen, K. R., Yang, Y. L., *PLoS ONE*, **2007**, e428.1-e428.12.

[47]Hung, H. C., Tseng, C. P., Yang, J. M., Ju, Y. W., Tseng, S. N., Chen, Y. F., Chao, Y. S., Hsieh, H. P., Shih, S. R., John, T., Hsu, A., *Antiviral Res.*, **2009**, *81*, 123-131.

[48]Wang, Y. L., Xiao, J., Suzek, T. O., Zhang, J., Wang, J., Bryant, S. H., *Nucleic Acids Res*, **2009**, *37*, 623 – 633.

IN VITRO BIOLOGICAL SCREENING AND NOVEL SYNTHESIS OF CHALCONES USING REUSABLE POLYAMINE CATALYST

A. N. Kasat,[a] R. L. Magar,[b] S. A. Dake,[b] S. B. Shinde,[b] V. K. Mourya,[c] U. A. Deokate,[c] V. M. Joshi[d] and R. P. Pawar[b]*

Keywords: chalcone synthesis; antibacterial activity; flavones; polyamine catalyst

A simple and efficient method for the synthesis of chalcone derivatives using polyamine catalyst has been described. The antibacterial activity of chalcones are also evaluated by using gram positive (*S. aureus, B. subtillus*) and gram negative bacteria (*Klebsiella pneumonia, P. aerugenosa*) microorganisms.

*Corresponding Author
        E-mail: rppawar@yahoo.com
[a]   Government College of Pharmacy, Aurangabad-431005, (MS), India
[b]   Department of Chemistry, Deogiri College, Station Road, Aurangabad-431005, (MS), India
[c]   Government College of Pharmacy, Amravati-444601, (MS), India
[d]   K. R. A. Arts, Science and Commerce College, Deola, Dist. Nashik, (MS), India

INTRODUCTION

Flavonoids are the largest group of naturally occurring phenolic compounds, abundantly occurs in different plant both in free state and as glycosides. The presence of these pigments is responsible for the various colors and combination of such colors exhibited by bark, leaves, flowers, fruits and seeds of plants.[1] Flavonoids are present in vegetables, fruits, berries and beverages such as tea, red wine and fruit juices, having similar effects as antioxidants. Acyclic flavonoids include chalcones & aurones which also contain C6-C3-C6 backbone.[2]

They were formerly considered to be minor flavonoids. Chalcones are open chain flavonoids in which two aromatic rings are joined by three carbons α, β-unsaturated carbonyl system. They are the important intermediates of flavonoids synthesis.

Aurones, (Z)-2-benzylidenebenzofuran-3-(2H)-ones are responsible for the bright yellow colour of some ornamental flowers.They are biosynthesized from chalcones by the key enzyme aureusidin synthase.[3] They contribute to the yellow flower color in several ornamental plants.

Chalcones are readily accessible via two well-established routes comprising a base catalyzed aldol condensation or acid mediated aldolisation of 2-hydroxyacetophenone and benzaldehyde. The base catalyzed aldol condensation is usually preferred route toward the chalcone formation.

Several methods have been reported for the synthesis of chalcones.[4] Under acidic conditions cyclization of chalcones leads to the formation of corresponding hydroxyl dihydrochalcone, 2-hydroxy heterochalcones. Chalcone derivatives are known as versatile physiologically active compounds.[5-6]

Chalcones have been reported to possess many useful properties, including anti-inflammatory,[7] anti-microbial,[8] antifungal,[9] antioxidant,[10] antitumor,[11] antimalarial,[12] antiprotozoal,[13] antibacterial properties,[14] antifilarial activity,[15] mosquito larvicidal activity,[16] anticonvulsant activity,[17] mammalian α-amylase inhibitory activity,[18] cyclo-oxygenase inhibitory activity,[19] monoamine oxidases inhibitory activity.[20]

In reported work, we developed a new methodology for the synthesis of biologically important chalcones using the mixture of aldehydes and acetophenones in presence of polyamine catalyst. The recovered polyamine catalyst was recycled and reused several times to carry out the same reaction, without any loss in its efficiency (Scheme 1).
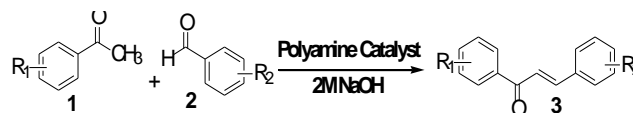
Scheme 1. Synthesis of chalcones by using polyamine catalysts

RESULTS AND DISCUSSION

Chalcones are synthesized using various catalysts like ionic liquid resins, clays, non-aqueous cation-exchange resin etc. Herein, we are reporting a simple and easy method for chalcone synthesis by using novel silica gel supported poly amine catalyst. The catalyst was prepared from solution of 3-aminopropyl-trimethoxy silane in dry toluene. The chalcone obtained using this catalyst is having more yields and it can be reusable. The activity of chalcones was found to be better. Structures of different chalcones synthesized are shown in Table 1.

Determination of minimum inhibitory concentration (MIC)

MIC of synthesized chalcone was determined using tube dilution technique against gram positive (*S. aureus,B. subtillus*) and gram negative bacteria (*Klebsiella pneumonia, P. aerugenosa*). The turbidity was measured by colorimeter at 620 nm. Colorimetrically, the MIC was found to be 125 μg mL^{-1}.

Table 1. Synthesis of chalcones using N,N-dibasic polyamine catalyst
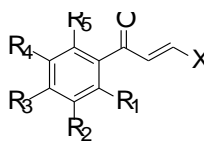
Comp. Codes	Substituent groups						M. p. (°C)	Yields (%)
	X	**R1**	**R2**	**R3**	**R4**	**R5**		
C1		OH	H	OH	H	H	187	93.32
C2		OH	H	OH	H	H	138	95.67
C3		OH	H	OH	H	H	124	87.45
C4		OH	H	OH	H		174	88.67
C5		OH	H	OH	H	H	96	76.45
C6		OH	H	OH	H	H	110	78.56
C7		OH	H	OH	H	H	5	73.45
C8		H	H	H	H	H	122	67.34
C9		H	H	H	H	H	94	87.78
C10		H	H	NO$_2$	H	H	118	68.78

Table 2. MIC Results of C9 compound against gram positive and gram negative bacteria

| Sr. No.	Concentration, µg mL^{-1}	Transmittance, %			
		S. aureus	*K. pneumonia*	*B. subtillus*	*P. aeruginosa*
C9a	1000	99	100	97	99
C9b	500	96	99	98	97
C9c	250	95	93	94	95
C9d	125	84	83	91	91
C9e	62.5	27	31	47	51

Table 3. MIC Results of C10 compound against gram positive and gram negative bacteria

Sr. No.	Concentration	Transmittance			
		S. aureus	*K. pneumonia*	*B. subtillus*	*P. aeruginosa*
C10a	1000	99	100	98	99
C10b	500	97	99	97	97
C10c	250	95	97	96	93
C10d	125	96	94	93	92
C10e	62.5	28	52	52	54

This concentration was used to study zone of inhibition of synthesized compounds. MIC results of chalcone C9 are shown in Table 2, Figure 1 and MIC results of chalcone C10 are shown in Table 3, Figure 2.
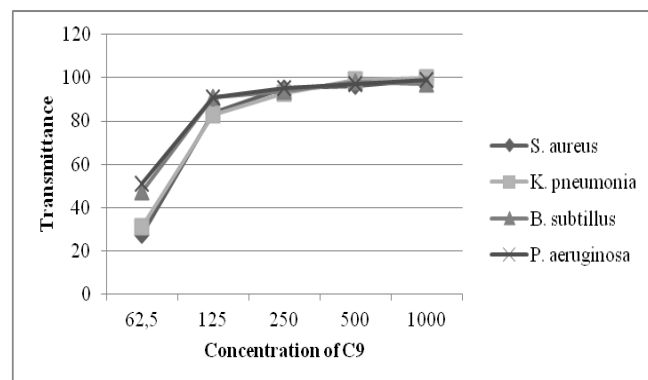
Figure 1. Graph indicating MIC of C9 against gram positive and gram negative bacteria
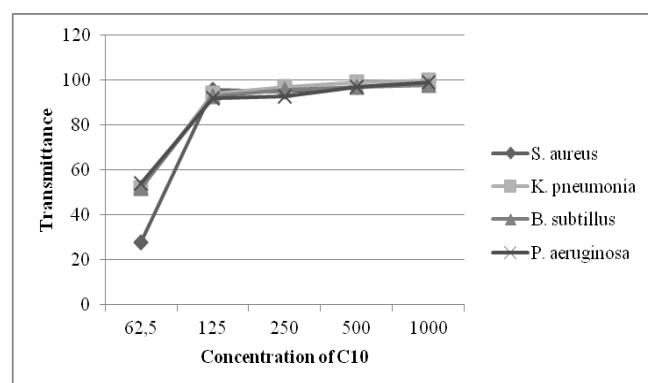
Figure 2. Graph indicating MIC of C10 against gram positive and gram negative bacteria

The results of MIC confirmed that the chalcone derivatives C9 and C10 showed inhibition growth of gram positive (*S. aureus, B. subtillus*) and gram negative bacteria (*K. pneumonia, P. aerugenosa*). MIC of 125µg/ml of testing compound is the concentration used to determine zone of inhibition against various microorganisms.[21]

Antibacterial activity of novel chalcone compounds

The chalcone are found to be antibacterial in nature. Various food borned pathogens are common agents responsible for various diseases. Several gram negative bacteria are harmful for human beings. The chalcone were used for bacterial growth inhibition. Compounds C9 and C10 are found to be antibacterial and showed a broad range of antibacterial activity. [22]

Zone of Inhibition

As per MIC results, it was founds that 125 µg/ml concentration is the minimum inhibitory concentration to inhibit further microbial growth. This concentration of compounds were used for the study of zone of inhibition on various microorganism. 100 µg of Ciprofloxacin was taken as standard and DMF were used as control.

Table 4. Zone of inhibition of compounds

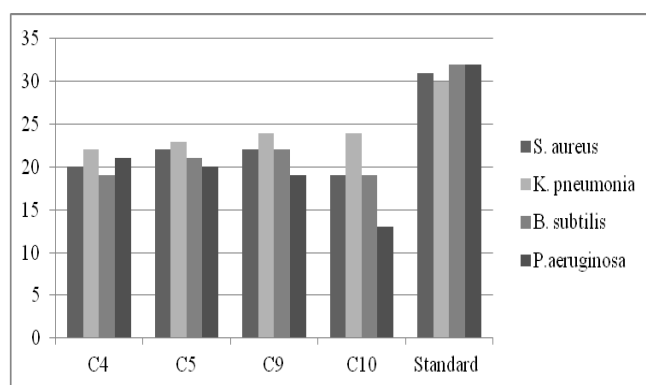| Compound code	Zone of inhibition(mm)			
	S. aureus	*K. pneu-monia*	*B. subtilis*	*P. aeru-ginosa*
C4	20	22	19	21
C5	22	23	21	20
C9	22	24	22	19
C10	19	24	19	13
Ciprofloxacin	31	30	32	32

Figure 3. Zone of inhibition of compounds

EXPERIMENTAL SECTION

Melting point of the synthesized compounds were determined in melting point apparatus made by viggo. The IR was monitored in the range of 400-4000 cm^{-1} IR spectra of final derivatives were recorded using a Shimadzu FT-IR spectrometer, MASS analyses of synthesized compounds were done on Micromass TOF mass spectrometer, and NMR analysis by VARIAN USA Mercury plus 300 MHz NMR spectrometer.

Preparation of silica gel supported polyamine catalyst

Silica gel supported polyamine catalyst was prepared by known literature processes. Silica gel was synthesized under acidic conditions. To control the population density of hydroxyl groups in the silica gel, it was calcinated at 600°c for 6 hours. Surface fictionalization of the silica gel was carried out by suspending the gel in solution of 3-aminopropyl-trimethoxy silane in dry toluene and refluxed at boiling temperature for 24 hours.[23]

General procedure for synthesis of chalcones derivatives

The substituted chalcone derivatives were prepared by stirring a mixture of substituted acetophenone (0.01 mol) and aromatic benzaldehyde (0.01 mol) in catalytic amount of polyamine catalyst in adequate amount of ethanol for 3-4 hrs in presence of 2M NaOH. The reaction mixture was poured on crushed ice and neutralized with dilute HCl. The precipitated product was filtered and purified by recrystallisation in ethanol.

Spectral data of selected compounds from Table 1.

(2E)-1-(2,4-dihydroxyphenyl)-3-[4-(dimethylamino)-phenyl]prop-2-en-1-one (C1): M.F. $C_{17}H_{17}NO_3$; FT-IR (KBr): ν=1629.85, 1693.50, 852.54, 852, 1300.02, 1261.45, 3552.88 cm^{-1}, ^{1}HNMR (300 MHz, CDCl$_3$, δppm): 3.04(6H,s,-N(CH$_3$)$_2$), 6.85(1H,d, α-H), 7.90 (1H,d, β-H), 7.05-7.80(7H,m, Ar-H), 9.25(1H,s, Ar-OH), 9.20(1H,s, Ar-OH), MS (EI, 70 eV): (M$^+$) 283.32, M+1= 284.10

(2E)-3-[4-(dimethylamino)phenyl]-1-phenylprop-2-en-1-one (C9): M.F. $C_{17}H_{17}NO$, FT-IR (KBr): γ =1602.85, 1641.42, 819.75, 850.61, 1230.58, 1307.74 cm^{-1}; ^{1}HNMR (300 MHz, CDCl$_3$, δppm): 7.90 (1H,d, β-H), 6.85(1H,d,αH), 3.05(6H,s, -N(CH$_3$)$_2$), 7.05-7.80(8H,m, Ar-H). MS (EI, 70 eV): (M$^+$) 251.32, M+1= 252.50

CONCLUSIONS

A new methodology for the synthesis of biologically important chalcones using the mixture of aldehydes and acetophenones and novel catalyst silica gel supported polyamine has been developed. The advantages of this catalyst is environmental friendly approach, recycled and reused several times, mild condition, etc. In biological screening C9 and C10 compounds were found to be potential antibacterial against gram positive and gram negative bacteria.

Compounds C9 and C10 were showed better zones of inhibition which confirms their effectiveness against the test microorganisms. These zone of inhibitions were measured in mm scale as shown in Table 4 and the respective graphs were plotted (Figure 3).

REFERENCES

[1]Bhat, S. V., Nagaswami, B. A., Sivakumar, M. *Chemistry of Natural products*; Narosa Publishing House Pvt Ltd page no.585.

[2]Malikov, V. M., Yuldashev, M. P. *Chem. Nat. Compound*, **2002,** *38,* 358.

[3]Nagao T, Abe F, Kinjo J, Okabe H. *Biol. Pharm. Bull.* **2002,** *7,* 875.

[4]aSarda, S. R., Jadhav, W. N., Bhusare, S. R., Wasmatkar, S. K., Dake S. A., Pawar, R. P., *Int. J. Chem, Tech, Res.,* **2009,** *1(2),* 265-269; bSarda, S. R., Jadhav, W. N., Tekale, S. U., Jadhav, G. V., Patil, B. R., Suryawanshi, G. S., Pawar, R. P., *Lett. Org. Chem.,* **2009,** *6(6),* 481-484; cSarda, S. R., Jadhav, W. N., Shete, A. S., Dhopte, K. B., Sadawarte, S. M., Gadge, P. J., Pawar, R. P. *Synth. Commun.,* **2010,** *40,* 2178-2184; dSarda, S. R.,, Mirgane, S. R., Jadhav, W. N., Bhosale, S. V., Domb, A. J., Kharat, K. R., Pawar, R. P., *Chalcones: The bioactive molecules,* "*The Biochemistry of Chalcones*", Lap Lambert Academic Publishing AG and Company Germany, **2011.**

[5]Detsi, A., Majdalani, M., Kontogiorgis, C. A., Dimitra, H. L., Kefalas, P., *Bioorg. Med. Chem.,* **2009,** *17,* 8073-8085.

[6]Hanson, J. R., *Natural Product Reports*, **2010,** *27,* 887–899.
[7]Yadav, H. L. Gupta, P., Pawar, P. S. Singour, P. K. Patil, U. K., *Med. Chem. Res.,* **2010,** *19,* 1-8.

[8]Rahman, M. A., *Chem. Sci. J.,* CSJ-**2011,** 29.

[9]Bag, S., Ramar, S., Degani. M. S., *Med. Chem. Res.,* **2009,** *18,* 309-316.

[10]Vasilev, R. F., Kancheva, V. D., Fedorova, G. F., Batovska, D. I., Trofimov, A. V., *Kinet. Catal.,* **2010,** *51,* 507-515.

[11]Achanta, G., Modzelewska, A., Feng, L. Khan, S. R., Huang, P., *Mol. Pharm.,* **2006,** *70,* 426-433.

[12]Motta, L. F., Gaudio, A. C., Takahata, Y., *Internet Electronic J. Mol. Design,* **2006**, *5,* 555-569.

[13]Lunardi, F., Guzela, M., Rodrigues, A. T., Corre, R., Eger-Mangrich, I., Steindel, M., Grisard, E. C., Assreuy, J., Calixto, J. B., Santos. A. R. S., *Antimicrob. Agents Chemotherapy,* **2003,** *47,* 1449-1451

[14]Hamdi, N., Fischmeister, C., Puerta, P. Valerga. M. C., *Med. Chem. Res.,* **2010,** *19,* 1-16.

[15]Awasthi, S. K., Mishra, N., Dixit, S. K., Singh, A., Yadav, M., Yadav, S. S., Rathaur, S., *Am. J. Tropical Med. Hygiene,* **2009,** *80,* 764-768.

[16]Begum, N. A., Roy, N. , Laskar, R. A., Roy, K., *Med. Chem. Res.,* **2010,** *19,* 1-14.

[17]Kaushik, S., Kumar, N., Drabu, S., *Pharm. Res.,* **2010,** *3,* 257-262.

[18]Najafian, M., Ebrahim-Habibi, A., Hezareh, N., Yaghmaei, P., Parivar, K., Larijani, B., *Mol. Biol. Reports,* **2010,** *10,* 271-274.

[19]Zarghi, A., Zebardast, T., Hakimion, F., Shirazi, F. H., Rao, P. N. P., Knaus, E. E., *Bioorg. Med. Chem.,* **2006,** *14,* 7044-7050.

[20]Chimenti, F., Fioravanti, R., Bolasco, P. Chimenti, A., Secci, D., Rossi, F., Yanez, M., Francisco, O. F., Ortuso, F., Alcaro, S., *J. Med. Chem.,* **2009,** *10,* 1-8 .

[21]*Indian pharmacopoeia.* New Delhi: Govt. of India, **1996,** *2(A),* 104-08.

[22]Ananthnarayan, R., Paniker, J. *Textbook of Microbiology;* 5th Ed., Madras: orient Longman, **1997,** 36-44.

[23]Espinola, J. G. P., Oliveria, S. F., Lemus, W. E. S., Airoldi, A. G., Moreria, J. C. A., *Colloids Surf. A. Physicochem. Eng. Aspects,* **2000,** *166,* 45.

DETERMINATION OF INTENSITY OF ENZYMES INHIBITION AND ACTIVATION

V. I. Krupyanko[a]

It was established that at increasing concentration of inhibitors (or activators) in the enzyme-substrate system the vector lengths of enzyme inhibition (and activation) retain a permanent tendency to increase, while the constants of enzyme inhibition (and activation) either remain unchangeable or change in any direction by studying the dependence of a course of change of vector length (l_i) and constants of enzyme inhibition (K_i) Examples are given of using the K_i constants and the vector lengths for the characterization of the strength of enzyme binding to inhibitor and the intensity of enzyme inhibition, respectively.

*Corresponding Authors
    Fax: (495) 956-3370;
    E-Mail: krupyanko@ibpm.pushchino.ru; pH76@mail.ru
[a] G. K. Skryabin Institute of Biochemistry and Physiology of
    Microorganisms, Russian Academy of Sciences, Pushchino,
   Prospect Nauki 5, Moscow region, 142290

Introduction

When studying the enzyme properties, a necessity often arises to characterize the intensity of effect of inhibitor (*i*) or activator (*a*) on enzyme. This question presents a great interest in experimental enzymology, because in the reacting enzyme-substrate system it is impossible to escape the presence of other components such as added activators and inhibitors and also the substances comprising a buffer part of the medium. Accumulated reaction products are also capable of decreasing enzyme activity. Before a vector method of representation of enzymatic reactions in the three-dimensional $K'_mV'I$ coordinate system (Figure 1),[1-5] where K'_m and V' – the effective determined in presence of inhibitor (*i*) or activator (*a*) Michaelis constant and maximum reaction rate, I – the common (printing) symbol of $K'_mV'I$ coordinate system, was unclear which parameters of catalyzed reaction can be used for these purposes: probably, the maximum reaction rate V' or – which is the same – the k_{+2} constant of reaction rate?

But simultaneously with change of this parameter of substrate cleavage the other important reaction parameter, i.e. the K^0_m Michaelis constant, also changes in most cases

$$v_0 = \frac{V^0}{1+\dfrac{K^0_m}{S}} \qquad (1)$$

where K^0_m and V^0 – the Michaelis constant and maximum reaction rate determined in absence of inhibitor (*i*) or activator (*a*), S – substrate concentration, v_0 – initial reaction rate.
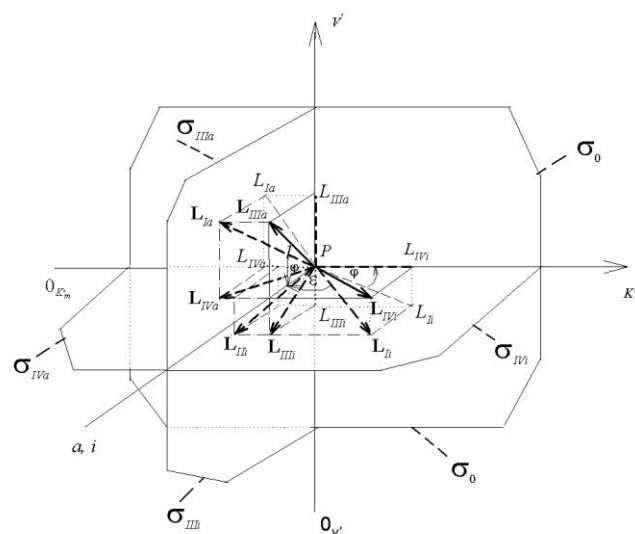
Figure 1. A three-dimensional $K'_mV'I$ system of rectangular coordinates with the coincident P_a and P_i semiaxes of molar concentrations of *i* and *a* (the $P_{a,i}$ semiaxis) convenient for analysis of the positions of three-dimensional vectors of enzyme inhibition: calf alkaline phosphatase – vector L_{Ii} , eel alkaline phosphatase – vector L_{IIi} and pyrimidine-specific RNase A-vector L_{IVa} analyzed as examples 1, 2 and 3 in the text. The symbols of the rest vectors L_{IIIi}, L_{IVi}… L_{Ia}, L_{Vaa}, and their projections L_{IIIi}, L_{IVi}… L_{Ia}, L_{Va} and the projections of directing planes σ_{IVi}, σ_{IIIi}, σ_{IVa}, σ_{IIIa} on the basic σ_0 plane and slope angles of vectors are considered in the text.

Sometimes the authors make attempts to characterize the intensity of effect of inhibitor on enzyme using a numerical value of the respective constant of enzyme inhibition K_i by the principle: the smaller the value of a calculated constant of enzyme inhibition is the stronger is the effect of inhibition on enzyme.[6-12]

However, a course of change of constants of enzyme inhibition may completely contradict such their application, because:

1) the constants of enzyme inhibition may remain unchangeable at increasing concentration of inhibitor (Figures 3A, 3B and Table 2) and

2)   their   values   may   augment   at   increasing concentration of inhibitor in the enzyme-substrate system (Figures 2A, 2B and Table 1).

There are examples of using the K_i constants of enzyme inhibition for characterization of strength of enzyme binding to inhibitor.[13-17] In some articles[18-21] the Tables of a course of change in the parameters of enzyme inhibition (or activation) are analyzed for explanation of such processes without construction of plots of a course of simultaneous change of both parameters. Such plotting becomes extremely difficult, if these parameters change in different directions (Table 1).

Table 1. Inhibitory effect of increasing concentration of WO_4^{2-} anions on calf alkaline phosphatase

Inhibitor, 10^{-4} M	K'_m, 10^{-5} M	V', $\mu mol\ min^{-1}$ $\mu g\ protein^{-1}$	K_{Ii}, 10^{-5} M	l_{Ii}, c.u.
0.0	4.45	2.56		
0.0625	5.28	2.51	3.33	0.834
(0.0625 c.u.)	(5.28 c.u.)	(2.51 c.u.)		
0.125	5.39	2.30	5.28	0.983
0.250	5.97	2.15	6.39	1.59
0.50	6.56	1.74	7.48	2.32

At data analysis by taking into account of a course of change of only one K'_m (or V') reaction parameter (Fig. 4A), the situation is simplified. But the researchers usually construct plots of the data obtained either in the $(tg\omega;i)$ coordinates of slopes, where $tg\ \omega = K'_m/V'$ or in the $(1/V';i)$ coordinates of intercepts, which is only convenient for calculation of the so-called K_{is}-slope and K_{ii}-intercept constants of enzyme inhibition but not for the characterization of intensity of effect of enzyme inhibition.

A vector method representation of enzymatic reactions in the three-dimensional $K'_mV'I$ coordinate system (Fig. 1) showed that the L vector length dependent on the concentration of inhibitor (Eq. 2) in the above coordinate system characterizes the intensity of effect of inhibitor (or activator) on enzyme, while the K_i constant of enzyme inhibition (or the K_a constant of enzyme activation) independent of the concentration of inhibitor – characterizes the strength of binding of enzyme to inhibitor.[1-5]

Let us consider the principle of construction and functioning of this system. If to designate the effective Michaelis constants determined in the presence of inhibitor (i) or activator (a) by the symbol K'_m and the Michaelis constants of initial (uninhibited $i = 0$ and nonactivated $a = 0$) enzymatic reaction by the symbol K^0_m, the $0K'_m$ axis of numerical values of K'_m parameters of enzymatic reactions shall be obtained with the point K^0_m on it. The construction of a scale of numerical values of the V' and V^0 maximum reaction rates of activated ($V' > V^0$) and inhibited ($V' < V^0$) enzymatic reactions is analogous.

If to intersect these axes at the right angle to each other at the points K^0_m and V^0 and draw from the obtained $P(K^0_mV^00)$ point a Pa,i semiaxis of molar concentrations of inhibitor (i) and activator (a) perpendicular to the basic σ_0 plane with the $0K'_m$ and the $0V'$ axes in it and also to draw through this

semiaxis and each of the directing PK'_m, PV', $P0_{Km}$ and $P0_V$ semiaxes a system of reciprocally-perpendicular σ_{Vi}, σ_{IIIi}, σ_{IVa}, σ_{IIIa} planes, we shall obtain a three-dimensional $K'_mV'I$ coordinate system with a coincident Pa,i semiaxis convenient for vector analysis of enzymatic reactions (Fig. 1).

According to the numerical values of K'_m, V' and i (or a) parameters, each inhibited or activated enzymatic reaction shall have in such a system its own vector of representation – a concrete three-dimensional L vector of this reaction.

Thus, the l length (module) of a vector:

$$l_i = \left(\left(K'_m - K^0_m \right)^2 + \left(V' - V^0 \right)^2 + \left(i - 0 \right)^2 \right)^{0.5} \quad (2)$$

shall characterize the intensity of proceeding of inhibited ($i > 0$) or activated ($a > 0$) enzymatic reaction, and a ratio of the lengths of L vector projections on the Pa,i semiaxis to the coordinates of this vector projection on the basic σ_0 plane shall be an equation for calculation of the K_i constant of enzyme inhibition (or the K_a constant of enzyme activation).[1-5]

Let us consider the possibility of using vector lengths at data analysis of the intensity of effect of inhibitor and activator on enzyme.

Materials and methods

Enzymes: calf and eel alkaline phosphatase (EC 3.1.3.1) – a preparation of Sigma (USA). Substrate: p-nitrophenyl phosphate·2CHA salt (pNPP) – a product of Serva (Germany). Inhibitors: sodium tungstate ($Na_2WO_4·2H_2O$) and isopropanol (i-PrOH) (high purity grade). The concentration of pNPP was changed within $0.294·10^{-4} – 0.98·10^{-4}$ M, the concentration of calf alkaline phosphatase and that of eel alkaline phosphatase were kept constant $0.978\ \mu g\ mL^{-1}$ and $2.46\ \mu g\ mL^{-1}$, respectively.

The course of pNPP cleavage catalyzed by all tested alkaline phosphatases was registered by a CF-4 DR Optica Milano spectrophotometer (Italy). Reactions were carried out on 0.05 M Tris-HCl buffer (pH 9.0) at ionic strength 0.1 by NaCl of high purity grade under constant stirring[1] and thermostatting (37 ^{0}C) at the wave length $+\Delta D_{400}$ of a solution containing the substrate, enzyme and inhibitor versus a solution of the same composition, but without the enzyme.

The 2nd enzyme: bovine pyrimidine-specific RNase A (EC 3.1.44.22) – a preparation of Sigma. Substrate of RNase A: cytidine-2′,3′-monophosphate (C>p), a product of Sigma. Activator of RNase A: sodium molybdate ($Na_2MoO_4·2H_2O$), a domestic preparation of high purity grade. Reactions were carried out under constant stirring and thermostatting (24 ^{0}C) in 0.05 M Na-acetate buffer (pH 5.8) at ionic strength 0.1 using NaCl of high purity grade. The concentration of C>p was changed within $6.58·10^{-4} – 1.645·10^{-4}$ M and that of enzyme was kept constant $8.46\ \mu g\ mL^{-1}$. A course of C>p cleavage was recorded by increase in the absorbance at the wave length $\lambda = 260$ nm.

The initial reaction rates v_0 (v_i and v_a) of substrate cleavage were determined by a slope angle of tangents to the initial segments of curves representing a course of reaction change in not less than five parallel experiments.

The kinetic parameters K'_m and V' of enzyme inhibition (or activation) were calculated by constructing plots in the (v^{-1}, S^{-1}) coordinates of Lineweaver-Burk by using a computer program SigmaPlot, version 2000 (USA).

The mean-square deviation a fivefold determination was as follows: $v = \pm 2.5\%$, K'_m and $V' = \pm 7.5\%$, $K_i = \pm 10\%$ and $l = \pm 10\%$.

Results and Discussions

Example 1. As it can be seen from Figs. 2A, 2B and Table 1, the inhibitory effect of anions of tungstic acid (WO_4^{2-}) on initial rates of pNPP cleavage by calf alkaline phosphatase is exhibited by increasing effective Michaelis constants and decreasing maximum reaction rates ($K'_m > K^0_m$, $V' < V^0$), in this case i.e. the K'_m and V' parameters change simultaneously in different directions.
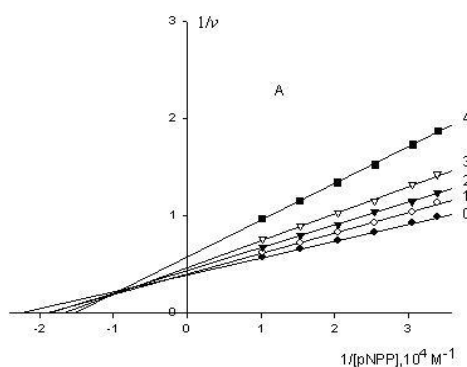
Figure 2A. Plots of the inhibitory effect of anions WO_4^{2-} on initial rates of pNPP cleavage catalyzed by calf alkaline phosphatase in the coordinates of Lineweaver-Burk. Note: line 1 – the concentration of inhibitor (10^{-4} M) is 0.0625, line 2 – 0.125, line 3 - 0.250, line 4 – 0.500. Line (0) – the inhibitor is absent. Designation: v, µmol·min^{-1} µg protein^{-1}.
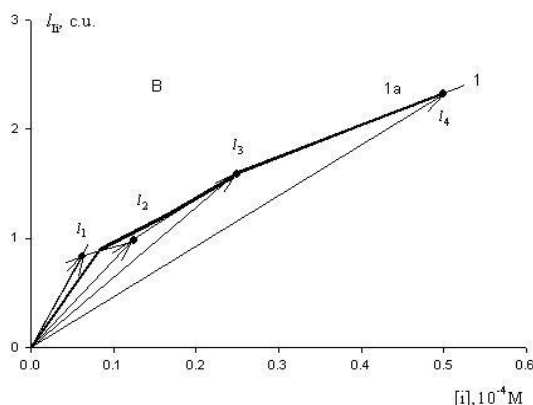
Figure 2B. Data representation of Figure 2A in the ($l_{Ii}; i$)) coordinates. Note: l_1, l_2 l_3 and l_4 are the lengths of L_{Ii} vectors. Line 1 – is a thin curve drawn by the positions of mobile vector ends, line 1a is a thick line drawn by taking into account the deviations at respective concentrations of WO_4^{2-}.

The attempt to use the K_{Ii} constants of enzyme inhibition (Table 1) for the characterization of intensity of inhibitory effect of WO_4^{2-} on enzyme indicated the weakening of binding of anions to enzyme, because the constants of enzyme inhibition augment at increasing concentration of WO_4^{2-}. But how to express the dependence of a course of change of the intensity of inhibitory effect of increasing concentrations of WO_4^{2-} on phosphatase as a function by using data of Fig. 2A and Table 1 seems unclear yet.

Substitution of the appropriate parameters of calf alkaline phosphatase inhibition in Equation (2) allows to obtain data on the dynamics of intensity of enzyme inhibition. For this purpose, it is necessary to express the dimensions of all parameters used in conventional units (c.u.).

It is noteworthy that because of using different definite ranges of concentration of the inhibitor ($10^{-3} – 10^{-6}$ M) explained by both the convenience in the obtaining of a desired effect on enzyme, the ability of inhibitors to suppress enzyme activity and an essential difference in the catalytic activity of enzymes proper (a range of difference in the V^0 and K^0_m parameters may be enumerated by orders in value), to choose a standard number of conventional units to be used in all possible cases of enzyme inhibition (and activation) is impossible now. The practice shows that a selection of conventional units (c.u.) when the determined vector lengths shall be expressed by small decimal digits (l_i= 1.000, 2.000 …) would be advisable. So, the conventional units for experimental data analysis of (Fig. 2A – 4A) were chosen according to the above reasons (this is marked by brackets in the 3rd line of each of Tables 1, 2 and 3).

Table 2. Inhibitory effect of increasing concentration of isopropanol on eel alkaline phosphatase

Inhibitor, 10^{-3} M	K'_m, 10^{-5} M	V, µmol·min^{-1} µg protein^{-1}	K_{IIi}, 10^{-3} M	l_{IIi}, c.u.
0.0	4.82	3.16		
0.2	4.47	2.93	1.77	0.4641
0.2 c.u.	4.47 c.u.	2.93 c.u.		
0.5	4.07	2.66	1.89	1.0308
1.0	3.53	2.31	1.91	1.8403

Table 3. Activating effect of increasing concentration of anions MoO_4^{2-} on RNase A

Activator, 10^{-3} M	K'_m, 10^{-4} M	V, µmol·min^{-1} µg protein^{-1}	K_{IVa}, 10^{-3} M	l_{IVa}, c.u.
0.0	5.446	8.17		
0.2	4.651	8.14	1.17	0.8198
0.2 c.u.	4.651 c.u.	8.14 c.u.		
0.5	3.732	8.13	1.09	1.7256
1.0	2.960	8.32	1.19	2.4940

Use of Equation (2) gives the possibility to calculate not only a course of change in the L vector lengths of calf alkaline phosphatase inhibition by WO_4^{2-}, but also to plot their vector length positions in the ($l_i; i$) (Fig.2B–3B) or ($l_a; a$)

Fig. 4B coordinate systems, thus allowing to take into account a simultaneous course of change of the K'_m and V' reaction parameters, which was impossible without vector analysis of enzymatic reactions in the three-dimensional $K'_m V'I$ coordinate system.

As seen from the obtained data (Table 1, Figs. 2A-B), the dynamics of intensity of enzyme inhibition (l_{Ii}) changed with retardation from linearity. This testifies to instability in the dynamics of effect of the above phosphatase by anions of tungstic acid and the disaccordante of this experiment with the criterion of stability of the mechanism of proceeding of this reac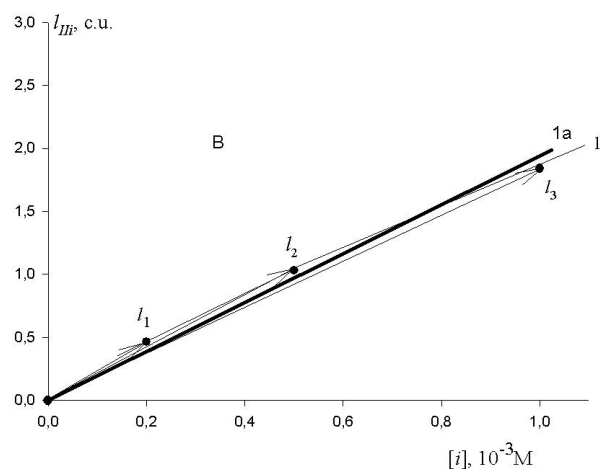tion, which should be characterized by constancy of the slope angles of **L** vectors of enzyme inhibition: azimuth (tg φ) – to the horizontal σ_{IVi} plane of Fig. 1 and tangential (tg ε) – to the vertical σ_{IIIi} plane of the same Figure 1:[3]

$$\text{tg } \varepsilon = \text{const, tg } \varphi = \text{const.} \qquad (3)$$

Example 2. In a course of reaction the values of two (K'_m and V') parameters of inhibited reaction change in one direction. As an example of analysis of such situation, it is convenient to analyze data of the study on the inhibitory effect of increasing concentrations of i-PrOH on initial rates of pNPP cleavage catalyzed by eel alkaline phosphatase (Fig. 3A and Table 2). The results show that although the K'_m and V' parameters of enzyme inhibition changed in one direction and at simultaneous increasing length of each subsequent pair of segments cut off on the coordinate axes by *n* times, where *n* is a coefficient of similarity of respective rectangular triangles cut off by respective lines on the coordinate axes at increasing concentration of isopropanol. This puts additional questions: the 1st one – should a researcher in this case analyze a course of change by only one parameter of enzyme inhibition, if so, which of the parameters ? And the 2nd question: what new information can be obtained from constancy of the values of K_{IIi} constants of enzyme inhibition?
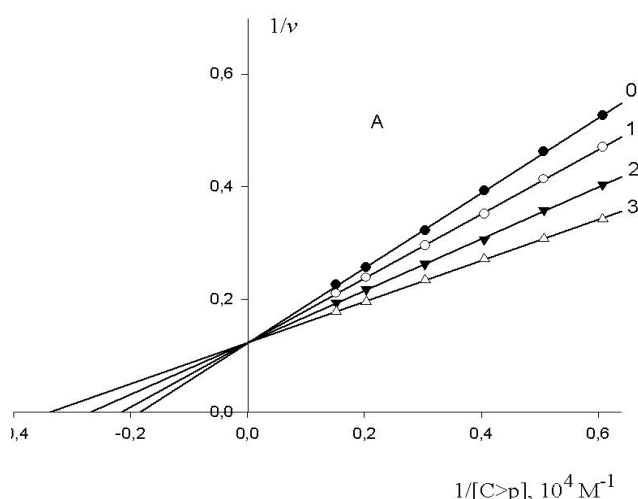

Figure 3A. Plots of the inhibitory effect of isopropanol on initial rates of pNPP cleavage catalyzed by eel alkaline phosphatase in the coordinates of Lineweaver-Burk. Note: line 1 – the concentration of inhibitor is 0.0002 M, line 2–0.0005 M, line 3–0.001 M. Line (0)–the inhibitor is absent. Designation: *v*, μmol· min⁻¹ μg protein⁻¹.

Figure 4A. Plots of the activating effect of anions MoO₄²⁻ on initial rates of C>p cleavage catalyzed by RNase A in the coordinates of Lineweaver-Burk. Note: line 1 – the concentration of inhibitor is 0.0002 M, line 2 – 0.0005 M, line 3 – 0.001 M. Line (0) – the inhibitor is absent. Designation:*v*, μmol· min⁻¹ μg protein⁻¹.
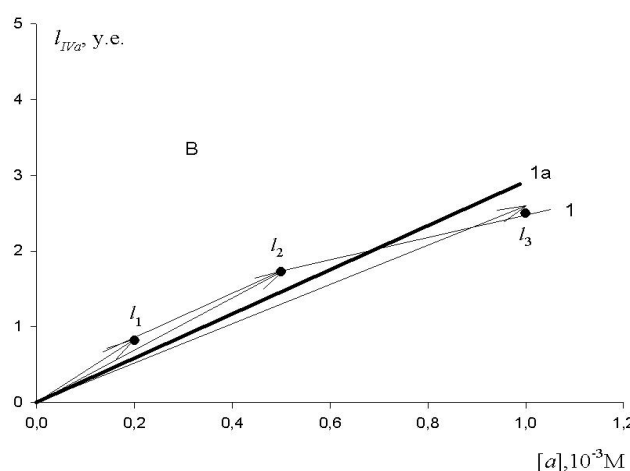

Figure 3B. Data representation of Figure 3A in the (l_{IIi};*i*) coordinates. Note: l_1, l_2 and l_3 are the lengths of **L**$_{IIi}$ vectors. Line 1 – is a thin curve drawn by the positions of mobile vector ends, line 1a is a thick curve drawn by taking into account the deviations at respective concentrations of i-PrOH by analogy to Figure 2A.

Figure 4B. Data representation of Figure 3A in the (l_{IIa}; *i*) coordinates. Note: l_1, l_2 and l_3 are the lengths of **L**$_{IIa}$ vectors Line 1 – is a thin curve drawn by the positions of mobile vector ends, line 1a is a thick curve drawn by taking into account the deviations at respective concentrations of MoO₄²⁻ by analogy to Figure 2B.

Construction of the positions of vector lengths l_{IIi} of calf alkaline phosphatase inhibition in the (l_{IIi};i) coordinate system (Fig. 3B) and the form of Eqn. (2) used for calculation of these lengths showed that since a change of the K'_{m} and V' parameters of inhibited reaction influences the position of each vector in this system and as these both parameters are found in Eqn. (2) used at calculation of vector modules, one shall have to obligatorily take into account a course of simultaneous change of the K'_{m} and V' parameters for characterization of the inhibitory effect of increasing concentrations of isopropanol on enzyme.

Example 3. Only the K'_{m} parameter of activated reaction is changed in the reaction course. Data analysis of the study on the activating effect of anions of molybdenic acid (MoO_4^{2-}) on initial rates of C>p cleavage catalyzed by pyrimidine-specific RNase A (Figs, 4A – 4B, Table 3) showed that a gradually increasing concentration of activator was accompanied by decrease in only the K'_{m} reaction parameter ($K'_{\text{m}} < K^0_{\text{m}}$, $V' = V^0$). The attempt to use anions of molybdate for the characterization of the intensity of activating effect on enzyme by taking into account a course of change of the $K_{\text{IV}a}$ constants of RNase A activation revealed that there was no such an effect on enzyme in that case because the values of the constants remained unchangeable at increasing concentration of activator on enzyme (Fig. 4A, Table 3).

At the same time, the calculation of vector $l_{\text{IV}a}$ lengths of RNase A activation (Table 3) and analysis of vector positions in the ($l_{\text{IV}a}$;a) coordinate system (Fig. 4B) showed that despite the constancy of values of the $K_{\text{IV}a}$ constants of enzyme activation their vector lengths increased directly proportional to the concentration of MoO_4^{2-}, which indicates the presence of the activating effect of molybdate anions on enzyme as well as on the stability of dynamics of enzyme activation.

References

[1]Krupyanko, V. I., *A Vector Method of Representation of Enzymic Reactions*. Moscow, Nauka, **1990**, (in Russian).

[2]Krupyanko, V. I., *Appl. Biochem. Microbiol. (Moscow)*, **1986**, *22* 440.

[3]Krupyanko, V. I., *Collect. Czech. Chem. Comm.*, **1998**, *53* 161.

[4]Krupyanko, V. I., Process Biochem., **2004,** *39* 825.

[5]Krupyanko, V. I., *J. Biol. Sci.*, **2005,** *5* 82.

[6]Andreassi, J. L., Moran, R. G., *Biochemistry*, **2002**, *41* 226.

[7]Wilson, J. E., Chung, V., *Arch. Biochem. Biophys.*, **1989**, *269* 517.

[8]Cuenllas, E., Gaitain, S., Bueren, J. A., Tejero, C., *Biochimie*, **1989**, *71* 763.

[9]Denicola-Seoane, A. D., Anderson, B. M., *J. Biol. Chem.*, **1990,** *265* 3691.

[10]Bhat, G. B., Iwase, K., Hummel, B. C. W., Walfish, P. G., *Biochem. J.,* **1989**, *258* 785.

[11]Whitman, M., Kaplan, D. Roberts, T. Cantley, L., *Biochem. J.,* **1987**, *247* 165.

[12]Hou, B., Lim, E-K., Higgins, G. S., Bowles, D. J., *J. Biol. Chem.*, **2004**, *279* 47822.

[13]Kazerounian, S., Pitari, G. M., Ruitz-Stewart, I., Schulz, S., Waldman, S. A., *Biochemistry*, **2002**, *41* 3396.

[14]Mau, C. J. D., Garneau, S., Scholte, A. A., Fleet, J. E., Vederas, J. C. and Cornish, K., *Eur. J. Biochem.,* **2003**, *230* 3939.

[15]Bhaird, N. A., Kumaravel, G., Gandour, R. D., Krueger, M. J., *Biochem. J.*, **1993**, *29*.

[16]Rangarajan M., Hartley, B. S., *Biochem. J.,* **1992**, *283* 223.

[17]Bakan, D. A., Saltman, P., Theriault, Y., Wright, P. E., *Biochim. Biophys. Acta*, **1991**, *1079* 162.

[18]Chan, M. Sim, T-S., *Biochem. Biophys. Res. Commun.*, **2005**, *326* 188.

[19]Tanizaki, M. M. Bittencourt, H. M. E., Chaimovich, H., *Biochim. Biophys. Acta*, **1977**, *485* 116.

[20]Folk, J. E., Wolff, E. C., Schirmer, E. W., Cornfield, J., *J. Biol. Chem.,* **1962**, *237* 3105.

[21]Kearns, A. E., Campbell, S. C., Westley, J., Schwartz, N. B., *Biochemistry*, **1991**, *30* 7477.

CONFORMATIONAL ISOMERISM IN A CONFORMATIONAL POLYMORPH OF 2,5-DIBENZYLIDENECYCLOPENTANONE: CRYSTALLOGRAPHIC AND QUANTUM CHEMICAL STRUCTURES

Ifzan Arshad,[a] Shumaila Ashraf,[a] Asghar Abbas,[a] Shahid Hameed,[a] Kong Mun Lo,[b] and Muhammad Moazzam Naseer[a]∗

A new polymorph (II) of 2,5-dibenzylidenecyclopentanone (DBCP) has been obtained by slow evaporation of ethanol solvent at room temperature. Interestingly, two conformational isomers of the title compound with slight difference in their bond lengths, torsion angles and dihedral angles were found within the same crystal lattice of polymorph (II). The crystal structure of polymorph (II) showed monoclinic $P2_1$ space group with a = 6.0983 (2) Å, b = 14.9200 (7) Å, c = 15.0740 (6) Å, V= 1368.69 Å^3, Z = 2 as compared to orthorhombic $C222_1$ space group with a = 11.803 (2) Å, b = 5.698 (4) Å, c = 20.872 (2) Å, V= 1403.6 Å^3, Z = 4 for previously reported polymorph (I) crystallized in CHC1$_3$/MeOH solvent. The concomitant origin of polymorphism and conformational isomerism was credited to C-H$^{...}$O, π-π and C-H$^{...}$π interactions resulting in intriguing supramolecular sheet-like multilayered molecular packing of polymorph (II). The results of the complementary electronic structure calculations, performed by DFT/B3LYP method using 6-31G* basis set were found in good agreement with the experimental results.

Corresponding Author
    Fax: +92 51 90642241 Phone: +92 51 90642129
    E-Mail: moazzam@qau.edu.pk (M.M. Naseer)
[a] Department of Chemistry, Quaid-i-Azam University, Islamabad 45320, Pakistan
[b] Department of Chemistry, University of Malaya, Kuala Lumpur 50603, Malaysia

Introduction

Polymorphism, a type of supramolecular isomerism is the ability of the same molecule to exist in more than one type of network superstructure resulting from interplay of kinetic and thermodynamic parameters and can therefore be related to structural isomerism at the molecular level.[1-8] The different nature of intermolecular forces, not only influence crystal packing but also affect physical, chemical and mechanical properties of the organic solid-state materials.[9-15] By slight variations in the crystallization environment such as temperature, solvent, using of additives and concentration; the same molecules can pack differently forming different crystal lattices or polymorphs.[5,16,17] The generality of this phenomenon can be estimated from this fact that 80-90% of active pharmaceutical ingredients are capable of existing in polymorphic forms[18] and hence may show distinguished physicochemical properties, bioavailabilities and therapeutic effects due to different arrangement of molecules in the crystal lattice.[19-21]

Molecules with conjugated backbone and spatially separated electron donor/acceptor functionalities have actively been investigated for their non-linear optical (NLO) and thermotropic properties.[22-28] Similar molecules with different substituents are also used as *in vivo* multiphoton fluorescent markers and in the control of blood coagulation pathways.[29] Among diverse conjugated systems recently explored, the molecular architectures having extended

donor-(π-spacer)-acceptor-(π-spacer)-donor (D-π-A-π-D) motifs were found potential biophotonic materials.[30] The double Claisen-Schmidt condensation reaction of a ketone having two active α,α′ sites with two equivalents of aldehyde is the best method to prepare compounds with (D-π-A-π-D) motif, often referred to by their generic name of *bis*-chalcone [31]. Recently, desirable NLO properties were obtained from piperidone-based *bis*-chalcones.[30]

In recent years, chalcones in general[32] and *bis*-chalcones[33-38] in particular, showed a number of biological applications. Therefore, controlling the polymorphic properties of this D-π-A-π-D class of compounds is important in medicinal chemistry and this can be achieved through combined experimental and computational approach to understand the interplay of intermolecular interactions and relative stability of different polymorphic forms of a compound. Herein, we report both experimental and computational results of second conformational polymorph of 2,5-dibenzylide-necyclopentanone which show conformational isomerism i-e two independent molecules with slightly different bond lengths, torsion angles and dihedral angles are present in its unit cell. The geometric parameters of two polymorphic forms are also compared through quantum chemical computations.

Experimental

Synthesis

2,5-dibenzylidenecyclopentanone (DBCP) was prepared by the reaction of cyclopentanone with benzaldehyde in 1:2 ratio by continuous stirring for 6 hours at room temperature in methanolic sodium hydroxide [39]. The single crystal suitable for X-ray analysis was obtained by slow evaporation of its ethanolic solution at room temperature.

X-ray Crystallography

Single crystal X-ray diffraction measurements for the title compound were carried out using Bruker APEX-II CCD area-detector equipped with the graphite monochromator at 140(2) K with MoK\α radiations (λ = 0.71073 Å). Structure solved by direct methods[40] full-matrix least-squares refinement[40] on F² and 355 parameters for 5355 unique intensities (R_{int} = 0.011). The crystal parameters are shown in Table 1. CCDC-983901 contains the supplementary crystallographic data for this paper.

Table 1. Crystallographic data for polymorph (II) of DBCP

| Crystal data	DBCP
CCDC Number	983901
M_r	516.60
Crystal system, space group	Monoclinic, P2$_1$
Temperature (K)	140
a,	6.0983(2),
b,	14.9200(7),
c (Å)	15.0740 (6)
β (°)	93.687 (3)
V (Å3)	1368.69 (10)
Z	2
Radiation type	Mo Ka
m (mm-1)	0.08
Crystal size (mm)	0.17 × 0.10 × 0.10
Data collection	
Diffractometer	Bruker APEX-II CCD area-detector diffractometer
Absorption correction	Multi-scan (SADABS; Sheldrick, 1996)
T_{min}, T_{max}	0.568, 0.746
No. of measured, independent and observed [I > 2s(I)] reflections	11078, 5355, 2558
R_{int}	0.246
Refinement	
$R[F2 > 2s(F2)]$,	0.111,
w$R(F2)$,	0.335,
S	0.98
No. of reflections	5355
No. of parameters	361
No. of restraints	1
H-atom treatment	H-atom parameters constrained
Δρmax, Δρmin (e Å-3)	0.84, -0.54

Computational Detail

The molecular structure of DBCP is optimized using DFT/B3LYP level of theory with 6–31G* basis set.[41-43] The initial guess of compound was first obtained from the X-ray coordinates. All calculations were performed using the ORCA 3.0.1 program package[44] with Gabedit graphical user interface[45] on a personal computer without specifying any symmetry for the title molecule.

Results and Discussion

Crystal structure of polymorph (II)

The crystal structure of polymorph (II) of 2,5-dibenzylidenecyclopentanone (DBCP) is shown in the ORTEP diagram with labeling in Figure 1. It crystallizes in the monoclinic P21 space group with Z = 2, Z' = 0 in contrast to the orthorhombic C2221 space group with Z = 4 for previously reported Polymorph (I).[39]
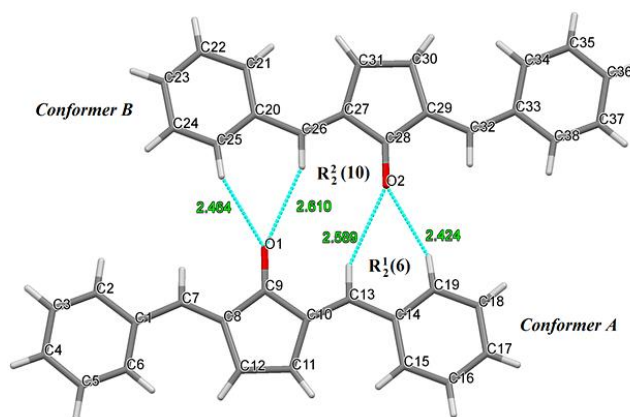

Figure 1. The crystal structure of polymorph (II) of DBCP having two conformational isomers.

Interestingly, in a unit cell of the polymorph (II), there are two different/independent molecules (called conformer A & conformer B) having slightly different bond lengths, dihedral angles and torsions angles. The peripheral phenyl rings and central cyclopentanone rings in both the conformers A & B are not coplanar. The angle between the least square planes of the rings containing the atoms C9 and C2, and C9 and C19 in conformer A = 5.67° and 5.68° and of the rings with C28 and C38, and C28 and C25 in conformer B = 3.87° and 3.38°. The Bond lengths for C=C-Car single bonds (C8-C9 1.496 Å, C10-C9 1.471 Å, C27-C28 1.463 Å, C29-C28 1.471 Å) in both the conformers are shorter than the normal single bond length due to conjugation and C=C-Car double bonds (C7-C8 1.320 Å, C10-C13 1.360 Å, C29-C32 1.368 Å, C26-C27 1.355 Å are also slightly different as compared to normal double bond length.[46] The bond lengths of carbonyl groups of two conformers are C9-O1 1.220 Å and C28-O2 1.254 Å, respectively. All the other bond lengths are also different in both the conformers. This difference in bond lengths, torsion angles and bond angles can be attributed to the varied amount of conjugation due to different conformations of two molecules.

Another important aspect of polymorph (II) of DBCP, other than having two different conformers in its unit cell, is its intriguing supramolecular sheet-like multilayered molecular packing stabilized mainly by C-H···O, π-π and C-H···π interactions (Figure 2a). Two conformers (A and B) are connected to each other in such a way that each A is connected with two B by means of cyclic $R^1_2(6)$ and $R^2_2(10)$ type C-H···O (C13-H13···O2= 2.589 Å, C19-H19···O2= 2.424 Å, C25-H25···O1= 2.464 Å, and C26-H26···O1= 2.610 Å) hydrogen bond motifs (Figure 1 & 2)[47]

and π-π (C9-C27 3.393 Å, C10-C28 3.339 Å, C13-C29 3.385 Å and C14-C32 3.381 Å) interactions [48] and vice versa making chains like structure (Figure 2b). Each 1D-supramolecular chain is further connected to the neighboring chain by means of H-H (C36-H36····H23-C23 2.393 Å) interactions[49,50] forming 2D-sheet like layer (Figure 2c). These sheet-like layers are then stacked one above the other by means of CH-π interactions (C22-C22····C16 2.891 Å)[48,51] forming sheet-like multilayered structure. It is interesting to mention here that chains of the every two neighboring layers are connected with each other in a head to tail fashion (Figure 2a).

(a)

(b)

(c)
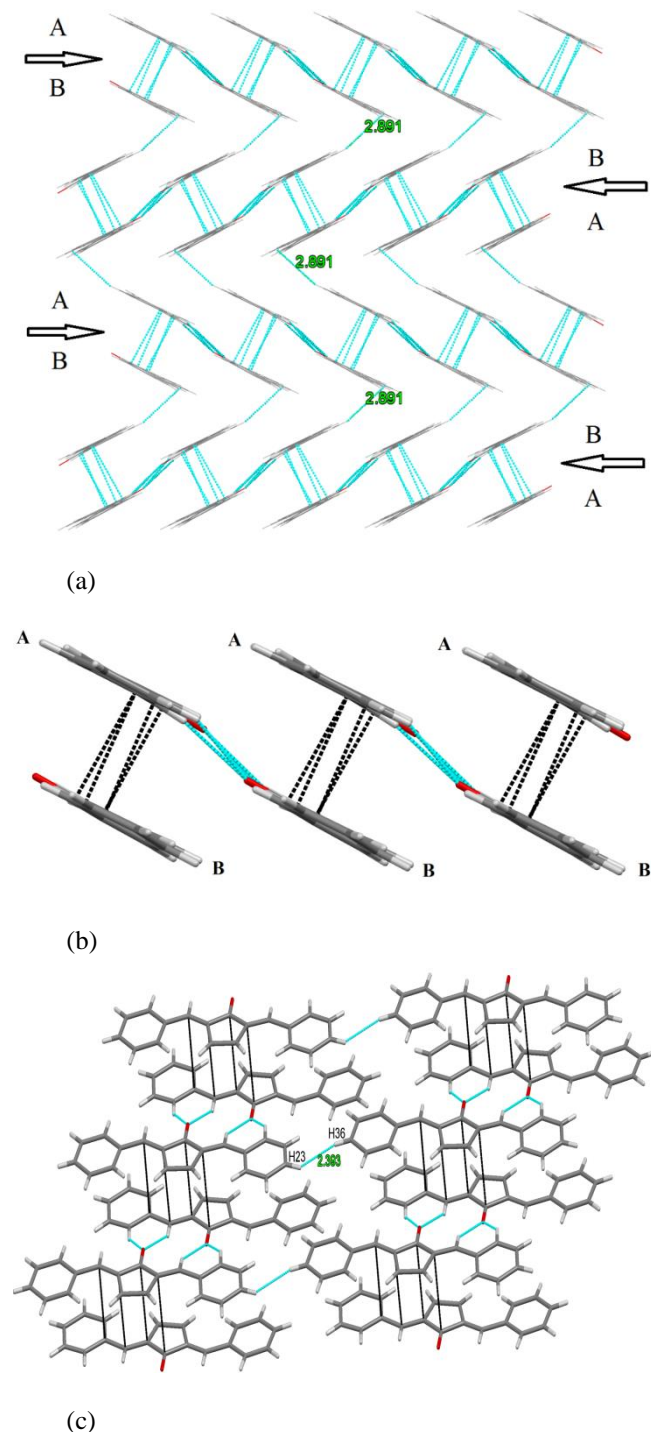
Figure 2. a) Sheet-like multilayered structure of polymorph (II) stabilized by C-H···O, π-π and C-H···π interactions. b) C-H···O and π-π interactions in 1D-Supramolecular chain (side view). c). Inter-chain hydrogen-hydrogen interactions between sheets forming 2D-sheet like layer.

Table 2. Measured and calculated bond lengths (Å).

Bond lengths, Å	X-ray	B3LYP/6-31G	
		Combined (A and B)	Conformer A
O1-C9	1.220	1.225	1.221
C1-C2	1.411	1.410	1.410
C1-C6	1.387	1.410	1.411
C1-C7	1.471	1.461	1.461
C2-C3	1.341	1.393	1.393
C3-C4	1.371	1.397	1.397
C4-C5	1.401	1.398	1.398
C5-C6	1.391	1.393	1.393
C7-C8	1.321	1.356	1.356
C8-C9	1.501	1.506	1.507
C8-C12	1.514	1.458	1.457
C9-C10	1.471	1.505	1.500
C10-C11	1.514	1.458	1.459
C10-C13	1.361	1.356	1.358
C11-C12	1.511	1.362	1.361
C13-C14	1.451	1.461	1.461
C14-C15	1.411	1.410	1.411
C14-C19	1.418	1.411	1.412
C15-C16	1.381	1.392	1.393
C16-C17	1.411	1.399	1.398
C17-C18	1.411	1.397	1.398
C18-C19	1.381	1.393	1.393
O2-C28	1.254	1.225	
C20-C21	1.386	1.411	
C20-C25	1.421	1.412	
C20-C26	1.461	1.461	
C21-C22	1.401	1.393	
C22-C23	1.381	1.398	
C23-C24	1.381	1.397	
C24-C25	1.341	1.393	
C26-C27	1.361	1.358	
C27-C28	1.451	1.500	
C27-C31	1.497	1.459	
C28-C29	1.471	1.507	
C29-C30	1.510	1.458	
C29-C32	1.371	1.356	
C30-C31	1.531	1.361	
C32-C33	1.441	1.461	
C33-C34	1.408	1.410	
C33-C38	1.409	1.410	
C34-C35	1.391	1.393	
C35-C36	1.391	1.398	
C36-C37	1.411	1.397	
C37-C38	1.391	1.393	

Geometry optimization

The molecular conformations present in the two conformer of polymorph (II) were investigated by geometry optimization calculations using B3LYP/6-31G* basis set,[41,43] computations were carried out for conformer A & B as such and for conformer A alone, initial geometry was defined using crystallographic information. Superposed structure of the molecule over X-ray structure is shown with small conformational discrepancies between them (Figure 3). These discrepancies are originated from dihedral angles between ring planes and also because of slight difference in estimated bond angles.

The small differences between the calculated and observed geometrical parameters can be attributed to the fact that the theoretical calculations were carried out with isolated molecules in the gaseous phase whereas the experimental values were based on the molecule in the crystalline state. Geometric parameters bond lengths and angles were listed in the Table 2 and Table 3, respectively along with the experimental results. As can be seen from the table all the bond lengths are extremely closed to experimental results and the biggest deviations of the selected bond lengths are 0.17 Å (C30-C31).

Table 3. Optimized bond angles of conformers A & B and conformer A in comparison with experimental results, (°).

| Bond angle (°) | X-ray | B3LYP/6-311G | |
		Combined A&B	Conformer A
C1-C7-C8	132.5	130.1	130.4
C7-C8-C9	119.3	120.7	120.4
C7-C8-C12	132.5	133.5	133.9
C9-C8-C12	108.0	105.6	105.6
O1-C9-C8	125.6	126.3	126.7
O1-C9-C10	126.0	127.0	126.8
C8-C9-C10	108.3	106.5	106.4
C9-C10-C11	109.0	105.5	105.6
C9-C10-C13	119.5	121.2	120.4
C11-C10-C13	131.5	133.2	133.8
C10-C13-C14	130.7	129.6	130.4
C20-C26-C27	132.3	129.5	
C26-C27-C28	120.1	121.3	
C26-C27-C31	130.9	133.1	
C28-C27-C31	108.9	105.5	
O2-C28-C27	126.6	127.1	
O2-C28-C29	124.1	126.2	
C27-C28-C29	109.3	106.5	
C28-C29-C30	108.7	105.6	
C28-C29-C32	120.5	120.7	
C30-C29-C32	130.7	133.5	
C29-C32-C33	132.0	130.2	

**Experimental and computed vibrational spectra**

It is normally observed that the calculated vibrational frequencies are higher than the normal due to the neglect of anharmonicity in the real system. Small differences between the theoretical and experimental values vibrational modes are observed. These differences can come from the non-covalent interactions. Also experimental results are for solid phase, and theoretical calculations belong to gaseous phase. Comparison of the experimental and calculated spectra is shown in Figure 4 and selected FT-IR and calculated vibrational wave numbers and assignments are listed in Table 4 for the conformer A and B considering a single molecule in a lattice.

The IR spectrum of the compound showed stretching band at 1687 cm-1 due to the carbonyl group while stretching for carbonyl groups are calculated at 1782-1784 cm-1 for the carbonyl groups of conformer A and B in a single lattice. The CH stretching modes, which were observed at 3054 and 2911 for the 5-member ring and phenyl group in the FT-IR spectrum, were calculated as 3257 and 3255 for CH stretching of cyclopentanone ring and number of stretching between 3220-3177 for the phenyl rings.
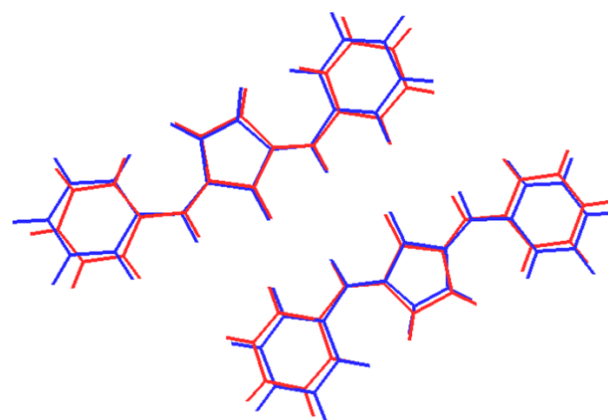
Figure 3. Atom-by-atom superimposition of the structures calculated (blue) on the X-ray structure (red) of polymorph (II) of DBCP.

As can be seen in table C=C (α,β-unsaturated) stretching mode, calculated as 1684-1674, were observed at 1622 in the FT-IR spectrum. These results obtained by the calculations have shown an adequate consistency with the experimental values, and small differences can be explained by the existence of intermolecular interactions like C-H…π and C-H…O.
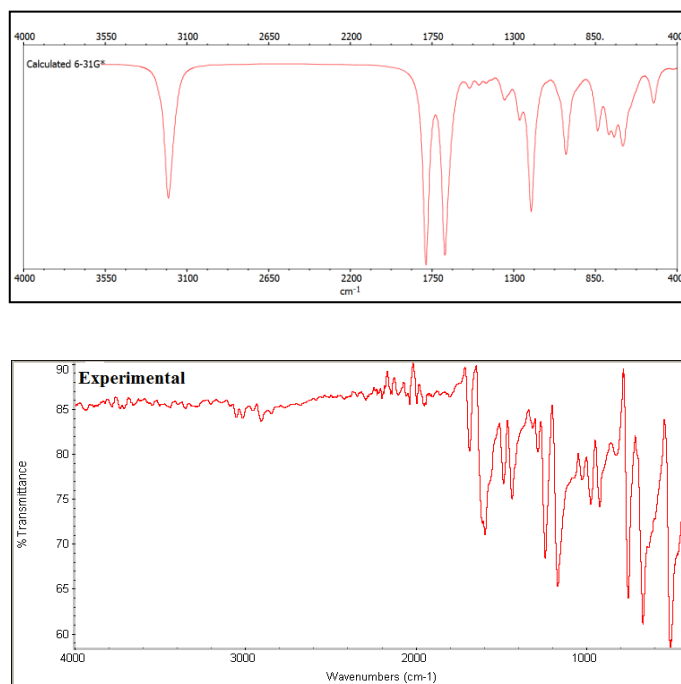
**Figure 4.** The experimental and calculated infrared spectra of the tiled compound.

Frontier Molecular Orbitals analysis

The most important frontier molecular orbitals (FMOs) such as highest occupied molecular orbital (HOMO) and lowest unoccupied molecular orbital (LUMO) plays a crucial part in the chemical stability of the molecule.[52] The HOMO represents the ability to donate an electron and LUMO as an electron acceptor represents the ability to accept an electron. The energy gap between HOMO and LUMO also determines the chemical reactivity, optical polarizability and chemical hardness–softness of the molecule.[53]

Table 4. Selected vibrational assignments (cm^{-1}) for polymorph (II).

Assignment	Experimental	Calculated 6-31G* for conformer A and B
5-member ring C-H str.	3054	3257, 3255
5-member ring C-H asym str.	3019	3240,3239
phenyl rings C-H str.	2911	3220-3177
α,β-unsaturated -C=C-H str.		3166-3149
carbonyl str.	1687	1784,1782
α,β-unsaturated C=C str.	1622	1683-1674
phenyl rings C=C str.	1600	1626-1653

In the present study, the HOMO and LUMO energies are predicted at B3LYP method with 6-31G* basis set. Accordingly to the results, the molecule contains 68 occupied molecular orbitals and 240 unoccupied molecular orbitals. Figure 5 shows the distributions and energy levels of HOMO and LUMO orbitals for the title molecule in gaseous phase.

HOMO (-0.1992 eV)

LUMO (-0.676 eV)
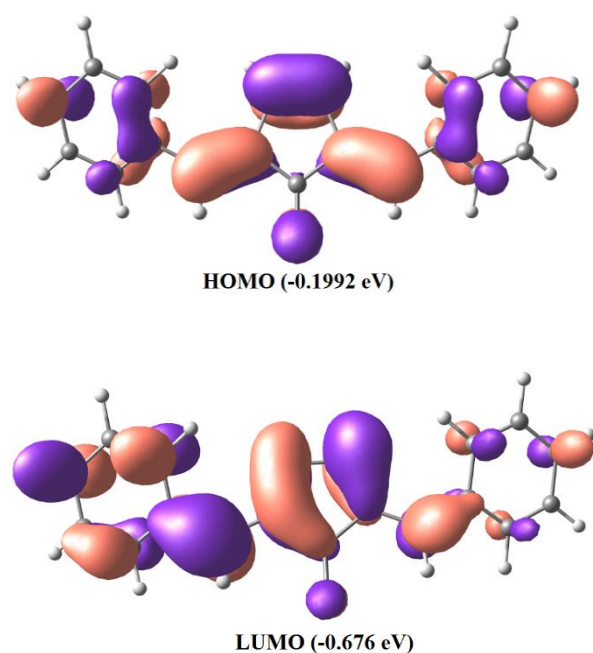
Figure 5. The molecular orbitals and energies for the HOMO and LUMO of 2,5-dibenzylidenecyclopentanone in gas phase.

It is clear from the Figure 5 that isodensity plot for the HOMO is well localized symmetrically over the cyclopentanone and on ipso, ortho and para position of the phenyl rings where the LUMO is populated on cyclopentanone and one of the phenyl ring along with the carbonyl group. The HOMO–LUMO energy separation can be used as a sign of kinetic stability. A large HOMO–LUMO gap implies high kinetic stability and low chemical reactivity.[54,55] As can be seen the magnitude of energy separation between HOMO and LUMO is 0.1768 eV this small gap indicates the chemical softness and high reactivity of compound.

Conclusion

The polymorph (II) of 2,5-dibenzylidenecyclopentanone (DBCP) having two conformationally different/independent molecules in its unit cell has been obtained by slow evaporation of ethanol solvent at room temperature and further investigated by the computational calculations using B3LYP method with 6-31G* basis set to explore its structural aspects in comparison to its previously reported polymorph (I). The polymorph (II) pack in 1D-supramolecular chains mainly stabilized by C-H…O hydrogen bonds, π-π, C-H…π interactions with every two neighbouring chains moving in opposite directions. The analysis of both the experimental and calculated molecular geometries of polymorph (II) shows good agreement with each other. In addition, all the vibrational modes are closed to the observed vibrations and small energy difference between the HOMO-LUMO orbitals frontier provides significant information regarding the softness and high reactivity of the molecule.

References

[1]Desiraju, G. R., *Angew. Chem.-Int. Ed. Engl.,* **1995,** *34*, (21), 2311-2327.

[2]Boistelle, R., *Actual. Néphrol.,*. **1985**, 159-202.

[3]Choudhury, A. R., Islam, K., Kirchner, M. T., Mehta, G., Row, T. N. G., *J. Am. Chem. Soc.,* **2004,** *126* (39), 12274-12275.

[4]Herbstein, F. H., *Crystal Growth Design,* **2004,** *4*(6), 1419-1429.

[5]Bernstein, J., Davey, R. J., Henck, J. O., *Angew. Chem.-Int. Ed. Engl.,* **1999,** *38*(23), 3440-3461.

[6]Braga, D., Maini, L., Polito, M., Scaccianoce, L., Cojazzi, G., Grepioni, F., *Coord. Chem. Rev.,* **2001,** *216*, 225-248.

[7]Kawamura, T., Miyazaki, Y., Sorai, M., *Chem. Phys. Lett.,* **1997,** *273*(5-6), 435-438.

[8]Kalman, A., Fabian, L., Argay, G., Bernath, G., Gyarmati, Z., *J. Am. Chem. Soc.,* **2003,** *125* (1), 34-35.

[9]Matsumoto, A., Tanaka, T., Tsubouchi, T., Tashiro, K., Saragai, S., Nakamoto, S., *J. Am. Chem. Soc.,* **2002,** *124*(30), 8891-8902.

[10]McMahon, J. A., Zaworotko, M. J., Remenar, J. F., *Chem. Commun.,* **2004**(3), 278-279.

[11]Barendt, J. M., Bent, E. G., Haltiwanger, R. C., Squier, C. A., Norman, A. D., *Inorg. Chem.,* **1989,** *28*(24), 4425-4427.

[12]Reger, D. L., Gardinier, J. R., Smith, M. D., Shahin, A. M., Long, G. J., Rebbouh, L., Grandjean, F., *Inorg. Chem.,* **2005,** *44*(6), 1852-1866.

[13]Reed, S. M., Weakley, T. J., Hutchison, J. E., *Crystal Eng.,* **2000,** *3*(2), 85-99.

[14]Ballester, L., Gil, A. M., Gutierrez, A., Perpinan, M. F., Azcondo, M. T., Sanchez, A. E., Amador, U., Campo, J., Palacio, F., *Inorg. Chem.,* **1997,** *36*(23), 5291-5298.

[15]Basavoju, S., Boström, D., Velaga, S. P., *Mol. Cryst. Liq.Cryst.,* **2012,** *562*(1), 254-264.

[16]Munshi, P., Venugopala, K. N., Jayashree, B. S., Row, T. N. G., *Crystal Growth Design,* **2004,** *4*(6), 1105-1107.

[17]Davey, R. J., Blagden, N., Potts, G. D., Docherty, R., *J. Am. Chem. Soc.,* **1997,** *119*(7), 1767-1772.

[18]Sarma, B., Chen, J., Hsi, H.-Y., Myerson, A., *Korean J. Chem. Eng.,* **2011,** *28*(2), 315-322.

[19]Aakeröy, C. B., Forbes, S., Desper, J., *J. Am. Chem. Soc.,* **2009,** *131*(47), 17048-17049.

[20]Chieng, N., Rades, T., Aaltonen, J., *J. Pharm. Biomed. Anal.,* **2011,** *55*(4), 618-644.

[21]Blagden, N., De Matas, M., Gavan, P., York, P., *Adv. Drug Deliv. Rev.,* **2007,** *59*(7), 617-630.

[22]Kawamata, J., Inoue, K., Inabe, T., *Appl. Physics Lett.,* **1995,** *66*(23), 3102-3104.

[23]Kawamata, J., Inoue, K., Inabe, T., *Bull. Chem. Soc. Jap.,* **1998,** *71*(12), 2777-2786.

[24]Kawamata, J., Inoue, K., Inabe, T., Kiguchi, M., Kato, M., Taniguchi, Y., *Chem. Phys. Lett.,* **1996,** *249*(1), 29-34.

[25]Ravindra, H., Chandrashekaran, K., Harrison, W., Dharmaprakash, S., *Appl.Phys. B.* **2009,** *94*(3), 503-511.

[26]Indira, J., Karat, P. P., Sarojini, B., *J. Cryst. Growth,* **2002,** *242*(1), 209-214.

[27]Nesterov, V. V., Antipin, M. Y., Nesterov, V. N., Penn, B. G., Frazier, D. O., Timofeeva, T. V., *Crystal Growth Design,* **2004,** *4*(3), 521-531.

[28]Nesterov, V. V., Antipin, M. Y., Nesterov, V. N., Moore, C. E., Cardelino, B. H., Timofeeva, T. V., *J. Phys. Chem., B.* **2004,** *108*(25), 8531-8539.

[29]Guilford, W. J., Shaw, K. J., Dallas, J. L., Koovakkat, S., Lee, W., Liang, A., Light, D. R., McCarrick, M. A., Whitlow, M., Ye, B., *J. Med. Chem.,* **1999,** *42*(26), 5415-5425.

[30]Nesterov, V. N., Timofeeva, T. V., Sarkisov, S. S., Leyderman, A., Lee, C. Y. C., Antipin, M. Y., *Acta Cryst. Sect. C.* **2003,** *59*(11), o605-o608.

[31]March, J., *Adv. Org. Chem.,* Wiley, New York, **1992**.

[32]Katsori, A. M., Hadjipavlou-Litina, D., *Expert. Opin. Ther. Path.,* **2011,** *21*(10), 1575-96.

[33]Asiri, A. M., Khan, S. A., *Molecules.* **2011,** *16* (1), 523-31.

[34]Husain, A., Rashid, M., Mishra, R., Kumar, D., *Acta Pol. Pharm.,* **2013,** *70*(3), 443-9.

[35]Solano, J. D., Gonzalez-Sanchez, I., Cerbon, M. A., Guzman, A., Martinez-Urbina, M. A., Vilchis-Reyes, M. A., Martinez-Zuniga, E. C., Alvarado, C., Quintero, A., Diaz, E., *Eur. J. Med. Chem.,* **2013,** *60*, 350-9.

[36]Dominguez, J. N., de Dominguez, N. G., Rodrigues, J., Acosta, M. E., Caraballo, N., Leon, C., *J. Enzyme Inhib. Med. Chem.,* **2013,** *28*(6), 1267-73.

[37]Vijaya Bhaskar Reddy, M., Shen, Y. C., Ohkoshi, E., Bastow, K. F., Qian, K., Lee, K. H., Wu, T. S., *Eur. J. Med. Chem.,* **2012,** *47*(1), 97-103.

[38]Modzelewska, A., Pettit, C., Achanta, G., Davidson, N. E., Huang, P., Khan, S. R., *Bioorg. Med. Chem.,* **2006,** *14*(10), 3491-5.

[39]Theocharis, C. R., Jones, W., Thomas, J. M., Motevalli, M., Hursthouse, M. B., *J. Chem. Soc., Perkin Trans. 2.* **1984**(1), 71-76.

[40]Sheldrick, G. M., *Acta Cryst., Sect. A. Found. Cryst.,* **2007,** *64*(1), 112-122.

[41]Becke, A. D., *J. Chem. Phys.,* **1993,** *98*(7), 5648-5652.

[42]Lee, C., Yang, W., Parr, R. G., *Phys. Rev. B.,* **1988,** *37*(2), 785.

[43]Hehre, W. J., Ditchfield, R., Pople, J. A., *J. Chem. Phys.,* **1972,** *56*(5), 2257-2261.

[44]Neese, F., *Wiley Interdiscipl. Rev.: Comput. Mol. Sci.,* **2012,** *2*(1), 73-78.

[45]Allouche, A. R., *J. Comput. Chem.,* **2011,** *32*(1), 174-182.

[46]Allen, F. H., Kennard, O., Watson, D. G., Brammer, L., Orpen, A. G., Taylor, R., *J. Chem. Soc., Perkin Trans. 2.,* **1987**(12), S1-S19.

[47]Etter, M. C., *Acc. Chem. Res.,* **1990,** *23*(4), 120-126.

[48]Naseer, M. M., Hameed, S., *Crystengcomm,* **2012,** *14*(13), 4247-4250.

[49]Casadesús, R., Moreno, M., González-Lafont, à., Lluch, J. M., Repasky, M. P., *J. Comput. Chem.,* **2004,** *25*(1), 99-105.

[50]Abbas, A., Nazir, H., Naseer, M. M., Bolte, M., Hussain, S., Hafeez, N., Hasan, A., *Spectrochim. Acta. A. Mol. Biomol. Spectr.,* **2014,** *120*, 176-84.

[51]Mikhailov, O. V., Chachkov, D. V., *Eur. Chem. Bull.,* **2014,** *3*(4), 367-371.

[52]Becker, H. G. O., *J. Prakt. Chem.,* **1978,** *320*(5), 879-880.

[53]Kosar, B., Albayrak, C., *Spectrochim. Acta Part A. Mol. Biomol.r Spectr.,* **2011,** *78*(1), 160-167.

[54]Özbek, N., Kavak, G., Özcan, Y., Ide, S., Karacan, N., *J. Mol. Struct.,* **2009,** *919*(1), 154-159.

[55]Kumar, P. S., Vasudevan, K., Prakasam, A., Geetha, M., Anbarasan, P., *Spectrochim. Acta Part A. Mol. Biomol. Spectr.,* **2010,** *77*(1), 45-50.

ORGANOCLAY PLURONIC F68 – MONTMORILLONITE, AS A SUSTAINED RELEASE DRUG DELIVERY VEHICLE FOR PROPRANOLOL HYDROCHLORIDE

Seema[a] and Monika Datta[a]*

Short half life of propranolol hydrochloride (PPN), an antihypertensive drug is a prime requirement to develop a formulation which could sustain the release of PPN in the human body and also eliminate daily multiple dosage of propranolol. In this study organoclay Pluronic F68 modified montmorillonite (Mt) has been explored as a sustained release carrier for oral delivery of PPN. The developed organoclay PF68-Mt was compared for adsorption capacity of PPN with pristine Mt. A detailed and systematic study to evaluate the effect of pH, time and initial PPN concentration on drug loading capacity of organoclay PF68-Mt and pristine Mt has been evaluated. The synthesized PF68-Mt-PPN composites were characterized by XRD, FTIR, TGA techniques. XRD studies suggested the intercalation of PPN within the pristine Mt and organoclay PF68 - Mt. In vitro drug release profile of PPN from organoclay PF68-Mt composites is compared with that of pristine Mt and the pure PPN, in simulated gastric and intestinal fluids. The release profile of loaded PPN in organoclay PF68-Mt shows pH dependent release in simulated gastrointestinal fluid. The release behaviour of PPN from PF68-Mt-PPN composites was appeared to be in more sustained manner than prisine Mt and pure PPN over a period of 24 hours. This study suggests that the modification of Mt with a non ionic tri block co polymer Pluronic F68 provides better controlled on the release of PPN as compared to pristine Mt and pure drug. The obtained PF68-Mt-PPN composites with high drug loading capacity and sustained drug release characteristics supposed to be a better oral drug delivery system, for a highly hydrophilic low molecular weight antihypertensive drug PPN. The PF68-Mt-PPN composites developed have the potential to minimize the drug dosing frequency and hence improving the patient compliance. Thus, proposing a new promising formulation for oral sustained release drug delivery.

*Corresponding Author
    Fax: +91-01127666605
    E-Mail: monikadatta_chem@yahoo.co.in
[a]   Analytical Research Laboratory, Department of Chemistry, University of Delhi, Delhi-110 007, India

INTRODUCTION

Recently there is a growing use of clays in delivery technology in order to confer slow release properties of the active ingredient, which is of particular interest in pharmaceutical industry.[1, 2]

Organoclays are extensively used in a wide range of applications as a basis for the synthesis of clay polymer nanocomposites, for photophysical applications, paints, cosmetics, refractory varnish, thixotropic fluids, or geochemical barriers in waste landfills.[3-7] Surface modifications of clay minerals in the form of organoclays allows the creation of new materials and new applications. However these materials are not widely explored in the area of drug delivery.

Organoclays combine the properties of natural clays such as a high surface area and a hydrophobic surface which allow the adsorption of organic compounds or the dispersion of clays into polymers.[3,6,8] Another feature is the strong increase of the interlayer height, comparatively small for the clay before modification,which makes easier the insertion of guest molecules whose orientations follow those of the previously adsorbed molecules used for the manufacture of organoclays.[9,10] The synthesis of organoclays is based on the mechanisms of the reactions that the clay minerals can have with the organic compounds.[3] Depending on the layer charge of the clay mineral and the chain length of the organic ion, different arrangements of organic molecules between the layers can be formed.

Being non toxic, biocompatible and FDA approved, montmorillonite (Mt) a smectite clay mineral is extensively explored for oral drug delivery applications in recent years. The advantageous characterstic physiochemical properties of Mt provides it all the properties of an ideal drug delivery vehicle.[1,2,11-14]
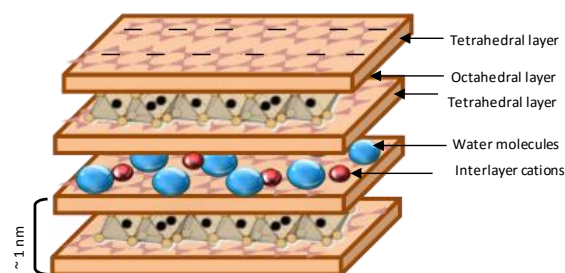
Figure 1. Structure of montmorillonite

Organo-montmorillonites, are mainly obtained by intercalating cationic surfactants such as quaternary ammonium compounds into the interlayer space through ion exchange.[3,15-16] The interlayer spacing of these organoclays generally increases as the surfactant loading increases and reaches a saturation limit which corresponds to or is larger than the clay cation exchange capacity (CEC).[11,15-16] However, the intercalation of a long alkyl tail surfactant

within the interlayer space is irreversible and prevents any further cationic exchanges which limit, as a result, the potential applications of the nanocomposites and/or the innovation of new hybrid materials.[17,18] Therefore, the synthesis of organoclays by using other surfactants is a new area of interest.

Pluronic F-68 a triblock copolymer has been approved for biomedical applications by US food and drug administration.[19] The properties of amphiphilic poly (ethylene oxide)-β-poly-(propylene oxide)-β-poly(ethylene oxide) (PEO–PPO–PEO) block copolymers in aqueous media have attracted a great deal of interest because of several important aspects.[19-20] PEO–PPO–PEO copolymers are commercially available surfactants (pluronics, synperonics, poloxamers), whose molecular weight and PEO/PPO composition ratio vary within a wide range. In water amobe their critical micelle concentration (CMC) value they usually spontaneously form nanosized core-shell micelles having a hydrophobic core composed predominantly of PPO segments and a shell dominated by hydrated PEO segments.[21-22] The PEO blocks have available functionality to which receptor-specific ligands could be attached. That is why the PEO–PPO–PEO copolymers meet the specific requirements for various applications, such as dispersion stabilization, emulsification, detergency, foaming, lubrication etc.[19-22] presently the PEO–PPO–PEO copolymers are being intensively evaluated as potential drug and gene delivery systems for multiple pharmaceutical applications as well as for diagnostic imaging as carriers for various contrasting agents. The hydrophobic PPO core may serve as a container for water insoluble drugs while the hydrophilic PEO shell provides steric stability.[19]

Propranolol hydrochloride, [(2RS)-1-(1-methylethyl)-amino-3-(naphthalen-1-yloxy)propan-2-ol hydrochloride] is widely used for the treatment of hypertension. The dose of propranolol hydrochloride (PPN) ranges from 40 to 80 mg day^{-1}.[23] Due to shorter half life (3.9 hours) the conventional PPN tablets has to be administrated 2 or 3 times daily so as to maintain adequate plasma levels of drug.[24.] Multiple drug administration results either in manifestation of side effects or reduction in drug concentration at the receptor site. Thus, the development of sustained-release dosage forms would clearly be advantageous.[4] Some researchers have formulated oral sustained-release products of PPN by various techniques.[12, 25-27]

In the present study FDA approved 2:1 smectite clay mineral Mt and a non ionic surfactant Pluronic F68 has been selected because of their structural, biological and industrial importance for the synthesis of organoclay PF68-Mt. To the best of our knowledge this system is reported for the first time and being further explored as a sustained release drug delivery vehicle for Propranolol hydrochloride (PPN) as a model drug.

The synthesized organoclay PF68-Mt was characterized by several complementary techniques including X-Ray diffraction (XRD), Fourier transform infrared spectroscopy (FTIR), TGA, DSC, and SEM.

A systematic study was carried out to obtain PPN loaded organoclay PF68-Mt composites by optimizing various experimental conditions for maximum adsorption capacity as a sustained release drug delivery vehicle. The obtained PF68-Mt-PPN composites were compared for their physiochemical properties and in vitro drug release profile with pristine Mt-PPN composites developed under similar conditions.

The obtained preliminary results suggest the potential of the synthesized orgnaoclay PF68-Mt-PPN composites for oral and sustained release drug delivery of PPN for the treatment of hypertension around the clock.

EXPERIMENTAL

Materials

Montmorillonite KSF, PPN (purity >99 %) and Pluronic F-68 with a molecular weight equal to 8500 Dalton were obtained from Sigma Aldrich St. Louise USA. Analytical grade HCl, KCl, NaOH, Potassium dihydrogen phosphate was ordered by MERCK (Germany). All other reagents whether specified or not were of analytical grade. Water used in the experiments was deionized and filtered (Milli-Q Academic, Millipore, France).
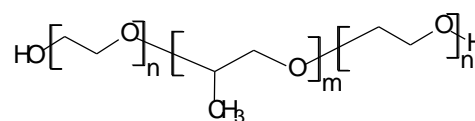
Figure 2. Structure of Pluronic F68, *n* = 75 oxyethylene units, *m* = 30 oxypropylene units
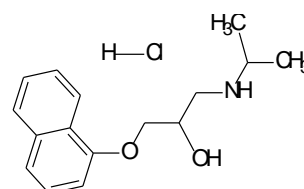
Figure 3. Structure of propranolol.HCl

Synthesis of organoclay Pluronic F68-montmorillonite

A nonionic triblock copolymer PF68 was selected as surfactant for the synthesis of organoclay PF68-Mt. In brief an aqueous Mt dispersion (1% w/v) was allowed to swell overnight at constant magnetic stirring of 500 rpm to form a stable Mt dispersion. A 2 % (w/v) PF68 solution was prepared separately and added gradually to the Mt dispersion to form a reaction media (above CMC of PF68) within a period of 2 hours followed by 6 hours stirring at normal room temperature. The resulted hydrophobic reaction media was centrifuged at 20,000 rpm followed by several washings to remove the unreacted PF68.

The obtained residue was lyophilized at –45 °C and pressure of 30 mTorr. Thus obtained organoclay PF68-Mt was characterized with suitable analytical techniques as discussed under characterization section and further used as an adsorbent for the PPN.

pH Stability study of the aqueous PPN Solution

To start with the experiment, stability of PPN molecule as a function of pH was evaluated in the pH range of 1-12. The pH of the 10 ppm drug solutions was maintained using 0.1N HCl and NaOH solutions using pH meter (Eutech instruments). The solutions thus prepared were analysed spectrometrically at λmax of 289 nm.

Synthesis of organoclay Mt-PF68-PPN composites and pristine Mt-PPN composites

In order to investigate the interaction of PPN with organoclay PF68-Mt, PF68-Mt-PPN composites were synthesized as per the reported method with certain modification as function of time, pH, Mt content and PPN content.[14]

Effect of pH on the adsorption efficiency of PPN on PF68-Mt, was investigated by treating 50 ml of 200 ppm aqueous PPN solution with organoclay PF68-Mt (0.1 g) in the pH range of 1 to 11 and allowed to stir on a magnetic stirrer for a period of 2 hours at 1000 rpm. In the next step, effect of contact time on the adsorption efficiency of PPN onto PF68-Mt surface was evaluated. The 50 ml aqueous PPN solution of 200 ppm concentration at pH 9.6 was treated with organoclay PF68-Mt (0.1 g) over a period of 0.25, 0.5, 0.75, 1, 2 and 3 h on a magnetic stirrer at 1000 rpm. Further, the effect of initial drug concentration on the adsorption capacity of PPN on PF68-Mt was evaluated. The 0.1 g of PF68-Mt was treated with 50 ml of PPN solution in the concentration range of 2 mg-20 mg/50 ml (40-400 mg L^{-1}) at the original aqueous drug solution pH (9.6) and allowed to stir on a magnetic stirrer for a period of 2 h at 1000 rpm.

After desired reaction time, PF68-Mt-PPN dispersion were centrifuged with 20,000 rpm for 30 minutes at 10 °C (Sigma, Sartorius, 3K30).The free PPN concentration in the supernatant were determined using UV–visible spectrophotometer (Analytic Jena) at 289 nm from the Lambert-Beer's plot and the percentage of the drug adsorbed, being calculated using equation 1.

$$\text{Drug adsorbed (\%)} = \frac{C_i - C_e}{C_i} \times 100 \qquad (1)$$

where

C_i is the initial drug concentration (mg L^{-1}) and

C_e is the concentration of the drug (mg L^{-1}) in the supernatant at the equilibrium stage.

The amount of drug adsorbed q_e (mg g^{-1}); was calculated via the mass-balance relationship as per the equation 2.

$$q_e = \frac{(c_i - c_e)V}{m} \qquad (2)$$

where

V is the volume of the reaction media in litre and

m is the mass of organo-Mt used for the studies in grams.

In order to compare and evaluate the effect of pristine Mt, experiments were also performed to synthesized pristine Mt-PPN composites and evaluated for drug adsorption capacity in a same manner as a function of time, pH, and PPN content as discussed above.

Characterizations of organoclay PF68-Mt, pristine PPN-Mt composites and PF68-Mt-PPN composites

Powder X-ray diffraction (PXRD) measurements of pristine Mt, organoclay PF68-Mt, PF68-Mt-PPN and pristine Mt-PPN composites were performed on a powder X-ray diffractometer (XPERT PRO Pananlytical, model PW3040160, Netherland) the measurement conditions were Cu K α radiation generated at 40 kV and 30 mA as X-ray source 2-40° (2θ) and step angle 0.01° s^{-1}. FTIR spectra of the same samples were recorded with an FTIR spectrophotometer (Perkin Elmer, Spectrum BXFTIR Spectrometer) using the KBr (Merck, Germany) disc method. Thermogravimetric analysis was carried out within 30 – 700 °C at 10 °C min^{-1} in nitrogen flow (TGA 2050 Thermal gravimetric Analyzer. Differential scanning calorimetric studies were conducted on DSC instrument (DSC Q200 V23.10 Build 79). The samples were purged with dry nitrogen at a flow rate of 10 ml min^{-1} and the temperature was raised at 5 °C min^{-1}. For surface morphology analysis, one drop of the samples was mounted on a stubs; sputter coated with gold in a vacuum evaporator and photographed using a scanning electron microscope model (ZEISS EVO 40) with an accelerating voltage of 20 KV. For particle shape and size, samples were examined by mounting a sample drop on the carbon coated copper grids, dried overnight and photographed using a transmission electron microscope (TECNAI G2 T30, U-TWIN) with an accelerating voltage of 300 kV. Zeta potential of the 0.01 % aqueous suspension of the samples were determined using Malvern zeta sizer Nano ZS.

In vitro drug release studies

In vitro drug release studies of pristine Mt-PPN composites and organoclay PF68-Mt-PPN composites, were evaluated in two dissolution media consisting of simulated intestinal fluid (PBS, pH 7.4) and simulated gastric fluid (HCl, pH 1.2) using the dialysis bag technique.[28] Both the dissolution media were prepared as per the reported method.[29]

Dialysis membranes (Sigma-Aldrich, Mw. 8405) were equilibrated overnight with the dissolution medium prior to experiments.

Weighed amount of pristine Mt-PPN composites and organoclay PF68-Mt-PPN composite with known drug content were taken in 5ml of dissolution media in the dialysis bag. Enclosed dialysis bag was dipped into the receptor compartment containing 100 ml dissolution medium, which was closed and maintained with 100 rpm at 37±0.5 °C. 5 ml of aliquote was withdrawn at regular time intervals and the same volume was replaced with a fresh dissolution medium maintained at 37°C. The withdrawn aliquotes were analyzed for PPN content by UV-Visible spectrophotometer (Analytic Jena) at 289 nm. Cumulative percentage of drug release was calculated by Lambert-Beer's plot of PPN obtained in the same dissolution media.

RESULTS AND DISCUSSION
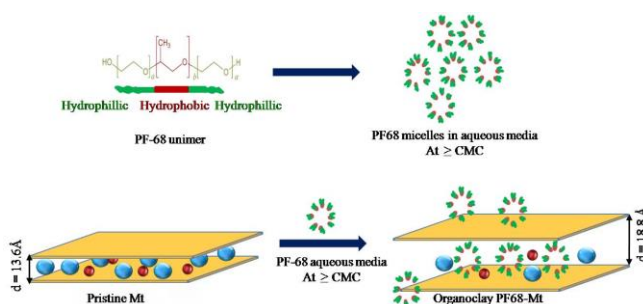
Characterization of Organoclay PF68-Mt

XRD studies

Pristine Mt showed a characteristic diffraction peak at 2θ of 6.4° (001 plane) representing d spacing of 13.4 Å.[30] In case of synthesized organoclay PF68-Mt a shifting in 2θ value from 6.4° to 4.6° and stronger intensity was observed (Figure 4). According to Bragg's law, shifting in 2θ value from higher diffraction angle to lower diffraction angle is because of increase in d spacing and intercalation of an organic moiety.[30,31] An increase of 9.2 Å was observed on intercalation of PF68 in Mt layers corresponding to the increase in d spacing from 13.6Å to 18.8 Å.
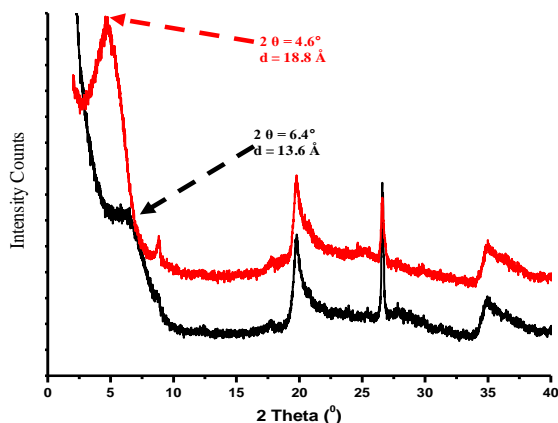
Figure 4. XRD pattern of Pristine Mt, organoclay PF68-Mt

Pluronic F68 a non ionic triblock copolymer of poly oxy ethylene, poly oxy propylene as already discussed earlier is known to form micelles in aqueous media above its critical micelle concentration (CMC).[19,22] During the synthesis process of organolay PF68-Mt, these PF68 micelles supposed to interact with the interlayer water molecules and polar groups of Mt, resulting in intercalation of PF68 with increase in d spacing from 13.6 to 18.8 Å.

A schematic representation for synthesis of organoclay PF68-Mt with PF68 is represented in Figure 5.

Figure 5. Schematic representation for the synthesis of organoclay PF68-Mt

FTIR studies

In order to confirm the presence of surfactant PF68 within the interlayer region of the Mt, FT-IR spectra were recorded in the region 400-4000 cm^{-1}. In the IR spectrum of Mt, the band at 1049 cm^{-1} has been assigned to Si-O stretching and is the characteristic band of Mt. The band at 3428 cm^{-1} and 3629 cm^{-1} has been assigned to H-O-H stretching vibrations from interlayer water and O-H stretching vibrations of the structural OH group. The absorption band at 1639 cm^{-1} corresponds to H-O-H bending. The absorption bands at 538 cm^{-1} and 474 cm^{-1} are strong bending vibrations corresponding to Al-O-Si and Si-O-Si respectively.[32-34] (Figure 6).
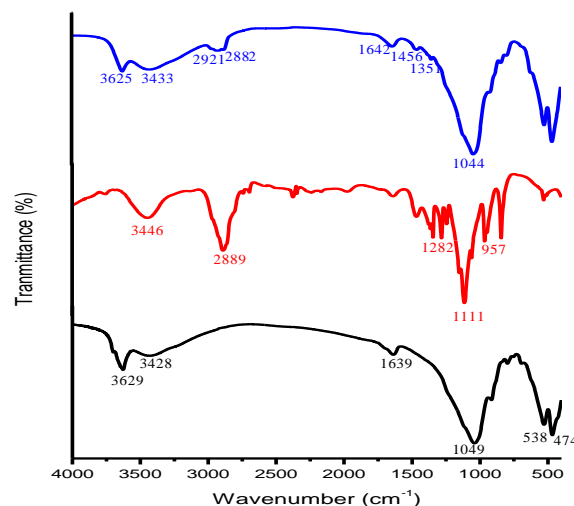
Figure 6. FTIR spectra of pristine Mt, Pluronic F68, organoclay PF68 - Mt

The major peaks observed around 3446 cm^{-1} in PF68 is assigned to the vibrations of hydroxyl (-OH) groups.[35] A strong absorption band at 2889 cm^{-1} was observed. The characteristic peaks at 957 cm^{-1} and 1111 cm^{-1} in PF68 were due to C–O symmetrical structure and C–O asymmetrical stretching vibrations of ether groups.

The peak at 1282 cm^{-1} is assigned to –CH$_2$ group vibration of PF68.[35] The presence of functional groups of PF68 on the surface of Mt is verified by peaks at about 2921cm^{-1} and 2882 cm^{-1} characteristic of the aliphatic C–H antisymmetric and symmetric vibrations respectively from the methylene group of PF68. Beside two new bands at 1351 cm^{-1} and 1456 cm^{-1} were also appeared. The presence of these bands in organoclay PF68-Mt indicates that PF-68, the neutral surfactant could interact with the Mt layers through an ion-dipole type interaction or hydrogen bonding between the hydrophilic or polar part of the PF68 and the water molecules around the exchange cations of the Mt.[36,37]

TG-DTA studies

The pristine Mt shows high thermal stability with weight loss of 10 % from 30-140 °C and is attributed to the loss of adsorbed and interlayer water followed by dehydroxylation in the temperature range from 600-750 °C respectively.[12] In case of organoclay PF68 a weight loss of 3.5 % was observed because of the loss of surface sorbed water in the temperature range of 25-35 °C (Figure 7).
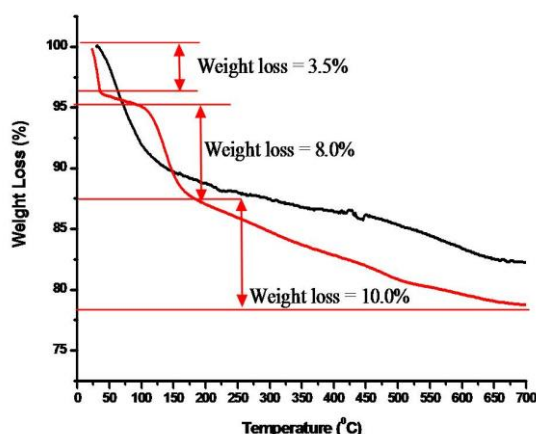

Figure 7. TG pattern: pristine Mt, organoclay PF68 - Mt

A second step weight loss of 8 % was observed from 105 °C to 180 °C due to the replacement of interlayer water by organic PF68 which thermally unstable in this region. In third step from 180 °C to 700 °C, a final weight loss of 10 % was observed and combindly attributed to the thermal decomposition of the PF68 and structural hydroxyl groups.
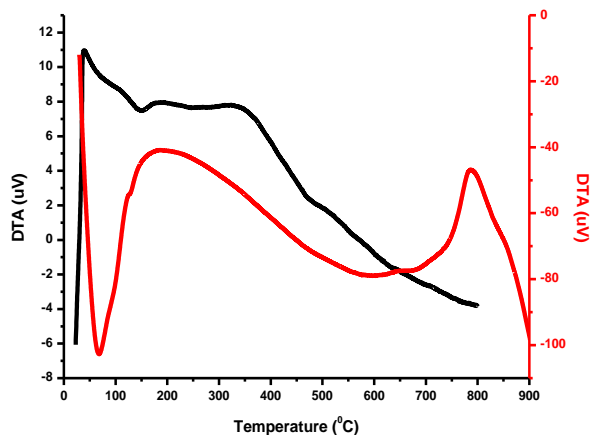

Figure 8. DTA pattern pristine Mt, organoclay PF68-Mt

The DTA thermo gram of pristine Mt resulted in a strong endothermic peak at 80 ºC and broad endothermic peak at 600 ºC corresponding to evaporation of the adsorbed water and loss of structural water respectively.[38,39] However, in case of organoclay PF-68 DTA pattern (Figure 8), an endothermic event at 149 °C corresponding to decomposition of intercalated surfactant moiety was observed.[36,37] This event is followed by an exothermic pattern which might be attributed to the thermal degradation of intercalated PF68 moiety.

DSC studies

In pristine Mt, the broad endotherm cantered at 110 °C is attributed to the dehydration of adsorbed water (Figure 9). In case of organoclay PF68-Mt a sharp endotherm at 63.9 °C corresponds to melting of intercalated PF68 within Mt layers was observed. Second endotherm at 153 °C is attributed to the decomposition of organic copolymer species[37,38] followed by broad endothermic region in the range of 285-355 °C attributed to the thermal degradation of PF68 within Mt layers.
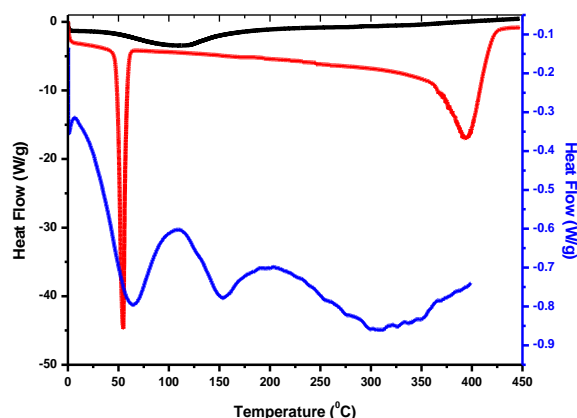

Figure 9. DSC curves: pristine Mt, Pluronic F68, organoclay PF68 - Mt

Surface morphology studies

Scanning electron microscopic (SEM) studies indicates that surface morphology of organoclay PF68-Mt was relatively porous compared to the pristine Mt. The particle size of PF68 modified Mt was found in the range of 1 to 2 μm (Figure 10) by SEM analysis.
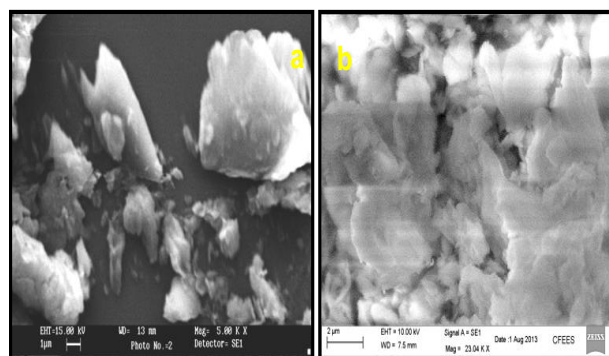

Figure 10. SEM of Mt (a) and PF68 modified Mt (b)

pH Stability study of the aqueous PPN solution

The pH stability of the aqueous PPN solution in the pH range 1 to 11 was investigated spectrophotometrically. The UV absorption spectra of PPN show two absorption peaks at 214 nm and 289 nm corresponding to different electronic transitions of the molecule. It has been found that PPN maintains its stability (Figure 11) within the experimental pH range as there is no change in the absorption spectra of PPN molecule was observed.
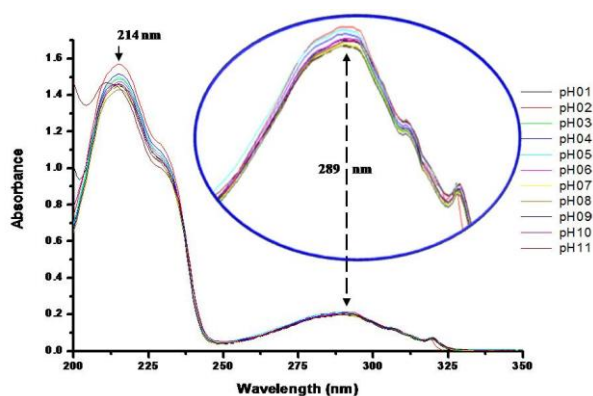

Figure 11. Absorption spectra of PPN as a function of pH of the PPN aqueous solution

Effect of pH on adsorption efficiency

The pH of the drug solution has always played a crucial role in adsorption process. pH effect of PPN aqueous solution on pristine Mt and organoclay PF68-Mt surface is shown in Figure 12. The results suggest that in the pH range of 5-10 adsorption of PPN on pristine Mt surface remain almost constant. But there was sharp decrease in adsorption when the pH was above 10 and below 5 up to 3. Whereas in case of organoclay PF68-Mt, the adsorption of PPN on PF68-Mt was found increase from (50 % to 85 % of 200 ppm drug solution) in the pH range of 2-10 followed by decrease up to 61 % at pH 11. This can be explained on the basis of pK$_a$ value of PPN (pK$_a$= 9.5).[25]

It has been reported that PPN undergo ionization under different pH conditions and about 75.8 % of it is in protonated form at pH 9 which increases to 99.7% and 99.9 % at pH 7 and pH 5 respectively. Hence, the high adsorption of PPN on pristine Mt surface (96-98 %) was observed at 200 ppm attributed to the strong affinity of negatively charge Mt surface for protonated form of PPN. However, decrease in adsorption (%) below pH 5 could be because of the competition between high concentrations of H$^+$ ions present at low pH which get adsorbed on the Mt surface. Besides at high pH values, the species of negetive PPN increases and slightly reduce the adsorption of drug at pH 11 due to repulsion between Mt and drug. With increase in pH, PPN exsist in the protonated form and positive charge on the surface of the PF68-Mt decreases resulting in high adsorption of PPN with PF68-Mt layers. At pH above pK$_a$, PPN is negatively charged, which restricts the adsorption of PPN as a result of the repulsive force between PPN and the negatively charged surface of the PF68-Mt leading to decreased adsorption % at pH 11.
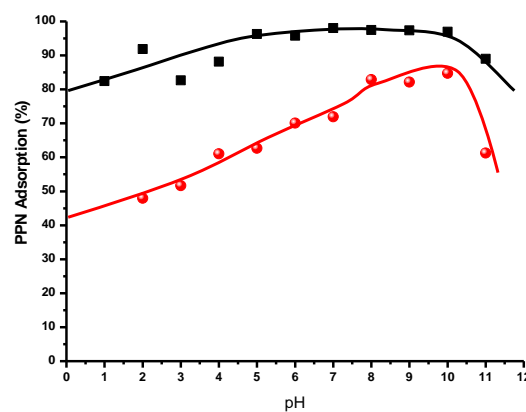
Figure 12. Effect of pH of PPN solution on adsorption efficiency at Mt, PF68-Mt with conc. 200 ppm and time 2 h

Effect of time on adsorption efficiency

Time dependent adsorption of PPN on pristine Mt shows 82 % adsorption of PPN (200 ppm) within a period of 30 minutes (Figure 13). The adsorption (%) increased up to 85 % in 2 hours and tends to decrease up to 84 % in 3 h. Negative surface charge as well as the rapid ion exchange process between Mt interlayer Na$^+$ ions and cationic PPN molecule is mainly attributed for the higher uptake of PPN. Time dependent adsorption of PPN on PF68-Mt shows 76.8 % adsorption of PPN (200 ppm) within a period of 30 minutes which increased up to 78.3 % over a period of 3 h.
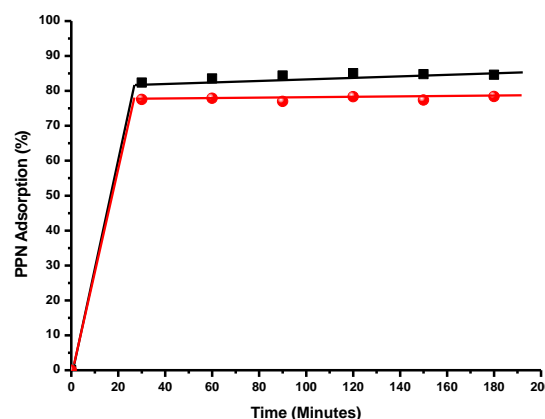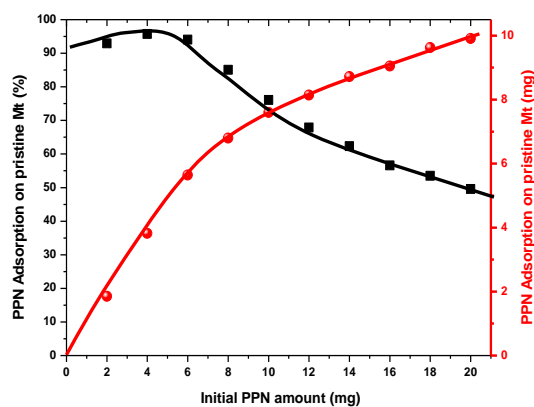

Figure 13. Effect of time on adsorption efficiency at pristine Mt, Organoclay PF68-Mt with conc. 200 ppm and pH 9.6

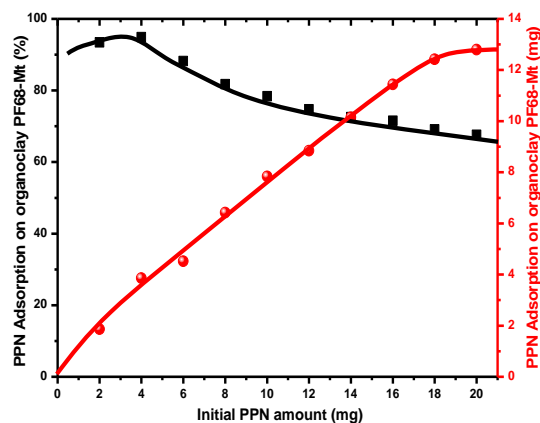**Effect of PPN concentration on adsorption efficiency**

At the natural pH of PPN (pH 9.6), the adsorption of PPN on pristine Mt and organoclay PF68-Mt is affected by its initial amount present in the solution (Figure 14). As the PPN amount in the solution increases from 2 to 4 mg (40 to 80 ppm), the adsorption % increases from 92 % to 95 %. With further increase in the initial drug amount up to 20 mg (400 mg L^{-1}) the adsorption % decreases upto 49.5 % and 67.6 % whereas the total amount of drug adsorbed increases from 1.8 mg to 9.9 mg and 1.86 mg to 12.8 mg for pristine Mt and organoclay PF68-Mt respectively. Therefore, it could be concluded that due to the higher availability of the adsorption sites, nearly 100 % adsorption was obtained at lower concentration of initial drug.

Modification of Mt with PF68 might have increased the surface area of the Mt, which has provided the larger adsorption site for interaction with PPN resulting in high adsorption % of PPN on organoclay PF68-Mt as compared to pristine Mt. The adsorption capacity 127 mg g^{-1} and 171mg g^{-1} was observed for pristine Mt and organoclay PF68-Mt respectively.

Figure 14. Effect of initial amount of PPN solution on adsorption efficiency of pristine Mt with equlibrium time 2 h and pH 9.6


Figure 15. Effect of initial concentration of PPN solution on adsorption efficiency of organoclay PF68-Mt with time equilibrium time 2 h and pH 9.6

Characterization of pristine Mt-PPN composites and organoclay PF68-Mt-PPN composites

XRD Studies

The XRD pattern of pristine Mt, pure PPN and pristine Mt-PPN composites are shown in **Figure 16.** Mt showed a distinct diffraction pattern (001 plane) at $2\theta = 6.4^{\circ}$ representing a 13.4 Å thickness of the Mt layer.[30] The Mt-PPN composites prepared at optimized conditions did not present the PXRD pattern of drug alone, suggesting that drug was in an amorphous form. In case of Mt-PPN composites a shifting in 2θ value from 6.4° to 5.6° and stronger intensity was observed. A previous study,[25] suggest stronger intensity of the basal spacing peak occurs when the drug molecule was intercalated within the Mt layers. According to Bragg's law, shifting in 2θ value from higher diffraction angle to lower diffraction angle is because of increase in *d* spacing. This indicates increase in the interlayer spacing upon intercalation of PPN in the Mt layers

from 13.6 Å to 15.6 Å with the replacement of interlayer cation by PPN. Subtracting the Mt layer thickness (9.6 Å) from the *d* spacing (15.6 Å) of the Mt-PPN complex, the Mt layer thickness was estimated to be 6Å.[30-31]
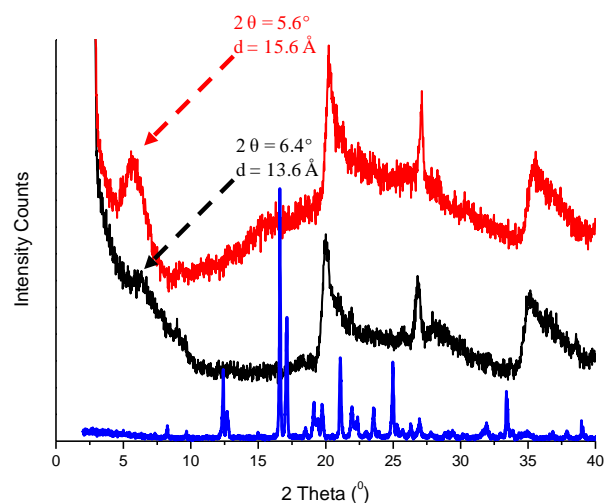
Figure 16. XRD pattern of pristine Mt, Mt-PPN composites, pure PPN

The result suggested that intercalated PPN form a monolayer with lying flat on the Mt surface as shown in Figure 17.

Figure 17. Diagrammatic representation of PPN intercalation within Mt layers

When organoclay PF68-Mt with *d* spacing of 18.8 Å was used as adsorbent for PPN the 2 θ value of optimized sample shift from lower to higher diffraction angle of 4.6° to 4.9° with decrease in *d* spacing from 18.8 Å to 18.05 Å (Figure 18).
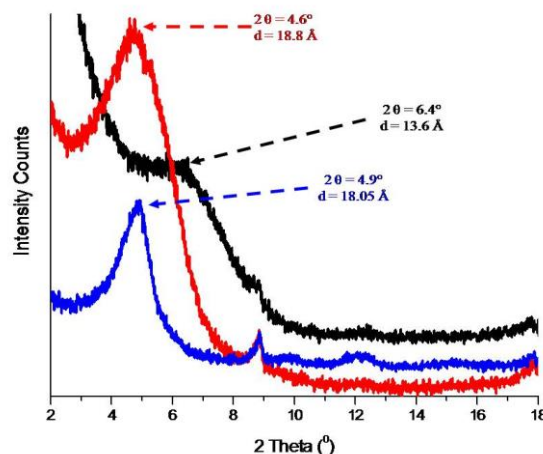
Figure 18. XRD pattern of pristine Mt, PF68-Mt, PF68-Mt-PPNcomplex

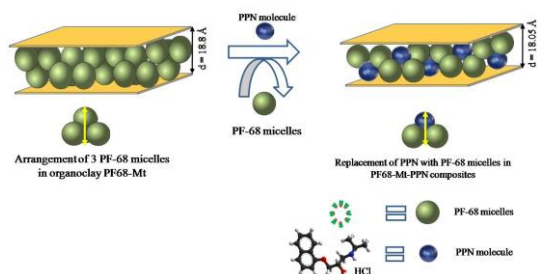The decrease in *d* spacing might be attributed to the replacement of certain intercalated PF68 (surfactant) moiety with PPN molecule. In order to accommodate the PPN molecule within the Mt layers, space is created by replacement of certain PF-68 (surfactant) molecule and the interaction of hydrophilic PEO with hydrophilic PPN moiety might be suggested.

Figure 19. Diagrammatic representation for intercalation of PPN within PF68-Mt

It has been well established, that above CMC, PF-68 molecule arranges itself into the spherical micellar form.[19-22] So, it can be suggested that because of hydrophilic-hydrophillic interaction the PPN molecule might get placed within hydrophilic corona of the PF68 micelles, (Figure 19) and hence being smaller in size, no significant change in the d spacing of PF68-Mt was observed.

On the basis of obtained XRD results it could be concluded that pristine Mt, organoclay PF68-Mt, pristine Mt-PPN composites and organoclay PF68 PF68- Mt-PPN composites followed the order of d spacing as:

$$Mt < Mt\text{-}PPN < PF68\text{-}Mt\text{-}PPN < PF68\text{-}Mt$$

FT-IR studies

The FT-IR spectrum of pristine Mt, pure PPN and Mt-PPN composites prepared by adsorption/ion exchange process is shown in Figure 20. The FT-IR spectra of PPN revealed the presence of peaks at 3323 and 3283 cm^{-1} corresponding to N-H and O-H stretching peaks. The aryl alkyl ether displayed a stretching band at 1268 cm^{-1} and the peak at 798 cm^{-1} was due to substituted naphthalene.[24,41-42]
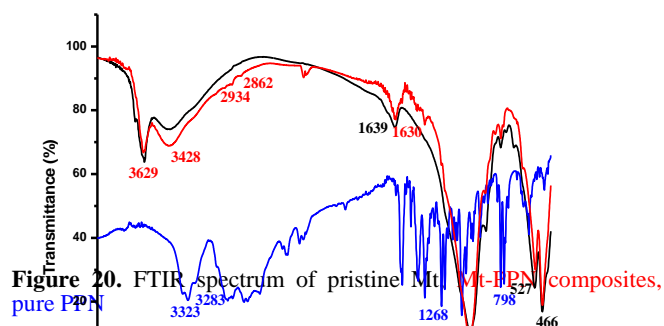
Figure 20. FTIR spectrum of pristine Mt, Mt-PPN composites, pure PPN

The principal peaks depicted in the IR spectra of PPN occur at wavenumbers 1103, 1270, 772, 1580, 795 and 1240 cm^{-1}. These peaks represent the stretching vibrations of the different functional groups that are present in the PPN structure. The wavenumbers 772 and 795 can be associated with the aromatic functional groups, 1240 and 1270 with the

amine functional group, 1103 with the OH group and 1580 with the ketone group respectively. [43]

The FT-IR spectrum of Mt has already been discussed under the section characterization of organclay PF68-Mt.

In case of pristine Mt-PPN composites, peaks at 2934 and 2862 appear because of the C–H stretching of the CH$_3$ group of PPN in the Mt-PPN composites. Not all characteristic bands belonging to Mt and PPN appear in the spectrum of PPN-Mt composites; several new bands in the region of 1250 cm^1 to 1500 cm^1 are also recognized. This also indicated that PPN interacts with the Mt layers.

However in the FT-IR spectra of organoclay PF68-Mt and PF68-Mt-PPN composites there is no significant difference was observed (Figure 21). The characteristic peaks related to PPN were not observed strengthening the fact of intercalation of PPN molecule with the organoclay PF68-Mt interlayer region.
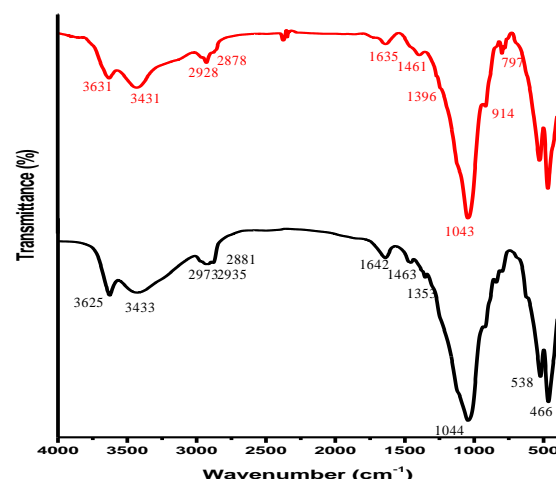
Figure 21. FTIR spectra: organoclay PF68-Mt, PF68-Mt-PPNcomposites

Zeta potential analysis

The zeta potential values of pristine Mt, organoclay PF68-Mt, pristine Mt-PPN composites and organoclay PF68-Mt-PPN composites at their natural pH in aqueous media were found to be negatively charged (Table 1). The negative charge of pristine Mt decreased after adsorption/intercalation of cationic drug PPN. Whereas, the same was increased after intercalation/surface adsorption of nonionic surfactant PF68, attributed to negatively charge terminal hydroxyl groups of poly oxy ethylene groups in PF68. When, organoclay PF68-Mt was used as an adsorbent for the PPN, it maintains the negative surface charge strengthening the fact of PPN intercalation within organoclay PF68-Mt layers as confirmed by XRD and FT-IR analysis.

Table 1. Zeta potential analysis

Code	Zeta potential (mV)
Pristine Mt	-33.9
Mt-PPN composites	-31.7
Organoclay PF68-Mt	-35.5

PF68-Mt-PPN composites	-35.3

TG Studies

The TG thermogram of pristine Mt shows high thermal stability in the temperature region of 30-700 °C with weight loss of 10% from 30-150°C corresponds to the evaporation of free water and water bound to the cations present within the interlayer (Figure 22). Weight loss in the temperature range from 600-750 °C is due to the loss of hydroxyl groups in the aluminosilicate structure and at this point the structure of the Mt layers collapses.[12,38,39]
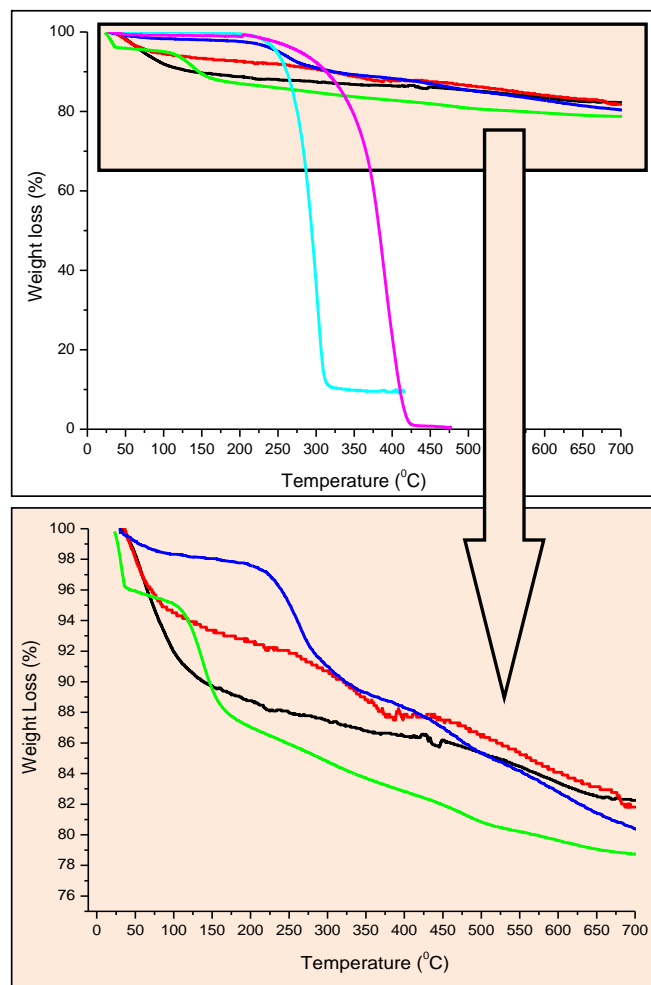
Figure 22. TG pattern: pristine Mt, PPN- Mt composites, organoclay PF68 - Mt, PF68-PPN- Mt composites, Pure PPN, Pure PF68

The thermogravimetric profile of pristine drug PPN (Figure 22) show a sharp weight loss at around 230-320°C corresponding to decomposition of the PPN molecule.[44] Pristine PF68 shows 100 % weight loss in the temperature range of 200 to 425°C.[45]

The pristine Mt-PPN composites (Figure 22) shows weight loss in three steps in the temperature region of 80-120 °C, 200-350 °C and 600-750 °C. The first weight loss of 6 % was observed from 80-150 °C suggesting replacement of interlayer water with PPN molecule. The weight loss observed was smaller than the pristine Mt (~10 %) because of the replacement of interlayer water with intercalated PPN which supposed to be stable and does not show any weight loss upto 200 °C. Weight loss from 600-750 °C might be attributed

to the loss of structural OH group in Mt-PPN composites. Decomposition of intercalated PPN within Mt layers took place in the temperature region of 250-400 °C evident by weight loss of 6 %.

In case of organoclay PF68-Mt, higher weight loss than PPN-Mt composites and degradation of PF68 at lower temperature than pure PF68 (Figure 21) was observed. Presence of less content of Mt is clearly evident from the thermo gram of organoclay PF68-Mt. When organoclay PF68-Mt was used for the adsorption of PPN, it shows the higher weight loss than PPN-Mt composites but less than PF68-Mt organoclay suggesting the fact of less surfactant content present within the PF68-PPN-Mt composites as has been concluded by XRD studies. Beside this, PF68-Mt-PPN composites follow the degradation pattern for both PF68 and PPN in the temperature range of 200-400 °C.

In case of pure Mt, pristine Mt-PPN composites, organoclay PF68 -Mt and PF68-Mt-PPN composites 82 %, 82 %, 80 % and 78 % residue was obtained in the temperature range of 20-700 °C, respectively, or otherwise it could be said that 18 %, 18 %, 20 % and 22 % weight loss was observed respectively. In case of PPN-Mt composites, replacement with PPN reduces the intercalated water content within Mt layers. Improved thermal stability of intercalated drug was also observed than the pure drug, followed by the same thermal behaviour as of pristine Mt.

Scanning Electron Micrographic studies

The surface morphology of pristine Mt particles (Figure 23a) was in platelet form and displayed many flakes on the surface. The pristine Mt-PPN composites had irregular shapes as shown in Figure 23b.
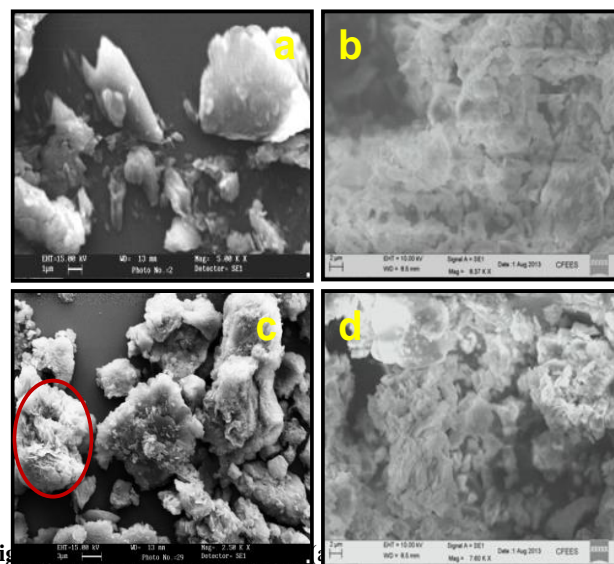
Figure ....-PPN composites (c) and PF68-Mt-PPN composites (d)

It has been found that the Mt-PPN composites had a different surface morphology when compared with that of pristine Mt alone as found to be more porous on surface leading to more open structure (encircled by red). Surface morphology of PF68-Mt-PPN composites were found to be irregular shaped particles with particle size in the range of 1-2 microns (Figure 22c). However no significant change in

the surface morphology as compared to organoclay PF68-Mt (Figure 22d) was observed.

Transmission electron micrographic studies

TEM images of pristine Mt clearly reveal the layered platelet structure of Mt with particle size in the range of 1.5 to 2μm (Figure 24a and b). TEM images of Mt-PPN composites are shown by (Figure 24 c and d). As a result of sonication required for sample preparation for TEM analysis, secretion of intercalated spherical drug particles of size 50-100 nm from Mt layers can be seen clearly (Figure 24c) further confirmed by the presence of PPN peakin UV spectra of sonicated sample of pristine Mt-PPN composites (Figure 24e).
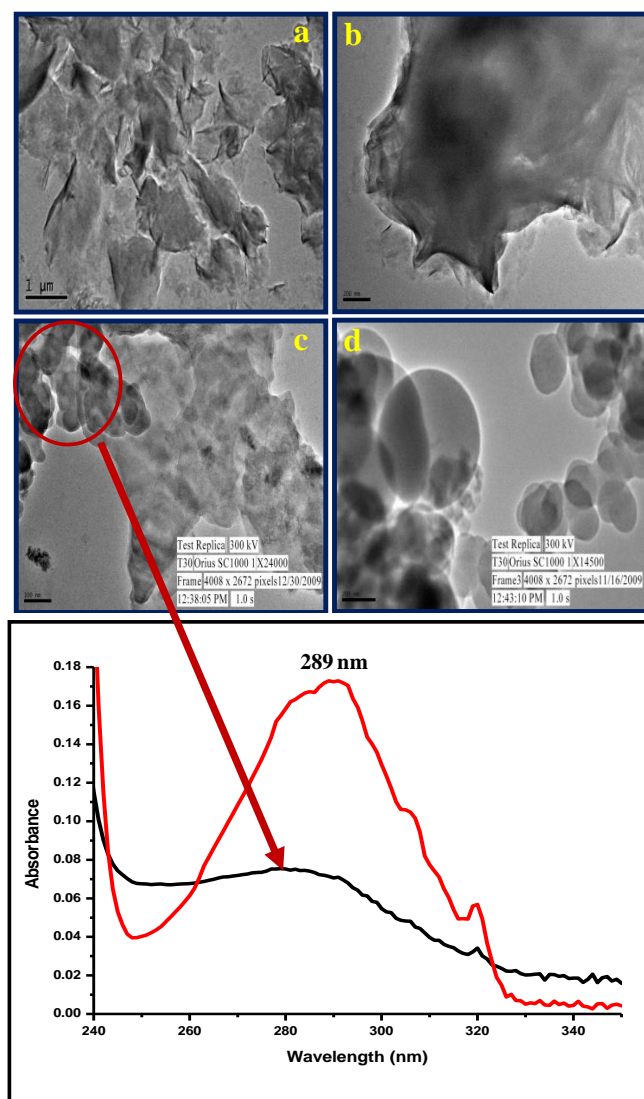

Figure 24. TEM images of pristine Mt (a and b) and Mt-PPN composites (c and d), UV spectra of aqueous PPN solution and sonicated Mt-PPN composites **e.**

In vitro drug release studies

In vitro release of pure PPN in simulated gastric (HCl, pH 1.2) and intestinal fluid (PBS, pH 7.4) at 37 °C was observed to be 84 % and 87 % (Figure 24) over a period of 4 h, respectively, approaches to 87 % and 90 % by the end of

8 h. In both the cases release pattern was not in a controlled manner (~ 36 % release per minute).[12]

When the pristine Mt-PPN composites exposed to the dissolution medium, the simultaneous penetration of the surrounding medium and cation exchange process occurred leading to a burst drug release of 40 % in simulated gastric fluid (SGF), and 23 % in simulated intestinal fluid (SIF) to initial first hour corresponds to adsorbed drug on the surface of the particles. Then the cation diffuses deep into the particles to exchange the drug, which leads to slow release of 57 % and 39 % by the end of 4 hours approaches to 75 % and 46 % by the end of 8 hours in SGF and SIF respectively (Figure 25). This study showed that release of PPN from the composites is controlled by a particle matrix that acts as diffusion barrier for drug release.[25] The difference in pH, presence of cations and higher solubility of PPN may be responsible for higher release of drug in acidic media. The percentage released of PPN was not up to 100 % probably due to the characteristic of ion-exchange reaction, i.e. this is an equilibrium process, and the interlayer cations cannot be exchanged completely.[46,47]
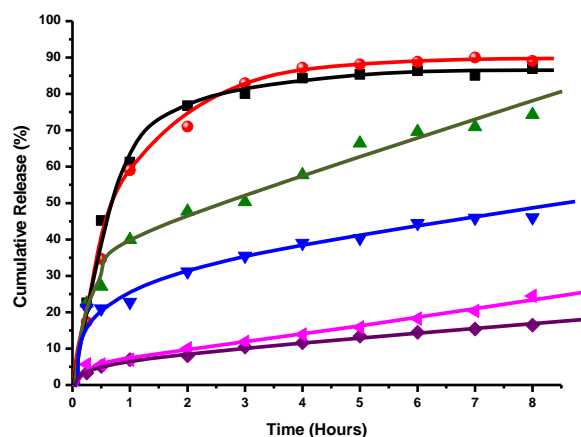
Figure 25. In vitro drug release profile in SGF (pH 1.2): pure PPN, Mt-PPN complex, PF68-Mt-PPN composites. In SIF (pH 7.4): pure PPN, Mt-PPN complex, PF68Mt-PPN composites

In case of PF68-Mt-PPN composites, initial burst release was substantially controlled by the presence of PF68 in both the dissolution media as only 7 % drug release was observed within first hour which approaches to 13 % and 11 % by the end of 4 h. The cumulative drug release of 16.4 % and 24.5 % over a period of 8 hours in SGF and SIF was obtained respectively which approaches to 20.9 % and 38.96 % by the end of 24 h (data not shown). In the present case it has been proposed that, triblock copolymer PF68 was intercalated within Mt layers in the form of micelles. So, the diffusion process is suggested to be responsible for the drug release from organoclay PF68-Mt. As a result of the interaction of PPN with hydrophilic parts of PF68 (PF 68 corona) the hydrophilic-hydrophilic interaction may prevents the release of drug in the dissolution media. However less release in SGF (HCl pH 1.2) is might be corresponds to the stability of Mt layers within the acidic media. Whereas, in case of pristine Mt, simply ion exchange process was the main driving force for release of drug in the dissolution media resulting in comparatively faster drug release process.

In vitro drug release data suggest that organoclay PF68-Mt-PPN composites are able to retain the high amount of PPN in simulated gastric fluid (the desired site of absorption), as compared to pristine Mt-PPN composites, with the advantage of gradual drug release over a longer period of time, thus able to increase the absorption, improve drug efficacy, and decrease dose requirements.

CONCLUSION

In the present work Pluronic F68 a non-ionic triblock copolymer has been reported for the first time for synthesis of organoclay PF68-Mt organoclay. The intercalation of PF68 moiety was confirmed by XRD, FT-IR, zeta potential and thermal studies.

The feasibility study of developed PF68-Mt organoclay is further being explored as a drug delivery vehicle for propranolol HCl, an antihypertension drug.

The developed PF68-Mt-PPN composites were compared for their physiochemical proerties and in vitro drug release behaviour with pristine Mt-PPN composites.

In case of pristine Mt-PPN composites developed by ion exchange/adsorption method, 127 mg g^{-1} of PPN was found to adsorb on the Mt surface. Intercalation of PPN was confirmed by XRD, FTIR, zeta potential and thermal studies. In vitro drug release profile of pristine Mt-PPN composites shows PPN release in simulated intestinal fluid was more sustained as compared to simulated gastric fluid over a period of 8 h governs by ion exchange process.

Organoclay PF68-Mt reveals enhanced negative surface charge with high adsorption capacity as compared to pristine Mt as adsorption capacity increase upto 171 mg g^{-1}. XRD studies suggested that organoclay PF68-Mt possesses highest d spacing followed by PF68-Mt-PPN composites, Mt-PPN composites and pristine Mt and confirms the intercalation of PPN within organoclay PF68 layers.

In vitro drug release profile of PF68-Mt-PPN composites suggest that, presence of intercalated PF68 in the composites significantly retarded the release of PPN in simulated gastric and intestinal fluid as compared to pristine Mt. The sustained release pattern of PPN might be attributed to the interaction of PPN with hydrophilic parts of PF68 intercalated within Mt layers.

Thus the developed PF68-Mt-PPN composites have promising potential to sustain the release of PPN than pristine Mt, able to reduce the dosing frequency and associated side effects. The obtained preliminary results suggest that synergism of FDA approved biocompatible Mt and Pluronic F68 can be further explored as a successful formulation of PPN as oral and sustained release drug delivery vehicle.

ACKNOWLEDGMENT

REFERENCES

[1]Borkar, S. R., Sawant, S. N., Shende, V. A., Dimble, S. K., *Int. J. Pharm. Sci. Nanotech.,* **2010,** *3,* 901–905.

[2]Rodrigues, L. A. S., Figueiras, A., Veiga, F., de Freitas, R. M., Nunes, L. C. C., da Silva Filho, E. C., da Silva Leite, C. M.,*Coll. Surf. B: Biointerfaces,* **2013,** *103,* 642– 651.

[3]de Paiva, L. B., Morales, A. R., Valenzuela Diaz, F. R., *Appl. Clay Sci.,* **2008,** *42,* 8–24.

[4]Gournis, D., Jankovicic, L., Maccallini, E., Benne, D., Rudolf, P., Colomer, J., Sooambar, C., Georgakilas, V., Prato, M., Fanti, M., Zerbetto, F., Sarova, G. H., Guldi, D. M. *J. Am. Chem. Soc.* **2006,** *128,* 6154–6163.

[5]Gournis, D., Georgakilas, V., Karakassides, M. A., Bakas, T., Kordatos, K., Prato, M., Fanti, M., Zerbetto, F., *J. Am. Chem. Soc.,* **2004,** *126,* 8561–8568.

[6]Guegan, R., Gautier, M., Beny, J. M., Muller, F., *Clays Clay Miner.,* **2009,** *57,* 502–509.

[7]Gautier, M., Muller, F., Leforestier, L., Beny, J. M., Guegan, R. *Appl. Clay Sci.,* **2010,** *49(3),* 247–254.

[8]Chua, Y. C., Lu, X., *Langmuir,* **2007,** *23,* 1701-1710.

[9]Othmani-Assmann, H., Benna-Zayani, M., Geiger, S., Fraisse, B., Kbir-Ariguib, N., Trabelsi Ayadi, M., Ghermani, N. E., Grossiord, J. L., *J. Phys. Chem., C,* **2007** *111,* 10869–10877.

[10]Lee, S. Y., Cho, W. J., Hahn, P. S., Lee, M., Lee, Y. B., Kim, K. J., *Appl. Clay Sci.,* **2005,** *30,* 174–180.

[11]Dong Y., Feng S. S. *Biomaterials,* **2005,** *26,* 6068–6076.

[12]Seema, Datta M., *Appl. Clay Sci.*, **2013,** *80–81,*85–92.

[13]Seema, Datta M., *Int. J. Pharm. Pharm. Sci.,* **2013,** *5(2),* 332–341.

[14]Seema, Datta M., *Eur. Chem. Bull.,* **2013***, 2(11),* 942–951.

[15]Kaur M., Datta M., *Adsorpt. Sci. Technol.,* **2011,** *29(3),* 309–318.

[16]Gelfer, M., Burger, C., Fadeev, A., Sics, I., Chu, B., Hsiao, B. S., Heintz, A., Kojo, K., Hsu, S., Si, M., Rafailovich, M., *Langmuir* **2004,** *20,* 3746–3758.

[17]Guegan, R., *Langmuir,* **2010,** *26(24),* 19175–19180.

[18]Guegan, R., Gautier, M., Beny, J. M., Muller, F., *Clays Clay Miner.,* **2009,** 57(4), 502–509, 2009.

[19]Batrakova, E. V., Kabanov, A. V., *J. Controll. Release,* **2008,** *130,*98–106.

[20]Batrakova, E. V., Alakhov V. Yu., *J. Controll. Release,* **2002,** *82* 189–212.

[21]Alexandridis, P., Hatton, T. A., *Colloids Surfaces A: Physicochem. Eng. Aspects,* **1995***, 96,* 1–46.

[22]Schmolka, I. R., *J. Am. Oil Chem. Soc.,* **1977,** *54,* 110–116.

[23]Dollery, S. C., *Therapeutic Drugs.* Churchill Livingstone, Edinburgh **1991**. 272–278.

[24]Chaturvedi, K., Umadevi, S., Vaghani, S., *Sci. Pharm.,* **2010,** *78,* 927–939.

[25]Rojtanatanya, S., Pongjanyakul, T., *Int. J. Pharm.,* **2010,** *383(1-2),* 106–115.

[26]Patra, C.N., Kumar, A. B., Pandit, H. K., Singh, S. K., Devi, M. V.,*Acta Pharm.,* **2007,** *57,* 479–489.

[27]Paker-Leggs, S., Neau, S. H., *Int. J. Pharm.,* **2009,** *369,* 96–104.

[28]Nagarwal R. C., Singh P. N., Shri Kant, Maiti P., Pandit J. K. *Chem. Pharm. Bull.,* **2011,** *59 (2),* 272-278.

[29]Joshi, G. V., Kevadiya, B. D., Patel, H. A., Bajaj, H. C., Jasra R.V., *Int. J. Pharm.*, **2009**, *374*, 53–57.

[30]Joshi, G.V., Kevadiya, B.D., Bajaj, H.C., *Micropor. Mesopor. Mater.,* **2010,** *132*, 526–530.

[31]Park, J. K., Choy, Y. B. Oh, J. M., Kim, J. Y., Hwang, S. J., Choy, J. H., *Int. J. Pharm.,* **2008**, *359*,198–204.

[32]Joshi, G. V., Patel, H. A., Kevadiya, B. D., Bajaj, H. C., *Appl. Clay Sci.* **2009,** *45*, 248–253.

[33]Chen B.Y., Lee Y. H., Lin W. C., Lin F. H., Lin K. F., *Biomed. Eng. Appl. Basis Comm*un., **2006,** *18(1),* 30–36.

[34]Meng, N., Zhou, N. L., Zhang, S. Q., Shen, J., *Int. J. Pharm.,* **2009**, *382*, 45–49.

[35]Sahu, A., Kasoju, N., Goswami P., Utpal Bora, *J. Biomater. Appl.* DOI: 10.1177/0885328209357110.

[36]Guegan, R, *Langmuir* **2010**, *26(24),* 19175–19180.

[37]Zhao, D., Huo, Q., Feng, J., Chmelka, B. F., Stucky, G. D., *J. Am. Chem. Soc.,* **1998**, *120 (24),* 6024-6036.

[39]Chen, Y., Zhou, A., Liu, B., Liang, J., *Appl. Clay Sci.* **2010**, *49(3)*, 108–112.

[40]Passerini, N., Albertini, B., Gonzalez-Rodrıguez M. L., Cavallari, C., Rodriguez, L., *Eur. J. Pharm. Sci*. **2002,** *15,* 71–78

[41]http:// Propranolol Information from Drugs.com.htm.

[42]Patra, C. N., Kumar, A. B., Pandit, H. K., Singh, S. K., Devi, M. V., *Acta Pharm.,* **2007,** *57*, 479–489.

[43]Sharan, G., Dey, B. K., Nagarajan, K., Das, S., Kumar, S. V., Dinesh, V., *Int. J. Pharm. Pharm. Sci.,* **2010,** *2(2),* 21–31.

[44]Macedo, R. O., Nascimento T. Gomes Do., Veras, J. W. E., *J. Therm. Anal. Calor.*, **2002**, *67,* 483–489.

[45]Wang, T., Wu, Y., Zeng, A. J., *Appl. Polym. Sci.,* **2009,** 605–613.

[46]Joshi, G. V., Kevadiya, B. D., Patel, H. A., Bajaj, H. C., Jasra, R. V., *Int. J. Pharm.,* **2009,** 53–57.

[47]Nunes, C. D., Vaz, P. D., Fernandes, A. C., Ferreira, P., Roma, C. C., Calhorda, M. J. *Eur. J. Pharm. Biopharm.,* **2007.** *66*, 357–365.

[38]Lakshmi, M. S., Sriranjani, M., Bakrudeen, H. B., Kannan, A. S., Mandal, A. B., Reddy, B. S.R., *Appl. Clay Sci.,* **2010**, *48*, 589–592.

EFFECTS OF GROWING FACTORS ON THE FORMATION OF BIOACTIVE COMPOUNDS IN CELERY (*APIUM GRAVEOLENS* L. CONVAR. *RAPACEUM*)

Mária Takács-Hájos [a]* and Mária Borbély-Varga [b]

Keywords: celery, bioactive compounds, leaves, tuber, polyphenols, flavonoids, vitamin C, growing method, row direction

The polyphenolic compounds of several plant products are not known, nor are the biotic and abiotic factors that influence their evaluation. Thus we have very few data about the effects of growing factors in case of root vegetables – for example soil type, light intensity, growing method (on open field, under glass, in soil or without soil cultivation). Our experiment were aimed to prove the effects of genotypes and growing method (direction of rows) on the enrichment of polyphenol, flavonoid and vitamin C content. In the experiments it was established that varieties reacted differently on to the incidence of light originated from the direction of rows. Polyphenol, flavonoid and dry material content of *Prágai óriás* were higher at North-South row directions, which originated from the favourable light luminous influence without fail. Variety *Neon* produced better results in nutritional values of leaves at South West row directions. The opposite was found for the polyphenol, flavonoid and dry matter contents of tubers. In this direction the sunshine from South warmed up the bed in which the tubers were developing. This factor was favourable for their production. The results of our experiments showed differences between the genotypes regarding their sensitivity, that is, the intensity of light that differed in the rows of different direction influenced the formation of secondary metabolites. Results proved that celery leaves contain more bioactive compounds (total polyphenols, flavonoids, vitamin C) than tubers. The difference in polyphenol content was threefold and six fold in flavonoid content. Vitamin C content in the tubers was 30 percent of the amount that was measured in leaves at very similar dry material content. Our data document the nutritional importance of celery leaves and emphasize the selection of the growing method to the needs of varieties to produce good quality vegetables for our foods.

Corresponding author
  E-mail: hajos@agr.unideb.hu
[a] University of Debrecen, Centre of Agricultural Science and Engineering, Faculty of Agriculture, Institute of Horticulture, 138 Böszörményi Str., Debrecen, H-4032, Hungary.
[b] University of Debrecen, Centre of Agricultural Science and Engineering, Faculty of Agriculture, Central Laboratory, 138 Böszörményi Str., Debrecen, H-4032, Hungary

Introduction

Researchers deal with evaluation of oxidative stress. Data support the fact that optimal quantity of vegetable, fruits and red vine in the diet has real effect on the human health, possibly due to the effect of polyphenols.[1] They are the most abundant antioxidants in the diet. If the total intake is as high as 1 g day^{-1}, they would be 10 times more efficient than vitamin C and 100 times more than carotenoids and vitamin E.[2,3,4] Several bioactive compounds have polyphenol structure. They are mainly products of secondary metabolites of plants which can protect against ultraviolet radiation and pathogenic attacks. Polyphenols contain several aromatic rings and hydroxyl groups. Distinctions are made between the following groups – phenolic acids, flavonoids, stilbens and lignin.[3]

Papers usually communicate mainly the total polyphenol content and very rarely the different components. Regarding the polyphenol content of apple, researchers have found values between 0.1 to 5 g per kg fresh fruits nearly in every variety. Only few varieties with higher acid content showed higher total polyphenol content (10 g kg^{-1}).[5,6]

Higher polyphenol content can be found in cabbage, celery, onion and parsley.[7,8] The highest polyphenol content [>250 mg gallic acid equivalent (GAE)/100g fresh product] was measured in artichokes, parsley and brussels sprouts, while the lowest in melon (*cv. Cantaloupe*). In the celery this content was 84.7 mg GAE in 100 g fresh product.[9]

Widely known is the fact that the synthesis of polyphenols is influenced by light intensity and the ripenness of the product.[10]

The amount and composition of total polyphenols are determined by the plant species, the variety (genotype), the soil composition, the growing conditions, ripening and the post harvest conditions.[11]

Stress conditions during the vegetation period, like temperature alterations, UV exposure and different pathogen attacks, can highly influence the synthesis of secondary assimilation products.[12]

It is very difficult to determine the reaction of plant family to environmental and growing factors. We have to pay attention to preparing the product for processing, because the deep peeling causes an increase in the loss of bioactive materials as these components are immediately under the skin of the product. Deep peeling can decrease the polyphenol content of the processed product.

Cooking has also negative effects on the polyphenol content. Researchers stated that the quercetin loss can be as high as 75-80 % in the onion and tomato, after 15 min cooking.[13]

As these compounds have great importance in prevention, the presence of polyphenols and flavonoids would be desirable beside that of vitamins, minerals and fibre content on the products. To resolve this problem we would like to present some data of our experiments about important root vegetables such as celery, because its leaf and tuber are equally important products in food the industry and in cooking too.

The enrichment of this component is influenced by the growing method, the direction of rows, since the length of sunny periods can influence the synthesis of bioactive molecules.

The data provides information on growing methods, as well as on choices of variety, and can also support the favourable dietary effects of celery leaves.

Experimental

Experiments were performed in the experiment garden of the Debrecen University. Raised beds were formed; the soil type was calcareous chernozem. In the two factorial experiments (growing method and varieties) random plot arrangement was used in four repetitions. Varieties *Prágai óriás* and *Neon* were sowed in North-South (N-S) and East–West (E-W) row directions on a plot of 2 m x 1 m size.

Beds were 15 cm high with four rows. Cultivation method – soil loosening, nutrient supply, mechanical and chemical weed control and plant protection – were selected for the varieties. Drip irrigation was used for the uniform water supply. Harvest was done on 8th October. Measurements were performed on 10-10 plants, and samples were prepared for the chemical analysis.

Total polyphenols in mg GAE/100 g fresh product were determined by Folin Ciocalteu colorimetric method, results were given in gallic acid equivalent value. Flavonoid content was determined using colorimetric method,[14] results were given in catechin equivalent value. Vitamin C content was determined by redox titration using iodine solution. Dry material content was measured by drying in oven at 105 °C.

Results and discussion

The light luminous influences of leaves were determined by the direction of rows. In our experiment in the tween-row production as a result of wide row spacing the sunlight reached the loft from side direction too. In case of N-S rows the loft could get light from west and east, too. When the raw direction was E-W, the light was less from the North, while too much from the South. In our experiment these effects on the formation of bioactive compounds in the leaves and the tubers were analysed.

### The formation of bioactive compounds in leaves

By examining the reaction of species to the row direction, we can get information about the demand of genotypes to form the best quality that is to accumulate the bioactive components in great amount.

Data are shown in Figure 1. We can establish that N-S row direction was favourable for the accumulation of polyphenols and flavonoids in case of *Pallagi óriás.*
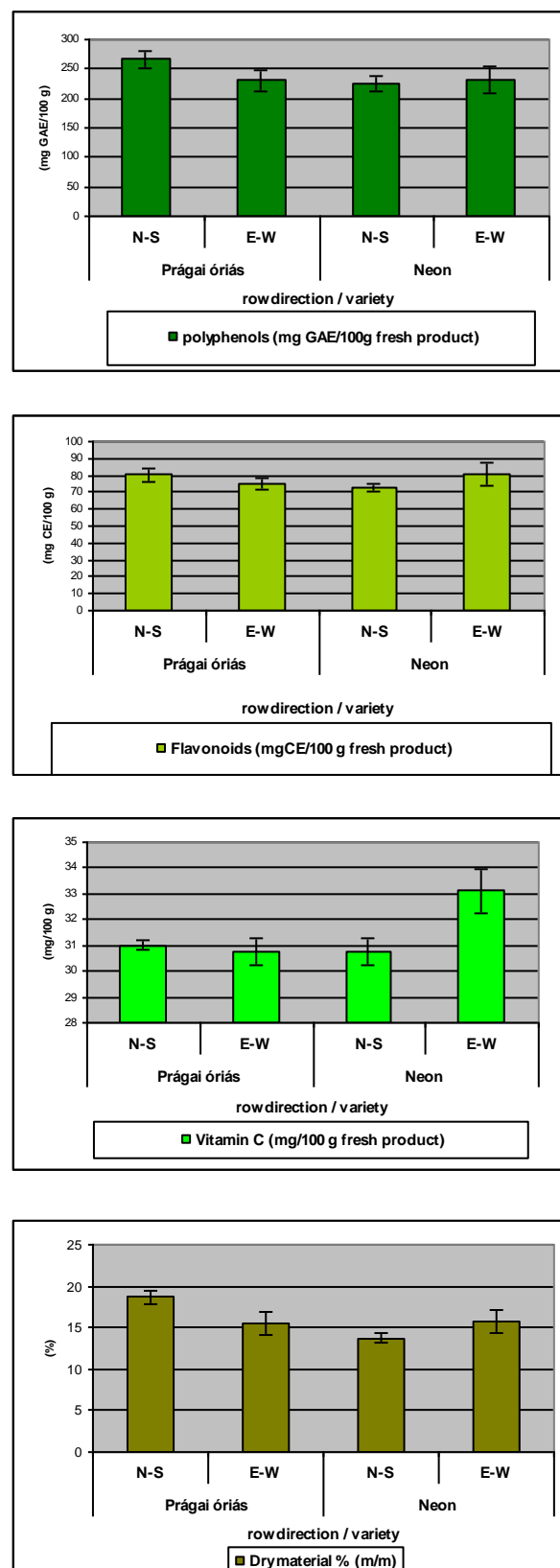
Figure 1. Bioactive compounds of celery loft with different row direction, Debrecen, 2013.

On the other hand, best results were found at E-W row direction in variety *Nero* for flavonoids, but there was no significant difference in the amount of total phenolic compounds.
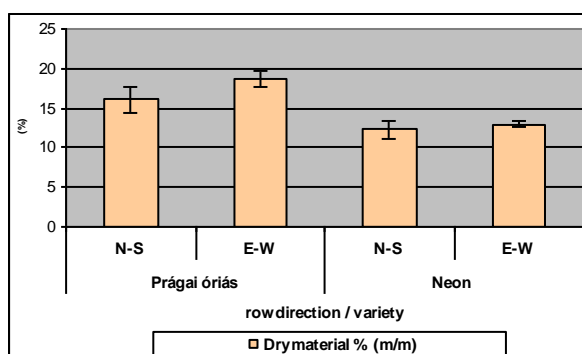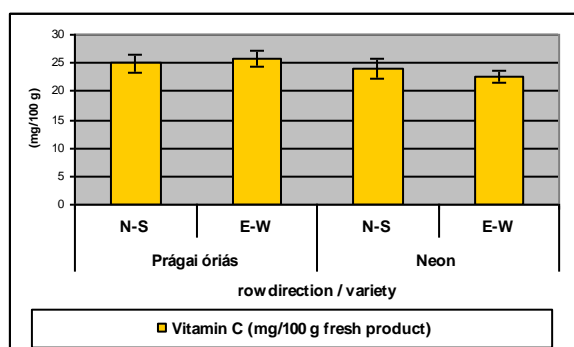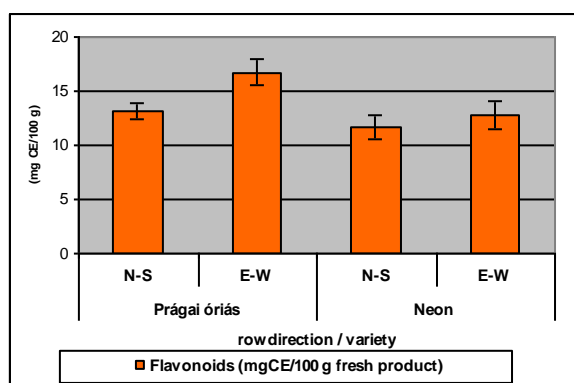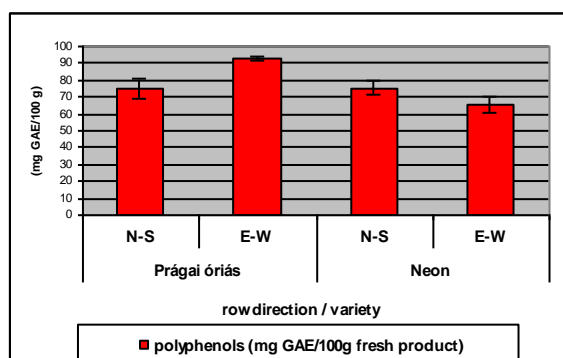
As regards to vitamin C, very high amount was found in *Nero* at E-W row direction, but the vitamin content was similar in both varieties at N-S row direction (30 mg in 100 g). Dry material content was higher in *Pallagi óriás* at N-W direction, while E-W proved to be favourable for *Nero*.

Formation of bioactive compounds in the tubers

As opposed to the loft, the S-W row directions resulted in the formation of most bioactive compounds in case of *Pallagi óriás* (Figure 2). The opposite effect was detected in variety *Neon* in the formation of flavonoids. In N-E rows more total phenolic compounds were measured than in South-East rows. Regarding flavonoid formation there was no significant difference, nor in vitamin C content.

The same tendency was found in dry material formation, the S-W direction was favourable for *Pallagi óriás*, but there was no difference in the variety *Neon*. Comparing the leafage and tubers we can say that the green parts of the plants are more abundant in bioactive compounds (Figure 3)
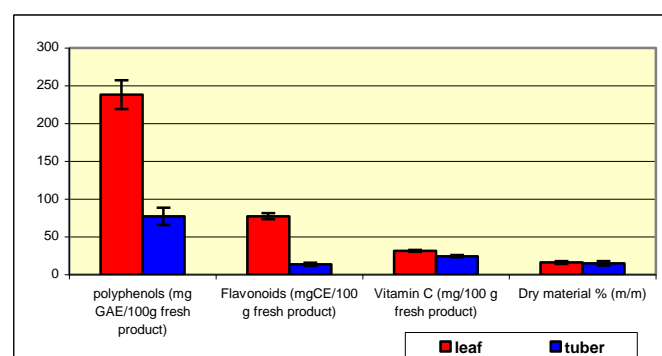
Figure 3. Comparison of nutritional values of leafage and tubers as a function of treatments and varieties, Debrecen, 2013.

Threefold difference was detected for polyphenols while the ratio was 7-8 times more for flavonoids. The leaf is more abundant in vitamin C than tubers (31.40 and 24.31 mg in 100 g), while the dry material contents were fairly similar. On the basis of data it can be established that celery leafage is very rich in bioactive compounds. This makes it important to keep in mind the state of health of celery so that it would be useable at the time of harvesting in autumn.Differences in leafage features as a function of treatment and varieties are presented in Figure 4.

Figure 2. Bioactive compounds of celery tubers at different row directions, Debrecen, 2013.
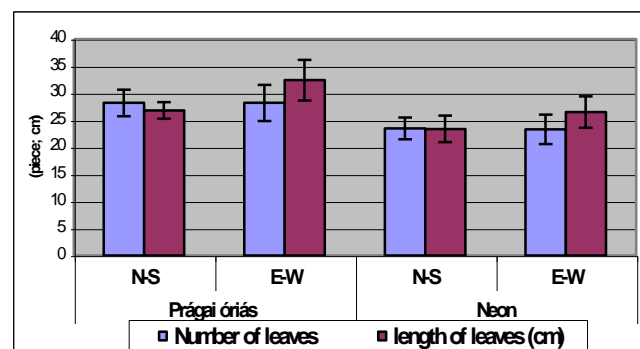
Figure 4. Leafage features at difference row directions, Debrecen, 2013.

Conclusion

It was found that variety *Prágai óriás* has more leaves and long stems than *Neon*. Leaves were longer in S-W row directions than at N-S. The differences were proved statistically.

References

[1]Arts, I. C. W., Hollman, C. H., *Am. J. Clin. Nutr.*, **2005**, *81*, 317–325.

[2]Scalbert, A., Williamson, G., *J. Nutr.,* **2000**, *130*, 2073S–85S.

[3]Manach, C., Scalbert, A., Morand, C., Rémésy, C., Jimenez, L., *Am. J. Clin. Nutr.,* **2004**, *79(5)*, 727–747.

[4]Scalbert, A., Johnston, I. T., Saltmarsh, M., *Am. J. Clin. Nutr.,* **2005**, *81*, 215–217.

[5]Guyot, S., Marnet, N., Laraba, D., Sanoner, P., Drilleau, J. F., *J. Agric. Food Chem.*, **1998**, *46*, 1698–705.

[6]Sanoner, P., Guyot, S., Marnet, N., Molle, D., Drilleau, J. F., *J. Agric. Food Chem.*, **1999**, *47*, 4847–4853.

[7]Bravo, L., *Nutr. Rev.,* **1998**, *56*, 317-333.

[8]Crozier, A., Burns, J., Aziz, A., Stewart, A., Rabiasz, H., Jenkins, G., Edwards, C., Lean, M., *Biol. Res.*, **2000**, *33*, 79-88.

[9]Brat, P., George, S., Bellamy, A., Du Chaffaut, L., Scalbert, A., Mennen, L., Arnault, N., Amiot, M. J., *J. Nutr.,*. **2006**, 2367-2373.

[10]Macheix, J. J., Fleuriet, A., Billot, J., Fruit Phenolics, *CRC Press*, **1990**, Boca Raton, 392.

[11]Jaffery, E. H., Brown, A. F., Kurilich, A. C., Keek, A. S., Matusheski, N., Klein, B. P., *J. Food Comp. Anal.*, **2003**, *16*, 323–330.

[12]Dixon, R. A., Paiva, N. L., *Plant Cell*, **1995**, *7*, 1085–1097.

[13]Crozier, A., Lean, M. E. J., McDonald, M. S., Black, C., *J. Agric. Food Chem.*, **1997**, *45*, 590–595.

[14] Lamaison, J. L., Carnat, A., *Pharm. Acta Helv.*, **1990**, *65,* 11, 315–320.

ANTIFUNGAL ACTIVITY OF AQUEOUS LEAF EXTRACT OF *OCIMUM SANCTUM* ON DOMINANT FUNGAL SPECIES OF MONUMENTS

S. P. Gupta[a]*, K. S. Rana[b], K. Sharma,[c] and B. S. Chhabra[d]

Four common species of fungi isolated *A. niger, Rizopous, Cladpsporium and Curvularia lunata* from archaeological site were subjected to laboratory experiment involving in vitro control of the fungal species using plant extracts. Aqueous leaves extract at 10 %, 20 %, 30 % and 40 % with the control (basal medium) concentrations tested on potato dextrose agar (PDA) for activity against mycelium growth were determined at 26 ± 1 ^{0}C with three replicated plates. Fungal growth values recorded were generally low compared with the control (without extract petri plate). Inhibitory action of the extract on fungal growth increased with increases in concentration of extract. A study was carried out to evaluate the antifungal properties of *Ocimum Sanctum Linn*. Aqueous extract on common fungal species, isolated from Bhand Deol temple at Arang of Chhattisgarh state using the well in PDA media. The in vitro studies have been performed by using leaf aqueous extract of *Ocimum Sanctum Linn*. (Tulsi plant). Extract showed antifungal activity. Different concentration viz. 10 %, 20 %, 30 % and 40 % of solution prepared for the study. It was found that the plant extract at 40 % concentration were effective in reducing the mycelial growth of *A. niger, Rizopous, Cladpsporium sp*. whereas 30 % of plant extract effective for *Curvularia lunata*. Concentrations of extract which inhibit 75 % and above having known as effective in this study. Plant extracts readily available and affordable and environmentally friendly in the control of fungal disease.

*Corresponding Authors
        E-Mail: guptasanjayprasad@gmail.com
[a & b]   Archaeological Survey of India, Dehradun
        (Uttrakhand), India
[c]   Govt. Arts & Commerce Girls College, Raipur
        (Chhattisgarh), India
[d]   Govt. College, Abhanpur, Raipur (Chhattisgarh),
        India

INTRODUCTION

The application of synthetic chemical on the monuments as a biocides are toxic and hazardous to the environment and to public health other than the stone itself. The biocide application can be harmful for conservators and the environment[1] and little is known about the consequences of repeated applications.[2] **The EC regulations (BPD 98/8/EC n 20 June 2004)** have had as consequence the elimination from the market of the most active (and toxic) compounds applied to this aim and new approaches are made in several sectors in order to overcome this problematic.

Alternative new approach based on natural antifouling substances, are recently experimented in the marine sector for the prevention of bio settlement on ships submerged structures. Natural sources or synthetic analogues must be found to ensure supplying at a reasonable cost.[3] Medicinal plants have been used for different ailments of human beings all over the world just from the beginning of civilization. Indian traditional medicinal system includes hundreds of medicinal plants related to multiple effects.[4] Throughout the old world and especially in the tropics *Ocimum sanctum* otherwise known as Tulsi or Holy Basil is cultivated abundantly for religious and medicinal purposes. It is commonly used in Ayurveda and across the wide region of south-east Asia is widely known as a medicinal plant as well as an herbal tea.[5] Exploitation of plant metabolites in monuments protection and preservation against bio-

deterioration of stone caused by fungi appear to be promising. In view of these, the authors screened some extracts one of them Tulsi (*Ocimum Sanctum Linn*.) against bio-deterioration causes by fungal species isolated and identified from the sample of Bhand Deol temple at Arang of Chhattisgarh.

MATERIALS AND METHODS

Sampling and isolation of fungi

Sample of monument was collected from Bhand Deol temple, Arang of Chhattisgarh for isolation and identification of fungal species. During the investigation period PDA media was used for the isolation of microorganisms. Sample was collected from the surface of the monument. Few drops of sample pour in the petridish and kept this petridish at 28 ± 1 ^{0}C for 7 days for incubation.[6] At the end of incubation period fungal colonies were counted, isolated and identified with the help of available literature and finally send this culture to authentic authority: National Center of Fungal Taxonomy Delhi for identification.

Preparation of plant leaf powder

The fully grown leaf of *Ocimum Tenuiflorum* (also known as *Ocimum sanctum*) was collected from campus of various temples at Bhilai (Chhattisgarh). The collected plant material thoroughly washed with tap water and then rinsed with sterile distilled water. The leaf of Tulsi was shed dried and grind in electric mixer. The powder material was kept in air tight glass bottles. This stock powder was used for further extraction.

Preparation of aqueous leaf extract

5.00±0.05 g of dried and ground leaves powder of Tulsi was placed in a thimble of soxlate apparatus. Sample was extracted in a Soxhlet extraction system using 150 ml of distilled water. The heating power was set to two cycles/h so that six cycles of extraction were achieved within 3 h. Distilled water used in this extraction process. The crude extract solutions obtained was then concentrated using a water bath at very low temperature to remove the solvent and completely dried in an atmospheric oven. High temperature treatment was avoided to minimize the component degradation[7]. Extract was then stored at room temperature before weighing gravimetrically to determine the yields after that prepared various dilution viz 10 %, 20 %, 30 %, 40 % and 50 % concentrations of extracts for inhibition of growth of fungal species. Control treatment was done without any plant extract in petriplate.

Percentage inhibition of fungi growth by the leaf extracts was calculated using the formula.[8]

$$FG = 100\frac{D_c - D_r}{D_c}$$

where:

FG = inhibition of fungi growth in %

D_c = diameter of control (mm)

D_r = diameter of test (mm)

Well in agar method

A loopful of the inoculums suspension of pure 04 cultured identified fungal organism were spread uniformly on the solidified sterile culture media (PDA) in the petriplate for uniform distribution of the organism. Using a sterile cork borer a well of 0.5 cm was made in the media and in each well, plant extract was filled so as to allow the diffusion of plant extract in the media. The petriplate were incubated at for 24 hours at 30±1°C temperature and the observations were recorded as diameter of inhibitory zone in mm. Well in agar plate filled with sterile distilled water was used as control in all the experiments[9]. All the experiments were in triplicate and mean has been considered in observation Table 1.

Table 1. Effect of *Ocimum tenuiflorum* aqueous extract on fungi growth (in %)

Fungal species↓	Concentration of extract				
	10 %	20%	30%	40%	50%
A. niger,	10	27	67	75	88
Rizopous,	16	27	70	82	90
Cladpsporium	17	28	71	77	87
Curvularia Lunata	19	31	77	88	91

RESULT AND DISCUSSION

At a concentration of 40 %, the leaf aqueous extract of Tulsi recorded effective for *A. niger, Rizopous* and *Cladpsporium* and their percentage of inhibition are 75 %, 82 % and 77 % for that concentration respectively while concentration of 30% leaf aqueous extract is effective for *Curvularia Lunata.* The minimum inhibition by leaf extract was recorded 10 % of *A. niger* sp. by 10 % of extract while 19 % of inhibition recorded for *Curvularia Lunata* by same concentration of the extract. Percentage of inhibition increases with the concentration of plant extract. Among the extracts assayed, the leaf aqueous extract of Tulsi having antifungal properties was observed. Results showed that radial growth in all the test organisms was impaired by the addition of the extracts in the culture medium used. The test organisms differed in their reaction to the different extracts but on the whole growth inhibition increased with the concentration of plant extract. The antifungal activity of the plant for the organisms was found is in increasing order with the concentration of extract.

This study showed that the leaf aqueous extract of *Ocimum Sanctum Linn.*(Tulsi) has fungicidal activity. Few previous studies have comprehensively investigated the activity of medicinal plant leaves, bark and other parts of plant against dermatophytes and other filamentous fungi.[10]

Many researchers already reported that, plant metabolites and plant based pesticides or biocides appear to be one of the better alternatives as they are known to have minimal environmental impact and eco-friendly to conservators/scientist involved in this fields as well as stone components in contrast to synthetic chemicals used as pesticides/biocides.[11-13] Studies on antifungal activity of different extracts of Cassia fistula and bioactivity guided isolation and identification of antifungal agent has been performed by Shilpakala et al.[14] Thus, there is a need to search for alternative eco-friendly approaches for conservation and preservation for our heritage.

ACKNOWLEDGMENT

REFERENCES

[1]Price, C. A., In: *Stone conservation: an overview of current research*, Keys, A. (ed). The Getty Conservation Institute, **1996.**

[2]Fortune, I. S., Alakomi, H. L., Young, M. E., Gorbushina, A. A., Krumbein, W. E., Maxwell, I., McCullagh, C., Robertson, P., Saarela, M., Valero, J. and Vendrell, M., *Assessing the suitability of novel biocides for use on historic surfaces in Heritage Microbiology and Science – Microbes, monuments and maritime materials*, Springer Verlag, Great Britain, **2008.**

[3]Yebra, D. M., Kiil, S. and Dam-Johansen, K., *Progr. Org. Coat.*, **2003,** *50*, 75-104.

[4]Rahal, A., Singh, V., Mehra, D., Rajesh, S., and Ahmad, A. H., *J. Nat. Prod.,* **2009,** *2,* 110-115.

[5]Kumar, A., Rahal, A., Chakraborty, S., Tiwari, R., Latheef S. K. and Dhama, K., *Int. J. Agron. Plant Product.,* **2013,** *4(7),* 1580-1589.

[6]Sharma, K. and Lanjewar, S., *J. Phytol.,* **2010,** *2(11)*, 47-49.

[7]Kumoro, A. C., Hasan, M. and Singh, H., *Sci. Asia,* **2009,** *35*, 306–309.

[8]Mondall, N. K., Mojumdar, A., Chatterje, S. K., Banerjee, A., Datta, J. K., and Gupta, S., *J. Appl. Sci. Environ. Manage,* **2009,** *13(1)*, 49-53.

[9]Shinde, V. and Dhale, D. A., *J. Phytol.,* **2011,** *3(12),* 41-44.

[10]Rajan, S., Jeevagangai, T. J., *J. Basic Appl. Biol.,* **2009,** *3(1-2),*76-81.

[11]Varma, J., and Dubey, N. K., *Curr. Sci.,* **1999,** *76(2),* 172–179.

[12]Harborne, J. B., *Phytochemical methods: A guide tomodern techniques of plant analysis*, 3rd ed. Chapman & Hall Pub., London, U. K, **1998,** 7–8.

[13]Gottlieb, O. R., Borin, M. R. and Brito, N. R., *Phytochemistry,* **2002,** *60(2),* 145–152.

[14]Shilpakala, S. R., Prathiba, J. and Malathi, R., *Eur. Rev. Med. Pharmacol. Sci.,* **2009,** *13*, 371-374.

PRECONCENTRATION AND RECOVERY OF PESTICIDES FROM SOIL AND WATER BY DISPERSIVE LIQUID-LIQUID EXTRACTION

Rajib Joarder,[a] Dhiman Santra,[a] Srimanta Marjit[a] and Mitali Sarkar[a]*

A simple method for the extraction and preconcentration of pesticides such as imidacloprid, flusilazole and atrazine from soil and water using dispersive liquid-liquid microextraction (DLLME) was described. The process was optimized by suitable selection of dispersive and extraction solvent. The sample was extracted by methanol (dispersive solvent) containing chloroform (extraction solvent) (3:7, v/v). Important factors such as the volume of extraction solvent, equilibration time, pH, and ionic strength were studied. pH and ionic strength found to have, significant influence for recovery and enrichment of solute. Extraction recovery value was found to be 98, 81 and 92 % respectively from water sample. The corresponding enrichment factor was found to be 742.01, 613.28 and 696.57 for imidacloprid, flusilazole and atrazine, respectively. The process was applied for extraction and recovery of the pesticides from soil and water system.

* Corresponding Authors
    E-Mail: mitaliku@gmail.com
[a]   Department of Chemistry, University of Kalyani, Kalyani
       741 235, West Bengal

Introduction

With the advent of chemical technology and synthesis of new materials some plant protecting chemicals are designed for the development of agricultural products. One among the classes is classified in different ways in terms of their origin, use or action popularly herbicide, fungicide and insecticide are collectively called as pesticides. Although the use of pesticide can be considered as one of the prime factors for green revolution their persistence in the environment poses a threat to the ecological balance. The interaction of pesticides with environmental parameters in addition may results in the alteration of their physicochemical properties. The pesticides as such or theirs residues and degradation products[1,2] may generate the toxicity with high residence times in different compartment of the ecosystem such as soil, water and organisms. Migration of pesticides into ground water via soil layers has serious consequences on the ecological balance.[3-6]

The identification and trace level determination of pesticide and residue becomes a challenging task to the analytical chemists. The enrichment of pesticides via separation and removal demands a high sensitive, selective and precise technique with wide range of applications.

The common chromatographic techniques such as HPLC,[7-15] GC,[16-19] capillary electrophoresis (CE)[20-22] and thin layer chromatography are applied for the determination of pesticide from different sample such as water, soil, food and vegetables. Among the well known enrichment techniques liquid-liquid extraction (LLE)[23-25] and solid phase extraction (SPE)[13,26,27] have some disadvantages viz. use of large volume of toxic organic solvent and generation of secondary pollutants respectively. Dispersive liquid-liquid extraction as an extension of liquid-liquid extraction utilizes extraction and dispersive solvent which are introduced in the aqueous solute sample. A very small volume of solvent requirement, quick equilibration time and high extraction efficiency makes the process very useful. The large contact surface area of immiscible phase assists the transfer of solute yielding high extraction efficiency while very small volume (μL) of extraction solvent ensures high enrichment factor.[28-37]

In the present communication the dispersive liquid-liquid extraction of imidacloprid, flusilazole and atrazine as the representative of insecticide, fungicide and herbicide respectively is described. The process was optimized for different operational variables such as nature and volume of dispersive and extraction solvent, time of equilibration, pH and ionic strength of the solution. The effect of different salts on the extraction efficiency and enrichment of the solute from water was determined. The applicability of process was judged from the extraction of solute from soil and water sample. Almost quantitative extraction (>80 %) and high enrichment factor (>630) offers the process quite applicable for trace analysis from complex matrices.

Experimental

Reagents and materials

Imidacloprid, flusilazole and atrazine were obtained from Sigma Aldrich (St Louis, MO, USA). HPLC grade solvents such as carbon tetrachloride, dichloromethane, chloroform, tetrachloroethane, acetone, methanol, and acetonitrile were purchased from Merck, India. All the other reagents used in the experiment were of the highest grade commercially available. Doubly distilled water was used throughout the experiment. All the experiments were performed at room temperature.

Instrumentation

A Shimadzu model UV-2401 PC UV-Vis recording spectrophotometer with quartz cells was used for recording absorption spectra. All spectral measurements were performed using the blank solution as reference. A Rotofix centrifuge was used to accelerate the phase separation process. Measurement of solution pH was done by Systronic digital pH meter. A Cecil (CE 4201) HPLC coupled with UV-Vis detector was used for analysis of the solutes.

Extraction procedure

For the DLLME, 5.0 ml of aqueous sample was placed in a 10 ml screw cap glass test tube with conical bottom. In a typical experiment 0.3 ml of methanol (as disperser solvent) containing 0.7 ml chloroform (as extraction solvent) were rapidly injected into the sample solution and the mixture was gently shaken. A cloudy solution was formed when the solute in the water sample was extracted into fine droplets. The mixture was centrifuged for 5 min at 4000 rpm and $CHCl_3$ was sedimented in the bottom of the conical test tube. The upper phase was withdrawn by a micropipette. The sediment phase was diluted to 6 ml using MeOH and the solute was analysed.

Critical parameter for extraction

In order to judge the feasibility and find out the extent of extraction two critical parameters viz. enrichment parameter and recovery parameter are of prime importance. The enrichment parameter (*EP*) may be defined as the ratio of analyte concentration in the sediment phase (C_{sed}) to the initial concentration of the analyte (C_0) as,

$$EP = \frac{C_{sed}}{C_0} \qquad (1)$$

The recovery parameter (*RP*) is defined as the fraction of solute transferred to the sediment phase, and is expressed in percentage as,

$$RP = 100\frac{W_{sed}}{W_0} = 100\frac{C_{sed}V_{sed}}{C_0V_0} \qquad (2)$$

where,

V_{sed} and V_0 are the volume of sediment phase and aqueous phase, respectively.

W_{sed} and W_0 are the amount of solute in sediment and aqueous phase respectively.

On combining equation (1) and (2) *EP* and *RP* can be correlated as,

$$RP = EP \, x100 \frac{V_{sed}}{V_0} \qquad (3)$$

Results and Discussion

Dispersive liquid-liquid extraction (DLLE) as an extension and improvement of conventional liquid-liquid utilizes a pair of solvents viz dispersive (DS) and extraction solvent (ES). Solute initially dissolved in aqueous phase if put in such a pair will tend to distribute between DS and ES in an equilibrium fashion depending on the nature as well as solubility criteria of the solute in the chosen pair of solvents. The mutual miscibility and density difference of DS and ES makes the phase separation effective .The factors that govern the extraction (both the extent and efficiency) are the nature and volume of DS and ES, time of equilibration, pH and ionic strength of the solution. Thus, optimization of the operational variables constitutes the first step of DLLE.

Influence of type and volume of dispersive solvent

The dispersive solvent is essentially be miscible with both the aqueous and extraction solvent. Further, it must disperse ES as very fine droplets in aqueous phase. In the present study acetone (DS1), methanol (DS2), and acetonitrile (DS3) were chosen as the DS. A typical experiment was performed using 0.3 vol. of each DS containing 0.7 vol. of a definite ES. Five replicate tests were performed for each combination of DS-ES to improve the precision of the operation.
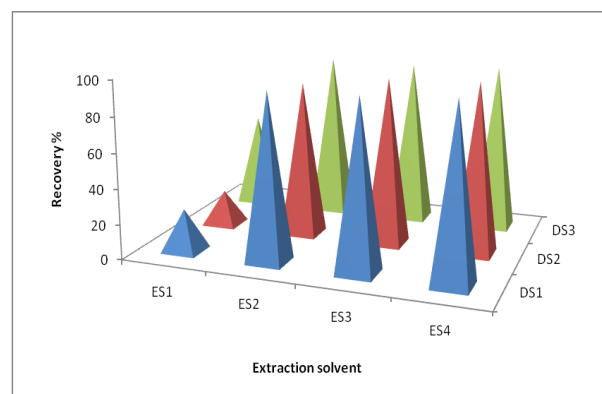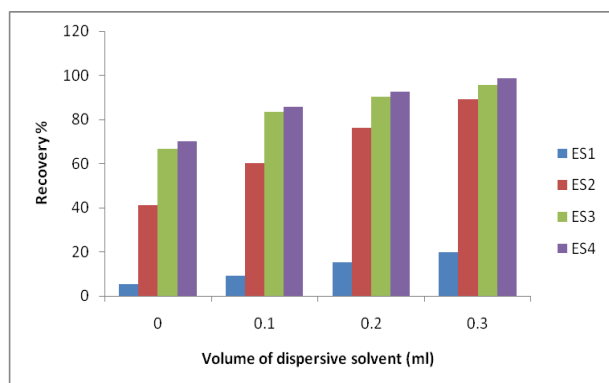

Figure 1. Effect of extraction solvent on the extraction recovery of imidacloprid.

The result indicates that CH_3CN (DS3) acts as the effective DS (Fig. 1) for imidacloprid. As the volume of DS is found to influence the formation of cloudy solution (aqueous-DS-ES) the optimization of the volume of DS is essential to maximize the degree of dispersion and extraction efficiency. The volume of DS was varied from 0.1 ml to 0.3 ml for a fixed volume 0.7 ml of ES.

In the typical study the extraction behavior of imidacloprid is illustrated for CH_3CN as DS and $C_2H_4Cl_4$ as ES.

It is found that for a fixed volume of ES, percent recovery increases with increasing volume of DS which then decreases with further volume of DS. The optimum volume of CH_3CN was chosen as 0.3 ml. At low volume DS cannot disperse ES properly and inhibits formation of the cloudy solution which results incomplete or poor extraction. On the other hand the solubility of imidacloprid in water increases as volume of DS increases. Similar trend is observed by changing either the ES or DS and for each combination a fixed optimum volume is needed to maximize the extraction. Again, different solutes show similar but distinct behavior.

Figure 2. Effect of the volume of acetonitrile (DS) on the extraction recovery of imidacloprid

Influence of type and volume of extraction solvent

In order to achieve the transfer of solute to ES the solute must have higher solubility in ES compared to that in water. The hydrophobicity and higher density, low solubility in water and the formation of the stable ternary phase system are the important parameters for selection of ES. Owing to the high density chlorinated solvents such as CCl_4 (ES1), CH_2CL_2 (ES2), $CHCl_3$, (ES3) and $C_2H_4Cl_4$ (ES4) are found to be the potential ES. In order to study the effect of the ES volume on the efficiency of the solute transfer the volume of the ES was varied (0.1-0.7 ml) for a fixed volume (0.3 ml) of a definite DS. It is inferred that high density solvents are effective due to quick settling at the bottom of the test tube. It is found that extraction increases with increase of volume of the extraction solvent for a fixed volume of the dispersive solvent.
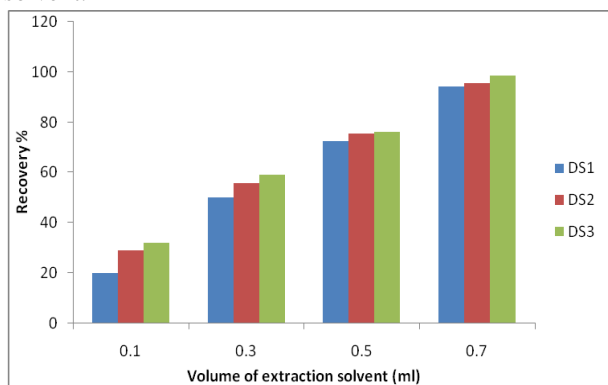

Figure 3. Effect of the volume of tetrachloroethane (ES) on the extraction recovery of imidacloprid

Figure. 3. demonstrates a typical situation for $C_2H_4Cl_4$ as ES for extraction of imidacloprid using acetone (DS1), methanol (DS2) and acetonitrile (DS3) as dispersive solvent.

However, the volume requirement of ES and extraction efficiency vary with change of the DS. Similar situation arises for a fixed DS and varying ES (Figure .2).

Effect of pH

The important parameters governing extraction with variation of solution pH are (a) solubility and (b) stability of the solute due to ionization. It is found (Figure .4) that with increase in pH the extraction of imidacloprid increases, reaches a maximum and decreases subsequently. The pH corresponding to maximum recovery is taken as the optimum pH for extraction.
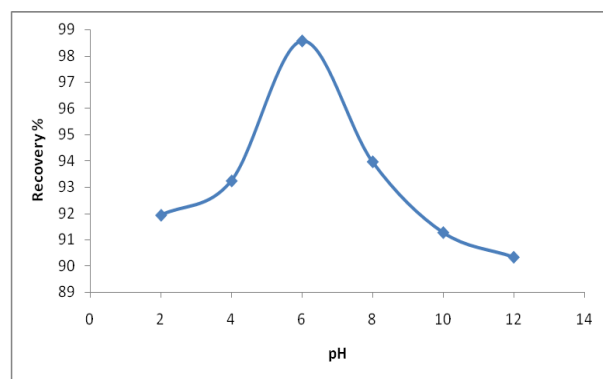
Figure 4. Effect of pH on the extraction recovery of imidacloprid

The extraction extent and pattern of the solute has distinct character in respect to variation of solution pH for a fixed combination of ES-DS. Figure 4. describes the pH effect of imidacloprid for $C_2H_4Cl_4$ as ES with CH_3CN as DS. The optimum pH was found to be 6, 10 and 5, for imidacloprid, flusilazole and atrazine, respectively.
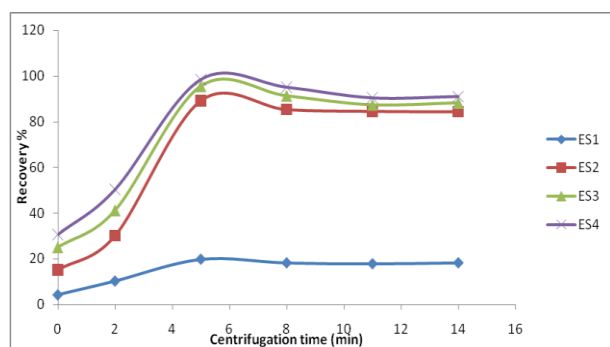
Effect of the extraction time

In order to have the present operation effective the solute transfer from aqueous to the extraction phase must be fast and thermodynamically feasible. The DLLE can be thought of as a two steps process viz,

(a) transfer of solute from aqueous to ES in an equilibrium fashion and

(b) formation of solute rich sediment phase.

It is expected that as the surface area between the aqueous and extraction solvent (in presence of DS at the cloudy state) is appreciably high the extraction is quite rapid and the equilibrium is reached within a very short time. Thus, aqueous-DS cloud formation and sedimentation of solute rich phase improves the efficiency of the said process. With CH_3CN as the DS, extraction profile of imidacloprid is presented in Figure 5.

It is found that with increase in centrifugation time the recovery percent increases and reaches a flat plateau after a certain time, considered as the equilibrium time, which may vary with the change of ES.

Figure 5. Effect of centrifugation time on the extraction recovery of imidacloprid

The effect of ionic strength

The ionic strength of the solution has some important influence governing the extraction efficiency. The ionic strength of the solution was varied by adding different salts of varying concentration. With salt addition the aqueous phase solubility of the extraction solvent and the solute will change affecting the extractability. It is found that the volume of the sediment phase and the extraction extent depend on the nature of the added electrolyte. Presence of chloride, sulfate, and carbonate typically decreases aqueous solubility of both the ES and the solute due to salting out effect. Thus, volume of sediment phase and the solubility of the solute in ES increase resulting *EP* decrease and *RP* increase. The extent of *EP* and *RP* vary with the nature of ES in presence of salt. The lower the lyotropic number of the salt, pronounced is the effect. In a typical study NaCl, KCl, KNO_3, $(NH_4)_2SO_4$, were examined. The carbonate salt was avoided due to the possibility of solution pH change. In all the cases electrolyte concentration was kept at 1×10^{-3} M. It is found that recovery percent increases in the order,: $(NH_4)_2SO_4 > KNO_3 > KCl > NaCl$. However, the volume of the sediment phase does not change appreciably with variation of electrolyte.

Table 1. Characteristic features for DLLE.

Parameters	Compounds		
	Imida-cloprid	Flusi-lazole	Atra-zine
Limit of detection, *LOD*, $\mu g\ L^{-1}$	0.1	0.08	0.05
Limit of quantification, *LOQ*, $\mu g\ L^{-1}$	0.3	0.24	0.15
Linear range, *LR,* $\mu g\ L^{-1}$	0.1-100	0.1-100	0.1-100
Correlation coefficient (*r*)	0.9924	0.9981	0.9944
Intra-day precision*, RSD %	2.1	2.9	2.7
Inter-day precision*, RSD %	3.8	4.2	4.0
Recovery Prameter, *RP* %	98	80.59	91.81
Enrichment Parameter, *EP*	742	610.18	695.13

*Five replication

The concentration of $(NH_4)_2SO_4$ was next varied from 10^{-2} to 10^{-4} M. It is found that volume of sediment phase increased from 25 to 28.5 µl and RP increased from 80.49 to 98.56 % corresponding to salt concentration of 10^{-3} M. In all subsequent experiment the salt concentration was kept at 10^{-3} M.

Efficiency of the method

At the optimized condition the analytical characteristics of the method, such as limit of detection (*LOD*), limit of quantification (*LOQ*), linear range (*LR*), correlation coefficient (*r*), repeatability (intra-day precision), reproducibility (inter-day precision), recovery parameter, (*RP*) and enrichment parameter (*EP*) are shown in Table 1.

The feasibility of the process was evaluated from the free energy change of the process.

Application of the method

The DLLE described so far was applied for the recovery of the studied pesticides from soil and water samples. Each sample was analysed 5 times and the results are presented as the mean.

Table 2. Recovery of imidacloprid, flusilazole and atrazine from soil and water.

Compounds	Sample	Conc., $\mu g\ L^{-1}$ (mean ± SD[#])	Recovery, % (mean ± SD[#])
Imidacloprid	soil	11.7 ± 0.02	96.8 ± 0.05
	water	4.1 ± 0.02	97.8 ± 0.04
Flusilazole	soil	20.1 ± 0.01	78.2 ± 0.05
	water	1.5 ± 0.02	79.7 ± 0.04
Atrazine	soil	27.8 ± 0.02	90.5 ± 0.04
	water	3.1 ± 0.01	90.9 ± 0.03

[#] standard deviation

References

[1]Liu, W.-P., Zheng, W., Ma, Y. and Liu, K. K., *J. Environ. Sci. Health B*, **2006**, *41*, 623-634.

[2]Yu, S., Qin, D., Wu, Q., Guo, X., Han, L. and Jiang, S., *Bull. Environ. Contam. Toxicol.*, **2011**, *86*, 319–322.

[3]Pang, G.-F., Fan, C.-L., Liu, Y.-M., Cao, Y.-Z, Zhang, J.-J., Fu, B.-L., Li, X.-M., Li, Z.-Y. and Wu, Y.-P., *Food Addit. Contam.*, **2006**, *23*, 777–810.

[4]Lehotay, S. J., De Kok, A., Hiemstra, M. and Van Bodegraven, P*., J. AOAC Int.*, **2005**, *88*, 595–614.

[5]Anagnostopoulos, C., Bourmpopoulou, A. and Miliadis, G., *Anal. Lett.*, **2013**, *46*, 2526–2541.

[6]Liu, H., Song, J., Zhang, S., Qu, L., Zhao, Y., Wu, Y. and Liu, H., *Pest Manag. Sci.*, **2005**, *61*, 511-514.

[7]Mauldin, R. E., Primus, T. M., Buettgenbach, T. A., John, J., Johnston, J. J. and Linz, G. M., *J. Liq. Chromatogr. R. T.*, **2006**, *29*, 339–348.

[8]Kumar, P., Singh, S. P., Shrikant, K. and Madhukar, D*., Turk. J. Vet. Anim. Sci.*, **2011**, *35,* 219-226.

[9]Kukusamude, C., Santalad, A., Boonchiangma, S., Burakham, R., Srijaranai, S. and Chailapakul, O., *Talanta*, **2010**, *81*, 486–492.

[10]Zhang, Q., Zhu, L., Han, C., Wang, J., Xie, H., Wang, J. and Sun, S., *J. Food Agric. Environ.*, **2011**, *9*, 659-662.

[11]Wang, Y., You, J., Ren, R., Xiao, Y., Gao, S., Zhang, H. and Yu, A., *J. Chromatogr. A*, **2010**, *1217*, 4241–4246.

[12]Rancan, M., Rossi, S. and Sabatini, A. G., *J. Chromatogr. A*, **2006**, *1123*, 60–65.

[13]Wang, P., Yang, X., Wang, J., Cui, J., Dong, A. J., Zhao, H. T., Zhang, L. W., Wang, Z. Y., Xu, P, Li, R. B., Zhang, W. J., Zhang, Y. C. and Jing, H., *Food Chem.*, **2012**, *134*, 1691–1698.

[14]Chen, L., Chen, J. M. and Xia, F. L., *Agro-environ. Protect.*, **2002**, *21*, 150–152.

[15]Farouk, M., Hussein, L. A. A. and Azab, N. F. E., *Intern. J. Environ. Anal. Chem.*, **2014**, *94*, 194-209.

[16]Wang,C., Qiu, L., Zhao, H., Wang, K. and Zhang, H., *Environ. Monit. Assess.*, **2013**, *185*, 9169–9176.

[17]Zang, X., Wang, J., Wang, O., Wang, M., Ma, J., Xi, G. and Wang, Z., *Anal. Bioanal. Chem.*, **2008**, *392*, 749–754.

[18]Amvrazi, E. G. and Tsiropoulos, N. G., *J. Chromatogr. A*, **2009**, *1216*, 2789–2797.

[19]Faria, A. M., Dardengo, R. P., Lima., C. F., Neves, A. A. and Queiroz, M. E. L. R., *Inter. J. Environ. Anal. Chem.*, **2007**, *87*, 249–258.

[20]Pico, Y., Rodríguez, R. and Mañes, J., *Trends Anal. Chem.*, **2003**, *22*, 133-151.

[21]Simpson Jr, S. L., Quirino, J. P. and Terabe, S., *J. Chromatogr. A*, **2008**, *1184*, 504–541.

[22]Palmer, J., Munro, N. J. and Landers, J. P., *Anal. Chem.*, **1999**, *71*, 1679–1687.

[23]Xie, S., Paau, M. C., Li, C. F., Xiao, D. and Choi, M. M. F., *J. Chromatogr. A*, **2010**, *1217*, 2306–2317.

[24]Lambropoulou, D. A. and Albanis, T. A., *J. Biochem. Biophys. Methods*, **2007**, *70*, 195–228.

[25]Jansson, C., Pihlstrom, T., Oterdahl., B. G., and Markides, K. E., *J. Chromatogr. A*, **2004**, *1023*, 93–104.

[26]Stajnbaher, D. and Zupancic-Kralj, L., *J. Chromatogr. A*, **2003**, *1015*, 185–198.

[27]Watanabe, E., Baba, K. and Eun, H., *J. Agric. Food Chem.*, **2007**, *55*, 3798–3804.

[28]Rezaee, M., Assadi, Y., Milani Hosseini, M. R., Aghaee, E., Ahmadi, F. and Berijani, S., *J. Chromatogr. A*, **2006**, *1116*, 1–9.

[29]Wang, Y., You, J., Ren, R., Xiao,Y., Gao, S., Zhang, H.and Yu., A., *J. Chromatogr. A*, **2010**, *1217*, 4241–4246.

[30]Zacharis, C. K., Rotsias, I., Zachariadis, P. G.and Zotos, A., *Food Chem.*, **2012**, *134*, 1665–1672.

[31]Qiao, F., Zhang, X., Wang, M. and Kang, Y., *Chromatographia*, **2010**, *72*, 331–335.

[32]Wu, Q., Li, Z., Wang, C., Wu, C., Wang, W. and Wang, Z., *Foods Anal. Meth.*, **2011**, *4*, 559–566.

[33]Zhang, S., Yang, X., Yin, X., Wang, C. and Wang, Z., *Food Chem.*, **2012**, *133*, 544–550.

[34]Jovanov, P., Guzsvány, V., Franko, M., Lazić, S., Sakač, M., Šarić, B. and Banjac, V., *Talanta*, **2013**, *111*, 125–133.

[35]Campillo, N.,Viñas, P., Férez-Melgarejo, G. and Hernández-Córdoba, M., *J. Agric. Food Chem.*, **2013**, *61*, 4799−4805.

[36]Vichapong, J., Burakham, R. and Srijaranai, S., *Talanta*, **2013**, *117*, 221–228.

[37]Pirsaheb, M., Fattahi, N., Shamsipur, M. and Khodadadi, T., *J. Sep. Sci.*, **2013**, *36*, 684–689.